Title	Chiral Behavior of S-Bridged M3M' 2 (M = AuI, AgI; M' = CoIII, RhIII) Pentanuclear Complexes with L-Cysteinate
Author(s)	Lee, Pei-Shan
Citation	大阪大学, 2014, 博士論文
Version Type	VoR
URL	https://doi.org/10.18910/34068
rights	Copyright © 2016 The Chemical Society of Japan. All Rights Reserved.
Note	

Chiral Behavior of S-Bridged $M_3M'_2$ ($M = Au^I, Ag^I$; $M' = Co^{III}, Rh^{III}$) Pentanuclear Complexes with L-Cysteinate

（L-システィンをもつ硫黄架橋 $M_3M'_2$（$M = Au^I, Ag^I$; $M' = Co^{III}, Rh^{III}$）五核錯体のキラル挙動）

Pei-Shan Lee

Department of Chemistry

Graduate School of Schience

Osaka University

2014

Contents

Chapter I. Introduction

Since Pasteur discovered that optical activity is derived from molecular structures by preparing chiral crystals of sodium ammonium tartrate, chiral compounds have attracted considerable interest in chemistry, biology, and material science.[1] Good examples of intriguing chiral compounds are biological macromolecules like proteins, DNA, and polysaccharides that are composed of chiral monomers like L-amino acids, nucleotides, and monosaccharides. These chiral structures are responsible for the origins of life. In these compounds, the chiral monomers are connected to each other not only through covalent bonds but also through intramolecular and intermolecular noncovalent bonding interactions, which leads to the formation of helical structures, such as double helices in DNA and triple helices in collagens, and permits the development of their specific functionalities.[2] Chirality also plays an important role in the development of nanotechnology such as chiral switches and chiral molecular machines.[3] The change in chirality induces change in the molecular structures or electronic properties of the system, which can simultaneously trigger particular functionalities to be modulated, such as fluorescence properties and molecular recognition behavior. Thus, due to the interests not only in the understanding of the origin of homochirality in the biological macromolecules but also in potential functional devices based on specific chiral structures, the chiral compounds have been widely studied in various research fields including supramolecular chemistry, biochemistry, and physical chemistry, as well as biology.

In the field of coordination chemistry, chiral coordination compounds are also receiving immense attention because of their fundamental importance in modern stereochemistry,[4] and potential applications such as catalysis, nonlinear optics, sensors, and multifunctional materials,[5] in recent years. The establishment of the construction of chiral compounds is one of the important subjects for the development of the research on chirality. There are mainly two ways to create chiral coordination compounds. One is the asymmetric synthesis, in which one of the possible enantiomers is formed in either partial or total excess by the use of chiral elements such as reagent, solvent, and catalyst.[6] This method is effective for preparing chiral organic compounds, but for coordination compounds, the number of examples is limited. The other way is the optical resolution of a racemic compound into its enantiomers, and most of chiral coordination compounds are isolated by this approach that includes spontaneous resolution, column chromatography, and use of chiral auxiliary.[7] The spontaneous resolution was found in sodium ammonium tartrate reported by Pasteur, but this type of resolution is still rare. The chromatography is a popular method to separate enantiomers or diastereomers on a preparative scale, and a

great number of chiral coordination compounds were separated using either chiral column or chiral eluant. The use of chiral auxiliary is also an effective approach, which leads to the formation of diastereomers with different physicochemical properties and leads to fractional crystallization. The formation of a diastereomeric ion pair is a powerful way, and optically pure organic compounds such as tartric acid and alkaloids have widely been used as resolving reagents for the separation of cationic and anionic coordination compounds, respectively.[8] The chiral ionic coordination compounds are also used as resolving reagents in this approach.[9]

The use of chiral ligands is one of the powerful ways to prepare diastereoselective coordination compounds.[10] L-Cysteine, one of the sulfur-containing amino acids, is known to act as a chiral ligand using its thiolate and amine groups to create chiralselective metal complexes. Treatment with Co^{III}, Rh^{III}, or Ir^{III} ions resulted in the formation of mononuclear structures with three bidentate-N,S L-cys ligands, Δ_{LLL}-[M(L-cys-*N*,*S*)$_3$]$^{3-}$ (L-H_2cys = L-cysteine).[11] Interestingly, the Δ_{LLL} isomer of the mononuclear complexes was easily obtained in these reactions. When these mononuclear complexes were reacted with octahedral metal ions, Δ_{LLL}-[M(L-cys-*N*,*S*)$_3$]$^{3-}$ acts as an S-donating metalloligand to form S-bridged trinuclear complexes. The chirality of the metal centers coordinated by L-cys ligands was found to be controlled by the metal ions used. Treatment of Δ_{LLL}-[Co(L-cys)$_3$]$^{3-}$ with Co^{III} gave the $(\Delta_{LLL})_2$ isomer of the L-cysteinato Co^{III}_3 complex, [Co_3(L-cys)$_6$]$^{3-}$, retaining the chirality around the Co^{III} centers, while treatment with Co^{II} gave the $(\Lambda_{LLL})_2$ isomer accompanied by the chiral inversion (Figure 1-1).[12] The reaction of Δ_{LLL}-[Rh(L-cys)$_3$]$^{3-}$ with Co^{II} gave a similar $Rh^{III}Co^{III}Rh^{III}$ trinuclear structure with $(\Delta_{LLL})_2$, $(\Lambda_{LLL})_2$, and $(\Delta_{LLL})(\Lambda_{LLL})$ configurations.[13a] These isomers were relatively easily separated because of their diastereomeric nature. On the other hand, when Δ_{LLL}-[Ir(L-cys)$_3$]$^{3-}$ was used, only the $(\Delta_{LLL})_2$ isomer of the $Ir^{III}Co^{III}Ir^{III}$ trinuclear complex was formed.[13b] Thus, the diastereoselective synthesis and the separation of the diastereomers were achieved by the use of chiral ligands. Furthermore, when Δ_{LLL}-[Co(L-cys)$_3$]$^{3-}$ was reacted with Zn^{II} with a tetrahedral coordination geometry, the $Co^{III}_4Zn^{II}_4$ octanuclear complex-anion $(\Delta_{LLL})_4$-[Co_4Zn_4O(L-cys)$_{12}$]$^{6-}$ was formed, in which four Δ_{LLL}-[Co(L-cys)$_3$]$^{3-}$ is connected with a [Zn_4O]$^{6+}$ core through thiolato groups (Figure 1-1).[14] The reaction of Δ_{LLL}-[Co(L-cys)$_3$]$^{3-}$ with a linear Ag^I ion afforded the S-bridged $Ag^I_3Co^{III}_2$ pentanuclear complex-anion $(\Delta_{LLL})_2$-[Ag_3Co_2(L-cys)$_6$]$^{3-}$ (Figure 1-1).[2d]

Thus, it was found that the use of Δ_{LLL}-[Co(L-cys)$_3$]$^{3-}$ as an S-donating metalloligand is a powerful way to create a variety of chiral structures. Because these L-cysteinato multinuclear complexes have free carboxylate groups available for a metal-coordination site or an acceptor site of hydrogen bonds, which is important for

the chiral recognition, the potential ability of the chiral separation in these complexes was investigated. The L-cysteinato multinuclear complexes have anionic nature, and thus have possibility to resolve cationic racemic metal complexes during the cocrystallization process. In fact, it has been reported that treatment of the $(\Lambda_{LLL})_2$ isomer of the L-cysteinato Co^{III}_3 complex-anion, $[Co_3(L\text{-cys})_6]^{3-}$, with the racemic Co^{III}_3 complex-cation, $[Co_3(aet)_6]^{3+}$ (aet = 2-aminoethanethiolate), which has an S-bridged Co^{III}_3 trinuclear structure, gave the cocrystallized compound consisting of $(\Lambda_{LLL})_2$-$[Co_3(L\text{-cys})_6]^{3-}$ and $[Co_3(aet)_6]^{3+}$ in a 1:1 ratio (Figure 1-2).[15] Of note is that only the $(\Delta)_2$ isomer of $[Co_3(aet)_6]^{3+}$ is exclusively incorporated in this compound, and the excellent optical resolving ability of the chiral multinuclear complex-anion toward the racemic complex-cation was successfully demonstrated. Furthermore, treatment of $(\Lambda_{LLL})_2$-$[Co_3(L\text{-cys})_6]^{3-}$ with $[Ag_3Co_2(aet)_6]^{3+}$, which has a similar S-bridged structure with $[Co_3(aet)_6]^{3+}$ having a $\{Ag^I_3\}$ moiety instead of the central Co^{III} ion, also afforded the cocrystallized compound $(\Lambda_{LLL})_2$-$[Ag_3Co_2(aet)_6][Co_3(L\text{-cys})_6]$ (Figure 1-3).[16] In this compound, the excellent chiralselective incorporation of the complex-cation was also observed, although in this case, the $(\Lambda)_2$ isomer of $[Co_3(aet)_6]^{3+}$ was selected.

In this thesis, the research on the optical resolving ability of chiral multinuclear complex-anions toward a racemic complex-cation is further developed. An S-bridged $Au^I_3Co^{III}_2$ pentanuclear complex-anion, $(\Delta_{LLL})_2$-$[Au_3Co_2(L\text{-cys})_6]^{3-}$, which has a similar structure with $(\Delta_{LLL})_2$-$[Co_3(L\text{-cys})_6]^{3-}$, except the presence of a $\{Au^I_3\}$ moiety between two terminal Δ_{LLL}-$[Co(L\text{-cys})_3]^{3-}$ units instead of the central Co^{III} ion, was newly prepared as a resolving reagent (Figure 1-4). The introduction of a $\{Au^I_3\}$ moiety with three linear Au^I centers can lead to the formation of additional intermolecular interactions such as metal-metal bonding interactions, which might induce different chiral behavior. When the chiralselectivity of this complex-anion toward the racemic complex-cation $[Co_3(aet)_6]^{3+}$ upon the cocrystallization was investigated, it was found that multiple chiral and structural conversions of the complex-anion occur during the crystallization process The mechanism of these unique conversions was elucidated, as well as its chiralselective behavior. Then, the chiralselectivity of a similar S-bridged $Ag^I_3Co^{III}_2$ pentanuclear complex-anion, $(\Delta_{LLL})_2$-$[Ag_3Co_2(L\text{-cys})_6]^{3-}$, was investigated (Figure 1-4). In this case, intermolecular coordination bonding interactions using the two-coordinated Ag^I ion were formed instead of metal-metal bonding interactions. The important factors for the chiral separation were discussed based on the structural comparison in detail. In addition, the $Au^I_3Rh^{III}_2$ and $Ag^I_3Rh^{III}_2$ pentanuclear complexes with L-cysteinate, $(\Delta_{LLL})_2$-$[Au_3Rh_2(L\text{-cys})_6]^{3-}$ and $(\Delta_{LLL})_2$-$[Ag_3Rh_2(L\text{-cys})_6]^{3-}$, have also been prepared and the chiral behavior was investigated for comparison (Figure 1-4).

In Chapter II, the L-cysteinato $Au^{I}_{3}Co^{III}_{2}$ pentanuclear complex-anion $(\Delta_{LLL})_2$-$[Au_3Co_2(L\text{-}cys)_6]^{3-}$ was newly prepared, and its cocrystallization behavior with the complex-cation $[Co_3(aet)_6]^{3+}$ was investigated. As a result, a cocrystallized compound, $(\Delta_{LLL})_2$-$[Co_3(aet)_6][Au_3Co_2(L\text{-}cys)_6]$, was obtained in neutral conditions, whereas the reaction in basic conditions led to chiral and structural conversions of the complex-anion to give a cocrystallized compound consisting of a L-cysteinato $Au^{I}_{6}Co^{III}_{4}$ pentanuclear complex-anion with the Λ_{LLL} configurational Co^{III} centers, $(\Lambda_{LLL})_2$-$[Au_6Co_4(L\text{-}cys)_{12}]^{6-}$, and $[Co_3(aet)_6]^{3+}$ in a 1:2 ratio. The mechanism of the unique conversions is discussed based on the spectral measurements. In Chapter III, the chiralselective behavior of three complex-anions, $(\Delta_{LLL})_2$-$[Au_3Co_2(L\text{-}cys)_6]^{3-}$, $(\Lambda_{LLL})_2$-$[Au_6Co_4(L\text{-}cys)_{12}]^{6-}$, and $(\Delta_{LLL})_2$-$[Ag_3Co_2(L\text{-}cys)_6]^{3-}$, toward the racemic complex-cation $[Co_3(aet)_6]^{3+}$ was investigated by means of absorption and CD spectral measurements, in combination with column chromatography. The factors that contribute to the chiralselective behavior are discussed based on the X-ray crystallography. In Chapter IV, the chiralselective behavior of two complex-anions, $(\Delta_{LLL})_2$-$[Au_3Rh_2(L\text{-}cys)_6]^{3-}$ and $(\Delta_{LLL})_2$-$[Ag_3Rh_2(L\text{-}cys)_6]^{3-}$, toward racemic complex-cation $[Co_3(aet)_6]^{3+}$ and the possibility to the chiral and structural conversions were investigated to clarify the influence of the presence of the inert Rh^{III} ions.

References

(1) (a) W. H. Pirkle, T. C. Pochapsky, *Chem. Rev.* **1989**, *89*, 347–362. (b) G. L. Hamilton, E. J. Kang, M. Mba, F. D. Toste, *Science* **2007**, *317*, 496–499. (c) K. Aikawa, M. Kojima, K. Mikami, *Angew. Chem. Int. Ed.* **2009**, *48*, 6073–6077. (d) S. Liao, B. List, *Angew. Chem. Int. Ed.* **2010**, *49*, 628–631.

(2) (a) J. D. Watson, F. C. Crick, *Nature* **1953**, *171*, 737–738. (b) B. Rosenberg, L. Van Camp, T. Krigas, *Nature* **1965**, *205*, 698−699. (c) K. Okamoto, S. Aizawa, T. Konno, H. Einaga, J. Hidaka, *Bull. Chem. Soc. Jpn.* **1986**, *59*, 3859–3864. (d) T. Konno, K. Tokuda, T. Suzuki, K. Okamoto, *Bull. Chem. Soc. Jpn.* **1998**, *71*, 1049–1054. (e) R. Kanaar, J. H. Hoeijmakers, D. C. van Gent, *Trends Cell Biol.* **1998**, *8*, 483−489. (f) A. J. T. Smith, R. Müller, M. D. Toscano, P. Kast, H. W. Hellinga, D. Hilvert, K. N. Houk, *J. Am. Chem. Soc.* **2008**, *130*, 15361–15373. (g) Y. Fu,; Q. Han, Q. Chen, Y.; Wang, J. Zhou, Q. Zhang, *Chem. Commun.* **2012**, *48*, 2322–2324. (h) S. Tabassum, A. Asim, R. A. Khan, Z. Hussain, S. Srivastav, S. Srikrishnac, F. Arjmand, *Dalton Trans.* **2013**, *42*, 16749–16761.

(3) (a) J. Zhang, M. T. Albelda, Y. Liu, J. W. Canary, *Chirality* **2005**, *17*, 404–420. (b) E. R. Kay, D. A. Leigh, F. Zerbetto, *Angew. Chem. Int. Ed.* **2007**, *46*, 72–191. (c) K. Ariga, T. Mori, J. P. Hill, *Adv. Mater.* **2012**, *24*, 158–176. (d) Y. Li, C. Xue, M. Wang, A. Urbas, Q. Li, *Angew. Chem. Int. Ed.* **2013**, *52*, 13703–13707. (e) P. Yin, T. Li, R. S. Forgan, C. Lydon, X. Zuo, Z. N. Zheng, B. Lee, D. Long, L. Cronin, T. Liu, *J. Am. Chem. Soc.* **2013**, *135*, 13425−13432.

(4) (a) M. Melnika, C. E. Holloway, *Coord. Chem. Rev.* **2006**, *250*, 2261–2270. (b) Y. Hirai, N. Yoshinari, A. Igashira-Kamiyama, T. Konno, *Inorg. Chem.* **2011**, *50*, 2040–2042.

(5) (a) P. FIscher, F. Hache, *Chirality* **2005**, *17*, 421–437. (b) Y. Liu, W. Xuan, Y. Cui, *Adv. Mater.* **2010**, *22*, 4112–4135. (c) W. J. Chen, S. Zhang, W. G. Zhang, J. Fan, X. Yin, S. R. Zheng, W. C. Su,; Z. Zhang, T. Hong, *Chirality* **2012**, *24*, 804–809. (d) K. Brak, E. N. Jacobsen, *Angew. Chem. Int. Ed.* **2013**, *52*, 534–561.

(6) (a) W. R. Cannon, S. F. Singleton, S. J. Benkovic, *Nat. Struct. Biol.* **1996**, *3*, 821–833. (b) H. J. Schneider, *Angew. Chem. Int. Ed.* **2009**, *48*, 3924–3977.

(7) (a) Y. Chikamoto, M. Hirotsu, T. Yamaguchi, T. Yoshimura, T. Konno, *Dalton Trans.* **2004**, 3654–3661. (b) H. Nakamura, M. Fujii, Y. Sunatsuki, M. Kojima, N. Matsumoto, *Eur. J. Inorg. Chem.* **2008**, 1258–1267.

(8) (a) M. Kita, K. Yamanari, Y. Shimura, *Chem. Lett.* **1980**, *3*, 275–278. (b) T. Tada, Y. Kushi, H. Yoneda, *Bull. Chem. Soc. Jpn.* **1982**, *55*, 1063–1072. (c) M. Sato, S. Yano, *Bull. Chem. Soc. Jpn.* **1989**, *62*, 3932–3938. (d) S. Yano, M. Kato, K.

Tsukahara, M. Sato, T. Shibahara, K. Lee, Sugihara, Y. M. Iida, K. Goto, S. Aoki, Y. Shibahara, H. Nakahara, Yanagisawa, S. H. Miyagawa, *Inorg*. *Chem*. **1994**, *33*, 5030–5035.

(9) (a) J. Lacour, V. Hebbe-Viton, *Chem*. *Soc*. *Rev*. **2003**, *32*, 373–382. (b) A. Macchioni, *Chem*. *Rev.* **2005**, *105*, 2039–2074. (c) J. Lacour, D. Moraleda, *Chem*. *Commun*. 2009, 7073–7089.

(10) (a) D. Marquarding, G. Gokel, P. Hoffman, I. K. Ugi, *J*. *Am*. *Chem*. *Soc*. **1970**, *92*, 5389–5393. (b) H. Barrera, J. Suades, M. C. Perucard, J. L. Brianso, *Polyhedron* **1984**, *3*, 839–843. (c) D. L. Caulder, R. E. Powers, T. N. Parac, K. N. Raymond, *Angew*. *Chem*. *Int*. *Ed*. **1998**, *37*, 1840–1843.

(11) (a) T. Konno, K. Nakamura, K. Okamoto, J. Hidaka, *Bull*. *Chem*. *Soc*. *Jpn*. **1993**, *66*, 2582–2589. (b) T. Konno, K. Okamoto, J. Hidaka, *Inorg*. *Chem*. **1994**, *33*, 538–544.

(12) T. Konno, S. Aizawa, K. Okamoto, J. Hidaka, *Chem*. *Lett*. **1985**, *7*, 1017–1020.

(13) (a) T. Konno, S. Aizawa, K. Okamoto, J. Hidaka, Bull. *Chem*. *Soc*. *Jpn*. **1990**, *63*, 792–798. (b) T. Konno, K. Nakamura, K. Okamoto, J. Hidaka, *Bull*. *Chem*. *Soc*. *Jpn*. **1993**, *66*, 2582–2589.

(14) N. Yoshinari, **2010**, doctor thesis.

(15) H. Q. Yuan, A. Igashira-Kamiyama, K. Tsuge, T. Konno, *Chem*. *Lett*. **2009**, *38*, 704–705.

(16) H. Q. Yuan, A. Igashira-Kamiyama, T. Konno, *Chem*. *Lett*. **2011**, *40*, 285–287.

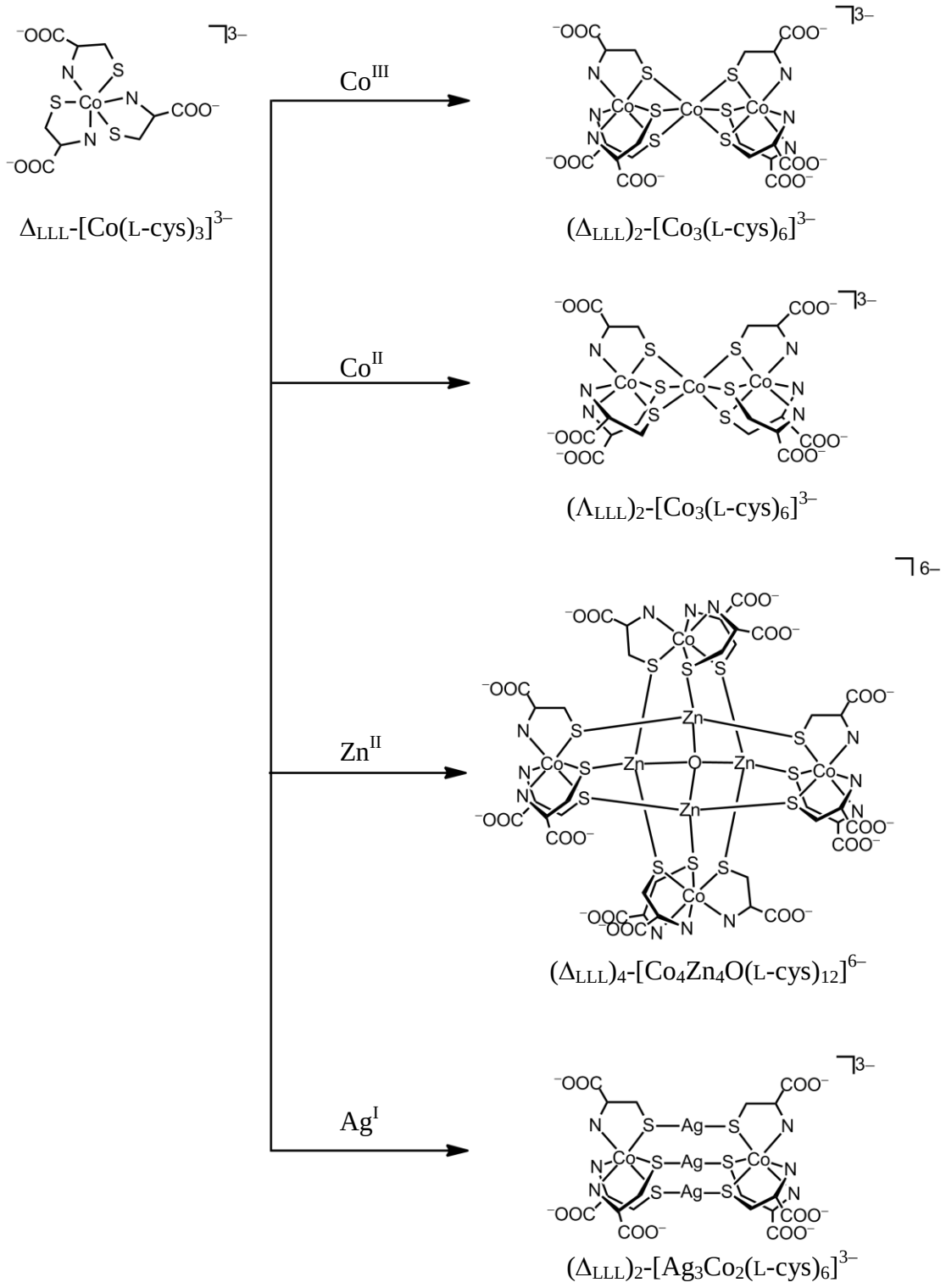

Figure 1-1. Reactions of Δ_{LLL}-$[Co(L\text{-}cys)_3]^{3-}$ with metal ions.

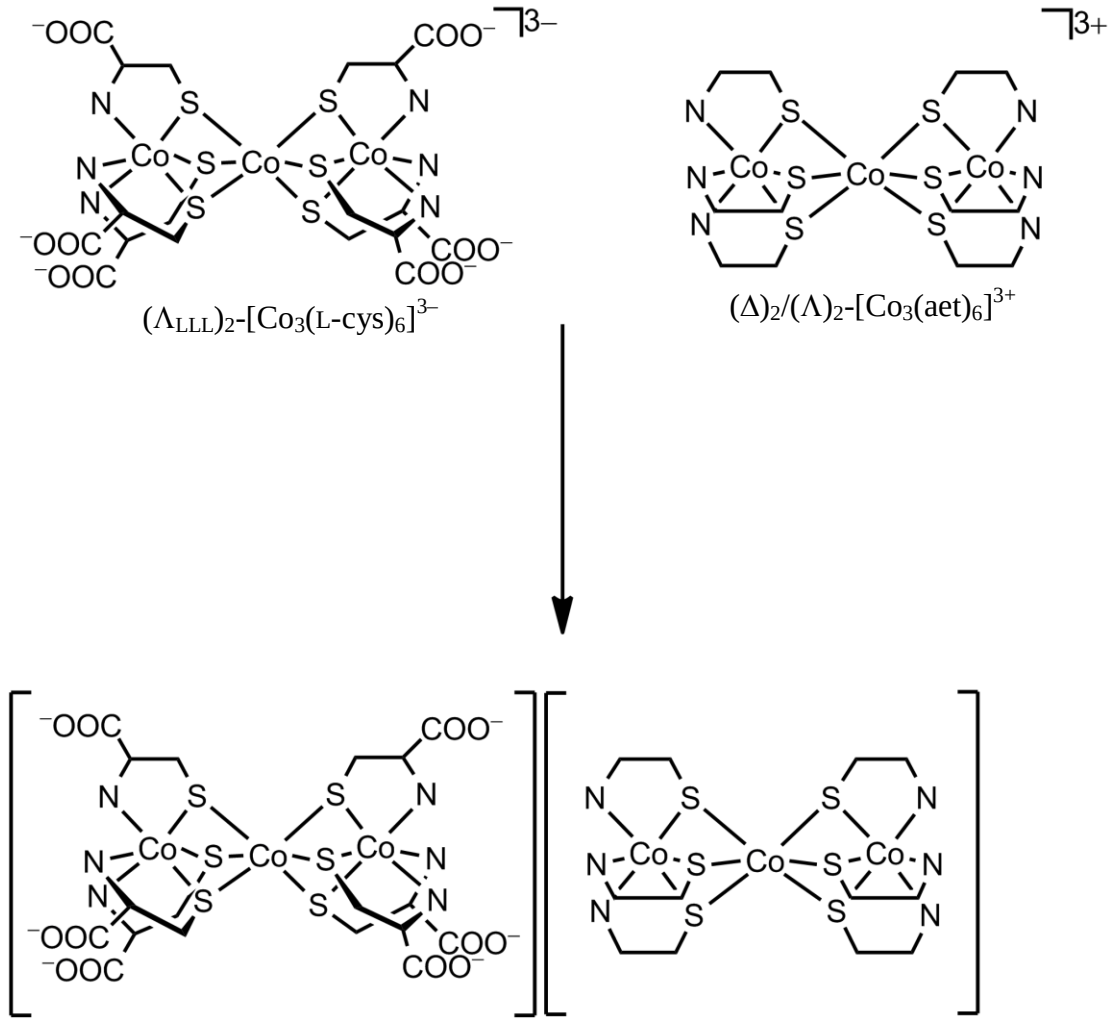

Figure 1-2. Chiral selective behavior by crystallization.

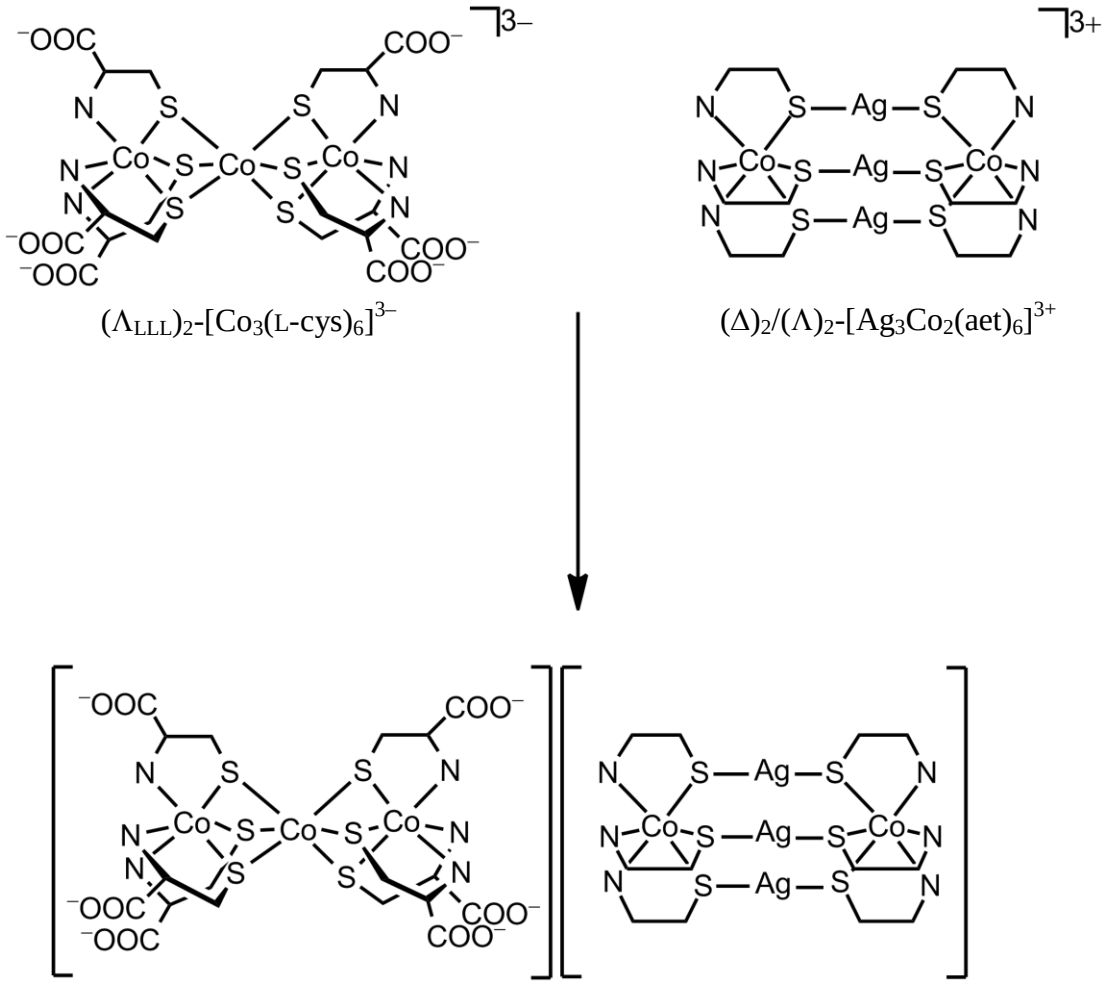

$(\Lambda_{LLL})_2$-$[Co_3(L\text{-}cys)_6]^{3-}$ $(\Delta)_2/(\Lambda)_2$-$[Ag_3Co_2(aet)_6]^{3+}$

$(\Lambda)_2(\Lambda_{LLL})_2$-$[Ag_3Co_2(aet)_6][Co_3(L\text{-}cys)_6]$

Figure 1-3. Chiral selective behavior by crystallization.

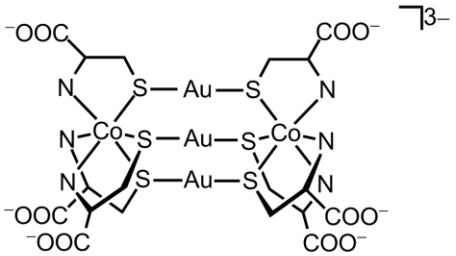

$(\Delta_{LLL})_2$-$[Au_3Co_2(L\text{-}cys)_6]^{3-}$

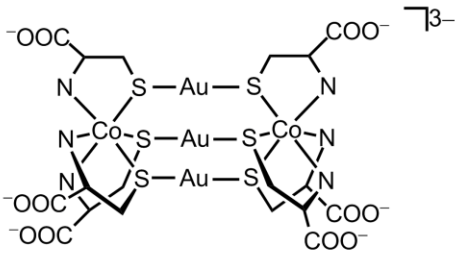

$(\Lambda_{LLL})_2$-$[Au_3Co_2(L\text{-}cys)_6]^{3-}$

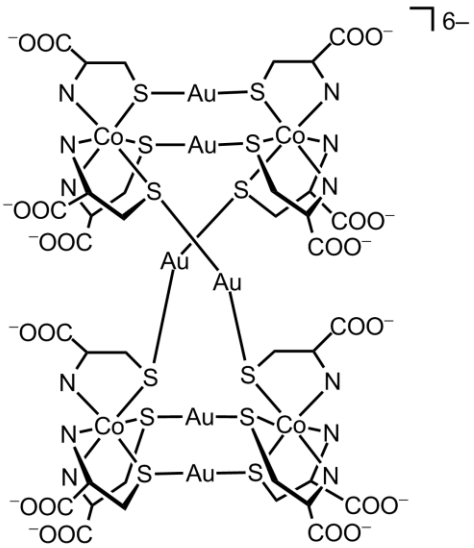

$(\Lambda_{LLL})_4$-$[Au_6Co_4(L\text{-}cys)_{12}]^{6-}$

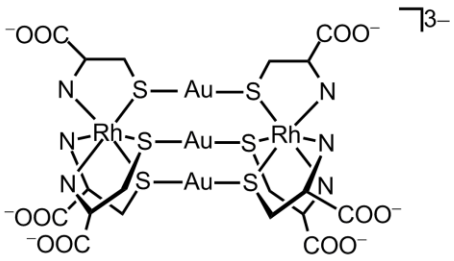

$(\Delta_{LLL})_2$-$[Au_3Rh_2(L\text{-}cys)_6]^{3-}$

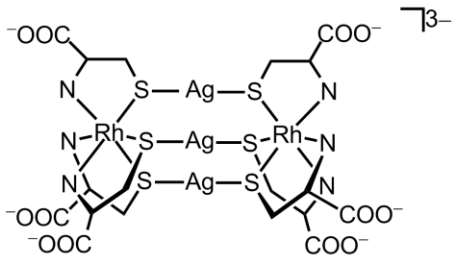

$(\Delta_{LLL})_2$-$[Ag_3Rh_2(L\text{-}cys)_6]^{3-}$

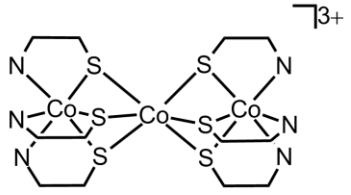

$(\Delta)_2/(\Lambda)_2$-$[Co_3(aet)_6]^{3+}$

Figure 1-4. Structures of complex-anions and complex-cation used in this thesis.

Chapter II. Chiral and Structural Conversions of S-Bridged $Au^{I}Co^{III}$ Complexes with L-Cysteinate

II-1 Introduction

Chiral inversion is one of the most important phenomena in various research fields including chemistry, biochemistry, pharmacy, and material science, because chirality controls not only molecular structures and their assembled structures but also their functionalities.[1] In coordination chemistry, chiral inversion processes have been investigated for a variety of chiral compounds that show chiral inversion between right-handed and left-handed helices, Δ and Λ configurations around metal centers in tris-chelating metal complexes, and *R* and *S* configurations of coordinated atoms in response to external stimuli such as solvents, counter ions, and additional ligands.[2] Metal complexes with labile metal centers are commonly utilized for these studies, and most of these compounds have a mononuclear structure and showed chiral inversion around the metal center. In some of these chiral convertible compounds, the inversion of the absolute configurations (Δ/Λ) leads to the overall chiral structural change like the inversion of helical chiralities,[3] and these compounds showing cooperative chiral inversions can be called as "strongly correlated chiral system". Because of the great potential as switching devices, the creation of such compounds is highly desired especially for the metal complexes with inert metal centers, which result in the formation of the relatively stable structures needed for the devices for use. However, the preparation of chiral convertible compounds having multi chiral centers is still challenging, because the inertness tends to prevent the conversions.

As mentioned in Chapter I, the use of chiral sulfur-containing amino acids such as cysteine and penicillamine as a ligand is an easy way to create chiral metal complexes.[4,5] Among them, the multinuclear compounds containing the L-cysteinato Co^{III} complex-anion $[Co(L\text{-}cys)_3]^{3-}$ as a metalloligand are good candidates for the construction of the strongly correlated chiral system, because the formed multinuclear complexes have multiple chiral centers around the Co^{III} centers and coordinated S atoms, and also, the Co^{III} mononuclear metalloligand is known to show the chiral inversion between Δ_{LLL} and Λ_{LLL} isomers in the solution state.[5] Actually, treatment of Δ_{LLL}-$[Co(L\text{-}cys)_3]^{3-}$ with Co^{II} gave the $(\Delta_{LLL})_2(S)_6$ isomer of the L-cysteinato Co^{III}_3 complex, $[Co_3(L\text{-}cys)_6]^{3-}$, retaining the chirality around the Co^{III} centers, while the

treatment with Co^{III} gave the $(\Lambda_{LLL})_2(R)_6$ isomer accompanied by the chiral inversion.[5a,b] Unfortunately, both the $(\Delta_{LLL})_2$ and $(\Lambda_{LLL})_2$ isomers of $[Co_3(L\text{-cys})_6]^{3-}$ did not show the chiral inversion in response to the external stimuli. In this chapter, the construction of an S-bridged $Au^{I}_3Co^{III}_2$ complex using Δ_{LLL}-$[Co(L\text{-cys})_3]^{3-}$ as a metalloligand and its cooperative multiple chiral inversions around not only Co^{III} centers but also coordinated S atoms are described. Reaction of Δ_{LLL}-$[Co(L\text{-cys})_3]^{3-}$ with Au^{I} gave $(\Delta_{LLL})_2$-$K_3[Au_3Co_2(L\text{-cys})_6]$ ($(\Delta_{LLL})_2$-K_3[**1**]), and this complex was crystallized with $[Co_3(aet)_6]^{3+}$ in a neutral aqueous solution gave an expected cocrystallized compound ($(\Delta_{LLL})_2$-$[Co_3(aet)_6]$[**1**]), as shown in Scheme 2-1. Remarkably, the similar reaction in a basic solution afforded a cocrystallized compound ($(\Lambda_{LLL})_4$-$[Co_3(aet)_6]_2$[**2**]) containing an $Au^{I}_6Co^{III}_4$ decanuclear structure in $(\Lambda_{LLL})_4$-$[Au_6Co_4(L\text{-cys})_{12}]^{6-}$ ($(\Lambda_{LLL})_4$-[**2**]$^{6-}$) and $[Co_3(aet)_6]^{3+}$ in a 1:2 ratio (Scheme 2-1). The X-ray crystallography of $(\Lambda_{LLL})_4$-$[Co_3(aet)_6]_2$[**2**] indicates that a chiral inversion from $(\Delta_{LLL})_2(S)_6$ to $(\Lambda_{LLL})_4(R)_{12}$ and a structural conversion occurred despite the inert character of Co^{III} and Au^{I} centers. To our knowledge, the creation of the coordination compounds with relatively inert metal centers showing such an unexpected multiple chiral inversion and a structural conversion is unprecedented. The reverse conversion as well as the proposed mechanism of the conversion by means of spectral measurements and the isolation of an intermediate species are also reported.

II-2 Experimental Section

II-2-1 Materials

The starting complexes, $(\Delta)_2/(\Lambda)_2$-$[Co_3(aet)_6](NO_3)_3$ and $(\Delta)_2/(\Lambda)_2$-$[CoRh_2(aet)_6](NO_3)_3$, were prepared by methods in the literature.[4d,6] All chemicals were used without further purifications.

II-2-2 Preparation of Au^ICo^{III} Complexes

(a) $(\Delta_{LLL})_2$-$K_3[Au^I_3Co^{III}_2(L\text{-cys})_6]$ ($(\Delta_{LLL})_2$-K_3[1])

To a solution of Δ_{LLL}-$K_3[Co(L\text{-cys})_3]\cdot 9H_2O\cdot 0.5KCl$ (0.50 g, 0.68 mmol) in 25 mL of water was added a mixture of $HAuCl_4$ (0.43 g, 1.02 mmol) and 2,2'-thiodiethanol (350 μL) in 25 mL of water. The resulting brown suspension was stirred at room temperature for 3 h, and the black precipitate was collected by filtration. The obtained black powder was suspended in 5 mL of H_2O, to which was added 1 M KOH aqueous solution until the suspension became a clear black solution (pH ~7). To the resulting solution was added a large amount of EtOH, which was stood at room temperature for 30 min. The resulting black powder was collected by filtration, and was washed with water and EtOH twice. Yield: 0.48 g (81%). Anal. Calcd for $K_3[Au_3Co_2(L\text{-cys})_6]\cdot 11H_2O$ = $C_{18}H_{52}Au_3Co_2S_6N_6O_{23}K_3$: C, 12.42; H, 3.01; N, 4.83%. Found: C, 12.43; H, 2.92; N, 4.57%. IR (KBr): 1606 cm^{-1} (COO^-). Electronic absorption spectrum in H_2O [λ / nm ($\log\varepsilon$ / mol^{-1} dm^3 cm^{-1})]: 553 (3.03), 254 (4.59), 230 (4.62). CD spectrum in H_2O [λ / nm ($\Delta\varepsilon$ / mol^{-1} dm^3 cm^{-1})]: 573 (–19.56), 455 (+11.17), 389 (–17.31), 339 (+29.80), 311 (–46.67), 253 (+89.28). Single crystals suitable for X-ray analysis were obtained by the crystallization of K_3[**1**] from an aqueous solution by adding K_2PtCl_4.

(b) $(\Lambda_{LLL})_2$-$K_3[Au^I_3Co^{III}_2(L\text{-cys})_6]$ ($(\Lambda_{LLL})_2$-K_3[1])

To a solution of $(\Delta_{LLL})_2$-K_3[**1**]$\cdot 11H_2O$ (0.20 g, 0.11 mmol) in 10 mL of water was added 0.1 M KOH aqueous solution (20 μL) to adjust the solution pH to ca. 9. The dark red solution was stood at room temperature for 2 weeks, and then, a large amount of EtOH was added to it. The resulting black powder was collected by filtration, which was recrystallized from water and EtOH twice. The resulting black powder was collected by filtration, and was washed with EtOH. Yield: 0.13 g (65%). Anal. Calcd for $K_3[Au_3Co_2(L\text{-cys})_6]\cdot 9H_2O$ = $C_{18}H_{48}Au_3Co_2K_3N_6O_{21}S_6$: C, 12.69; H, 2.84; N, 4.93%. Found: C, 12.72; H, 2.72; N, 4.97%. IR (KBr): 1600 cm^{-1} (COO^-). Electronic absorption

spectrum in H_2O [λ / nm (logε / mol^{-1} dm^3 cm^{-1})]: 561 (3.06), 255 (4.58), 230 (4.66). CD spectrum in H_2O [λ / nm ($\Delta\varepsilon$ / mol^{-1} dm^3 cm^{-1})]: 580 (+20.71), 458 (–10.30), 389 (+16.48), 359 (+22.01), 332 (+9.39), 284 (+42.22), 252 (–70.86).

II-2-3 Preparation of Cocrystallized Compounds

(a) (Δ_{LLL})$_2$-[Co$^{III}_3$(aet)$_6$][Au$^{I}_3$Co$^{III}_2$(L-cys)$_6$] ((Δ_{LLL})$_2$-[Co$^{III}_3$(aet)$_6$][1])

To a solution containing 30 mg (0.036 mmol) of *rac*-$[Co_3(aet)_6](NO_3)_3 \cdot H_2O$ in 10 mL of water was added a solution containing 30 mg (0.017 mmol) of (Δ_{LLL})$_2$-$K_3[Au_3Co_2(L\text{-}cys)_6] \cdot 11H_2O$ ((Δ_{LLL})$_2$-K_3[**1**]$\cdot 11H_2O$) in 10 mL of water. The black solution was allowed to stand at room temperature for 1 week. The resulting black crystals of (Δ_{LLL})$_2$-[Co$_3$(aet)$_6$][**1**] were collected by filtration. Yield: 20 mg (48%). Calcd for $[Co_3(aet)_6][Au_3Co_2(L\text{-}cys)_6] \cdot 18H_2O = C_{30}H_{102}N_{12}O_{30}S_{12}Co_5Au_3$: C, 15.12; H, 4.31; N, 7.06%. Found: C, 14.95; H, 4.16; N, 6.95%. Electronic absorption spectrum in a saturated $NaNO_3$ aqueous solution [λ / nm (log ε / mol^{-1} dm^3 cm^{-1})]: 560 (3.52), 437 (3.85), 339 (4.45), 280 (4.73), 257 (4.79). CD spectrum in a saturated $NaNO_3$ aqueous solution [λ / nm ($\Delta\varepsilon$ / mol^{-1} dm^3 cm^{-1})]: 573 (–20.27), 520 (+1.80), 450 (+12.25), 385 (–21.17), 355 (–21.07), 311 (–48.94), 254 (+104.81), 234 (+8.59), 221 (–4.91), 207 (+48.81). One of single crystals was used for X-ray measurement.

(b) (Λ_{LLL})$_4$-[Co$^{III}_3$(aet)$_6$]$_2$[Au$^{I}_6$Co$^{III}_4$(L-cys)$_{12}$] ((Λ_{LLL})$_4$-[Co$^{III}_3$(aet)$_6$]$_2$[2])

Method A. To a solution containing 50 mg (0.029 mmol) of (Δ_{LLL})$_2$-K_3[**1**]$\cdot 11H_2O$ in 10 mL of water was added a solution containing 48 mg (0.058 mmol) of *rac*-$[Co_3(aet)_6](NO_3)_3 \cdot H_2O$ in 10 mL of water. To the black reaction solution was added 0.1 M KOH aqueous solution (150 μL) until the solution pH became ca. 9. The resulting black solution was allowed to stand at room temperature for 1 day to give a small amount of mircocrystals of (Δ_{LLL})$_2$-[Co$_3$(aet)$_6$][**1**]. The solution containing black microcrystals was stood at room temperature without filtration. After 1 week, the microcrystals disappeared and larger block black crystals of (Λ_{LLL})$_4$-[Co$_3$(aet)$_6$]$_2$[**2**] appeared, which were collected by filtration. Yield: 27 mg (61%). Calcd for $[Co_3(aet)_6]_2[Au_6Co_4(L\text{-}cys)_{12}] \cdot 48H_2O = C_{60}H_{228}N_{24}O_{72}S_{24}Co_{10}Au_6$: C, 14.47; H, 4.62; N, 6.75%. Found: C, 14.21; H, 4.40; N, 6.61%. IR (KBr): 1612 cm^{-1} (COO$^-$). Electronic absorption spectrum in a saturated $NaNO_3$ aqueous solution [λ / nm (log ε / mol^{-1} dm^3 cm^{-1})]: 574 (3.74), 439 (4.15), 343 (4.70). CD spectrum in a saturated $NaNO_3$ aqueous solution [λ / nm ($\Delta\varepsilon$ / mol^{-1} dm^3 cm^{-1})]: 561 (39.90), 467 (–25.00), 392 (29.15), 301

(+16.75), 288 (17.46). One of single crystals was used for X-ray measurement.

Method B. To a solution containing 50 mg (0.026 mmol) of $(\Lambda_{LLL})_2$-K_3[**1**]·12H_2O·2.5KOH in 10 mL was added a solution containing 45 mg (0.053 mmol) of *rac*-$[Co_3(aet)_6](NO_3)_3$·H_2O in 10 mL of water. The black solution was allowed to stand at room temperature for 1 week. The resulting black crystals of $(\Lambda_{LLL})_4$-$[Co_3(aet)_6]_2$[**2**] were collected by filtration. Yield: 30 mg (57%).

(c) $(\Lambda_{LLL})_4$-$[Co^{III}Rh^{III}_2(aet)_6]_2[Au^{I}_6Co^{III}_4(L\text{-}cys)_{12}]$ ($(\Lambda_{LLL})_4$-$[Co^{III}Rh^{III}_2(aet)_6]_2$[2])

To a solution containing 30 mg (0.016 mmol) of $(\Lambda_{LLL})_2$-K_3[**1**]·9H_2O in 5mL was added a solution containing 31 mg (0.033 mmol) of *rac*-$[CoRh_2(aet)_6](NO_3)_3$·1.5H_2O in 5 mL of water. The black solution was allowed to stand at room temperature for 1 week. The resulting black crystals of $(\Lambda_{LLL})_4$-$[CoRh_2(aet)_6]$[**2**] were collected by filtration. Yield: 21 mg (53%). Calcd for $[CoRh_2(aet)_6][Au_6Co_4(L\text{-}cys)_{12}]$·46$H_2O$ = $C_{60}H_{224}N_{24}O_{70}S_{24}Co_6Au_6Rh_4$: C, 14.07; H, 4.41; N, 6.56%. Found: C, 14.25; H, 4.15; N, 6.55%. IR (KBr): 1592 cm^{-1} (COO^-). Electronic absorption spectrum in a $NaNO_3$ aqueous solution [λ / nm (log ε / mol^{-1} dm^3 cm^{-1})]: 585 (3.02), 423 (3.77). CD spectrum in an $NaNO_3$ aqueous solution [λ / nm ($\Delta\varepsilon$ / mol^{-1} dm^3 cm^{-1})]: 619 (–7.80), 556 (+12.37), 469 (–10.66), 411 (51.54), 365 (+21.00), 334 (45.46).

(d) $(\Lambda_{LLL})_2$-$[Co^{III}(en)_3][Au^{I}_3Co^{III}_2(L\text{-}cys)_6]$ ($(\Lambda_{LLL})_2$-$[Co^{III}(en)_3]$[1])

To a solution containing 20 mg (0.011 mmol) of $(\Lambda_{LLL})_2$-K_3[**1**]·9H_2O in 20mL was added a solution containing 9.2 mg (0.022 mmol) of *rac*-$[Co(en)_3](NO_3)_3$ in 20 mL of water. The brown suspension was allowed to stand at room temperature for 1 week. The resulting brown crystals of $(\Lambda_{LLL})_2$-$[Co(en)_3]$[**1**] were collected by filtration. Yield: 9.6 mg (43%). Calcd for $[Co(en)_3][Au_3Co_2(L\text{-}cys)_6]$·16$H_2O$ = $C_{24}H_{86}N_{12}O_{28}S_6Co_3Au_3$: C, 14.77; H, 4.44; N, 8.61%. Found: C, 14.95; H, 4.25; N, 8.38%. IR (KBr): 1601 cm^{-1} (COO^-). Electronic absorption spectrum in H_2O [λ / nm (log ε / mol^{-1} dm^3 cm^{-1})]: 573 (2.84), 443 (3.02). CD spectrum in H_2O [λ / nm ($\Delta\varepsilon$ / mol^{-1} dm^3 cm^{-1})]: 579 (2.79), 457 (–1.85), 360 (3.09).

II-2-4 Physical Measurements

The electronic absorption spectra were recorded with a JASCO V-660 or a JASCO V-630 spectrophotometers using a 1 cm quartz cell at room temperature. The diffuse reflectance spectra were recorded on a JASCO V-570 spectrophotometer at room

temperature by using $MgSO_4$. The CD spectra were recorded with a J-820 spectrometer at room temperature using a 1 cm quartz cell for the solution state and using KBr disks for the solid state. The IR spectra were recorded on a JASCO FT/IR-4100 infrared spectrometer using KBr disks at room temperature. The elemental analyses (C, H, N) were performed at Osaka University. X-ray fluorescence analyses were made on a HORIBA MESA-500 or SHIMADZU EDX-720 spectrometer. The ^{1}H NMR spectra were recorded with a JEOL ECA500 (500 MHz) spectrometer at room temperature in D_2O, using sodium 4,4'-dimethyl-4-silapentane-1-sulfonate (DSS) as the internal standard.

II-2-5 X-ray Structural Determination

Single-crystal X-ray diffraction measurements for complexes $(\Delta_{LLL})_2$-K_3[**1**]·7.5H_2O, $(\Delta_{LLL})_2$-[Co_3(aet)$_6$][**1**]·18H_2O, and $(\Lambda_{LLL})_4$-[Co_3(aet)$_6$]$_2$[**2**]·20H_2O were performed on a Rigaku R-AXIS VII imaging plate and Vari-Max with graphite monochromated Mo-Kα radiation (λ = 0.71075 Å) at 200 K. The intensity data were collected by the ω-scan technique and empirically corrected for absorption. The structures of complexes were solved by a direct method using SHELXS97.[7] The structure refinements were carried out using full matrix least-squares (SHELXL-97).[7] All calculations were performed using the Yadokari-XG software package.[7] For $(\Delta_{LLL})_2$-K_3[**1**]·7.5H_2O, Au, Co, and S atoms were refined anisotropically, while the others were refined isotropically. H atoms were included in calculated positions except those of water molecules. A half of K^+ atoms were not refined because of the severe disorder. DFIX restraint and EADP constraint were used to model one disordered carboxylate group. For $(\Delta_{LLL})_2$-[Co_3(aet)$_6$][**1**]·18H_2O, all non-hydrogen atoms except the disordered carboxylate groups, C and N atoms in aet ligands, and water molecule were refined anisotropically, while the others are refined isotropically. Hydrogen atoms were included in calculated positions except those of aet ligands and water molecules. DFIX and FLAT restraints were used to model a part of disordered carboxylate groups. For $(\Lambda_{LLL})_4$-[Co_3(aet)$_6$]$_2$[**2**]·20H_2O, Au, Co, and S atoms in $(\Lambda_{LLL})_4$-[**2**]$^{6-}$ and Co atoms in [Co_3(aet)$_6$]$^{3+}$ were refined anisotropically, while the others were refined isotropically. Hydrogen atoms were included in calculated positions except those of aet ligands and water molecules. DFIX restraint and EADP constraint were used to model a part of disordered carboxylate groups, and DFIX restraint was used to model aet ligands.

II-3 Results and Discussion

II-3-1 Synthesis and Characterization of $Au^{I}Co^{III}$ Complexes

(a) $(\Delta_{LLL})_2$-K_3[$Au^{I}_3Co^{III}_2$(L-cys)$_6$] ($(\Delta_{LLL})_2$-K_3[**1**])

Reaction of Δ_{LLL}-K_3[Co(L-cys)$_3$] with Au^{I} in a 1:1.5 ratio gave a dark brown suspension. After filtration, the obtained reddish brown crude product was dissolved in water by adding a KOH aqueous solution, and then a large amount of EtOH was added to it to give a reddish brown powder of $(\Delta_{LLL})_2$-K_3[**1**].

As shown in Figure 2-1, the IR spectrum of $(\Delta_{LLL})_2$-K_3[**1**] shows the band at 1606 cm^{-1} assigned to COO^{-}, suggestive of the presence of L-cys. The X-ray fluorescence spectroscopy implies that $(\Delta_{LLL})_2$-K_3[**1**] contains Au and Co atoms, and elemental analytical data are agreement with the formula for $K_3[Au_3Co_2(L\text{-cys})_6]\cdot 11H_2O$. The ^1H NMR spectrum in D_2O shows two methylene signals (δ 2.91 and 3.31 ppm) and one methine signal (δ 3.07 ppm) attributed to the L-cys ligand (Figure 2-2). The presence of single set of signals suggests that $(\Delta_{LLL})_2$-K_3[**1**] has a symmetrical structure with all L-cys ligands being equivalent. The absorption spectrum of $(\Delta_{LLL})_2$-K_3[**1**] in water shows the d-d absorption band at 553 nm and the sulfur to cobalt charge transfer band at around 250 nm with a shoulder at lower energy side (Figure 2-3, Table 2-5). The CD spectrum shows negative bands at 573, 389, and 311 nm and positive bonds at 455, 339 and 253 nm (Figure 2-3, Table 2-5). The absorption and CD spectral features are similar to those of $(\Delta_{LLL})_2$-$K_3[Ag_3Co_2(L\text{-cys})_6]$,[4d] suggesting that $(\Delta_{LLL})_2$-K_3[**1**] has a similar S-bridged structure having Δ_{LLL} configurational $[Co(L\text{-cys})_3]^{3-}$ units. The reflection and CD spectra in the solid state are essentially the same as the absorption and CD spectra in the solution state, showing bands at 560 and 435 nm for the reflection spectrum, and negative bands at 510 and 405 nm and a positive band at 446 nm for the CD spectrum, respectively (Figure 2-4). Single crystals suitable for X-ray analysis were obtained by the recrystallization of $(\Delta_{LLL})_2$-K_3[**1**] from an aqueous solution by adding K_2PtCl_4. The X-ray analysis demonstrated that $(\Delta_{LLL})_2$-K_3[**1**] has an S-bridged $Au^{I}_3Co^{III}_2$ pentanuclear structure in $K_3[Au_3Co_2(L\text{-cys})_6]$, in which two Δ_{LLL}-$[Co(L\text{-cys})_3]^{3-}$ moieties are bridged by three linear Au^{I} atoms (*vide infra*).

(b) $(\Lambda_{LLL})_2$-K_3[$Au^{I}_3Co^{III}_2$(L-cys)$_6$] ($(\Lambda_{LLL})_2$-K_3[**1**])

To a solution of $(\Delta_{LLL})_2$-$K_3[Au_3Co_2(L\text{-cys})_6]$ ($(\Delta_{LLL})_2$-K_3[**1**]) in water was added an aqueous solution of KOH to adjust the solution pH to about 9, and the resulting reddish

brown solution was stood at room temperature for 2 weeks. An addition of a large amount of EtOH to the resulting solution gave a brown powder of $(\Lambda_{LLL})_2$-K_3[**1**].

X-ray fluorescence spectroscopy indicates that $(\Lambda_{LLL})_2$-K_3[**1**] contains Au and Co atoms, and elemental analytical data are agreement with the formula for $K_3[Au_3Co_2(L\text{-cys})_6]\cdot 9H_2O$. The IR spectrum of $(\Lambda_{LLL})_2$-K_3[**1**] shows the presence of L-cys ligands based on the band at 1600 cm^{-1} assigned to the deprotonated COO^- group (Figure 2-1). The ^1H NMR spectrum in D_2O shows one set of signals attributed to the L-cys ligand with the chemical shifts of 3.06 and 3.19 ppm for two methylene protons and 3.89 ppm for one methine protons (Figure 2-5), which are different from those of $(\Delta_{LLL})_2$-K_3[**1**]. The ESI mass spectrum in methanol/water (1:1) showed a trianionic signal at *m*/*z* 474.20, which corresponds to $[Au_3Co_2(L\text{-cys})_6]^{3-}$ (Figure 2-6). The absorption and CD spectra of $(\Lambda_{LLL})_2$-K_3[**1**] in water are shown in Figure 2-3 and their data are summarized in Table 2-5. The absorption spectrum of $(\Lambda_{LLL})_2$-K_3[**1**] in water shows the d-d absorption band at 561 nm and the sulfur to cobalt charge transfer band at ca. 250 nm with a shoulder at lower energy side. This spectral feature is similar to that of $(\Delta_{LLL})_2$-K_3[**1**]. On the other hand, the CD spectrum shows positive bonds at 580, 389, 359, and 284 nm and negative bonds at 458 and 252 nm, of which spectral pattern is almost enantiometric to that of $(\Delta_{LLL})_2$-K_3[**1**]. These absorption and CD spectral features indicate that $(\Lambda_{LLL})_2$-K_3[**1**] has a similar structure with $(\Delta_{LLL})_2$-K_3[**1**], but the chirality around the Co^{III} center is opposite. The reflection and CD spectra in the solid state are essentially the same as the absorption and CD spectra in the solution state, exhibiting a band at 560 nm for the reflection spectrum, and positive bands at 522 and 410 nm and a negative bands at 450 nm for the CD spectrum, respectively (Figure 2-4). Unfortunately, many attempts to obtain crystals suitable for X-ray analysis were unsuccessful. However, from the above-mentioned descriptions, we concluded that $(\Lambda_{LLL})_2$-K_3[**1**] has an S-bridged $Au^I_3Co^{III}_2$ pentanuclear structure in $K_3[Au_3Co_2(L\text{-cys})_6]$, in which two Λ_{LLL} configurational $[Co(L\text{-cys})_3]^{3-}$ units are bridged by three Au^I atoms (Scheme 2-1).

(c) $(\Delta_{LLL})_2$-$[Co^{III}_3(aet)_6][Au^I_3Co^{III}_2(L\text{-cys})_6]$ ($(\Delta_{LLL})_2$-$[Co^{III}_3(aet)_6]$[1])

Treatment of $(\Delta_{LLL})_2$-$K_3[Au_3Co_2(L\text{-cys})_6]$ ($(\Delta_{LLL})_2$-K_3[**1**]) with $(\Delta)_2/(\Lambda)_2$-$[Co_3(aet)_6](NO_3)_3$ in a 1:2 ratio in water, followed by allowing to stand at room temperature for 1 week, gave black block crystals of $(\Delta_{LLL})_2$-$[Co_3(aet)_6]$[**1**].

The IR spectrum shows a strong sharp C=O stretching band at 1604 cm^{-1} assigned to COO^-, suggestive of the presence of L-cys (Figure 2-1). X-ray fluorescence

spectroscopy indicates that this compound contains Au and Co atoms, and the elemental analytical data are in agreement with the formula for a 1:1 adduct of $[Co_3(aet)_6]^{3+}$ and $[Au_3Co_2(L\text{-}cys)_6]^{3-}$. The reflection and CD spectra of the crystals are shown in Figure 2-7. The reflection spectrum shows two bands at 560 and 437 nm, and the CD spectrum shows negative bands at 577 and 398 nm and a positive band at 450 nm in the region of 700 to 350 nm. The crystals of $(\Delta_{LLL})_2$-$[Co_3(aet)_6]$[**1**] are almost insoluble in water but are soluble in a saturated $NaNO_3$ aqueous solution. The absorption spectrum of the crystals in the solution state shows four absorption bands at 560, 437, 339, and 280 nm (Figure 2-8), the first band of which is similar to that of $(\Delta_{LLL})_2$-$[\mathbf{1}]^{3-}$ and the latter two bands are very similar to those of $[Co_3(aet)_6]^{3+}$. On the other hand, the CD spectrum is reminiscent of that of $(\Delta_{LLL})_2$-$[\mathbf{1}]^{3-}$, showing negative bands at 573, 385, and 355 nm and positive bands at 520 and 450 nm (Figure 2-8). The ^1H NMR spectrum of $(\Delta_{LLL})_2$-$[Co_3(aet)_6]$[**1**] in a $NaNO_3$ solution of D_2O shows the presence of $(\Delta_{LLL})_2$-$[\mathbf{1}]^{3-}$ and $[Co_3(aet)_6]^{3+}$ in a 1:1 ratio. Single-crystal X-ray analysis demonstrated that $(\Delta_{LLL})_2$-$[Co_3(aet)_6]$[**1**] is composed of $(\Delta_{LLL})_2$-$[\mathbf{1}]^{3-}$ and $[Co_3(aet)_6]^{3+}$ in a 1:1 ratio, and the structures of both complex-cation and complex-anion units are retained during the reaction (*vide infra*). Focused on the chirality of the $[Co_3(aet)_6]^{3+}$ unit, both $(\Delta)_2$ and $(\Lambda)_2$ isomers of $[Co_3(aet)_6]^{3+}$ are contained in $(\Delta_{LLL})_2$-$[Co_3(aet)_6]$[**1**] with the severe disorder. This is also indicated by the CD spectrum that is not affected by the presence of $[Co_3(aet)_6]^{3+}$. The chiralselectivity of $(\Delta_{LLL})_2$-$[\mathbf{1}]^{3-}$ toward $[Co_3(aet)_6]^{3+}$ will be discussed in detail in Chapter III.

(d) $(\Lambda_{LLL})_4$-$[Co^{III}_3(aet)_6]_2[Au^{I}_6Co^{III}_4(L\text{-}cys)_{12}]$ ($(\Lambda_{LLL})_4$-$[Co^{III}_3(aet)_6]_2$[2])

Treatment of $(\Delta_{LLL})_2$-$K_3[Au_3Co_2(L\text{-}cys)_6]$ ($(\Delta_{LLL})_2$-K_3[**1**]) with $(\Delta)_2/(\Lambda)_2$-$[Co_3(aet)_6](NO_3)_3$ in a 1:2 ratio in a basic aqueous solution, of which solution pH was adjusted to ca. 9 by adding a KOH aqueous solution, gave a black solution. The mixture was stood at room temperature overnight to give black microcrystals of $(\Delta_{LLL})_2$-$[Co_3(aet)_6]$[**1**], which was characterized by spectral measurements as well as elemental analysis. When the reaction mixture containing black microcrystals was stood without filtration, the microcrystals disappeared and black block crystals appeared with time, and only newly formed block crystals ($(\Lambda_{LLL})_4$-$[Co_3(aet)_6]_2$[**2**]) existed after 2 weeks. The same crystals were also obtained by the reaction of $(\Lambda_{LLL})_2$-K_3[**1**] with $(\Delta)_2/(\Lambda)_2$-$[Co_3(aet)_6](NO_3)_3$ in a 1:2 ratio in water.

The IR spectrum of $(\Lambda_{LLL})_4$-$[Co_3(aet)_6]_2$[**2**] shows the presence of the carboxylate

group of L-cys based on the band at 1612 cm^{-1} (Figure 2-1). X-ray fluorescence spectroscopy indicates that this compound contains Au and Co atoms, and elemental analytical data are in agreement with the formula for a 1:1 adduct of $[Co_3(aet)_6]^{3+}$ and $[Au_3Co_2(L\text{-}cys)_6]^{3-}$. The reflection and CD spectra in the solid state are shown in Figure 2-7. The reflection spectrum is similar to that of $(\Delta_{LLL})_2$-$[Co_3(aet)_6]$[**1**], showing bands at 580, 450, and 360 nm. However, the CD spectrum shows almost opposite pattern to that of $(\Delta_{LLL})_2$-$[Co_3(aet)_6]$[**1**], showing positive bands at 560, 395, and 355 nm and a negative band at 460 nm. This spectral pattern is similar to that of $(\Lambda_{LLL})_2$-$[\mathbf{1}]^{3-}$, indicative of the presence of the Λ_{LLL} configurational $[Co(L\text{-}cys)_3]^{3-}$ unit in $(\Lambda_{LLL})_4$-$[Co_3(aet)_6]_2$[**2**]. The black crystals of $(\Lambda_{LLL})_4$-$[Co_3(aet)_6]_2$[**2**] are also insoluble in water but are soluble in a saturated $NaNO_3$ aqueous solution. The absorption spectrum in the solution state shows three bands at 574, 439, and 343 nm (Figure 2-8), which is very similar to that of $(\Delta_{LLL})_2$-$[Co_3(aet)_6]$[**1**]. Its CD spectrum shows positive bands at 561, 392, 301, and 288 nm and a negative band at 467 nm in this region (Figure 2-8). These absorption and CD spectral features in the solution state are essentially the same as the reflection and CD spectral features in the solid state. The structure of $(\Lambda_{LLL})_4$-$[Co_3(aet)_6]_2$[**2**] was determined by single-crystal X-ray analysis, which showed the presence of decanuclear complex-anion of $(\Lambda_{LLL})_4$-$[Au_6Co_4(L\text{-}cys)_{12}]^{6-}$ ($(\Lambda_{LLL})_4$-$[\mathbf{2}]^{6-}$) and complex-cation ($[Co_3(aet)_6]^{3+}$) in a 1:2 ratio (*vide infra*). This indicates that $(\Delta_{LLL})_2$-$[\mathbf{1}]^{3-}$ was converted to $(\Lambda_{LLL})_4$-$[\mathbf{2}]^{6-}$ by the reaction with $[Co_3(aet)_6]^{3+}$ under the basic condition. Therefore, the chiral inversion from the Δ_{LLL} to Λ_{LLL} isomers and the structural conversion from the $Au^{I}_3Co^{III}_2$ pentanuclear to $Au^{I}_6Co^{III}_4$ decanuclear structures occurred during the reaction. Focused on the chirality of the $[Co_3(aet)_6]^{3+}$ unit, both $(\Delta)_2$ and $(\Lambda)_2$ isomers of $[Co_3(aet)_6]^{3+}$ are contained in $(\Lambda_{LLL})_4$-$[Co_3(aet)_6]_2$[**2**] with the severe disorder, which is also indicated by the CD spectrum that is not affected by the presence of $[Co_3(aet)_6]^{3+}$. The chiralselectivity of $(\Lambda_{LLL})_4$-$[\mathbf{2}]^{6-}$ toward $[Co_3(aet)_6]^{3+}$ will be discussed in detail in Chapter III. The ^1H NMR spectrum of $(\Lambda_{LLL})_4$-$[Co_3(aet)_6]_2$[**2**] dissolving in a $NaNO_3$ solution of D_2O shows three sets of L-cys signals in addition to the signals of $[Co_3(aet)_6]^{3+}$, indicative of the presence of $(\Lambda_{LLL})_4$-$[\mathbf{2}]^{6-}$ with a D_2 symmetry in solution (Figure 2-11).

(e) $(\Lambda_{LLL})_4$-$[Co^{III}Rh^{III}_2(aet)_6]_2[Au^{I}_6Co^{III}_4(L\text{-}cys)_{12}]$ ($(\Lambda_{LLL})_4$-$[Co^{III}Rh^{III}_2(aet)_6]_2$[2])

Treatment of $(\Lambda_{LLL})_2$-$K_3[Au_3Co_2(L\text{-cys})_6]$ ($(\Lambda_{LLL})_2$-K_3[**1**]) with $(\Delta)_2/(\Lambda)_2$-$[CoRh_2(aet)_6](NO_3)_3$ in a 1:2 ratio in water gave black crystals of $(\Lambda_{LLL})_4$-$[CoRh_2(aet)_6]_2$[**2**].

The IR spectrum of $(\Lambda_{LLL})_4$-$[CoRh_2(aet)_6]_2$[**2**] shows the presence of the carboxylate group of L-cys based on the band at 1592 cm^{-1} (Figure 2-1). X-ray fluorescence spectroscopy indicates that this compound contains Au, Rh, and Co atoms, and elemental analytical data are in agreement with the formula for a 1:1 adduct of $[CoRh_2(aet)_6]^{3+}$ and $[Au_3Co_2(L\text{-cys})_6]^{3-}$. The reflection and CD spectra in the solid state are shown in Figure 2-9. The reflection spectrum is similar to that of $(\Delta_{LLL})_2$-$[Co_3(aet)_6]$[**1**], showing bands at 579, 539, and 336 nm. However, the CD spectrum is similar to that of $(\Lambda_{LLL})_4$-$[Co_3(aet)_6]_2$[**2**], showing positive bands 553, 416, and 370 nm and a negative band at 632 nm. The black crystals of $(\Lambda_{LLL})_4$-$[CoRh_2(aet)_6]_2$[**2**] are also insoluble in water but are soluble in a saturated $NaNO_3$ aqueous solution. The absorption spectrum in the solution state shows two bands at 585 and 423 nm in the region of 700 to 300 nm (Figure 2-10), which is very similar to that of $(\Delta_{LLL})_2$-$[Co_3(aet)_6]$[**1**]. Its CD spectrum shows positive bands at 556, 411, 365, and 334 nm and negative bands at 619 and 469 nm in this region (Figure 2-10). These absorption and CD spectral features in the solution state are essentially the same as the reflection and CD spectral features in the solid state. The structure of $(\Lambda_{LLL})_4$-$[CoRh_2(aet)_6]_2$[**2**] was preliminarily determined by single-crystal X-ray analysis, which showed the presence of decanuclear complex-anion of $(\Lambda_{LLL})_4$-$[Au_6Co_4(L\text{-cys})_{12}]^{6-}$ ($(\Lambda_{LLL})_4$-[**2**]$^{6-}$) and complex-cation ($[CoRh_2(aet)_6]^{3+}$) in a 1:2 ratio (see Appendix). This indicates that $(\Lambda_{LLL})_2$-[**1**]$^{3-}$ was converted to $(\Lambda_{LLL})_4$-[**2**]$^{6-}$ upon the crystallization with $[CoRh_2(aet)_6]^{3+}$. The ^1H NMR spectrum of $(\Lambda_{LLL})_4$-$[CoRh_2(aet)_6]_2$[**2**] dissolving in a $NaNO_3$ solution of D_2O shows three sets of L-cys signals, of which chemical shifts are same as that of $(\Lambda_{LLL})_4$-[**2**]$^{6-}$ in $(\Lambda_{LLL})_4$-$[Co_3(aet)_6]_2$[**2**], indicative of the presence of $(\Lambda_{LLL})_4$-[**2**]$^{6-}$ in solution (Figure 2-11). The signals of $[CoRh_2(aet)_6]^{3+}$ are also observed, and the integration ratio of $(\Lambda_{LLL})_4$-[**2**]$^{6-}$ and $[CoRh_2(aet)_6]^{3+}$ is 1:2.

(f) $(\Lambda_{LLL})_2$-$[Co^{III}(en)_3][Au^{I}_3Co^{III}_2(L\text{-cys})_6]$ ($(\Lambda_{LLL})_2$-$[Co^{III}(en)_3]$[1])

Treatment of $(\Lambda_{LLL})_2$-$K_3[Au_3Co_2(L\text{-cys})_6]$ ($(\Lambda_{LLL})_2$-K_3[**1**]) with $(\Delta)_2/(\Lambda)_2$-$[Co(en)_3](NO_3)_3$ in a 1:2 ratio in water gave black microcrystals of $(\Lambda_{LLL})_2$-$[Co(en)_3]$[**1**].

The IR spectrum of $(\Lambda_{LLL})_2$-$[Co(en)_3]$[**1**] shows the presence of the carboxylate group of L-cys based on the band at 1601 cm^{-1} (Figure 2-1). X-ray fluorescence spectroscopy indicates that this compound contains Au and Co atoms, and elemental analytical data are in agreement with the formula for a 1:1 adduct of $[Co(en)_3]^{3+}$ and $[Au_3Co_2(L\text{-}cys)_6]^{3-}$. The reflection and CD spectra in the solid state are shown in Figure 2-12. The reflection spectrum is similar to that of $(\Delta_{LLL})_2$-$[Co_3(aet)_6]$[**1**], showing bands at 572, 436, and 340 nm. The CD spectrum is almost opposite to that of $(\Delta_{LLL})_2$-$[Co_3(aet)_6]$[**1**] and is similar to that of $(\Lambda_{LLL})_4$-$[Co_3(aet)_6]_2$[**2**], showing positive bands at 520, 410, 375, and 320 nm and a negative band at 450 nm. The black crystals of $(\Lambda_{LLL})_2$-$[Co(en)_3]$[**1**] are also soluble in a saturated $NaNO_3$ aqueous solution, and the spectral measurements in the solution state were performed. The absorption spectrum shows two bands at 573 and 443 nm in the region of 700 to 300 nm (Figure 2-12), which is very similar to that of $(\Delta_{LLL})_2$-$[Co_3(aet)_6]$[**1**]. Its CD spectrum shows positive bands at 579 and 360 nm and a negative band at 457 nm in this region (Figure 2-12). These absorption and CD spectral features in the solution state are essentially the same as the reflection and CD spectral features in the solid state. Unfortunately, many trials to obtain single crystals suitable for the X-ray diffraction measurement were failed, but the presence of $(\Lambda_{LLL})_2$-$[\mathbf{1}]^{3-}$ was confirmed by its ^1H NMR spectrum. The ^1H NMR spectrum of $(\Lambda_{LLL})_2$-$[Co(en)_3]$[**1**] dissolving in a $NaNO_3$ solution of D_2O showed one set of L-cys signals corresponding to $(\Lambda_{LLL})_2$-$[\mathbf{1}]^{3-}$, and no signals of $(\Lambda_{LLL})_4$-$[\mathbf{2}]^{6-}$ were observed (Figure 2-11). The signals of $[Co(en)_3]^{3+}$ were also observed. From these results, it was found that the structure of $(\Lambda_{LLL})_2$-$[\mathbf{1}]^{3-}$ was retained upon the crystallization with $[Co(en)_3]^{3+}$, and the conversion to $(\Lambda_{LLL})_4$-$[\mathbf{2}]^{6-}$ did not occur.

II-3-2 Crystal Structures of Au^ICo^{III} Complexes

(a) $(\Delta_{LLL})_2$-$K_3[Au^I_3Co^{III}_2(L\text{-}cys)_6]$ ($(\Delta_{LLL})_2$-K_3[**1**])

The crystal structure of $(\Delta_{LLL})_2$-K_3[**1**]$\cdot 7.5H_2O$ was established by single-crystal X-ray crystallography. The asymmetric unit contains two independent half complex-anions, potassium ions, and water molecules. A part of potassium ions were not defined because of the severe disorder. The molecular and packing structures are shown in Figures 2-13, 2-14, and 2-15. The crystallographic data are summarized in Table 2-1 and the selected bond distances and angles are listed in Table 2-2.

The complex-anion of $(\Delta_{LLL})_2$-$[\mathbf{1}]^{3-}$ has an S-bridged $Au^I_3Co^{III}_2$ pentanuclear structure. Each Co^{III} atom has an octahedral geometry coordinated by three bidentate

L-cys-*N*,*S* ligands in a facial fashion (av. Co–S = 2.24 Å, Co–N = 2.00 Å), and adopts a Δ configuration. Two Δ_{LLL}-$[Co(L\text{-}cys)_3]^{3-}$ units are linked by three linear Au^I atoms through S atoms (av. Au–S = 2.31 Å, S–Au–S = 175.9°). All six S atoms adopt an *S* configuration, and only the $(\Delta_{LLL})_2(S)_6$ isomer exists in crystal. The L-cys N,S-chelate rings in the Δ configurational $[Co(L\text{-}cys)_3]^{3-}$ units adopt a *lel* (λ for Δ) conformation with free COO^- groups pointing to an equatorial orientation. Three Au^I atoms are arranged in a triangle form with the averaged Au···Au distance of 2.98 Å, indicative of the presence of an aurophilic interaction,[8] and three S–Au–S linkages are twisted to form a triple-stranded helical structure with a left handedness. The $(\Delta_{LLL})_2$-$[\mathbf{1}]^{3-}$ units are connected to each other through intermolecular Au···Au interactions (av. Au···Au = 2.99 Å) to form a right-handed helical chain structure (Figure 2-14). The helical chains are arranged in a parallel manner, and are connected to each other through hydrogen bonds between amine and carboxylate groups (av. NH···O = 2.984 Å) and through coordination bonds between carboxylate groups and potassium ions (Figure 2-15).

(b) $(\Delta_{LLL})_2$-$[Co^{III}_3(aet)_6][Au^I_3Co^{III}_2(L\text{-}cys)_6]$ ($(\Delta_{LLL})_2$-$[Co^{III}_3(aet)_6][1]$)

The crystal structure of $(\Delta_{LLL})_2$-$[Co_3(aet)_6][\mathbf{1}]$ consists of a trinuclear complex-cation ($[Co_3(aet)_6]^{3+}$) and a pentanuclear complex-anion ($[\mathbf{1}]^{3-}$) besides water molecules of crystallization. The molecular and packing structures are shown in Figures 2-16, 2-17, 2-18 and 2-19. The crystallographic data are summarized in Table 2-1 and the selected bond distances and angles are listed in Table 2-3.

The structure of $(\Delta_{LLL})_2$-$[\mathbf{1}]^{3-}$ in $(\Delta_{LLL})_2$-$[Co_3(aet)_6][\mathbf{1}]$ is essentially the same as that in $(\Delta_{LLL})_2$-$K_3[\mathbf{1}]$, having an S-bridged $Au^I_3Co^{III}_2$ pentanuclear structure (Figure 2-16). The coordination geometry around the Co^{III} centers is N_3S_3 octahedral, coordinated by three bidentate-*N*,*S* L-cys ligands (av. Co–S = 2.26 Å, Co–N = 2.04 Å). Two $[Co(L\text{-}cys)_3]^{3-}$ units are linked by three Au^I ions, and each Au^I center is in an S_2 linear coordination environment (av. Au–S = 2.29 Å, S–Au–S = 176.1°). Two Co^{III} centers take a Δ_{LLL} configuration, and all six S atoms adopt an *S* configuration to give only the $(\Delta_{LLL})_2(S)_6$ isomer. The L-cys N,S-chelate rings in the Δ_{LLL} configurational $[Co(L\text{-}cys)_3]^{3-}$ units adopt a *lel* (λ for Δ) conformation with free COO^- groups pointing to an equatorial orientation. There exist intramolecular aurophilic interactions between the triangular Au^I ions (av. Au···Au = 2.975(3) Å), and three S–Au–S linkages have a left-handed helical arrangement. For the cationic part, the S-bridged Co^{III}_3 trinuclear structure is retained, and it was found that the $(\Delta)_2$ and $(\Lambda)_2$ isomers are disordered in a

ca. 3:2 ratio. In the packing structure, $(\Delta_{LLL})_2$-[**1**]$^{3-}$ units are connected to each other through hydrogen bonds between amine and carboxylate groups (av. NH···O = 2.932 Å) to form a hydrogen-bonded 1D chain structure (Figure 2-17). The 1D chains are arranged in a parallel manner, and the disordered $[Co_3(aet)_6]^{3+}$ units are incorporated between the chains through hydrogen bonds (av. NH···O = 2.950 Å), such that each complex-cation is surrounded by two complex-anions (Figure 2-18). Each complex-anion is surrounded by two complex-anions and two complex-cations (Figure 2-19), and as a result, complex-anions and complex-cations are alternately arranged to construct a 3D hydrogen-bonding network structure (Figure 2-19).

(c) $(\Lambda_{LLL})_4$-$[Co^{III}_3(aet)_6]_2[Au^{I}_6Co^{III}_4(L\text{-}cys)_{12}]$ ($(\Lambda_{LLL})_4$-$[Co^{III}_3(aet)_6]_2$[2])

The asymmetric unit of $(\Lambda_{LLL})_4$-$[Co_3(aet)_6]_2$[**2**] contains one complex-anion ($(\Lambda_{LLL})_4$-[**2**]$^{6-}$) and two complex-cations ($[Co_3(aet)_6]^{3+}$), besides water molecules. The molecular and the packing structures of $(\Lambda_{LLL})_4$-$[Co_3(aet)_6]_2$[**2**] are shown in Figures 2-20, 2-21, 2-22, 2-23, and 2-24. The crystallographic data are summarized in Table 2-1, and the selected bond distances and angles are listed in Table 2-4.

The complex-anion ($(\Lambda_{LLL})_4$-[**2**]$^{6-}$) has an S-bridged $Au^{I}_6Co^{III}_4$ decanuclear structure. In $(\Lambda_{LLL})_4$-[**2**]$^{6-}$, two $[Co(L\text{-}cys)_3]^{3-}$ units are bridged by two Au^{I} ions, and two of the resulting $Au^{I}_2Co^{III}_2$ tetranuclear units are further connected by two linear Au^{I} ions through S atoms to form an $Au^{I}_6Co^{III}_4$ decanuclear structure with a D_2 symmetry. Each of the Co^{III} centers in $(\Lambda_{LLL})_4$-[**2**]$^{6-}$ is in an N_3S_3 octahedral geometry coordinated by three bidentate-*N*,*S* L-cys ligands (av. Co–S = 2.25 Å, Co–N = 2.00 Å), and six Au^{I} centers are in an S_2 linear coordination geometry (av. Au–S = 2.31Å, S–Au–S = 169.6°). All four Co^{III} centers take a Λ configuration, and twelve S atoms take an *R* configuration. Thus, only the $(\Lambda_{LLL})_4(R)_{12}$ isomer was formed. Two of the three N,S-chelate rings in each $[Co(L\text{-}cys)_3]^{3-}$ unit adopt an *ob* (λ for Λ) conformation with free carboxylate groups pointing to an equatorial orientation, while the remaining one N,S-chelate ring has a *lel* (δ for Λ) conformation with the carboxylate group pointing to an axial orientation. The axially oriented carboxylate is hydrogen bonded with the adjacent amine group within the complex-anion (av. NH···O = 2.973 Å). There are seven intramolecular aurophilic interactions in $(\Lambda_{LLL})_4$-[**2**]$^{6-}$ with the average Au···Au distance of 3.05 Å. For the complex-cations, two units are crystallographically independent. Both have the similar S-bridged Co^{III}_3 structure with six aet ligands, and are disordered into two parts. In the one complex-cation, the S and N atoms are

disordered, and the $(\Delta)_2$ and $(\Lambda)_2$ isomers exist in a 3:7 ratio. In the other complex-cation, all atoms are disordered into two parts in an 8:2 ratio. While the major Co^{III}_3 structure takes a $(\Delta)_2$ configuration, only the Co_3S_6 framework was refined in the minor part and the chirality about the Co^{III} centers was not determined. Totally, the $(\Delta)_2$ or $(\Lambda)_2$ isomers of $[Co_3(aet)_6]^{3+}$ exist at an almost equal ratio, and the preference of two isomers was not determined. In the parking structure, each complex-anion is connected to six complex-anions through hydrogen bonds between the amine and carboxylate groups to form a wave-like 2D structure (Figure 2-21). One of the two crystallographically independent complex-cations is positioned so as to fill the space of the anionic wave-like structure forming a 2D sheet-like structure (Figure 2-22). In this sheet, the complex-anion and complex-cation are connected through a single NH···OOC hydrogen bond. As a result, in the sheet-like structure, each complex-anion is surrounded by six complex-anions and two complex-cations, whereas each complex-cation is surrounded by two complex-anions (Figure 2-23). The other independent complex-cation is positioned in between the hydrogen-bonded 2D network without significant intermolecular interactions (Figure 2-24).

II-3-3 Chiral and Structural Conversions between $(\Delta_{LLL})_2$-$[Au^I_3Co^{III}_2(L\text{-cys})_6]^{3-}$ ($(\Delta_{LLL})_2$-$[\mathbf{1}]^{3-}$), $(\Lambda_{LLL})_2$-$[Au^I_3Co^{III}_2(L\text{-cys})_6]^{3-}$ ($(\Lambda_{LLL})_2$-$[\mathbf{1}]^{3-}$), and $(\Lambda_{LLL})_4$-$[Au^I_6Co^{III}_4(L\text{-cys})_{12}]^{6-}$ ($(\Lambda_{LLL})_4$-$[\mathbf{2}]^{6-}$)

The reaction of $(\Delta_{LLL})_2$-$K_3[\mathbf{1}]$ with $(\Delta)_2/(\Lambda)_2$-$[Co_3(aet)_6](NO_3)_3$ in a 1:2 ratio in a neutral aqueous solution (pH ~7) gave the cocrystallized compound of the starting materials ($(\Delta_{LLL})_2$-$[Co_3(aet)_6][\mathbf{1}]$). On the other hand, the similar reaction in a basic solution (pH ~9) led to the chiral inversion and structural conversion of the complex-anion to afford the cocrystallized compound of $(\Lambda_{LLL})_4$-$[Co_3(aet)_6]_2[\mathbf{2}]$. To clarify the mechanism of such unique chiral inversion and structural conversion that occurred only in a basic condition, the influence of the solution pH on the conversions was investigated by the absorption, CD, and ^{1}H NMR spectral measurements of $(\Delta_{LLL})_2$-$K_3[\mathbf{1}]$ in different pH conditions. The absorption and CD spectra in a neutral aqueous solution (pH ~7) did not change for 1 week (Figure 2-25), indicative of the retention of the $Au^I_3Co^{III}_2$ structure with the Δ configurational $[Co(L\text{-cys})_3]^{3-}$ moieties. On the other hand, the CD spectral pattern in a basic solution (pH ~9) changed with time to show an almost opposite pattern after 1 week, while the absorption spectra did not change significantly (Figure 2-26). These results indicate that the chirality about the

Co^{III} centers in $(\Delta_{LLL})_2$-[**1**]$^{3-}$ was inverted from Δ to Λ only in a basic condition. The ^{1}H NMR spectra of $(\Delta_{LLL})_2$-[**1**]$^{3-}$ in D_2O in both neutral and basic conditions were also measured. As expected, the ^{1}H NMR spectrum of $(\Delta_{LLL})_2$-[**1**]$^{3-}$ showed one set of L-cys signals (Figure 2-27), and no spectral change was observed in a neutral solution (pH ~7) (Figure 2-27). On the other hand, in a basic solution (pH ~9), the signals of $(\Delta_{LLL})_2$-[**1**]$^{3-}$ became smaller and another set of L-cys signals appeared with time (Figure 2-28). Consequently, there exists newly formed single species as a main product in the solution after 8 days (Figure 2-28). If the D_2 symmetrical structure of $(\Lambda_{LLL})_4$-[**2**]$^{6-}$ exists in solution, three sets of L-cys signals should be observed. The presence of only one set of signals in the ^{1}H NMR spectrum indicates that this new species does not have the $Au^I_6Co^{III}_3$ decanuclear structure, but has another symmetrical structure with the Λ configurational Co^{III} centers. This compound was successfully isolated as potassium salts ($(\Lambda_{LLL})_2$-K_3[**1**]) by adding EtOH to the solution. Absorption and CD spectra of $(\Lambda_{LLL})_2$-K_3[**1**] in water are similar to those of the reaction solution, respectively (Figure 2-3). Elemental analytical data are consistent with the formula for the potassium salt of the L-cysteinato $Au^I_3Co^{III}_2$ complex. Unfortunately, many trials to get good single crystals of $(\Lambda_{LLL})_2$-K_3[**1**] were failed, but the ESI mass spectrum in methanol/water (1:1) showed a trianionic signal at *m*/*z* 474.20, which corresponds to [**1**]$^{3-}$ (Figure 2-6). From these results, it is assumed that the new compound has an $Au^I_3Co^{III}_2$ pentanuclear structure in $(\Lambda_{LLL})_2$-$[Au_3Co_2(L\text{-cys})_6]^{3-}$ ($(\Lambda_{LLL})_2$-[**1**]$^{3-}$), in which two Λ_{LLL} configurational $[Co(L\text{-cys})_3]^{3-}$ units are bridged by three linear Au^I atoms. The same complex, $(\Lambda_{LLL})_2$-$[Au_3Co_2(L\text{-cys})_6]^{3-}$, was synthesized by the stepwise reaction of $[Ni(L\text{-cys})_2]^{2-}$ and Au^I, followed by the metal substitution of Ni^{II} ion to Co^{III} ion.[5c] The spectral features are same as the reported one. Since the molecular modeling study demonstrated that the coordinated S atoms should adopt the *R* configuration, only the $(\Lambda_{LLL})_2(R)_6$ isomer might be formed. Focused on the chiral inversion behavior, the $(\Delta_{LLL})_2(S)_6$ isomer in $(\Delta_{LLL})_2$-[**1**]$^{3-}$ was inverted to the $(\Lambda_{LLL})_2(R)_6$ isomer in $(\Lambda_{LLL})_2$-[**1**]$^{3-}$ at once, and thus, the cooperative multiple chiral inversion successfully occurred with the retention of the S-bridged $Au^I_3Co^{III}_2$ structure only in a basic solution.

From the pH dependent spectral changes, $(\Delta_{LLL})_2$-[**1**]$^{3-}$ was found to show the multiple chiral inversion to give $(\Lambda_{LLL})_2$-[**1**]$^{3-}$ in a basic solution, but the factor that causes the structural conversion from $(\Lambda_{LLL})_2$-[**1**]$^{3-}$ to $(\Lambda_{LLL})_4$-[**2**]$^{6-}$ is still unclear. As mentioned in Scheme 2-1, the structural conversion occurred to afford black crystals of $(\Lambda_{LLL})_4$-$[Co_3(aet)_6]_2$[**2**], when $(\Lambda_{LLL})_2$-[**1**]$^{3-}$ was mixed with $[Co_3(aet)_6]^{3+}$ in water. To

check whether the $Au^{I}_{6}Co^{III}_{4}$ decanuclear structure was formed in the solution state in the presence of $[Co_3(aet)_6]^{3+}$, the ^{1}H NMR spectra of the mixture of $(\Lambda_{LLL})_2$-[**1**]$^{3-}$ and $[Co_3(aet)_6]^{3+}$ in D_2O was measured. As a result, only the signals attributed to $(\Lambda_{LLL})_2$-[**1**]$^{3-}$ as an anionic component were observed (Figure 2-29). Therefore, we concluded that the Λ configurational $Au^{I}_{6}Co^{III}_{4}$ decanuclear structure in $(\Lambda_{LLL})_4$-[**2**]$^{6-}$ was formed upon the crystallization with $[Co_3(aet)_6]^{3+}$. This might be due to the stabilization by the presence of seven intramolecular aurophilic interactions (Figure 2-20). A good shape matching between $(\Lambda_{LLL})_4$-[**2**]$^{6-}$ and $[Co_3(aet)_6]^{3+}$ also contributes to the formation of $(\Lambda_{LLL})_4$-[**2**]$^{6-}$ because of the presence of the efficient intermolecular anion-anion and cation-anion hydrogen bonding interactions that leads to the quite low solubility of $(\Lambda_{LLL})_4$-$[Co_3(aet)_6]_2$[**2**] into water. To show the importance of the molecular shape, the similar reaction using $[CoRh_2(aet)_6]^{3+}$ that has a similar S-bridged trinuclear structure with $[Co_3(aet)_6]^{3+}$, instead of $[Co_3(aet)_6]^{3+}$, was performed. Expectedly, treatment of $(\Lambda_{LLL})_2$-K_3[**1**] and $[CoRh_2(aet)_6](NO_3)_3$ resulted in the structural conversion to give the cocrystallized compound consisting of $(\Lambda_{LLL})_4$-[**2**]$^{6-}$ and $[CoRh_2(aet)_6]^{3+}$ in a 1:2 ratio. This was evidenced by the ^{1}H NMR, absorption, and CD spectral measurements as well as elemental analysis and preliminary single-crystal X-ray analysis. On the other hand, the reaction of $(\Lambda_{LLL})_2$-K_3[**1**] and $[Co(en)_3](NO_3)_3$ did not lead to the formation of $(\Lambda_{LLL})_4$-[**2**]$^{6-}$, but gave the cocrystallized compound of two starting materials, $(\Lambda_{LLL})_2$-$[Co(en)_3]$[**1**]. Together with the fact that $(\Delta_{LLL})_2$-[**1**]$^{3-}$ was not converted to the corresponding $Au^{I}_{6}Co^{III}_{4}$ decanuclear structure upon the crystallization with $[Co_3(aet)_3]^{3+}$, the molecular shape of the complex-cation is essential for the formation of the $Au^{I}_{6}Co^{III}_{3}$ decanuclear structure in $(\Lambda_{LLL})_4$-[**2**]$^{6-}$.

Considering the speculation of the importance of the good shape matching for the structural conversion, $(\Lambda_{LLL})_4$-[**2**]$^{6-}$ is possible to revert back to $(\Lambda_{LLL})_2$-[**1**]$^{3-}$ upon dissolution, because $(\Lambda_{LLL})_4$-[**2**]$^{6-}$ is essentially not affected by $[Co_3(aet)_6]^{3+}$ and behaves as a well-isolated species in the solution state. Thus, the structure of $(\Lambda_{LLL})_4$-[**2**]$^{6-}$ in the solution state was studied by the ^{1}H NMR spectral measurements. As shown in Figure 2-30, the spectrum of $(\Lambda_{LLL})_4$-$[Co_3(aet)_6]_2$[**2**] just after dissolving in a $NaNO_3$ solution of D_2O shows three sets of L-cys signals attributed to $(\Lambda_{LLL})_4$-[**2**]$^{6-}$. The signals of $(\Lambda_{LLL})_4$-[**2**]$^{6-}$ disappeared almost completely after 9 h, and instead, those of $(\Lambda_{LLL})_2$-[**1**]$^{3-}$ were observed, suggesting that the $Au^{I}_{6}Co^{III}_{4}$ decanuclear species ($(\Lambda_{LLL})_4$-[**2**]$^{6-}$) was converted to the $Au^{I}_{3}Co^{III}_{2}$ pentanuclear species ($(\Lambda_{LLL})_2$-[**1**]$^{3-}$) retaining the Λ_{LLL} configuration around the Co^{III} centers. Therefore, the reversible

structural conversion between $(\Lambda_{LLL})_2$-[**1**]$^{3-}$ and $(\Lambda_{LLL})_4$-[**2**]$^{6-}$ upon crystallization/dissolution was successful.

Because the understanding of the mechanism of the multiple chiral inversion between $(\Delta_{LLL})_2$-[**1**]$^{3-}$ and $(\Lambda_{LLL})_2$-[**1**]$^{3-}$ in basic/acidic conditions is important, the structures of $(\Delta_{LLL})_2$-[**1**]$^{3-}$ and $(\Lambda_{LLL})_4$-[**2**]$^{6-}$ are compared in detail focused on the *lel*/*ob* conformations and the directions of free carboxylate groups (equatorial/axial). In general, the *lel* conformation (λ for Δ and δ for Λ) is thermodynamically stable than the *ob* conformation (δ for Δ and λ for Λ), and the equatorial orientation of a free carboxylate group is favorable than the axial orientation.[9] In $(\Delta_{LLL})_2$-[**1**]$^{3-}$, all the L-cys N,S-chelate rings in the Δ configurational [Co(L-cys)$_3$]$^{3-}$ units adopt a *lel* (λ for Δ) conformation with free COO^- groups pointing to an equatorial orientation. This indicates that $(\Delta_{LLL})_2$-[**1**]$^{3-}$ is a thermodynamically favorable product. On the other hand, in each of the Λ configurational [Co(L-cys)$_3$]$^{3-}$ unit in $(\Lambda_{LLL})_4$-[**2**]$^{6-}$, two of three L-cys N,S-chelate rings adopt an *ob* (λ for Λ) conformation with free carboxylate groups pointing to an equatorial orientation, while the remaining one N,S-chelate ring has a *lel* (δ for Λ) conformation with carboxylate groups pointing to an axial orientation. This thermodynamically unstable structure is stabilized by intramolecular hydrogen bonds between the axially oriented carboxylate and adjacent amine groups. Similar hydrogen bonding interactions were also observed in $(\Lambda_{LLL})_2$-[Co$_3$(L-cys)$_6$]$^{3-}$ and $(\Lambda_{LLL})_2$-[Au$_3$Ni$_2$(L-cys)$_6$]$^{5-}$.[4a,5c] Unfortunately, the structural features of the *lel*/*ob* conformations and the orientation of carboxylate groups in $(\Lambda_{LLL})_2$-[**1**]$^{3-}$ could not be determined due to the low crystallinity. However, it is speculated that the Λ configuration around the Co^{III} centers in $(\Lambda_{LLL})_2$-[**1**]$^{3-}$ might be also stabilized by the intramolecular hydrogen bonding interactions. In the basic condition, these intramolecular hydrogen bonds easily formed compared with the neutral condition, because of the presence of the completely deprotonated carboxylate groups. In the neutral condition, the hydrogen bonds are not stable compared with the basic condition, because the carboxylate groups might be partially protonated. Therefore, we suppose that the most conceivable factor responsible for determining the chirality around the Co^{III} centers is the protonation/deprotonation of the carboxy groups. Previously, the similar Δ_L-Λ_L chiral inversion in the ruthenabenzene with L-cysteinate induced by the protonation/deprotonation of the carboxy group was reported.[10] The chiral inversions from $(\Lambda_{LLL})_2(R)_6$ to $(\Delta_{LLL})_2(S)_6$ isomers did not occur, which might be because it is difficult to cleave the stable intramolecular hydrogen bonds in the solid state.

II-4 Summary

In this chapter, the unique multiple chiral inversion and structural conversion in the L-cysteinato $Au^{I}Co^{III}$ system was demonstrated. The reaction of $(\Delta_{LLL})_2$-$[Au_3Co_2(L\text{-}cys)_6]^{3-}$ ($(\Delta_{LLL})_2$-$[\mathbf{1}]^{3-}$) and $[Co_3(aet)_6]^{3+}$ in a neutral aqueous solution gave black crystals of $(\Delta_{LLL})_2$-$[Co_3(aet)_6][\mathbf{1}]$ with the retention of both cationic and anionic structures. On the other hand, the similar reaction in a basic solution gave black crystals of $(\Lambda_{LLL})_4$-$[Co_3(aet)_6]_2[Au_6Co_4(L\text{-}cys)_{12}]$ ($(\Lambda_{LLL})_4$-$[Co_3(aet)_6]_2[\mathbf{2}]$), accompanied with the chiral and structural conversions. From the spectral measurements, it was found that the multiple chiral inversion from $(\Delta_{LLL})_2$-$[\mathbf{1}]^{3-}$ to $(\Lambda_{LLL})_2$-$[\mathbf{1}]^{3-}$ was induced by the pH control, and subsequently, the structural conversion to $(\Lambda_{LLL})_4$-$[\mathbf{2}]^{6-}$ occurred upon the crystallization with $[Co_3(aet)_6]^{3+}$. In the chiral inversion process, the cooperative multiple chiral inversion occurred from $(\Delta_{LLL})_2(S)_6$ to $(\Lambda_{LLL})_2(R)_6$ retaining the $Au^{I}{}_3Co^{III}{}_2$ pentanuclear structure, and this system belongs to "strongly correlated chiral system" that shows cooperative multiple chiral inversions. The further structural conversion from the $Au^{I}{}_3Co^{III}{}_2$ pentanuclear to $Au^{I}{}_6Co^{III}{}_4$ decanuclear structures retaining the chirality around the Co^{III} centers is promoted by the stabilization through the formation of the many intramolecular aurophilic interactions, as well as by the good shape matching of the complex-cation and complex-anion that leads to the quite low solubility. The similar structural conversion was not observed using $(\Delta_{LLL})_2$-$[\mathbf{1}]^{3-}$. The creation of such a unique coordination compound that has relatively inert metal centers and shows a multiple chiral inversion and a structural conversion is unprecedented. Interestingly, the $Au^{I}{}_6Co^{III}{}_4$ decanuclear structure in $(\Lambda_{LLL})_4$-$[\mathbf{2}]^{6-}$ was converted back to $(\Lambda_{LLL})_2$-$[\mathbf{1}]^{3-}$ by dissolution. Thus, we succeeded in the construction of "strongly correlated chiral system" that also shows the structural conversion in the coordination system with the inert metal centers.

II-5 References

(1) (a) I. Agranat, H. Caner, J. Caldwell, *Nat. Rev. Drug Disc*. **2002**, *1*, 753–768. (b) J. J. D. de Jong, L. N. Lucas, R. M. Kellogg, J. H. van Esch, B. L. Feringa, *Science* **2004**, *304*, 278–281. (c) R. A. van Delden, M. K. J. tar Wiel, M. M. Pollard, J. Vicario, N. Koumura, B. L. Feringa, *Nature* **2005**, *437*, 1337–1340. (d) R. Elekema, M. M. Pollard, J. Vicario, N. Katsonis, B. S. Ramon, C. W. M. Bastiaansen, D. J. Broer, B. L. Feringa, *Nature* **2006**, *440*, 163. (e) M. Mellah, A. Voituriez, E. Schulz, *Chem. Rev*. **2007**, *107*, 5133−5209. (f) C. Gautier, T. Bürgi, *J. Am. Chem. Soc*. **2008**, *130*, 7077–7084. (g) R. Rasappan, D. Lanventine, O. Reiser, *Coord. Chem. Rev*. **2008**, *252*, 702–714. (h) R. Sessoli, A. K. Powell, *Coord. Chem. Rev*. **2009**, *253*, 2328–2341. (i) J. Clayden, W. J. Moran, P. J. Edwards, S. R. LaPlante, *Angew. Chem. Int. Ed*. **2009**, *48*, 6398–6401. (j) M. Bartók, *Chem. Rev*. **2010**, *110*, 1663–1705. (k) J. Suk, V. R. Naidu, X. Liu, M. S. Lah, K.-S. Jeong, *J. Am. Chem. Soc*. **2011**, *133*, 13938–13941. (l) H. Hayasaka, T. Miyashita, M. Nakayama, K. Kuwada, K. Akagi, *J. Am. Chem. Soc*. **2012**, *134*, 3758–3765. (m) Y. Wang, Q. Li, *Adv. Mater*. **2012**, *24*, 1926–1945. (n) H. Hayasaka, T. Miyashita, M. Nakayama, K. Kuwada, K. Akagi, *J. Am. Chem. Soc*. **2012**, *134*, 3758−3765. (o) G. Chelucci, *Coord. Chem. Rev*. **2013**, *257*, 1887–1932.

(2) (a) R. S. Vagg, *Inorg. Chim. Acta* **1981**, *51*, 61–65. (b) S. Zahn, J. W. Canary, *Science* **2000**, *288*, 1404–1407. (c) J. Gregolíński, J. Lisowski, *Angew. Chem. Int. Ed*. **2006**, *45*, 6122–6126. (d) H. Sato, A. Yamagishi, *J. Photochem. Photobiol. C* **2007**, *8*, 67–84. (e) D.-X. Xue, W.-X. Zhang, X.-M. Chen, Wang, H.-Z. *Chem. Commun*. **2008**, 1551–1553. (f) S. Akine, S. Hotate, T. Nabeshima, *J. Am. Chem. Soc*. **2011**, *133*, 13868–13871. (g) S. Takashima, H. Abe, M. Inoue, *Chem. Commun*. **2011**, *47*, 7455–7457. (h) H. Miyake, M. Ueda, S. Murota, H. Sugimoto, H. Tsukube, *Chem. Commun*. **2012**, *48*, 3721–3723. (i) H. Miyake, H. Tsukube, *Chem. Soc. Rev*. **2012**, *41*, 6977–6991. (j) N. Ousaka, J. K. Clegg, J. R. Nitschke, *Angew. Chem. Int. Ed*. **2012**, *51*, 1464 –1468. (k) L. Chen, X. Ding, L. Gong, Meggers, E. *Dalton Trans*. **2013**, *42*, 5623–5626.

(3) (a) H. Miyake, K. Yoshida, H. Sugimoto, H. Tsukube, *J. Am. Chem. Soc*. **2004**, *126*, 6524–6525. (b) H. Miyake, M. Hikita, M. Itazaki, H. Nakazawa, H. Sugimoto, H. Tsukube, *Chem. Eur. J*. **2008**, *14*, 5393–5396.

(4) (a) T. Konno, S. Aizawa, K. Okamoto, J. Hidaka, *Chem. Lett*. **1985**, *14*, 1017–1020.

(b) K. Okamoto, S. Aizawa, T. Konno, H. Einaga, J. Hidaka, *Bull. Chem. Soc. Jpn*. **1986**, *59*, 3859–3864. (c) S. Miyanowaki, Konno, T.; K. Okamoto, J. Hidaka, *Bull. Chem. Soc. Jpn.* **1988**, *61*, 2987–2989. (d) T. Konno, K. Tokuda, T. Suzuki, K. Okamoto, *Bull. Chem. Soc. Jpn*. **1998**, *71*, 1049–1054. (e) T. Konno, T. Yoshimura,; K. Aoki, K. Okamoto, M. Hirotsu, *Angew. Chem. Int. Ed*. **2001**, *40*, 1765–1768. (f) T. Konno, Y. Shimazaki, T. Yamaguchi, T. Ito, M. Hirotsu, *Angew. Chem. Int. Ed*. **2002**, *41*, 4711–4715. (g) T. Konno, *Bull. Chem. Soc. Jpn*. **2004**, *77*, 627–649. (h) M. Taguchi, A. Igashira-Kamiyama, T. Kajiwara, T. Konno, *Angew. Chem. Int. Ed.* **2007**, *46*, 2422–2425. (i) T. Aridomi, K. Takamura, A. Igashira-Kamiyama, T. Kawamoto, T. Konno, *Chem. Eur. J*. **2008**, *14*, 7752–7755. (j) N. Yoshinari, A. Igashira-Kamiyama, T. Konno, *Chem. Eur. J.* **2010**, *16*, 14247–14251. (k) A. Igashira-Kamiyama, T. Konno, *Dalton Trans*. **2011**, *40*, 7249–7263.

(5) (a) A. P. Arnold, W. G. Jackson, *Inorg. Chem*. **1990**, *29*, 3618–3620. (b) M. Kita, K. Yamanari, *J. Chem. Soc., Dalton Trans*. **1999**, 1221–1226. (c) Y. Sameshima, N. Yoshinari, K. Tsuge, A. Igashira-Kamiyama, T. Konno *Angew. Chem. Int. Ed.* **2009**, *48*, 8469–8472.

(6) T. Konno, S. Aizawa, K. Okamoto, J. Hidaka, *Bull. Chem. Soc. Jpn*. **1990**, *63*, 792–798.

(7) (a) G. M. Sheldrick, *Acta Crystallogr*. **2008**, *A64*, 112–122. (b) C. Kabuto, S. Akine, E. Kwon, *J. Cryst. Soc. Jpn*. **2009**, *51*, 218–224.

(8) P. Pyykkö, *Chem. Rev*. **1997**, *97*, 597−636.

(9) (a) E. J. Corey, J. C. Bailar Jr., *J. Am. Chem. Soc*. **1959**, *81*, 2620−2629. (b) J. K. Beattie, *Acc. Chem. Res*. **1971**, *4*, 253−259. (c) S. R. Niketić, K. Rasmussen, *Acta Chem. Scand.* **1978**, *A32*, 391−400. (d) K. P. C. Vollhardt, N. E. Schore, *Organic Chemistry*, 2nd ed.; W. H. Freeman and Company: New York, **1994**, chap. 4.

(10) R. Lin, H. Zhang, S. Li, L. Chen, W. Zhang, T. B. Wen, H. Zhang, H. Xia, *Chem. Eur. J*. **2011**, *17*, 2420–2427.

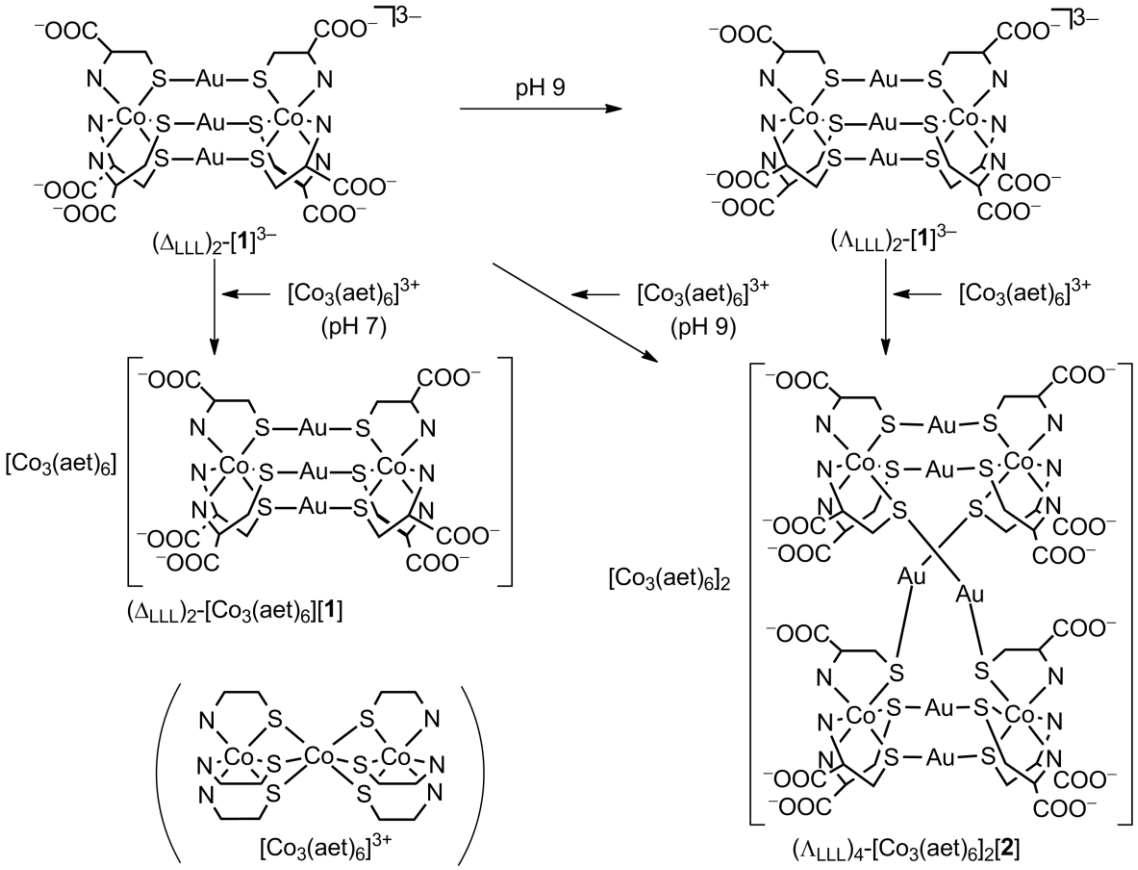

Scheme 2-1. Chiral and structural conversions between $(\Delta_{LLL})_2$-$[Au_3Co_2(L\text{-cys})_6]^{3-}$ ($(\Delta_{LLL})_2$-[**1**]$^{3-}$), $(\Lambda_{LLL})_2$-$[Au_3Co_2(L\text{-cys})_6]^{3-}$ ($(\Lambda_{LLL})_2$-[**1**]$^{3-}$), and $(\Lambda_{LLL})_4$-$[Au_6Co_4(L\text{-cys})_{12}]^{6-}$ ($(\Lambda_{LLL})_4$-[**2**]$^{6-}$).

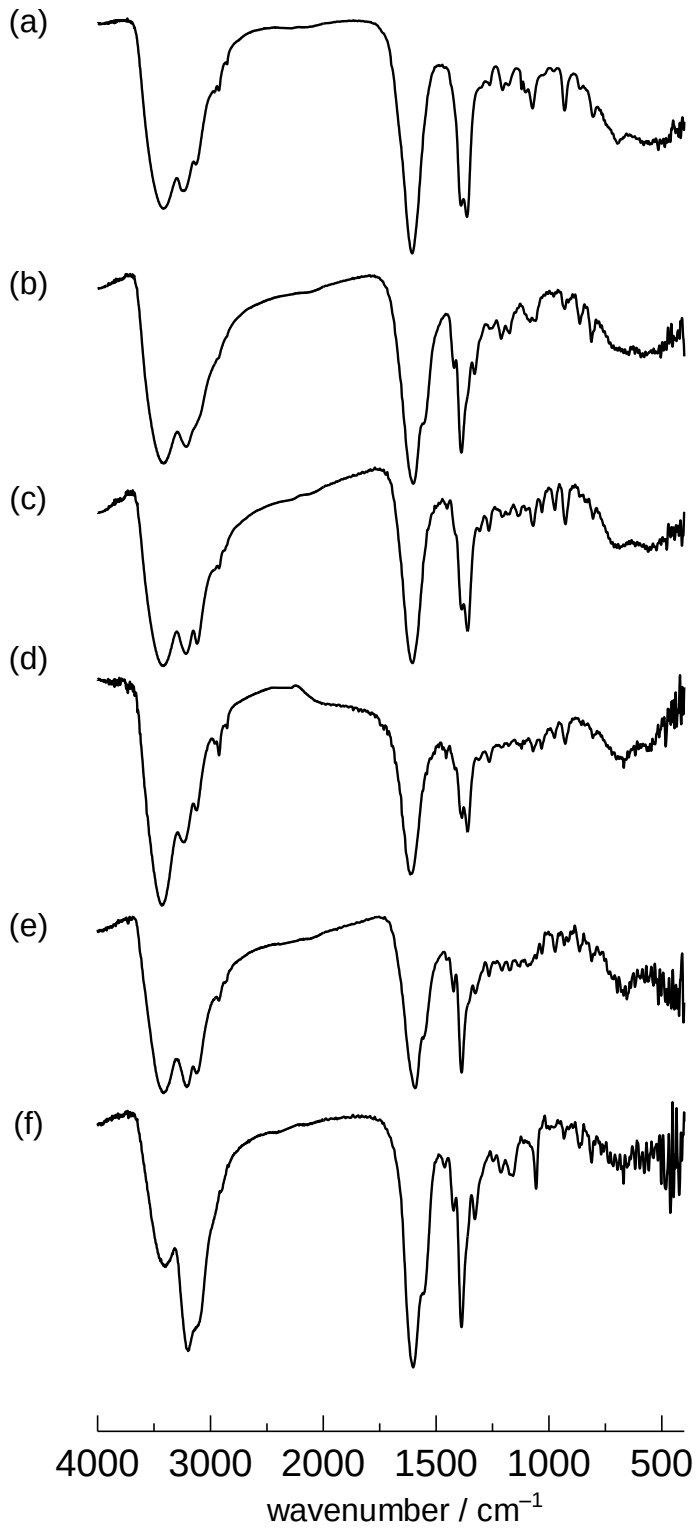

Figure 2-1. IR spectra of (a) $(\Delta_{LLL})_2$-K_3[**1**], (b) $(\Lambda_{LLL})_2$-K_3[**1**], (c) $(\Delta_{LLL})_2$-$[Co_3(aet)_6]$[**1**], (d) $(\Lambda_{LLL})_4$-$[Co_3(aet)_6]_2$[**2**], (e) $(\Lambda_{LLL})_4$-$[CoRh_2(aet)_6]_2$[**2**], and (f) $(\Lambda_{LLL})_2$-$[Co(en)_3]$[**1**] (KBr disk).

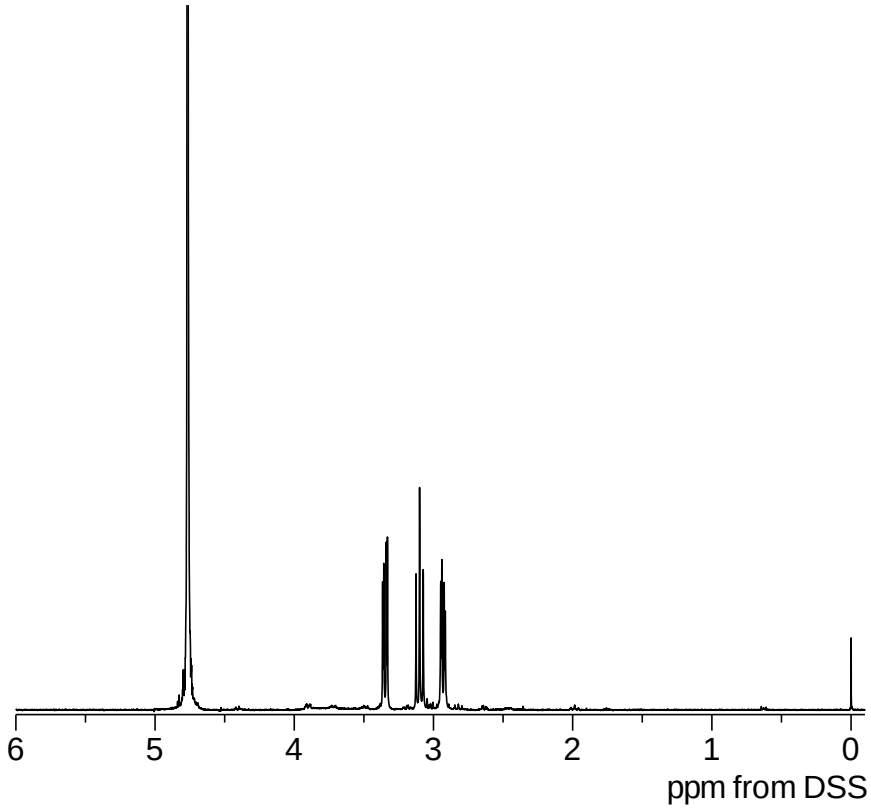

Figure 2-2. ^{1}H NMR spectrum of $(\Delta_{LLL})_2$-K_3[**1**] in D_2O.

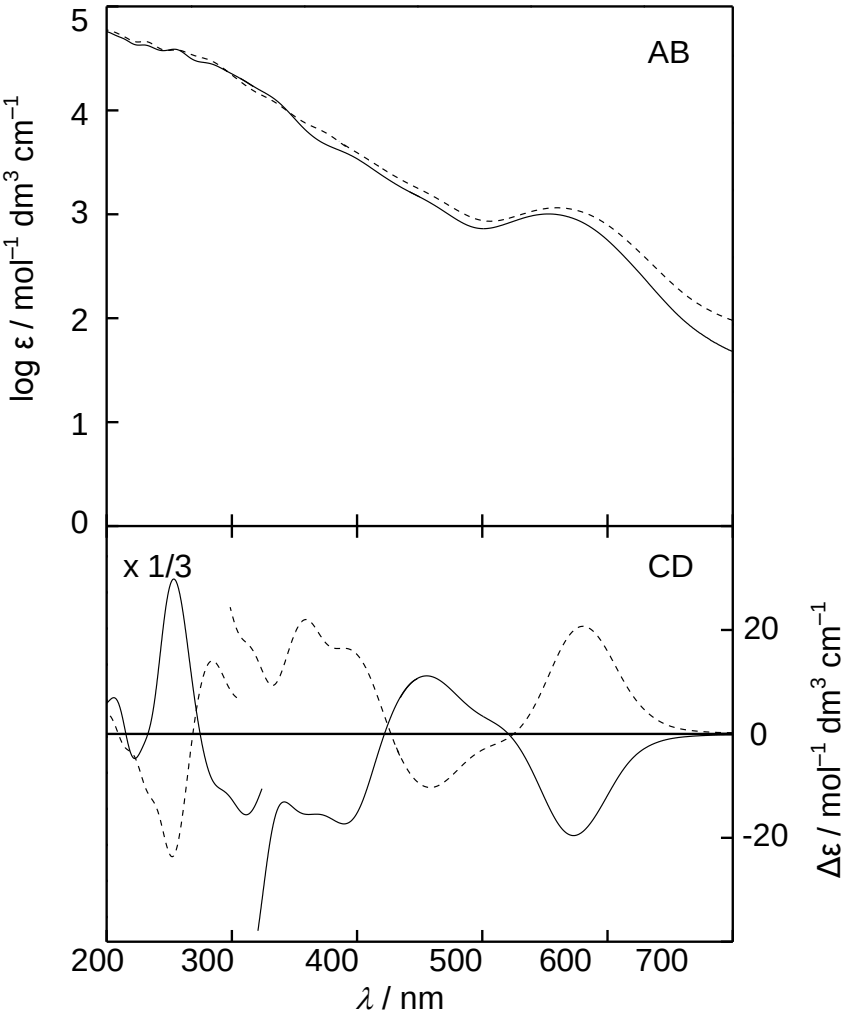

Figure 2-3. Absorption and CD spectra of $(\Delta_{LLL})_2$-K_3[**1**] (—) and $(\Lambda_{LLL})_2$-K_3[**1**] (---) in water.

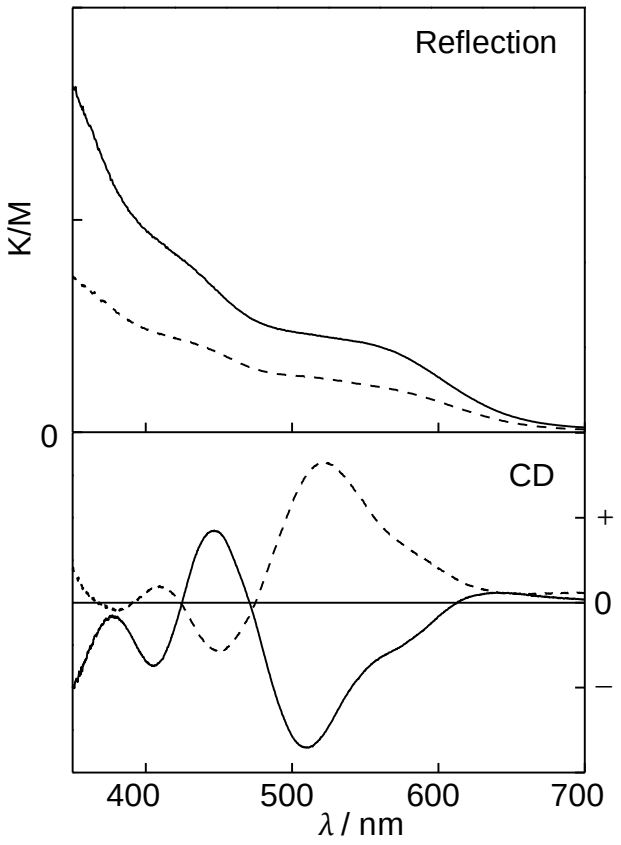

Figure 2-4. Reflection and CD spectra of $(\Delta_{LLL})_2$-K_3[**1**] (—) and $(\Lambda_{LLL})_2$-K_3[**1**] (---) in the solid state. For $(\Delta_{LLL})_2$-K_3[**1**], reflection spectrum [λ / nm]: 560, 434; CD spectrum [λ / nm]: 509 (–), 447 (+), 404 (–), 376 (–). For $(\Lambda_{LLL})_2$-K_3[**1**], reflection spectrum [λ / nm]: 550, 434; CD spectrum [λ / nm]: 522 (+), 450 (–), 410 (+), 377 (–).

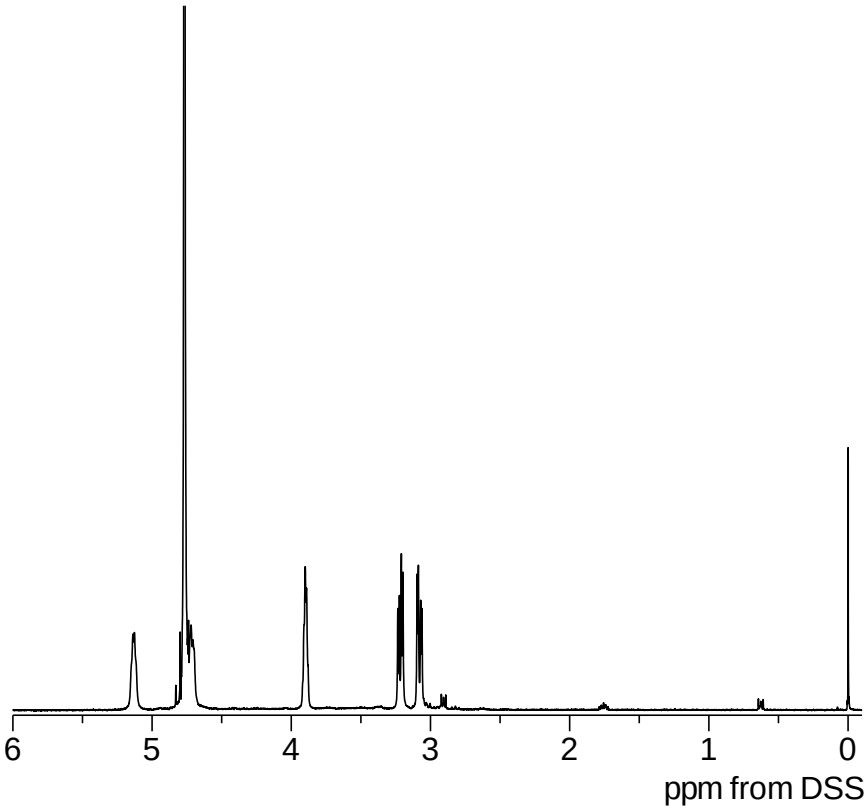

Figure 2-5. ^{1}H NMR spectrum of $(\Lambda_{LLL})_2$-K_3[**1**] in D_2O.

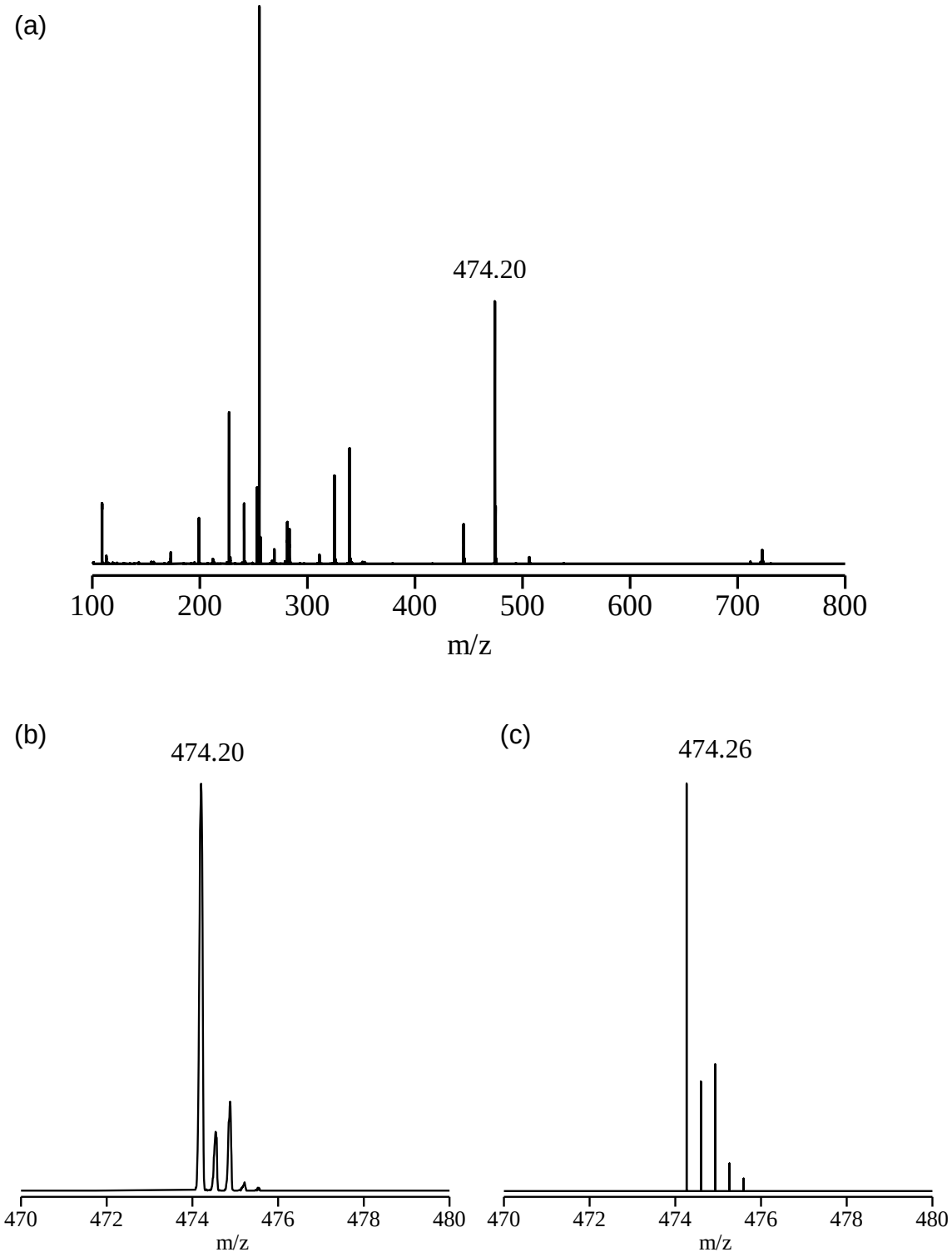

Figure 2-6. (a) ESI mass spectrum of $(\Lambda_{LLL})_2$-K_3[**1**] in water/methanol (1:1). (b) The observed spectrum and (c) the calculated isotope pattern of the dominant signal (*m*/*z* = 474.26).

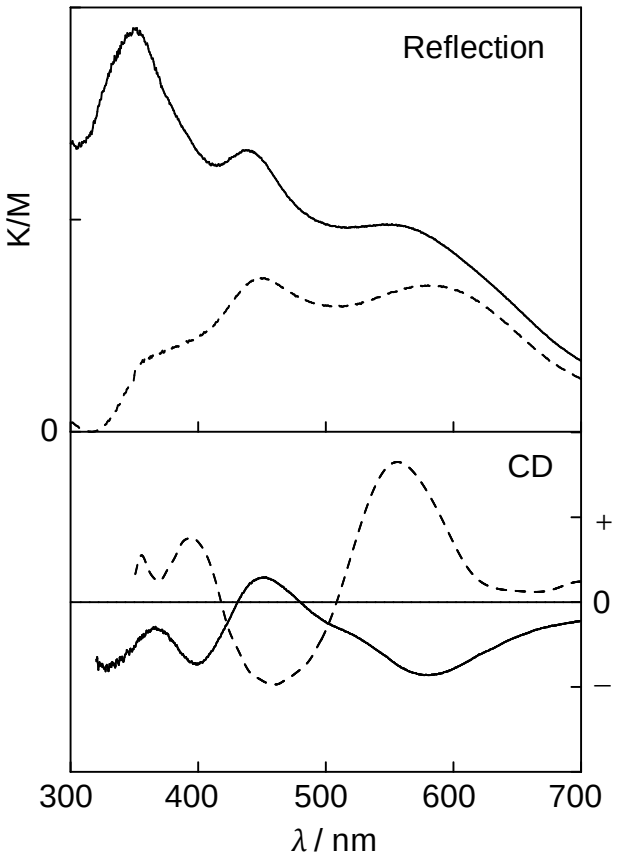

Figure 2-7. Reflection and CD spectra of $(\Delta_{LLL})_2$-$[Co_3(aet)_6]$[**1**] (—) and $(\Lambda_{LLL})_4$-$[Co_3(aet)_6]_2$[**2**] (---) in the solid state. For $(\Delta_{LLL})_2$-$[Co_3(aet)_6]$[**1**], reflection spectrum [λ / nm]: 560, 437, 348; CD spectrum [λ / nm]: 577 (–), 451 (+), 398 (–), 365 (–). For $(\Lambda_{LLL})_4$-$[Co_3(aet)_6]_2$[**2**], reflection spectrum [λ / nm]: 580, 450, 360; CD spectrum [λ / nm]: 560 (+), 460 (–), 395 (+), 355 (+).

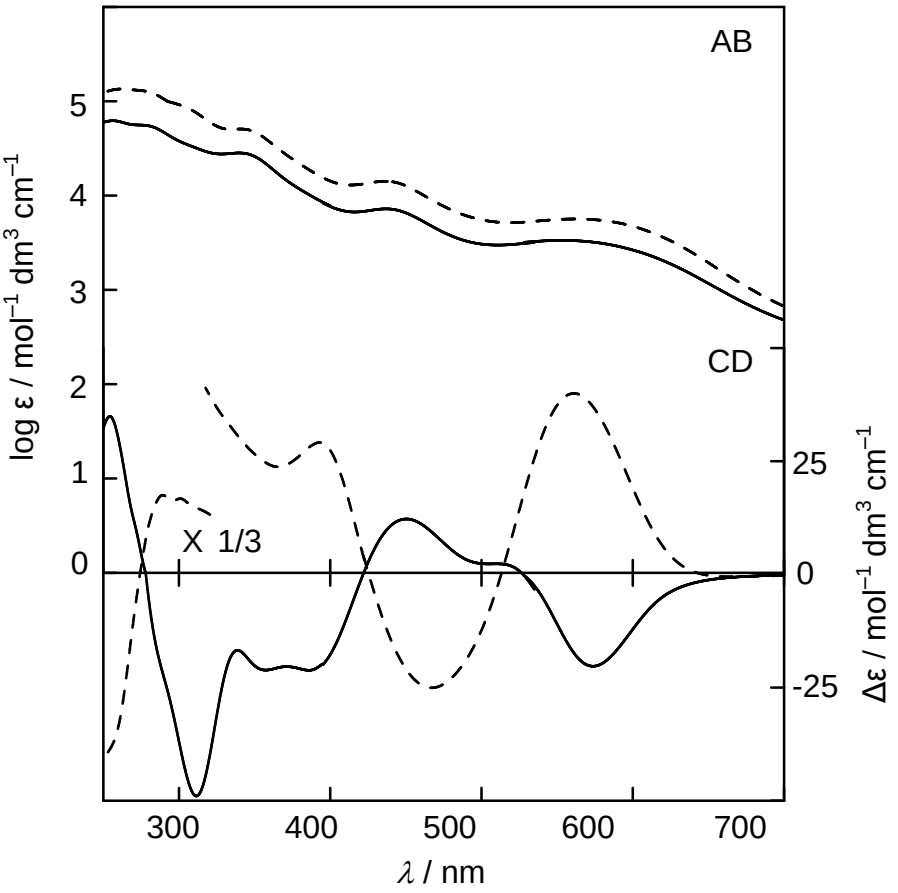

Figure 2-8. Absorption and CD spectra of $(\Delta_{LLL})_2$-$[Co_3(aet)_6]$[**1**] (—) and $(\Lambda_{LLL})_4$-$[Co_3(aet)_6]_2$[**2**] (---) in a $NaNO_3$ aqueous solution. For $(\Delta_{LLL})_2$-$[Co_3(aet)_6]$[**1**], absorption spectrumn [λ / nm (log ε / mol^{-1} dm^3 cm^{-1})]: 560 (3.52), 437 (3.85), 339 (4.45), 280 (4.73), 257 (4.79); CD spectrum [λ / nm ($\Delta\varepsilon$ / mol^{-1} dm^3 cm^{-1})]: 573 (–20.27), 520 (+1.80), 450 (+12.25), 385 (–21.17), 355 (–21.07), 311 (–48.94), 254 (+104.81), 234 (+8.59), 221 (–4.91), 207 (+48.81). For $(\Lambda_{LLL})_4$-$[Co_3(aet)_6]_2$[**2**], absorption spectrum [λ / nm (log ε / mol^{-1} dm^3 cm^{-1})]: 574 (3.74), 439 (4.15), 343 (4.70); CD spectrum [λ / nm ($\Delta\varepsilon$ / mol^{-1} dm^3 cm^{-1})]: 561 (+39.90), 467 (–25.00), 392 (+29.15), 301 (+16.75), 288 (+17.46).

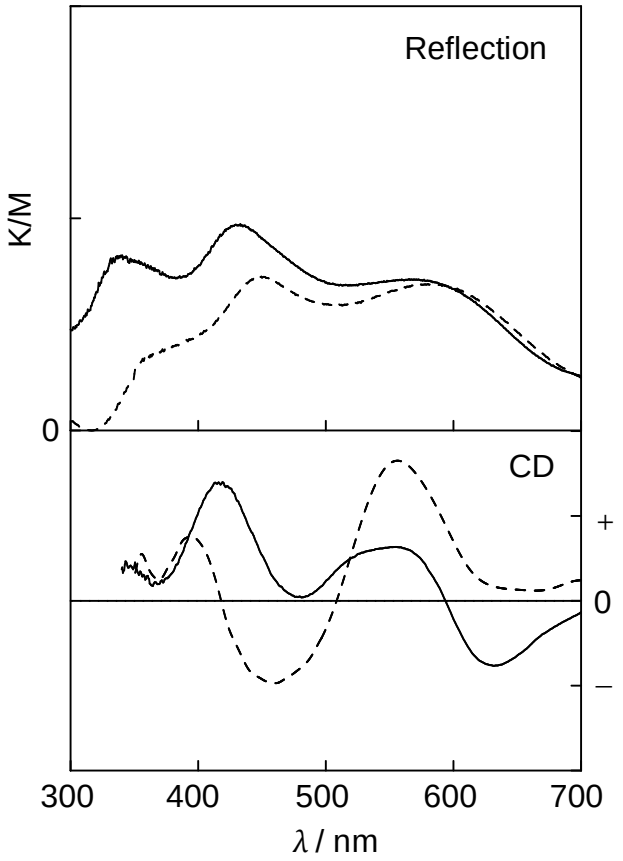

Figure 2-9. Reflection and CD spectra of $(\Lambda_{LLL})_4$-$[CoRh_2(aet)_6]_2$[**2**] (—) together with those of $(\Lambda_{LLL})_4$-$[Co_3(aet)_6]_2$[**2**] (---) in the solid state. For $(\Lambda_{LLL})_4$-$[CoRh_2(aet)_6]_2$[**2**], reflection spectrum [λ / nm]: 579, 539, 336; CD spectrum [λ / nm]: 632 (–), 553 (+), 416 (+), 370 (+).

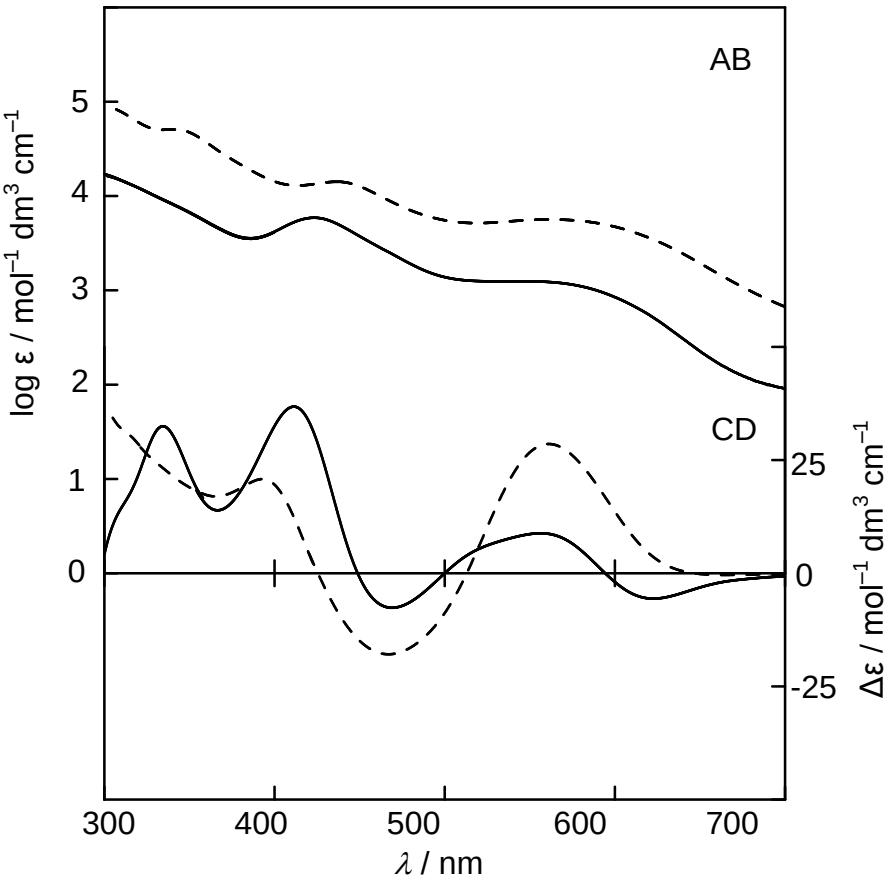

Figure 2-10. Absorption and CD spectra of $(\Lambda_{LLL})_4$-$[CoRh_2(aet)_6]_2$[**2**] (—) in a $NaNO_3$ aqueous solution together with those of $(\Lambda_{LLL})_4$-$[Co_3(aet)_6]_2$[**2**] (---). For $(\Lambda_{LLL})_4$-$[CoRh_2(aet)_6]_2$[**2**], absorption spectrum [λ / nm (log ε/ mol^{-1} dm^3 cm^{-1})]: 585 (3.02), 423 (3.77); CD spectrum [λ / nm ($\Delta\varepsilon$ / mol^{-1} dm^3 cm^{-1})]: 619 (–7.80), 556 (+12.37), 469 (–10.66), 411 (+51.54), 365 (+21.00), 334 (+45.46).

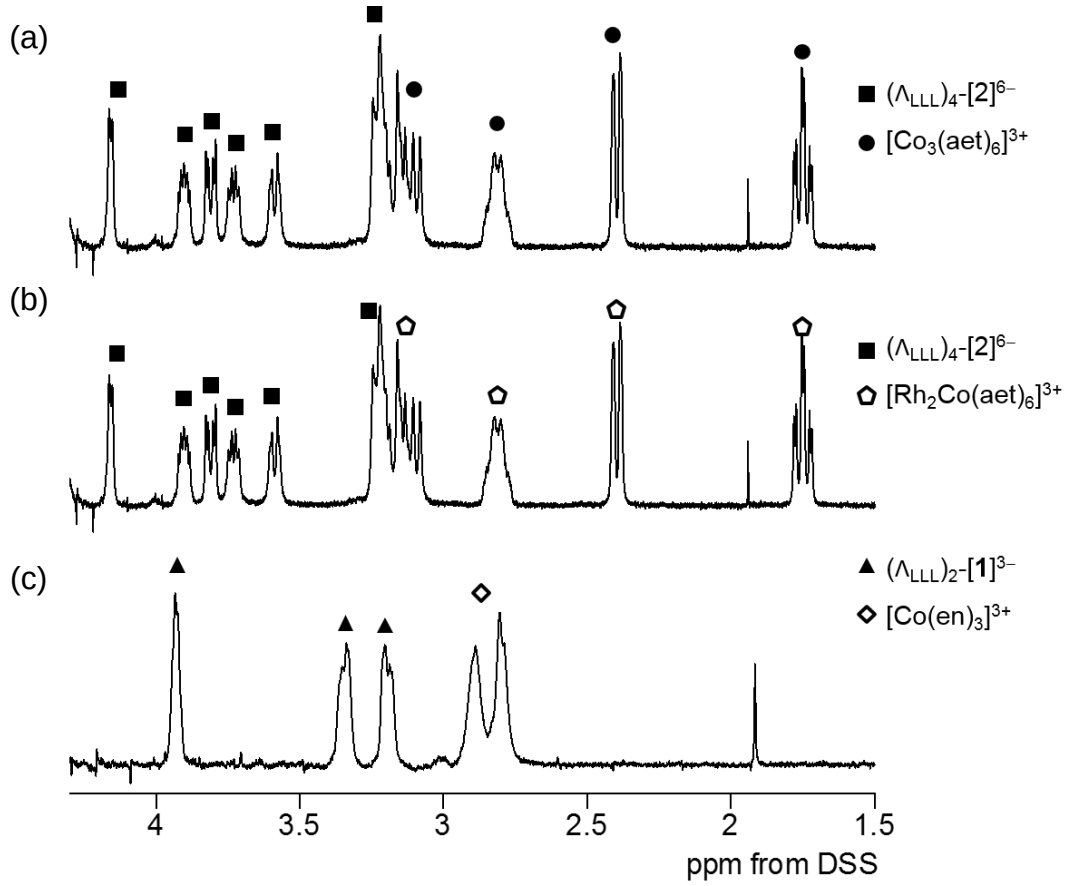

Figure 2-11. ^{1}H NMR spectra of (a) $(\Lambda_{LLL})_4$-$[Co_3(aet)_6]_2$[**2**], (b) $(\Lambda_{LLL})_4$-$[CoRh_2(aet)_6]_2$[**2**], and (c) $(\Lambda_{LLL})_2$-$[Co(en)_3]$[**1**] in a $NaNO_3$ solution of D_2O.

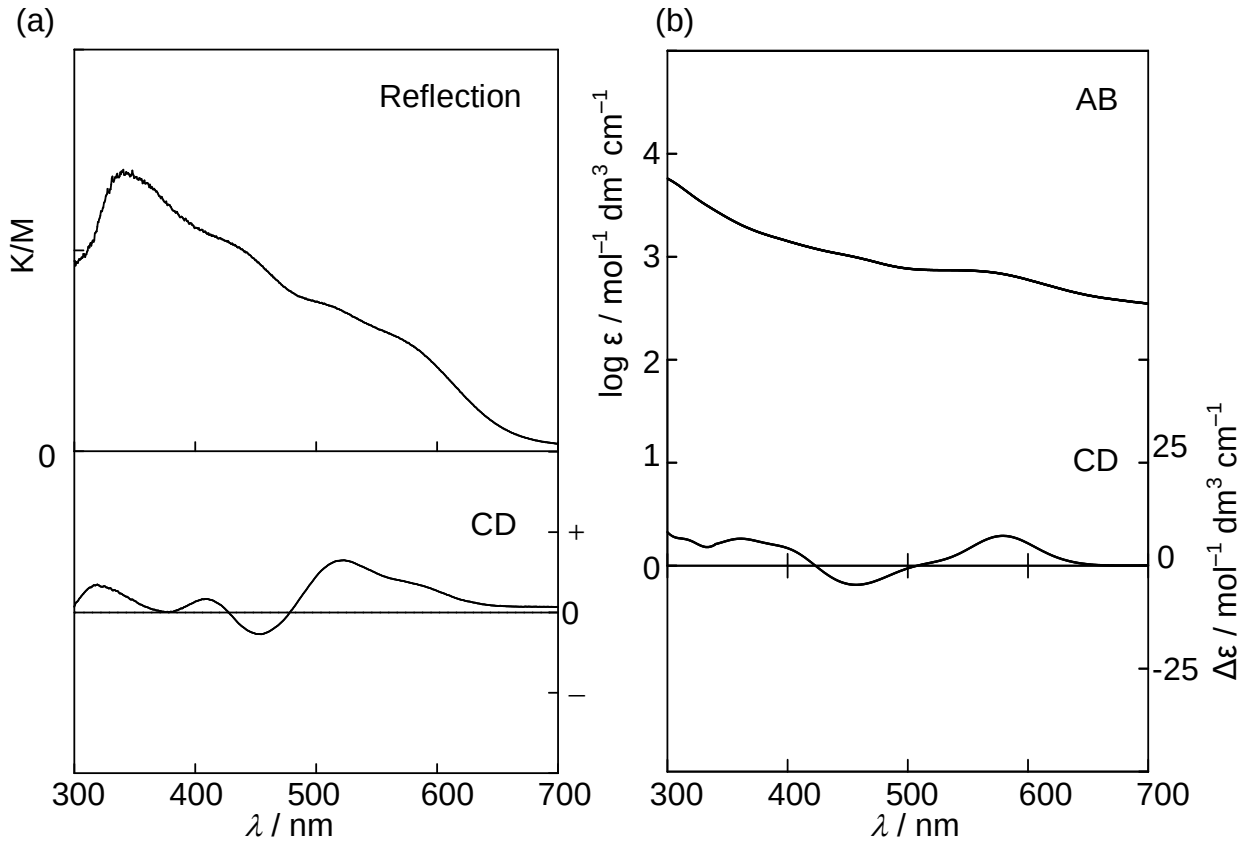

Figure 2-12. (a) Reflection and CD spectra of $(\Lambda_{LLL})_2$-[Co(en)$_3$][**1**] in the solid state. (b) Absorption and CD spectra of $(\Lambda_{LLL})_2$-[Co(en)$_3$][**1**] in a $NaNO_3$ aqueous solution. For reflection spectrum [λ / nm]: 572, 436, 340; CD spectrum [λ / nm]: 520 (+), 450 (–), 410 (+), 375 (+), 320 (+). For absorption spectrum [λ / nm (log ε / mol^{-1} dm^3 cm^{-1})]: 573 (2.84), 443 (3.02); CD spectrum [λ / nm ($\Delta\varepsilon$ / mol^{-1} dm^3 cm^{-1})]: 579 (+2.79), 457 (–1.85), 360 (+3.09).

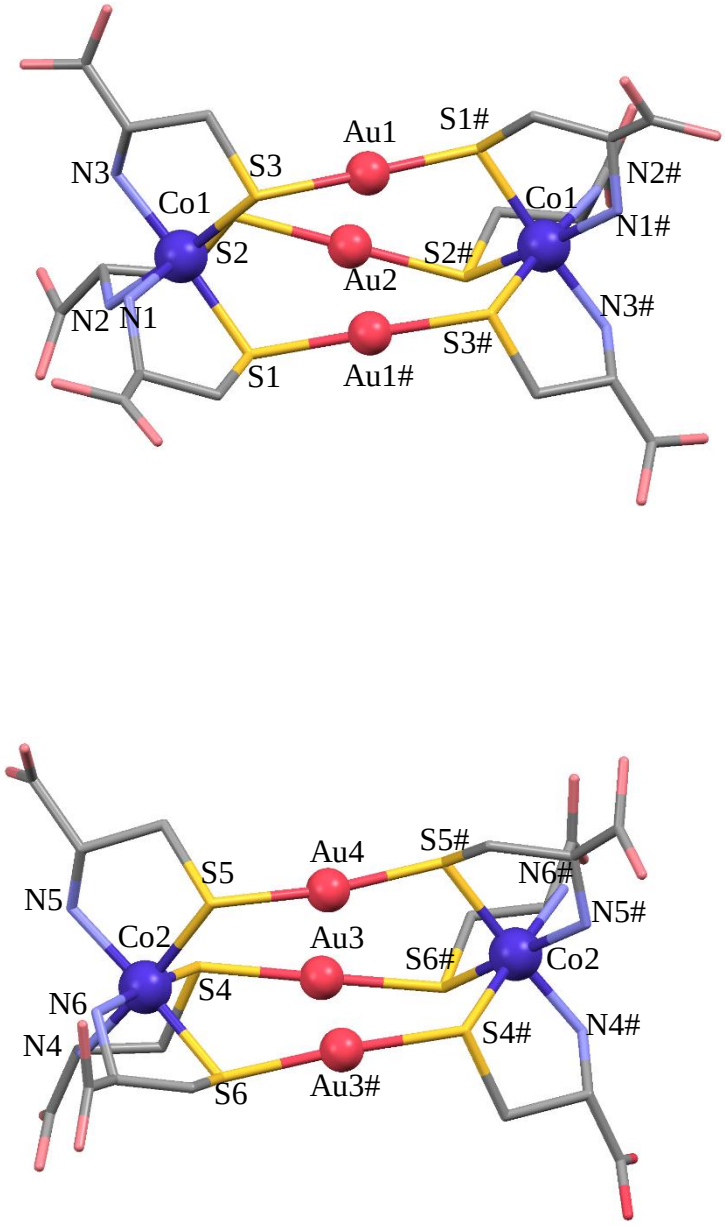

Figure 2-13. Perspective views of $(\Delta_{LLL})_2$-$[\mathbf{1}]^{3-}$ in $(\Delta_{LLL})_2$-$K_3[\mathbf{1}]\cdot 7.5H_2O$ with the atomic labeling scheme. Symmetry code: (#) x,–y+1,–z+1.

(a)

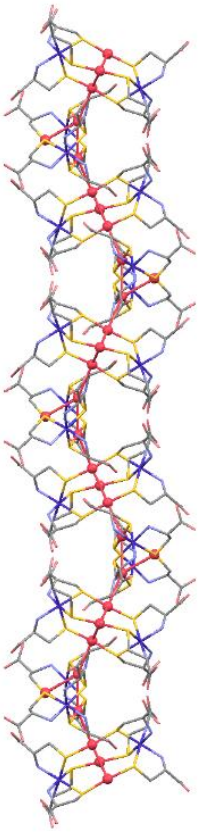

(b)

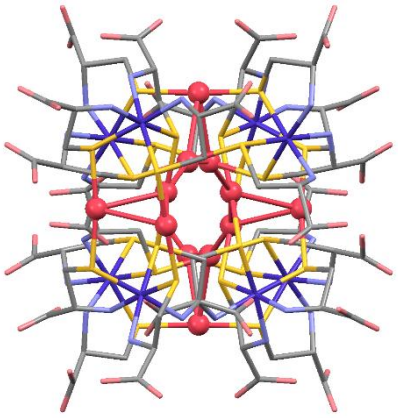

Figure 2-14. Perspective views of a right-handed helical chain structures of $(\Delta_{LLL})_2$-K_3[**1**] (a) along *a* axis and (b) along *c* axis.

(a)

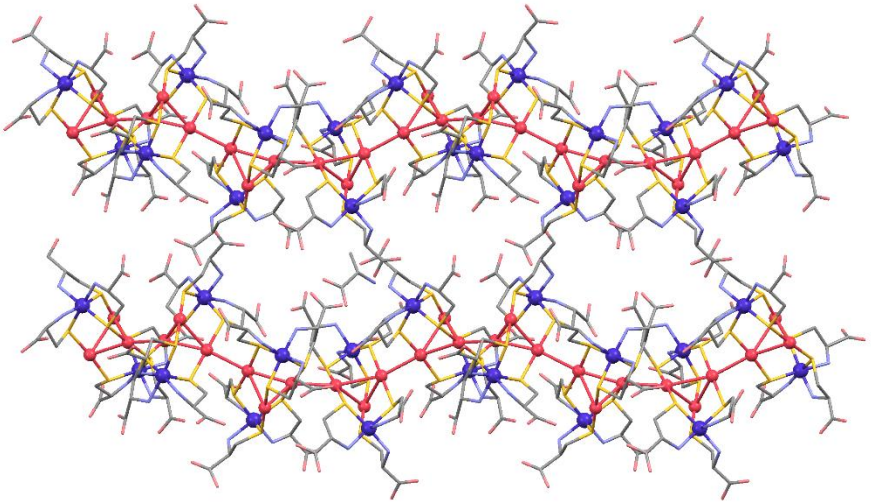

(b)

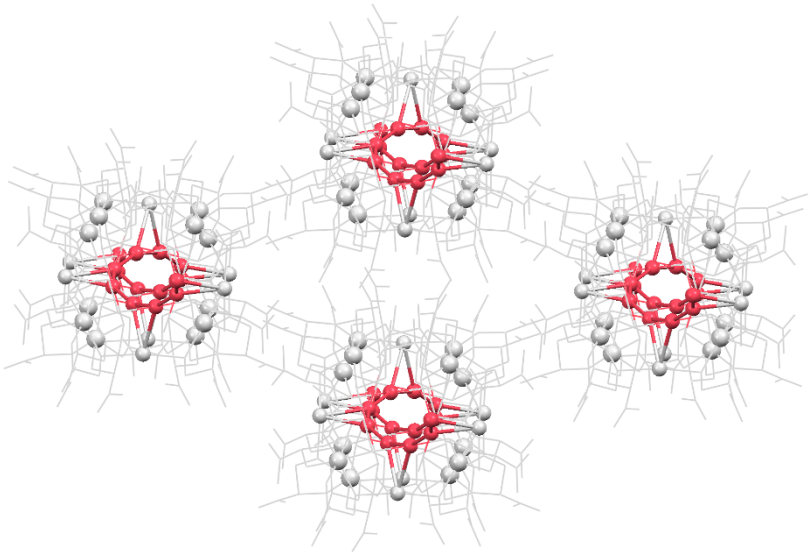

Figure 2-15. Packing structure of $(\Delta_{LLL})_2$-K_3[**1**] (a) along *b* axis and (b) along *c* axis.

(a)

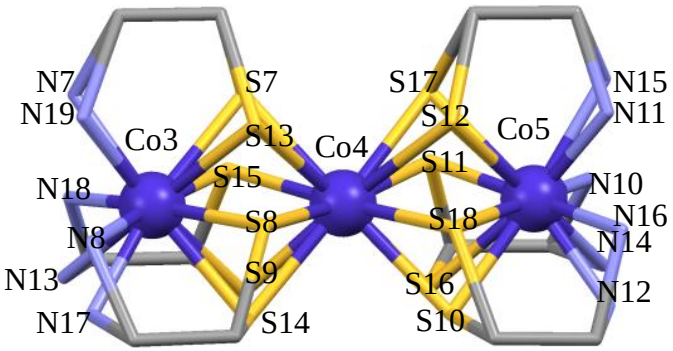

(b)

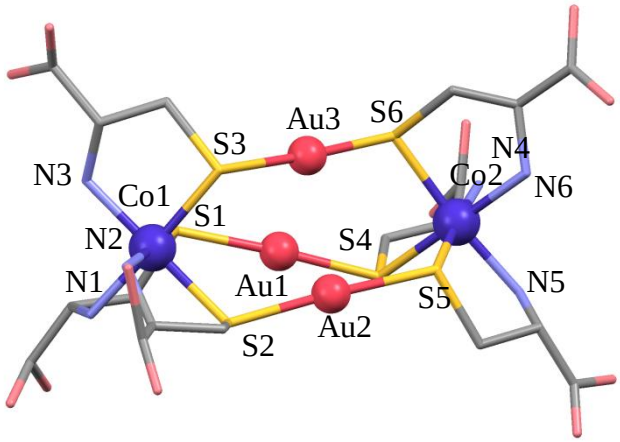

Figure 2-16. Perspective views of (a) $[Co_3(aet)_6]^{3+}$ and (b) $[\mathbf{1}]^{3-}$ in $(\Delta_{LLL})_2$-$[Co_3(aet)_6][\mathbf{1}]$ with the labeling scheme. Hydrogen atoms are omitted for clarity.

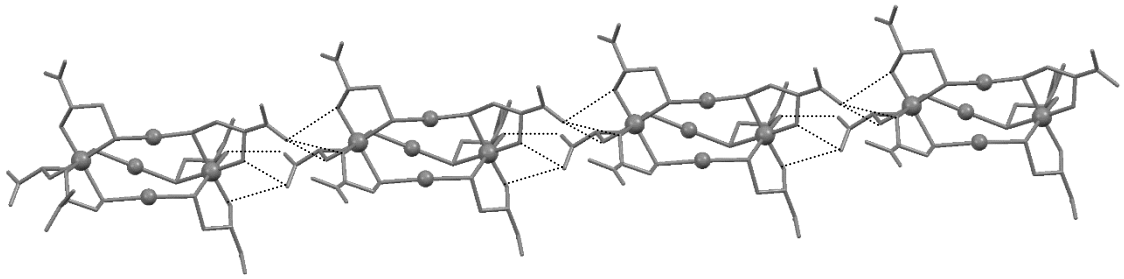

Figure 2-17. 1D chain structure composed of the complex-anions in $(\Delta_{LLL})_2$-$[Co_3(aet)_6][\mathbf{1}]$. Dashed line represents hydrogen bonds.

(a)

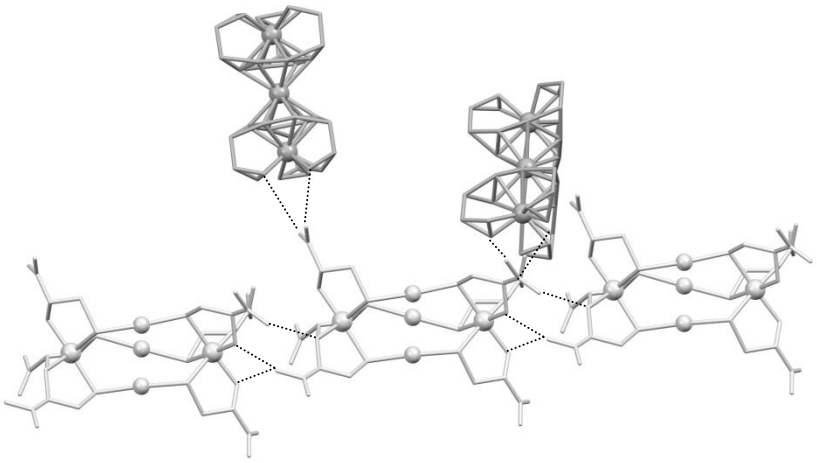

(b)

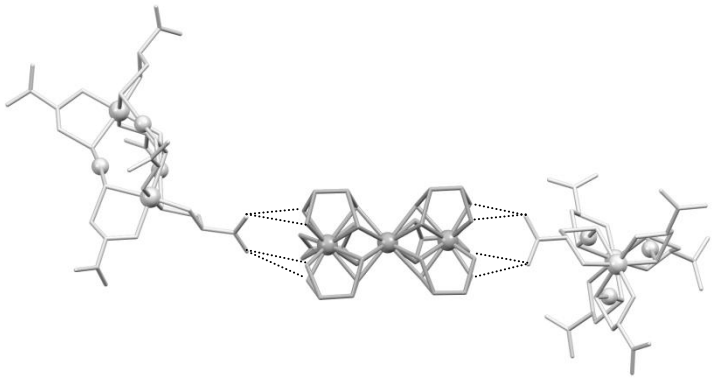

Figure 2-18. Perspective view of intermolecular interactions (a) around each complex-anion and (b) around each complex-cation in $(\Delta_{LLL})_2$-$[Co_3(aet)_6]$[**1**].

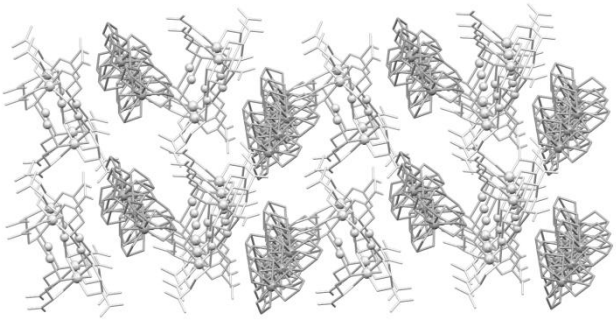

Figure 2-19. Crystal structure of $(\Delta_{LLL})_2$-$[Co_3(aet)_6]$[**1**] viewing from *a* axis. Dark gray and light gray molecules represent complex-cation and complex-anion, respectively.

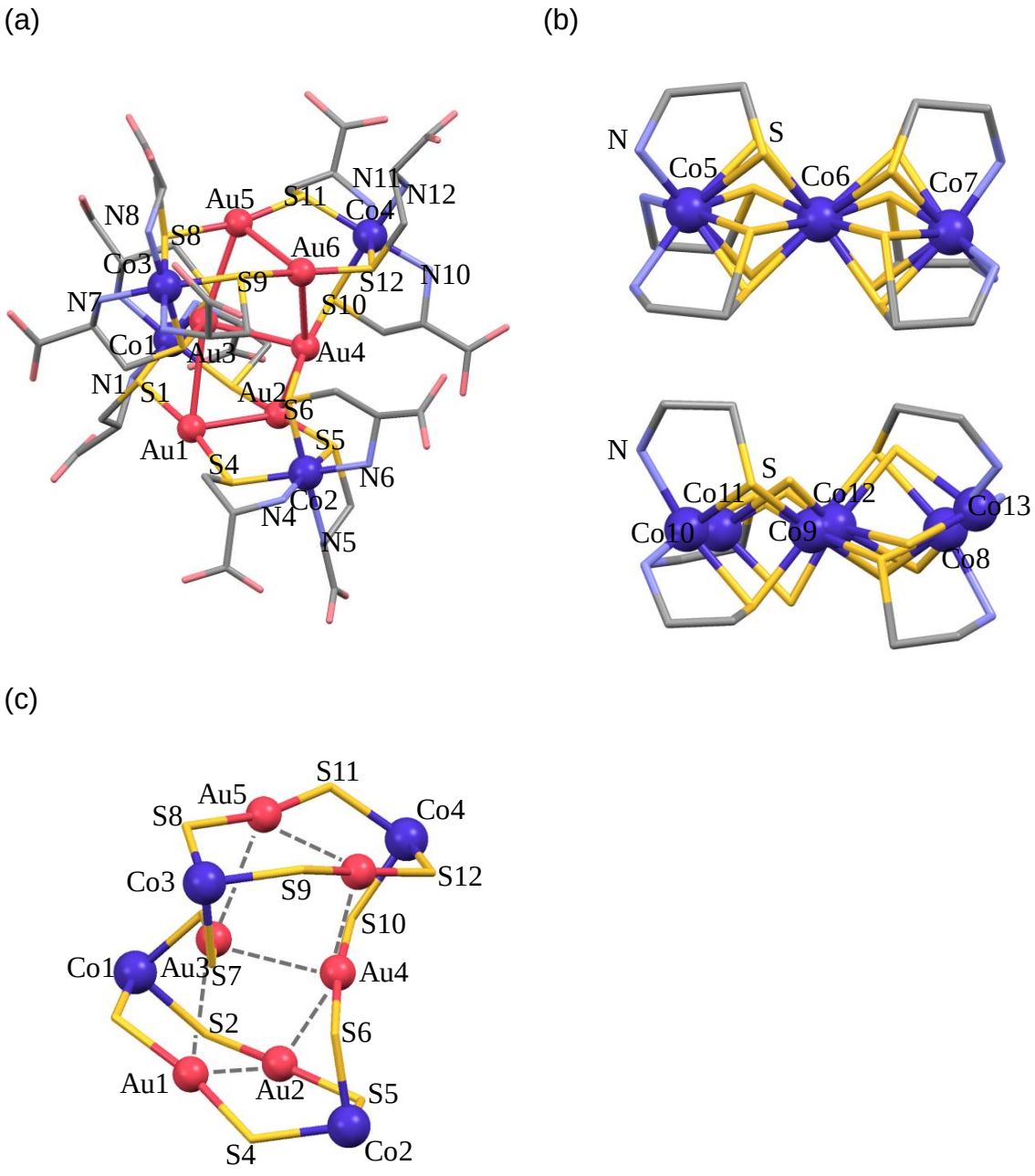

Figure 2-20. Crystal structural description of (a) complex-anion, (b) complex-cations, and (c) intramolecular aurophilic interactions in $(\Lambda_{LLL})_4$-$[Co_3(aet)_6]_2$[**2**].

(a)

(b)

Figure 2-21. Perspective view of wave-like 2D structure composed of complex-anions in $(\Lambda_{LLL})_4$-$[Co_3(aet)_6]_2$[**2**] viewing from (a) *a* axis and (b) *c* axis.

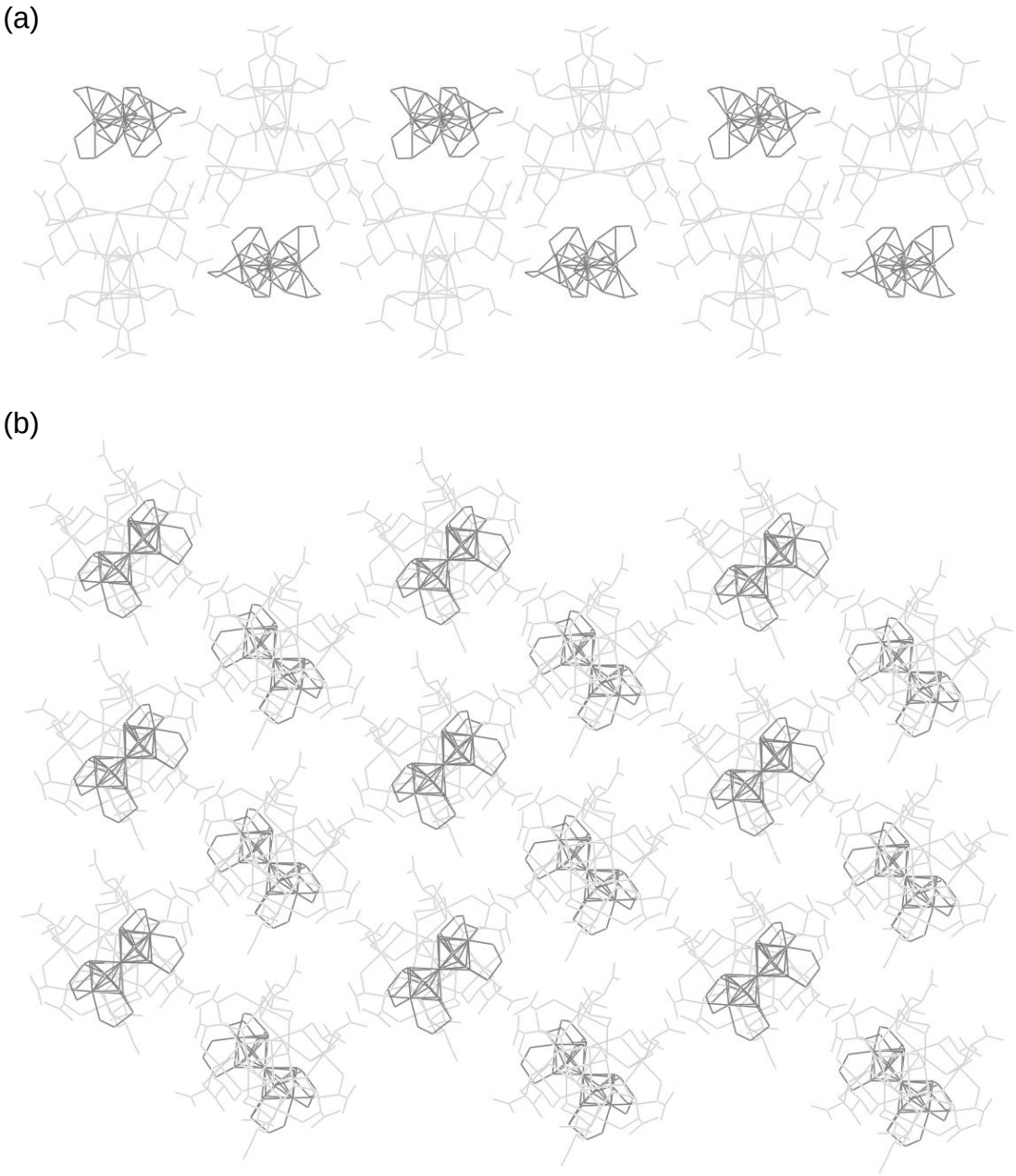

Figure 2-22. Perspective views of 2D sheet-like structure composed of complex-anions and complex-cations in $(\Lambda_{LLL})_4$-$[Co_3(aet)_6]_2$[**2**] viewing from (a) *a* axis and (b) *c* axis. Dark gray and light gray molecules represent complex-cation and complex-anion, respectively.

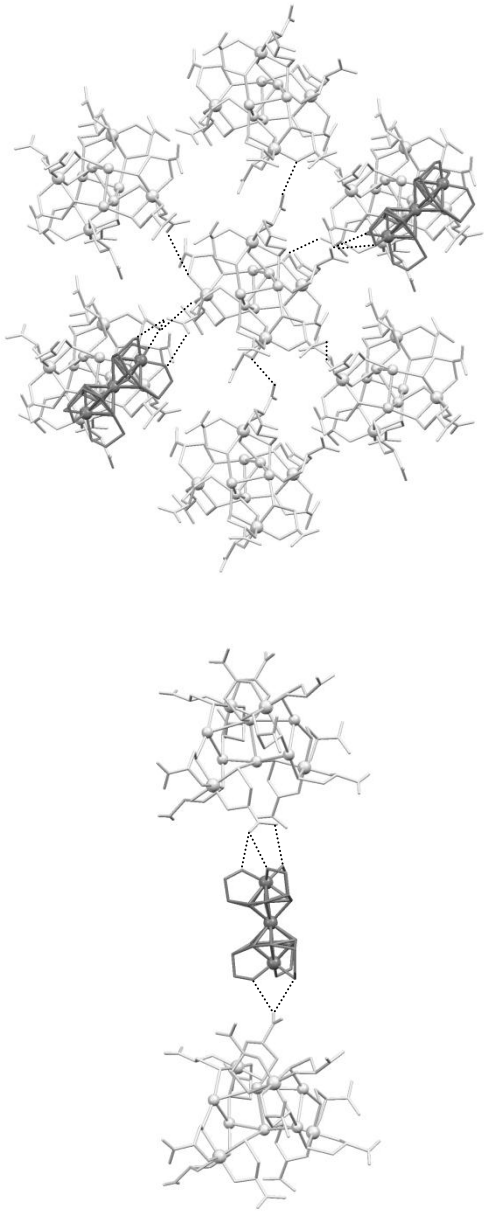

Figure 2-23. Perspective views of intermolecular interactions (a) around each complex-anion and (b) around each complex-cation in $(\Lambda_{LLL})_4$-$[Co_3(aet)_6]_2$[**2**]. Dark gray and light gray molecules represent complex-cation and complex-anion, respectively.

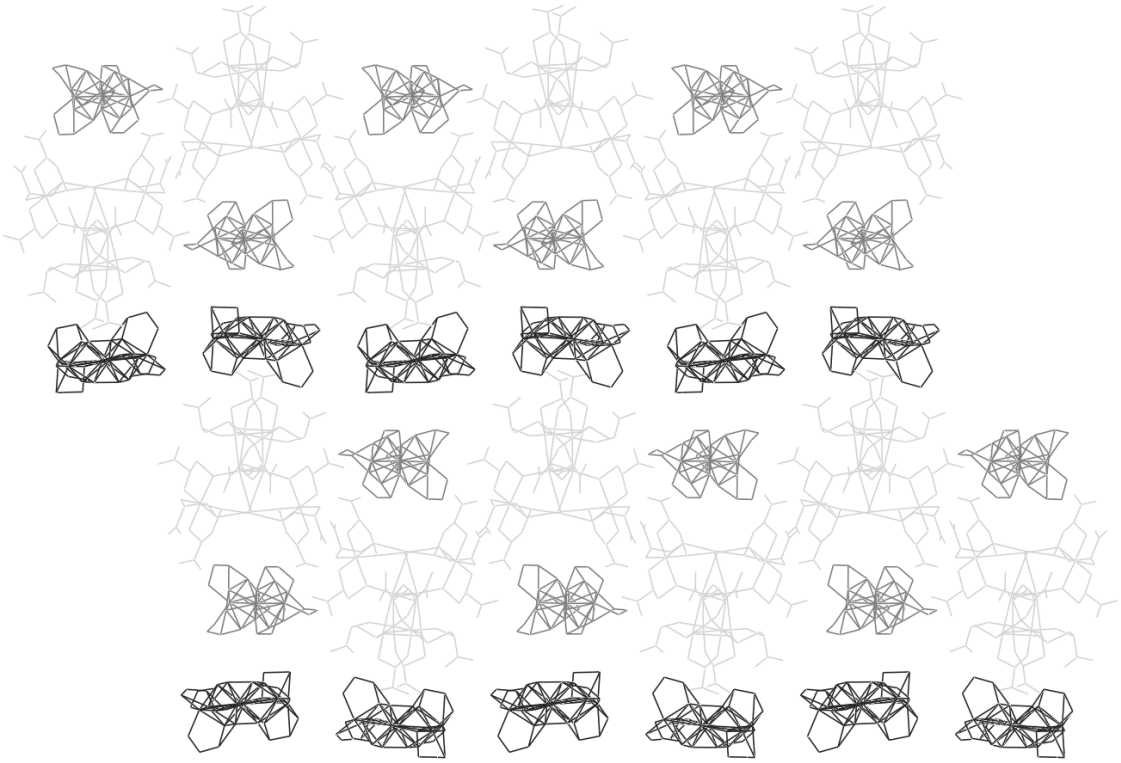

Figure 2-24. Packing structure of $(\Lambda_{LLL})_4$-$[Co_3(aet)_6]$[**2**] viewing from *a* axis. Dark gray, gray, and light gray molecules represent complex-cation forming no significant intermolecular interactions, complex-cation forming intermolecular hydrogen bonds, and complex-anion, respectively.

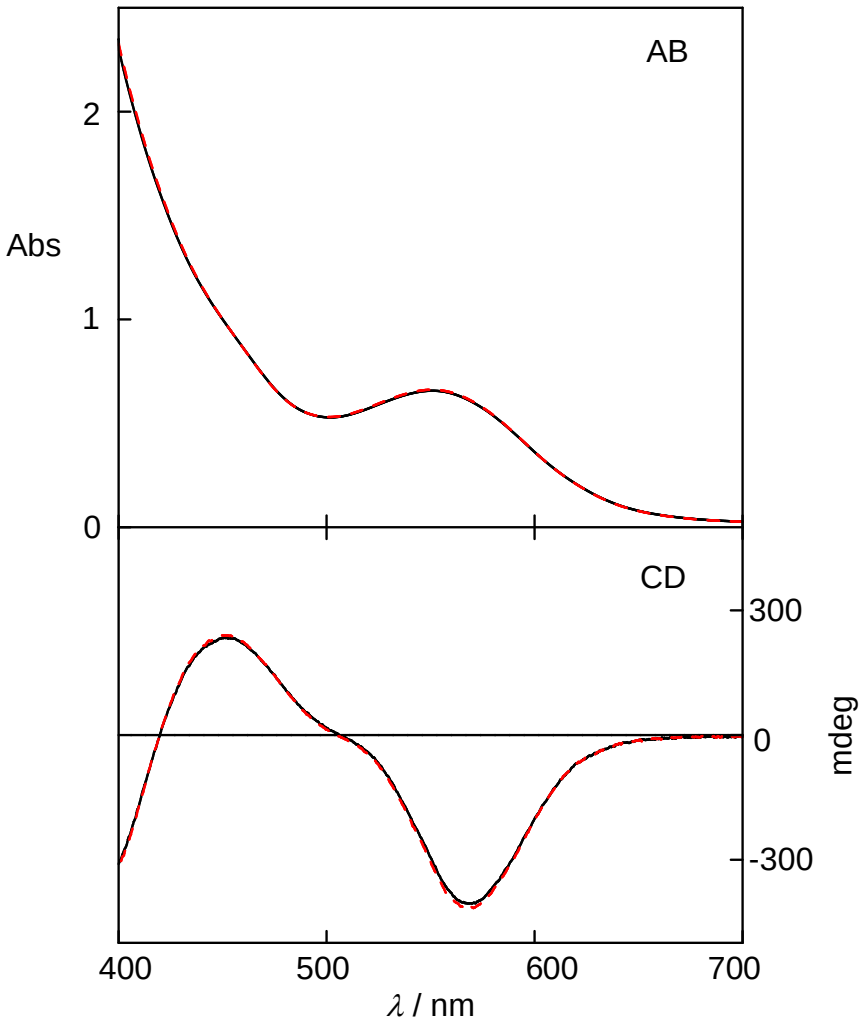

Figure 2-25. Absorption and CD spectral change of $(\Delta_{LLL})_2$-[**1**]$^{3-}$ in water (pH 7). The mixture was stood at room temperature for 1 week. Start (—) and after 1 week (---).

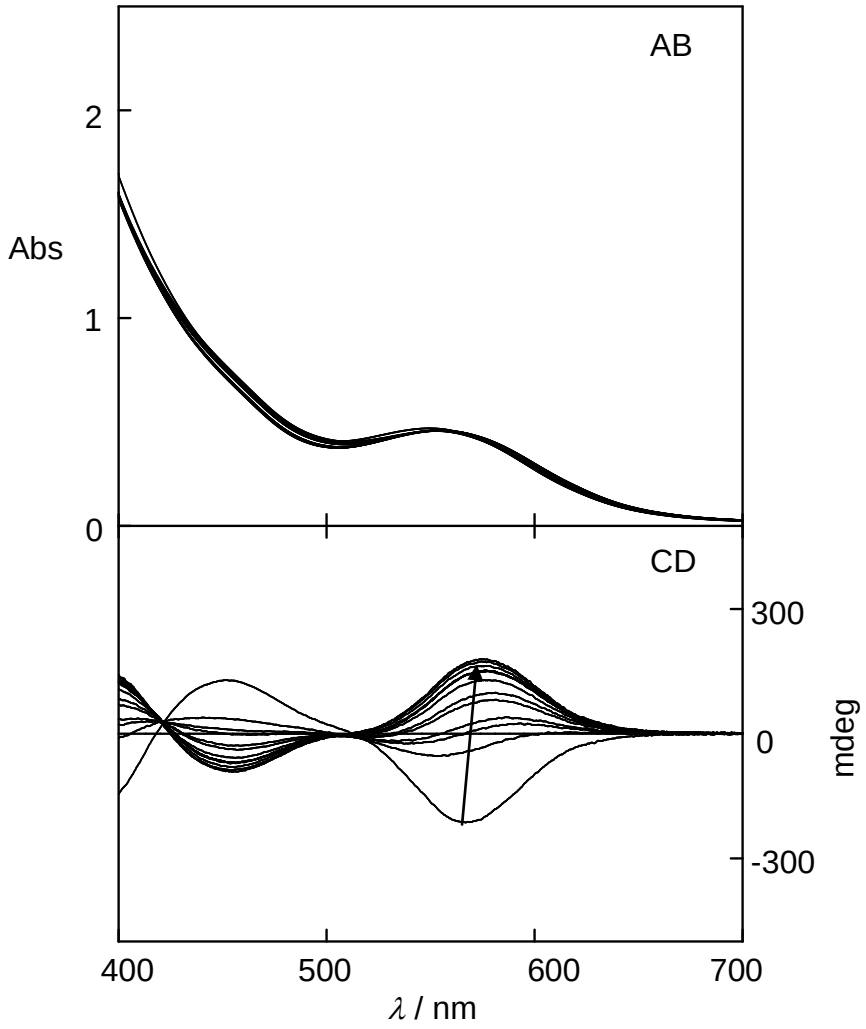

Figure 2-26. Absorption and CD spectral change of $(\Delta_{LLL})_2$-[**1**]$^{3-}$ in a basic aqueous solution (pH 9). The mixture was stood at room temperature for 1 week.

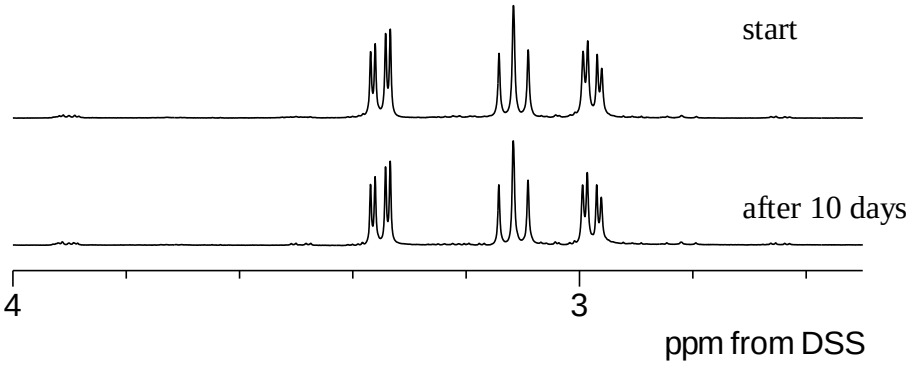

Figure 2-27. The ^{1}H NMR spectral change of $(\Delta_{LLL})_2$-[**1**]$^{3-}$ in a neutral aqueous solution (pH 7).

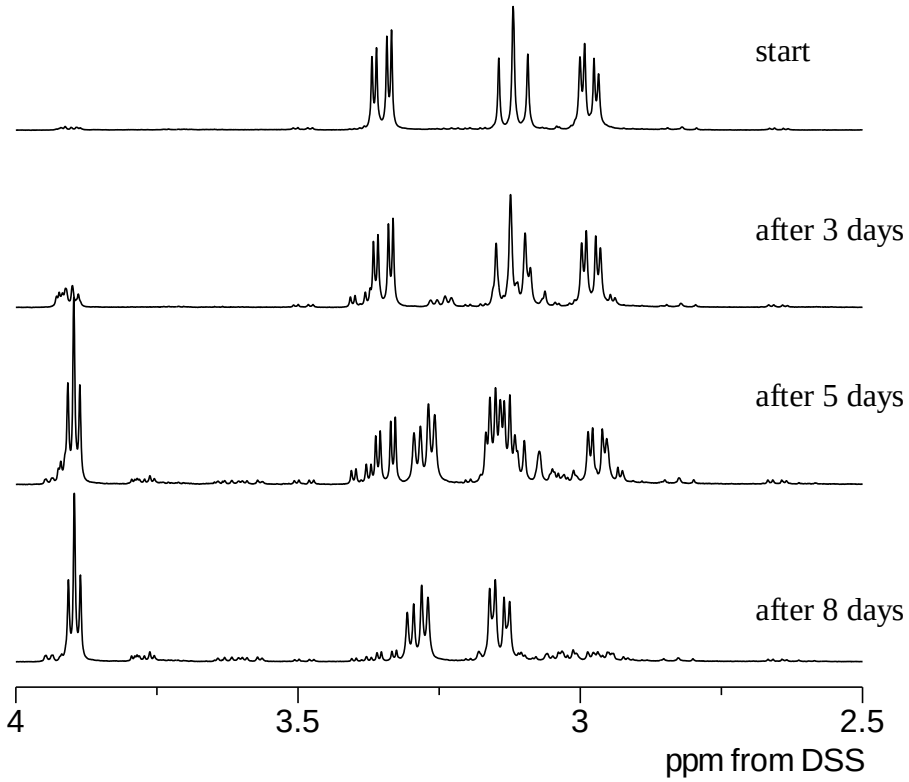

Figure 2-28. The ^{1}H NMR spectral change of $(\Delta_{LLL})_2$-[**1**]$^{3-}$ in a basic aqueous solution (pH 9).

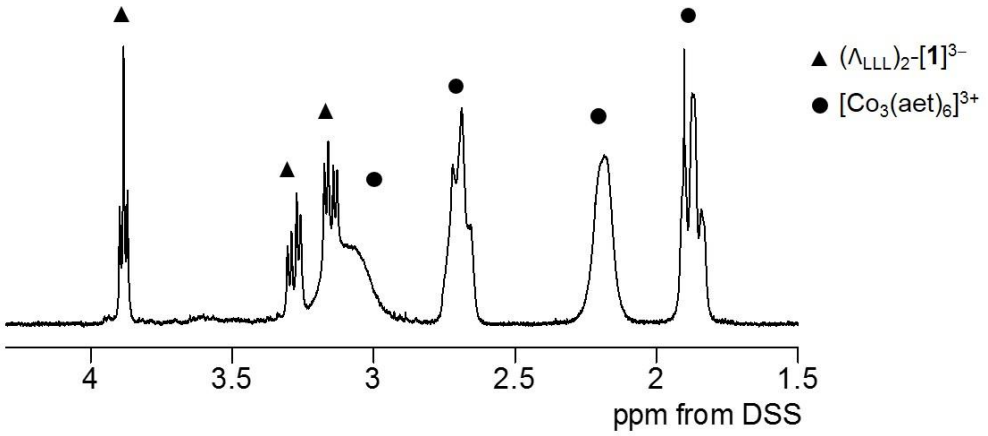

Figure 2-29. ^{1}H NMR spectrum of the mixture of $(\Lambda_{LLL})_2$-[**1**]$^{3-}$ and $[Co_3(aet)_6]^{3+}$ in D_2O.

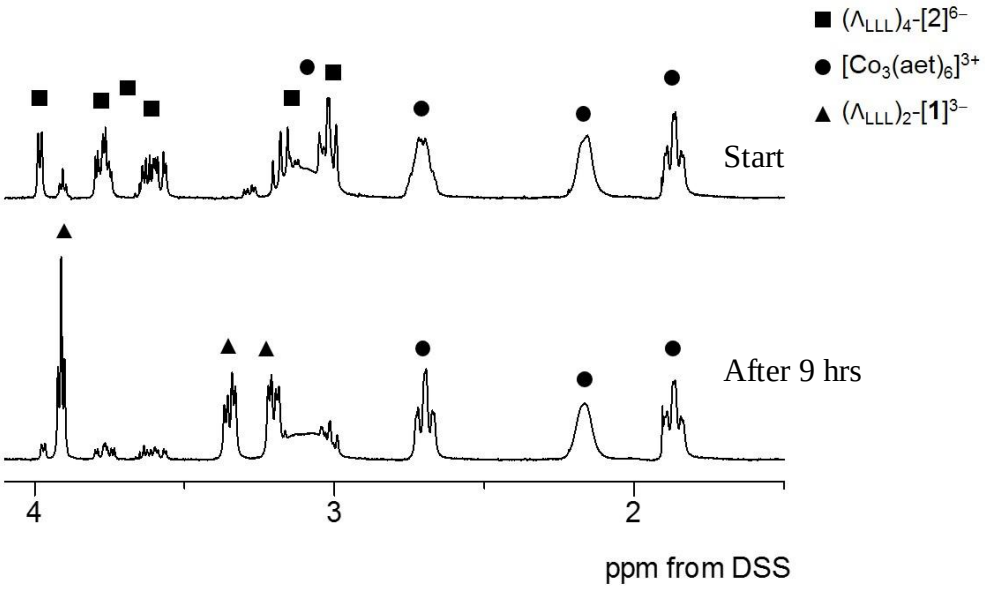

Figure 2-30. The ^{1}H NMR spectral change of $(\Lambda_{LLL})_4$-$[Co_3(aet)_6]_2$[**2**] in a $NaNO_3$ aqueous D_2O solution.

Table 2-1. Crystallographic data of complexes.

	$(\Delta_{LLL})_2$-K_3[**1**]·7.5H_2O	$(\Delta_{LLL})_2$-[$Co_3(aet)_6$][**1**]·18H_2O	$(\Lambda_{LLL})_4$-[$Co_3(aet)_6$]$_2$[**2**]·20H_2O
Empirical formula	$C_{18}H_{45}Au_3Co_2K_3N_6O_{19.5}S_6$	$C_{30}H_{102}Au_3Co_5N_{12}O_{30}S_{12}$	$C_{60}H_{172}Au_6Co_{10}N_{24}O_{44}S_{24}$
Formula weight	1676.02	2381.51	4474.76
Crystal system	Orthorhombic	Monoclinic	Orthorhombic
Space group	$C222_1$	$P2_1$	$P2_12_12_1$
a / Å	14.0324(16)	12.6999(3)	14.2119(14)
b / Å	27.535(3)	26.2905(6)	22.117(2)
c / Å	21.739(3)	12.9054(3)	52.158(5)
β / °		114.946(8)	
V / Å^3	8399.5(17)	3906.94(16)	6394(3)
Z	8	2	4
T / K	200(2)	200(2)	200(2)
I(int)	0.1531	0.1531	0.0600
ρ_{calcd} / g cm^{-3}	2.651	2.024	1.813
μ(Mo $K\alpha$) / cm^{-1}	11.891	7.041	6.699
θ_{Max}	54.96	54.96	54.98
Total no. of data	33491	30845	107851
No. of unique data	9623	16779	36933
No. of parameters	289	725	841
R1, wR2 (I>2σ(I))[a,b]	0.1005, 0.1688	0.0479, 0.1261	0.0885, 0.2318
R1, wR2 (all data)[a,b]	0.1757, 0.1921	0.0507, 0.1294	0.1089, 0.2387

a) $R1 = \Sigma|(|F_o| - |F_c|)|/\Sigma(|F_o|)$. b) $wR2 = \{\Sigma w(|F_o| - |F_c|)^2/\Sigma w(|F_o|)^2\}^{1/2}$.

Table 2-2. Selected bond distances and angles of $(\Delta_{LLL})_2$-K_3[**1**].

Bond distances (Å)			
Au(1)-S(1)	2.312(6)	Au(4)-Au(3)#2	2.9848(16)
Au(1)-S(3)#1	2.313(7)	Co(2)-N(4)	1.951(19)
Au(1)-Au(2)	2.9642(16)	Co(2)-N(6)	2.04(2)
Au(1)-Au(3)	2.9847(14)	Co(2)-N(5)	2.06(2)
Au(1)-Au(1)#1	2.996(2)	Co(2)-S(4)	2.216(8)
Au(2)-S(2)#1	2.282(8)	Co(2)-S(6)	2.255(8)
Au(2)-S(2)	2.282(8)	Co(2)-S(5)	2.257(9)
Au(2)-Au(1)#1	2.9642(16)	Au(3)-S(6)#2	2.317(7)
Co(1)-N(2)	1.97(2)	Au(3)-S(4)	2.328(6)
Co(1)-N(3)	1.975(19)	Au(3)-Au(3)#2	2.961(2)
Co(1)-N(1)	2.016(18)	Au(3)-Au(4)	2.9848(16)
Co(1)-S(1)	2.245(7)	Au(4)-S(5)#2	2.296(7)
Co(1)-S(2)	2.251(8)	Au(4)-S(5)	2.296(7)
Co(1)-S(3)	2.258(7)	Au(4)-Au(3)#2	2.9848(16)
Au(3)-S(6)#2	2.317(7)	Co(2)-N(4)	1.951(19)
Au(3)-S(4)	2.328(6)	Co(2)-N(6)	2.04(2)
Au(3)-Au(3)#2	2.961(2)	Co(2)-N(5)	2.06(2)
Au(3)-Au(4)	2.9848(16)	Co(2)-S(4)	2.216(8)
Au(4)-S(5)#2	2.296(7)	Co(2)-S(6)	2.255(8)
Au(4)-S(5)	2.296(7)	Co(2)-S(5)	2.257(9)

Angles (°)			
S(1)-Au(1)-S(3)#1	179.0(2)	N(1)-Co(1)-S(2)	174.4(6)
S(2)#1-Au(2)-S(2)	176.6(4)	S(1)-Co(1)-S(2)	91.0(3)
S(2)-Au(2)-Au(1)#1	83.56(18)	N(2)-Co(1)-S(3)	176.0(7)
S(6)#2-Au(3)-S(4)	174.6(2)	N(3)-Co(1)-S(3)	88.0(6)
S(5)#2-Au(4)-S(5)	172.1(4)	N(1)-Co(1)-S(3)	92.0(6)
S(5)-Au(4)-Au(3)#2	87.9(2)	S(1)-Co(1)-S(3)	93.4(3)
N(2)-Co(1)-N(3)	88.5(8)	S(2)-Co(1)-S(3)	93.5(3)
N(2)-Co(1)-N(1)	86.0(8)	N(4)-Co(2)-N(6)	90.6(9)
N(3)-Co(1)-N(1)	89.1(8)	N(4)-Co(2)-N(5)	87.2(8)
N(2)-Co(1)-S(1)	90.0(7)	N(6)-Co(2)-N(5)	92.7(9)
N(3)-Co(1)-S(1)	176.6(6)	N(4)-Co(2)-S(4)	86.5(6)
N(1)-Co(1)-S(1)	87.8(6)	N(6)-Co(2)-S(4)	176.4(7)
N(2)-Co(1)-S(2)	88.5(6)	N(5)-Co(2)-S(4)	89.4(6)
N(3)-Co(1)-S(2)	92.0(6)	N(4)-Co(2)-S(6)	90.7(6)

Table 2-2. (continued)

N(6)-Co(2)-S(6)	84.7(7)	N(5)-Co(2)-S(5)	88.1(6)
N(5)-Co(2)-S(6)	176.6(7)	N(6)-Co(2)-S(5)	89.8(7)
S(4)-Co(2)-S(6)	93.1(3)	S(4)-Co(2)-S(5)	93.3(3)
N(4)-Co(2)-S(5)	175.3(7)	S(6)-Co(2)-S(5)	94.0(3)

Symmetry codes: (#1) –x,y,–z+3/2, (#2) x,–y+1,–z+1.

Table 2-3. Selected bond distances and angles of $(\Delta_{LLL})_2$-$[Co_3(aet)_6]$[**1**].

Bond distances (Å)			
Au(1)-S(4)	2.2905(8)	Co(3)-S(15)	2.2204(15)
Au(1)-S(1)	2.2919(7)	Co(3)-S(7)	2.260(2)
Au(1)-Au(3)	2.96699(17)	Co(3)-S(8)	2.279(2)
Au(1)-Au(2)	2.9737(2)	Co(3)-S(9)	2.2795(19)
Au(2)-S(5)	2.2846(7)	Co(4)-S(9)	2.182(2)
Au(2)-S(2)	2.2908(7)	Co(4)-S(7)	2.223(2)
Au(2)-Au(3)	2.9854(2)	Co(4)-S(18)	2.2279(16)
Au(3)-S(6)	2.2993(7)	Co(4)-S(17)	2.2353(15)
Au(3)-S(3)	2.3038(7)	Co(4)-S(16)	2.2524(13)
Co(1)-N(3)	1.981(3)	Co(4)-S(8)	2.255(2)
Co(1)-N(2)	2.000(3)	Co(4)-S(13)	2.2733(15)
Co(1)-N(1)	2.007(2)	Co(4)-S(11)	2.284(2)
Co(1)-S(1)	2.2457(10)	Co(4)-S(14)	2.2919(15)
Co(1)-S(2)	2.2557(10)	Co(4)-S(10)	2.301(2)
Co(1)-S(3)	2.2578(8)	Co(4)-S(15)	2.3026(17)
Co(2)-N(6)	1.976(2)	Co(4)-S(12)	2.312(2)
Co(2)-N(4)	2.001(3)	Co(5)-N(11)	1.902(5)
Co(2)-N(5)	2.008(3)	Co(5)-N(12)	1.953(5)
Co(2)-S(5)	2.2549(10)	Co(5)-N(16)	1.959(6)
Co(2)-S(4)	2.2579(8)	Co(5)-N(10)	1.997(6)
Co(2)-S(6)	2.2780(9)	Co(5)-N(14)	2.031(8)
Co(3)-N(19)	1.945(7)	Co(5)-N(15)	2.075(7)
Co(3)-N(18)	1.961(10)	Co(5)-S(11)	2.156(2)
Co(3)-N(7)	2.005(6)	Co(5)-S(10)	2.190(2)
Co(3)-N(8)	2.005(5)	Co(5)-S(18)	2.2197(14)
Co(3)-N(17)	2.013(7)	Co(5)-S(17)	2.2587(15)
Co(3)-N(13)	2.036(6)	Co(5)-S(12)	2.261(2)
Co(3)-S(14)	2.2083(15)	Co(5)-S(16)	2.2865(13)
Co(3)-S(13)	2.2186(18)		

Angles (°)			
S(4)-Au(1)-S(1)	174.80(3)	N(2)-Co(1)-N(1)	89.47(11)
S(5)-Au(2)-S(2)	176.22(3)	N(3)-Co(1)-S(1)	88.63(9)
S(6)-Au(3)-S(3)	177.16(3)	N(2)-Co(1)-S(1)	175.90(7)
N(3)-Co(1)-N(2)	90.48(12)	N(1)-Co(1)-S(1)	86.55(8)
N(3)-Co(1)-N(1)	91.34(11)	N(3)-Co(1)-S(2)	175.97(9)

Table 2-3. (continued)

N(2)-Co(1)-S(2)	85.85(9)	N(17)-Co(3)-N(13)	60.8(2)
N(1)-Co(1)-S(2)	90.30(9)	N(19)-Co(3)-S(14)	143.7(2)
S(1)-Co(1)-S(2)	95.15(3)	N(18)-Co(3)-S(14)	120.7(2)
N(3)-Co(1)-S(3)	86.42(7)	N(7)-Co(3)-S(14)	173.37(19)
N(2)-Co(1)-S(3)	91.14(8)	N(8)-Co(3)-S(14)	90.39(16)
N(1)-Co(1)-S(3)	177.68(9)	N(17)-Co(3)-S(14)	68.9(2)
S(1)-Co(1)-S(3)	92.80(3)	N(13)-Co(3)-S(14)	93.65(16)
S(2)-Co(1)-S(3)	91.98(3)	N(19)-Co(3)-S(13)	75.7(3)
N(6)-Co(2)-N(4)	90.48(10)	N(18)-Co(3)-S(13)	140.9(2)
N(6)-Co(2)-N(5)	88.27(11)	N(7)-Co(3)-S(13)	87.91(19)
N(4)-Co(2)-N(5)	89.19(12)	N(8)-Co(3)-S(13)	93.09(16)
N(6)-Co(2)-S(5)	89.83(9)	N(17)-Co(3)-S(13)	123.6(2)
N(4)-Co(2)-S(5)	176.12(8)	N(13)-Co(3)-S(13)	174.61(16)
N(5)-Co(2)-S(5)	86.96(10)	S(14)-Co(3)-S(13)	85.58(6)
N(6)-Co(2)-S(4)	176.99(9)	N(19)-Co(3)-S(15)	122.4(2)
N(4)-Co(2)-S(4)	86.55(7)	N(18)-Co(3)-S(15)	69.8(3)
N(5)-Co(2)-S(4)	91.19(8)	N(7)-Co(3)-S(15)	94.87(18)
S(5)-Co(2)-S(4)	93.10(3)	N(8)-Co(3)-S(15)	176.09(18)
N(6)-Co(2)-S(6)	85.80(8)	N(17)-Co(3)-S(15)	137.92(16)
N(4)-Co(2)-S(6)	90.02(8)	N(13)-Co(3)-S(15)	89.24(16)
N(5)-Co(2)-S(6)	174.01(8)	S(14)-Co(3)-S(15)	85.90(6)
S(5)-Co(2)-S(6)	93.86(3)	S(13)-Co(3)-S(15)	85.39(6)
S(4)-Co(2)-S(6)	94.69(3)	N(19)-Co(3)-S(7)	90.0(2)
N(19)-Co(3)-N(18)	92.2(4)	N(18)-Co(3)-S(7)	94.1(3)
N(19)-Co(3)-N(7)	32.1(3)	N(7)-Co(3)-S(7)	75.3(2)
N(18)-Co(3)-N(7)	65.5(3)	N(8)-Co(3)-S(7)	139.11(14)
N(19)-Co(3)-N(8)	60.5(3)	N(17)-Co(3)-S(7)	169.5(2)
N(18)-Co(3)-N(8)	113.3(3)	N(13)-Co(3)-S(7)	125.34(17)
N(7)-Co(3)-N(8)	88.7(2)	S(14)-Co(3)-S(7)	101.34(7)
N(19)-Co(3)-N(17)	96.0(3)	S(13)-Co(3)-S(7)	49.81(7)
N(18)-Co(3)-N(17)	94.2(3)	S(15)-Co(3)-S(7)	41.00(6)
N(7)-Co(3)-N(17)	114.1(3)	N(19)-Co(3)-S(8)	97.5(3)
N(8)-Co(3)-N(17)	40.9(2)	N(18)-Co(3)-S(8)	169.9(3)
N(19)-Co(3)-N(13)	107.7(3)	N(7)-Co(3)-S(8)	122.56(18)
N(18)-Co(3)-N(13)	36.2(3)	N(8)-Co(3)-S(8)	74.38(18)
N(7)-Co(3)-N(13)	92.9(2)	N(17)-Co(3)-S(8)	87.7(2)
N(8)-Co(3)-N(13)	92.3(2)	N(13)-Co(3)-S(8)	140.88(16)

Table 2-3. (continued)

S(14)-Co(3)-S(8)	50.95(6)	S(7)-Co(4)-S(11)	92.90(8)
S(13)-Co(3)-S(8)	40.75(6)	S(18)-Co(4)-S(11)	97.51(7)
S(15)-Co(3)-S(8)	102.23(7)	S(17)-Co(4)-S(11)	37.62(5)
S(7)-Co(3)-S(8)	83.01(8)	S(16)-Co(4)-S(11)	50.38(5)
N(19)-Co(3)-S(9)	172.2(2)	S(8)-Co(4)-S(11)	171.28(7)
N(18)-Co(3)-S(9)	87.6(3)	S(13)-Co(4)-S(11)	133.00(6)
N(7)-Co(3)-S(9)	142.97(18)	S(9)-Co(4)-S(14)	40.24(7)
N(8)-Co(3)-S(9)	126.58(15)	S(7)-Co(4)-S(14)	99.89(7)
N(17)-Co(3)-S(9)	91.82(18)	S(18)-Co(4)-S(14)	99.93(5)
N(13)-Co(3)-S(9)	76.53(17)	S(17)-Co(4)-S(14)	174.47(6)
S(14)-Co(3)-S(9)	40.17(7)	S(16)-Co(4)-S(14)	94.64(5)
S(13)-Co(3)-S(9)	99.63(7)	S(8)-Co(4)-S(14)	50.26(6)
S(15)-Co(3)-S(9)	50.35(6)	S(13)-Co(4)-S(14)	82.41(5)
S(7)-Co(3)-S(9)	82.19(7)	S(11)-Co(4)-S(14)	138.45(5)
S(8)-Co(3)-S(9)	82.43(8)	S(9)-Co(4)-S(10)	94.44(8)
S(9)-Co(4)-S(7)	85.27(8)	S(7)-Co(4)-S(10)	175.34(7)
S(9)-Co(4)-S(18)	132.60(7)	S(18)-Co(4)-S(10)	46.34(6)
S(7)-Co(4)-S(18)	136.13(6)	S(17)-Co(4)-S(10)	99.34(7)
S(9)-Co(4)-S(17)	134.26(7)	S(16)-Co(4)-S(10)	42.63(6)
S(7)-Co(4)-S(17)	77.68(7)	S(8)-Co(4)-S(10)	100.22(7)
S(18)-Co(4)-S(17)	85.12(6)	S(13)-Co(4)-S(10)	134.90(6)
S(9)-Co(4)-S(16)	77.68(6)	S(11)-Co(4)-S(10)	82.62(7)
S(7)-Co(4)-S(16)	132.97(6)	S(14)-Co(4)-S(10)	82.76(6)
S(18)-Co(4)-S(16)	83.55(5)	S(9)-Co(4)-S(15)	50.47(7)
S(17)-Co(4)-S(16)	83.64(5)	S(7)-Co(4)-S(15)	40.54(6)
S(9)-Co(4)-S(8)	85.21(8)	S(18)-Co(4)-S(15)	176.60(4)
S(7)-Co(4)-S(8)	84.40(8)	S(17)-Co(4)-S(15)	92.95(6)
S(18)-Co(4)-S(8)	78.98(7)	S(16)-Co(4)-S(15)	99.04(5)
S(17)-Co(4)-S(8)	133.71(6)	S(8)-Co(4)-S(15)	100.46(7)
S(16)-Co(4)-S(8)	136.12(6)	S(13)-Co(4)-S(15)	82.26(6)
S(9)-Co(4)-S(13)	100.94(7)	S(11)-Co(4)-S(15)	82.57(7)
S(7)-Co(4)-S(13)	49.59(7)	S(14)-Co(4)-S(15)	82.11(6)
S(18)-Co(4)-S(13)	95.28(6)	S(10)-Co(4)-S(15)	136.91(6)
S(17)-Co(4)-S(13)	99.46(5)	S(9)-Co(4)-S(12)	173.52(8)
S(16)-Co(4)-S(13)	176.60(5)	S(7)-Co(4)-S(12)	99.64(7)
S(8)-Co(4)-S(13)	40.49(6)	S(18)-Co(4)-S(12)	41.19(6)
S(9)-Co(4)-S(11)	102.86(7)	S(17)-Co(4)-S(12)	51.57(7)

Table 2-3. (continued)

S(16)-Co(4)-S(12)	101.65(7)	N(16)-Co(5)-S(18)	138.54(18)
S(8)-Co(4)-S(12)	91.02(8)	N(10)-Co(5)-S(18)	170.59(19)
S(13)-Co(4)-S(12)	79.37(7)	N(14)-Co(5)-S(18)	72.2(2)
S(11)-Co(4)-S(12)	81.24(7)	N(15)-Co(5)-S(18)	122.62(18)
S(14)-Co(4)-S(12)	133.95(7)	S(11)-Co(5)-S(18)	101.64(7)
S(10)-Co(4)-S(12)	81.02(7)	S(10)-Co(5)-S(18)	47.70(5)
S(15)-Co(4)-S(12)	135.68(6)	N(11)-Co(5)-S(17)	89.70(17)
N(11)-Co(5)-N(12)	97.8(2)	N(12)-Co(5)-S(17)	171.22(15)
N(11)-Co(5)-N(16)	111.3(3)	N(16)-Co(5)-S(17)	126.6(2)
N(12)-Co(5)-N(16)	54.6(2)	N(10)-Co(5)-S(17)	91.29(19)
N(11)-Co(5)-N(10)	95.6(2)	N(14)-Co(5)-S(17)	136.41(17)
N(12)-Co(5)-N(10)	92.5(2)	N(15)-Co(5)-S(17)	73.7(2)
N(16)-Co(5)-N(10)	40.3(2)	S(11)-Co(5)-S(17)	38.47(5)
N(11)-Co(5)-N(14)	56.3(2)	S(10)-Co(5)-S(17)	102.02(7)
N(12)-Co(5)-N(14)	47.6(2)	S(18)-Co(5)-S(17)	84.76(5)
N(16)-Co(5)-N(14)	93.4(3)	N(11)-Co(5)-S(12)	69.98(17)
N(10)-Co(5)-N(14)	116.1(3)	N(12)-Co(5)-S(12)	126.67(14)
N(11)-Co(5)-N(15)	36.4(3)	N(16)-Co(5)-S(12)	178.2(2)
N(12)-Co(5)-N(15)	115.1(3)	N(10)-Co(5)-S(12)	138.92(17)
N(16)-Co(5)-N(15)	94.5(3)	N(14)-Co(5)-S(12)	88.3(2)
N(10)-Co(5)-N(15)	64.0(2)	N(15)-Co(5)-S(12)	85.9(2)
N(14)-Co(5)-N(15)	88.1(3)	S(11)-Co(5)-S(12)	85.25(8)
N(11)-Co(5)-S(11)	122.62(17)	S(10)-Co(5)-S(12)	84.61(7)
N(12)-Co(5)-S(11)	136.62(13)	S(18)-Co(5)-S(12)	41.81(6)
N(16)-Co(5)-S(11)	93.0(2)	S(17)-Co(5)-S(12)	51.95(7)
N(10)-Co(5)-S(11)	70.3(2)	N(11)-Co(5)-S(16)	171.34(17)
N(14)-Co(5)-S(11)	173.3(2)	N(12)-Co(5)-S(16)	89.87(14)
N(15)-Co(5)-S(11)	93.3(2)	N(16)-Co(5)-S(16)	76.4(2)
N(11)-Co(5)-S(10)	136.45(16)	N(10)-Co(5)-S(16)	88.08(18)
N(12)-Co(5)-S(10)	69.37(15)	N(14)-Co(5)-S(16)	128.70(19)
N(16)-Co(5)-S(10)	95.01(19)	N(15)-Co(5)-S(16)	142.0(2)
N(10)-Co(5)-S(10)	125.46(16)	S(11)-Co(5)-S(16)	51.42(6)
N(14)-Co(5)-S(10)	89.3(2)	S(10)-Co(5)-S(16)	43.34(6)
N(15)-Co(5)-S(10)	170.23(19)	S(18)-Co(5)-S(16)	82.95(5)
S(11)-Co(5)-S(10)	88.25(8)	S(17)-Co(5)-S(16)	82.35(5)
N(11)-Co(5)-S(18)	92.96(16)	S(12)-Co(5)-S(16)	102.19(7)
N(12)-Co(5)-S(18)	90.28(14)		

Table 2-4. Selected bond distances and angles of $(\Lambda_{LLL})_4$-$[Co_3(aet)_6]_2$[**2**].

Bond distances (Å)			
Au(1)-S(4)	2.293(4)	Co(4)-S(11)	2.236(6)
Au(1)-S(1)	2.310(4)	Co(4)-S(10)	2.263(5)
Au(1)-Au(2)	2.8857(10)	Co(4)-S(12)	2.267(6)
Au(1)-Au(3)	3.1563(9)	Co(5)-N(13)	1.95(3)
Au(2)-S(5)	2.285(4)	Co(5)-N(14)	2.00(3)
Au(2)-S(2)	2.298(4)	Co(5)-N(15)	2.13(3)
Au(2)-Au(4)	3.1556(9)	Co(5)-S(19)	2.15(2)
Au(3)-S(7)	2.316(4)	Co(5)-S(15)	2.198(8)
Au(3)-S(3)	2.322(4)	Co(5)-S(14)	2.200(9)
Au(4)-S(10)	2.305(4)	Co(5)-S(21)	2.22(2)
Au(4)-S(6)	2.322(4)	Co(5)-S(13)	2.290(8)
Au(5)-S(11)	2.305(5)	Co(5)-S(20)	2.45(2)
Au(5)-S(8)	2.337(5)	Co(5)-Co(6)	2.844(4)
Au(6)-S(12)	2.301(5)	Co(6)-S(22)	2.127(19)
Au(6)-S(9)	2.306(5)	Co(6)-S(19)	2.24(2)
Co(1)-N(1)	1.939(16)	Co(6)-S(14)	2.247(8)
Co(1)-N(3)	2.021(15)	Co(6)-S(15)	2.251(8)
Co(1)-N(2)	2.032(15)	Co(6)-S(13)	2.252(8)
Co(1)-S(1)	2.237(5)	Co(6)-S(23)	2.261(18)
Co(1)-S(3)	2.246(5)	Co(6)-S(21)	2.27(2)
Co(1)-S(2)	2.247(5)	Co(6)-S(18)	2.275(8)
Co(2)-N(6)	1.995(15)	Co(6)-S(17)	2.293(8)
Co(2)-N(4)	2.011(13)	Co(6)-S(16)	2.294(8)
Co(2)-N(5)	2.107(13)	Co(6)-S(20)	2.304(19)
Co(2)-S(6)	2.224(5)	Co(6)-S(24)	2.33(2)
Co(2)-S(4)	2.257(5)	Co(7)-N(18)	1.91(3)
Co(2)-S(5)	2.278(5)	Co(7)-N(17)	1.95(2)
Co(3)-N(7)	1.962(15)	Co(7)-N(16)	1.96(2)
Co(3)-N(9)	1.977(15)	Co(7)-S(16)	2.207(7)
Co(3)-N(8)	2.00(2)	Co(7)-S(24)	2.21(2)
Co(3)-S(8)	2.228(6)	Co(7)-S(17)	2.213(8)
Co(3)-S(7)	2.239(5)	Co(7)-S(18)	2.282(8)
Co(3)-S(9)	2.251(5)	Co(7)-S(23)	2.28(2)
Co(4)-N(11)	1.968(17)	Co(7)-S(22)	2.29(2)
Co(4)-N(12)	1.975(17)	Co(8)-N(21)	2.07(3)
Co(4)-N(10)	1.992(17)	Co(8)-S(26)	2.143(14)

Table 2-4. (continued)

Co(8)-N(19)	2.15(5)	Co(10)-S(28)	2.247(12)
Co(8)-N(20)	2.19(4)	Co(10)-S(30)	2.251(11)
Co(8)-S(25)	2.275(13)	Co(11)-S(32)	2.12(5)
Co(8)-S(27)	2.335(16)	Co(11)-S(31)	2.26(4)
Co(8)-Co(9)	2.970(10)	Co(11)-S(33)	2.47(4)
Co(9)-S(28)	2.135(14)	Co(11)-Co(12)	2.57(2)
Co(9)-S(30)	2.141(12)	Co(12)-S(33)	1.83(4)
Co(9)-S(29)	2.181(16)	Co(12)-S(31)	1.98(4)
Co(9)-S(26)	2.253(14)	Co(12)-S(32)	2.12(5)
Co(9)-S(27)	2.270(18)	Co(12)-S(34)	2.19(2)
Co(9)-S(25)	2.291(14)	Co(12)-S(36)	2.39(3)
Co(9)-Co(10)	2.768(10)	Co(12)-S(35)	2.45(4)
Co(10)-N(22)	1.96(3)	Co(13)-S(35)	2.22(4)
Co(10)-N(23)	2.00(2)	Co(13)-S(34)	2.25(3)
Co(10)-N(24)	2.05(4)	Co(13)-S(36)	2.37(4)
Co(10)-S(29)	2.220(17)		

Angles (°)

S(4)-Au(1)-S(1)	169.01(16)	S(1)-Co(1)-S(2)	96.66(18)
S(5)-Au(2)-S(2)	168.72(16)	S(3)-Co(1)-S(2)	89.89(18)
S(7)-Au(3)-S(3)	172.12(16)	N(6)-Co(2)-N(4)	89.2(6)
S(10)-Au(4)-S(6)	172.40(15)	N(6)-Co(2)-N(5)	91.9(6)
S(11)-Au(5)-S(8)	168.38(18)	N(4)-Co(2)-N(5)	92.2(5)
S(12)-Au(6)-S(9)	167.23(18)	N(6)-Co(2)-S(6)	88.0(4)
N(1)-Co(1)-N(3)	91.0(7)	N(4)-Co(2)-S(6)	90.4(4)
N(1)-Co(1)-N(2)	90.3(7)	N(5)-Co(2)-S(6)	177.4(4)
N(3)-Co(1)-N(2)	90.6(6)	N(6)-Co(2)-S(4)	174.1(5)
N(1)-Co(1)-S(1)	85.8(5)	N(4)-Co(2)-S(4)	85.3(4)
N(3)-Co(1)-S(1)	87.8(5)	N(5)-Co(2)-S(4)	90.5(4)
N(2)-Co(1)-S(1)	175.8(5)	S(6)-Co(2)-S(4)	89.81(17)
N(1)-Co(1)-S(3)	179.0(6)	N(6)-Co(2)-S(5)	89.6(5)
N(3)-Co(1)-S(3)	88.7(4)	N(4)-Co(2)-S(5)	176.6(4)
N(2)-Co(1)-S(3)	90.6(5)	N(5)-Co(2)-S(5)	84.7(4)
S(1)-Co(1)-S(3)	93.25(17)	S(6)-Co(2)-S(5)	92.66(17)
N(1)-Co(1)-S(2)	90.5(5)	S(4)-Co(2)-S(5)	95.93(18)
N(3)-Co(1)-S(2)	175.4(5)	N(7)-Co(3)-N(9)	90.4(6)
N(2)-Co(1)-S(2)	84.9(5)	N(7)-Co(3)-N(8)	91.8(8)

Table 2-4. (continued)

N(9)-Co(3)-N(8)	92.0(8)	S(19)-Co(5)-S(15)	101.9(6)
N(7)-Co(3)-S(8)	89.0(5)	N(13)-Co(5)-S(14)	92.2(10)
N(9)-Co(3)-S(8)	178.1(5)	N(14)-Co(5)-S(14)	92.8(8)
N(8)-Co(3)-S(8)	86.2(7)	N(15)-Co(5)-S(14)	170.9(8)
N(7)-Co(3)-S(7)	87.6(5)	S(19)-Co(5)-S(14)	39.3(6)
N(9)-Co(3)-S(7)	89.1(5)	S(15)-Co(5)-S(14)	85.3(3)
N(8)-Co(3)-S(7)	178.7(7)	N(13)-Co(5)-S(21)	125.5(10)
S(8)-Co(3)-S(7)	92.6(2)	N(14)-Co(5)-S(21)	134.6(10)
N(7)-Co(3)-S(9)	174.7(5)	N(15)-Co(5)-S(21)	68.4(10)
N(9)-Co(3)-S(9)	84.3(5)	S(19)-Co(5)-S(21)	88.2(8)
N(8)-Co(3)-S(9)	88.4(7)	S(15)-Co(5)-S(21)	47.0(6)
S(8)-Co(3)-S(9)	96.3(2)	S(14)-Co(5)-S(21)	102.5(7)
S(7)-Co(3)-S(9)	92.3(2)	N(13)-Co(5)-S(13)	87.3(8)
N(11)-Co(4)-N(12)	91.7(7)	N(14)-Co(5)-S(13)	175.9(8)
N(11)-Co(4)-N(10)	90.6(7)	N(15)-Co(5)-S(13)	88.7(8)
N(12)-Co(4)-N(10)	89.8(7)	S(19)-Co(5)-S(13)	52.0(6)
N(11)-Co(4)-S(11)	85.3(5)	S(15)-Co(5)-S(13)	83.7(3)
N(12)-Co(4)-S(11)	90.2(6)	S(14)-Co(5)-S(13)	84.4(3)
N(10)-Co(4)-S(11)	175.9(5)	S(21)-Co(5)-S(13)	43.7(6)
N(11)-Co(4)-S(10)	91.5(5)	N(13)-Co(5)-S(20)	137.4(10)
N(12)-Co(4)-S(10)	175.8(6)	N(14)-Co(5)-S(20)	74.4(9)
N(10)-Co(4)-S(10)	87.4(5)	N(15)-Co(5)-S(20)	128.0(9)
S(11)-Co(4)-S(10)	92.86(19)	S(19)-Co(5)-S(20)	81.9(7)
N(11)-Co(4)-S(12)	175.8(5)	S(15)-Co(5)-S(20)	44.0(5)
N(12)-Co(4)-S(12)	84.4(6)	S(14)-Co(5)-S(20)	48.4(5)
N(10)-Co(4)-S(12)	87.9(5)	S(21)-Co(5)-S(20)	84.4(7)
S(11)-Co(4)-S(12)	96.1(2)	S(13)-Co(5)-S(20)	101.5(5)
S(10)-Co(4)-S(12)	92.39(18)	S(22)-Co(6)-S(19)	103.0(7)
N(13)-Co(5)-N(14)	95.8(11)	S(22)-Co(6)-S(14)	137.6(6)
N(13)-Co(5)-N(15)	93.4(11)	S(19)-Co(6)-S(14)	38.0(5)
N(14)-Co(5)-N(15)	93.8(11)	S(22)-Co(6)-S(15)	128.2(6)
N(13)-Co(5)-S(19)	71.0(11)	S(19)-Co(6)-S(15)	97.3(6)
N(14)-Co(5)-S(19)	126.5(10)	S(14)-Co(6)-S(15)	83.0(3)
N(15)-Co(5)-S(19)	137.1(9)	S(22)-Co(6)-S(13)	73.7(6)
N(13)-Co(5)-S(15)	170.8(8)	S(19)-Co(6)-S(13)	51.4(6)
N(14)-Co(5)-S(15)	93.1(8)	S(14)-Co(6)-S(13)	84.2(3)
N(15)-Co(5)-S(15)	88.1(7)	S(15)-Co(6)-S(13)	83.4(3)

Table 2-4. (continued)

S(22)-Co(6)-S(23)	85.2(7)	S(14)-Co(6)-S(20)	49.8(5)
S(19)-Co(6)-S(23)	171.0(7)	S(15)-Co(6)-S(20)	45.3(5)
S(14)-Co(6)-S(23)	133.0(5)	S(13)-Co(6)-S(20)	107.3(6)
S(15)-Co(6)-S(23)	80.4(6)	S(23)-Co(6)-S(20)	89.1(7)
S(13)-Co(6)-S(23)	136.2(6)	S(21)-Co(6)-S(20)	86.6(8)
S(22)-Co(6)-S(21)	89.2(8)	S(18)-Co(6)-S(20)	75.2(6)
S(19)-Co(6)-S(21)	84.5(8)	S(17)-Co(6)-S(20)	138.8(5)
S(14)-Co(6)-S(21)	99.3(6)	S(16)-Co(6)-S(20)	128.4(6)
S(15)-Co(6)-S(21)	45.8(6)	S(22)-Co(6)-S(24)	86.7(8)
S(13)-Co(6)-S(21)	43.6(6)	S(19)-Co(6)-S(24)	93.8(8)
S(23)-Co(6)-S(21)	99.7(8)	S(14)-Co(6)-S(24)	82.0(6)
S(22)-Co(6)-S(18)	103.1(6)	S(15)-Co(6)-S(24)	139.1(5)
S(19)-Co(6)-S(18)	134.6(6)	S(13)-Co(6)-S(24)	132.2(6)
S(14)-Co(6)-S(18)	101.4(3)	S(23)-Co(6)-S(24)	82.7(7)
S(15)-Co(6)-S(18)	94.9(3)	S(21)-Co(6)-S(24)	175.1(8)
S(13)-Co(6)-S(18)	173.9(3)	S(18)-Co(6)-S(24)	51.7(5)
S(23)-Co(6)-S(18)	37.8(5)	S(17)-Co(6)-S(24)	98.2(6)
S(21)-Co(6)-S(18)	132.2(6)	S(16)-Co(6)-S(24)	35.3(5)
S(22)-Co(6)-S(17)	33.6(5)	S(20)-Co(6)-S(24)	97.8(7)
S(19)-Co(6)-S(17)	133.0(5)	N(18)-Co(7)-N(17)	97.5(10)
S(14)-Co(6)-S(17)	170.8(3)	N(18)-Co(7)-N(16)	92.8(10)
S(15)-Co(6)-S(17)	102.4(3)	N(17)-Co(7)-N(16)	96.6(9)
S(13)-Co(6)-S(17)	88.9(3)	N(18)-Co(7)-S(16)	87.6(8)
S(23)-Co(6)-S(17)	55.9(5)	N(17)-Co(7)-S(16)	173.5(8)
S(21)-Co(6)-S(17)	79.7(6)	N(16)-Co(7)-S(16)	87.3(7)
S(18)-Co(6)-S(17)	85.7(3)	N(18)-Co(7)-S(24)	67.5(9)
S(22)-Co(6)-S(16)	58.1(6)	N(17)-Co(7)-S(24)	142.1(8)
S(19)-Co(6)-S(16)	81.6(6)	N(16)-Co(7)-S(24)	117.9(9)
S(14)-Co(6)-S(16)	92.4(3)	S(16)-Co(7)-S(24)	37.0(5)
S(15)-Co(6)-S(16)	173.7(3)	N(18)-Co(7)-S(17)	171.6(8)
S(13)-Co(6)-S(16)	100.6(3)	N(17)-Co(7)-S(17)	87.9(8)
S(23)-Co(6)-S(16)	99.8(6)	N(16)-Co(7)-S(17)	92.9(8)
S(21)-Co(6)-S(16)	139.8(6)	S(16)-Co(7)-S(17)	86.6(3)
S(18)-Co(6)-S(16)	81.6(3)	S(24)-Co(7)-S(17)	104.4(6)
S(17)-Co(6)-S(16)	82.8(3)	N(18)-Co(7)-S(18)	85.9(7)
S(22)-Co(6)-S(20)	172.2(7)	N(17)-Co(7)-S(18)	92.7(7)
S(19)-Co(6)-S(20)	83.2(7)	N(16)-Co(7)-S(18)	170.6(7)

Table 2-4. (continued)

S(16)-Co(7)-S(18)	83.4(3)	N(21)-Co(8)-S(27)	86.3(12)
S(24)-Co(7)-S(18)	53.1(6)	S(26)-Co(8)-S(27)	83.3(6)
S(17)-Co(7)-S(18)	87.5(3)	N(19)-Co(8)-S(27)	91.7(13)
N(18)-Co(7)-S(23)	118.9(9)	N(20)-Co(8)-S(27)	166.4(12)
N(17)-Co(7)-S(23)	72.1(9)	S(25)-Co(8)-S(27)	80.3(5)
N(16)-Co(7)-S(23)	147.1(9)	N(21)-Co(8)-Co(9)	125.4(12)
S(16)-Co(7)-S(23)	101.8(5)	S(26)-Co(8)-Co(9)	49.1(4)
S(24)-Co(7)-S(23)	84.9(8)	N(19)-Co(8)-Co(9)	123.7(13)
S(17)-Co(7)-S(23)	56.7(5)	N(20)-Co(8)-Co(9)	117.6(11)
S(18)-Co(7)-S(23)	37.5(5)	S(25)-Co(8)-Co(9)	49.7(4)
N(18)-Co(7)-S(22)	143.4(9)	S(27)-Co(8)-Co(9)	48.9(4)
N(17)-Co(7)-S(22)	118.6(9)	S(28)-Co(9)-S(30)	88.8(5)
N(16)-Co(7)-S(22)	77.7(9)	S(28)-Co(9)-S(29)	86.0(6)
S(16)-Co(7)-S(22)	57.0(5)	S(30)-Co(9)-S(29)	84.8(5)
S(24)-Co(7)-S(22)	85.7(7)	S(28)-Co(9)-S(26)	100.3(5)
S(17)-Co(7)-S(22)	33.1(5)	S(30)-Co(9)-S(26)	98.5(5)
S(18)-Co(7)-S(22)	97.8(5)	S(29)-Co(9)-S(26)	172.9(7)
S(23)-Co(7)-S(22)	81.0(7)	S(28)-Co(9)-S(27)	174.9(7)
N(18)-Co(7)-Co(6)	119.5(8)	S(30)-Co(9)-S(27)	95.1(6)
N(17)-Co(7)-Co(6)	121.4(8)	S(29)-Co(9)-S(27)	91.1(6)
N(16)-Co(7)-Co(6)	122.6(7)	S(26)-Co(9)-S(27)	82.4(6)
S(16)-Co(7)-Co(6)	52.2(2)	S(28)-Co(9)-S(25)	94.9(5)
S(24)-Co(7)-Co(6)	53.2(6)	S(30)-Co(9)-S(25)	176.1(6)
S(17)-Co(7)-Co(6)	52.1(2)	S(29)-Co(9)-S(25)	96.7(6)
S(18)-Co(7)-Co(6)	51.3(2)	S(26)-Co(9)-S(25)	79.6(5)
S(23)-Co(7)-Co(6)	50.9(5)	S(27)-Co(9)-S(25)	81.3(6)
S(22)-Co(7)-Co(6)	47.4(5)	N(22)-Co(10)-N(23)	105.3(16)
N(21)-Co(8)-S(26)	105.8(14)	N(22)-Co(10)-N(24)	92.8(17)
N(21)-Co(8)-N(19)	78.9(18)	N(23)-Co(10)-N(24)	100.4(16)
S(26)-Co(8)-N(19)	172.8(14)	N(22)-Co(10)-S(29)	166.6(13)
N(21)-Co(8)-N(20)	105.6(17)	N(23)-Co(10)-S(29)	83.2(12)
S(26)-Co(8)-N(20)	87.0(12)	N(24)-Co(10)-S(29)	95.8(14)
N(19)-Co(8)-N(20)	97.0(16)	N(22)-Co(10)-S(28)	86.8(11)
N(21)-Co(8)-S(25)	163.4(13)	N(23)-Co(10)-S(28)	92.7(10)
S(26)-Co(8)-S(25)	82.2(5)	N(24)-Co(10)-S(28)	166.5(12)
N(19)-Co(8)-S(25)	91.9(13)	S(29)-Co(10)-S(28)	82.5(5)
N(20)-Co(8)-S(25)	89.0(12)	N(22)-Co(10)-S(30)	89.6(13)

Table 2-4. (continued)

N(23)-Co(10)-S(30)	164.4(12)	S(32)-Co(12)-S(34)	89.9(14)
N(24)-Co(10)-S(30)	83.1(11)	S(33)-Co(12)-S(36)	162.0(17)
S(29)-Co(10)-S(30)	81.3(5)	S(31)-Co(12)-S(36)	85.9(15)
S(28)-Co(10)-S(30)	83.4(4)	S(32)-Co(12)-S(36)	98.3(17)
S(32)-Co(11)-S(31)	78.2(15)	S(34)-Co(12)-S(36)	78.7(12)
S(32)-Co(11)-S(33)	77.1(15)	S(33)-Co(12)-S(35)	89.6(17)
S(31)-Co(11)-S(33)	82.4(13)	S(31)-Co(12)-S(35)	109.2(16)
S(33)-Co(12)-S(31)	109.5(17)	S(32)-Co(12)-S(35)	164.6(18)
S(33)-Co(12)-S(32)	92.6(17)	S(34)-Co(12)-S(35)	74.9(12)
S(31)-Co(12)-S(32)	84.5(16)	S(36)-Co(12)-S(35)	76.2(13)
S(33)-Co(12)-S(34)	87.1(14)	S(35)-Co(13)-S(34)	78.7(14)
S(31)-Co(12)-S(34)	162.7(15)	S(35)-Co(13)-S(36)	81.1(15)

Table 2-5. Absorption and CD spectral data for $(\Delta_{LLL})_2$-K_3[**1**] and $(\Lambda_{LLL})_2$-K_3[**1**] in water.

Complex	Absorption maxima: λ / nm (log ε / mol^{-1} dm^3 cm^{-1})
$(\Delta_{LLL})_2$-K_3[**1**]	553 (3.03), 254 (4.59), 230 (4.62)
$(\Lambda_{LLL})_2$-K_3[**1**]	561 (3.06), 255 (4.58), 230 (4.66)

Complex	CD extrema: λ / nm ($\Delta\varepsilon$ /mol^{-1} dm^3 cm^{-1})
$(\Delta_{LLL})_2$-K_3[**1**]	573 (–19.56), 455 (+11.17), 389 (–17.31), 339 (+29.80), 311 (–46.67), 253 (+89.28)
$(\Lambda_{LLL})_2$-K_3[**1**]	580 (+20.71), 458 (–10.30), 389 (+16.48), 359 (+22.01), 332 (+9.39), 284 (+42.22), 252 (–70.86)

Table 2-6. Absorption and CD spectral data for $(\Delta_{LLL})_2$-[Co_3(aet)$_6$][**1**], $(\Lambda_{LLL})_4$-[Co_3(aet)$_6$]$_2$[**2**], $(\Lambda_{LLL})_4$-[$CoRh_2$(aet)$_6$]$_2$[**2**], and $(\Lambda_{LLL})_2$-[Co(en)$_3$][**1**] in a $NaNO_3$ aqueous solution.

Complex	Absorption maxima: λ / nm (log ε / mol^{-1} dm^3 cm^{-1})
$(\Delta_{LLL})_2$-[Co_3(aet)$_6$][**1**]	560 (3.52), 437 (3.85), 339 (4.45), 280 (4.73), 257 (4.79)
$(\Lambda_{LLL})_4$-[Co_3(aet)$_6$]$_2$[**2**]	574 (3.74), 439 (4.15), 343 (4.70)
$(\Lambda_{LLL})_4$-[$CoRh_2$(aet)$_6$]$_2$[**2**]	585 (3.02), 423 (3.77)
$(\Lambda_{LLL})_2$-[Co(en)$_3$][**1**]	573 (2.84), 443 (3.02)

Complex	CD extrema: λ / nm ($\Delta\varepsilon$ /mol^{-1} dm^3 cm^{-1})
$(\Delta_{LLL})_2$-[Co_3(aet)$_6$][**1**]	573 (–20.27), 520 (+1.80), 450 (+12.25), 385 (–21.17), 355 (–21.07), 311 (–48.94), 254 (+104.81), 234 (+8.59), 221 (–4.91), 207 (+48.81)
$(\Lambda_{LLL})_4$-[Co_3(aet)$_6$]$_2$[**2**]	561 (+39.90), 467 (–25.00), 392 (+29.15), 301 (+16.75), 288 (+17.46)
$(\Lambda_{LLL})_4$-[$CoRh_2$(aet)$_6$]$_2$[**2**]	619 (–7.80), 556 (+12.37), 469 (–10.66), 411 (+51.54), 365 (+21.00), 334 (+45.46)
$(\Lambda_{LLL})_2$-[Co(en)$_3$][**1**]	579 (+2.79), 457 (–1.85), 360 (+3.09)

Table 2-7. Absorption and CD spectral data for $(\Delta_{LLL})_2$-K_3[**1**], $(\Lambda_{LLL})_2$-K_3[**1**], $(\Delta_{LLL})_2$-$[Co_3(aet)_6]$[**1**], $(\Lambda_{LLL})_4$-$[Co_3(aet)_6]_2$[**2**], $(\Lambda_{LLL})_4$-$[CoRh_2(aet)_6]_2$[**2**], and $(\Lambda_{LLL})_2$-$[Co(en)_3]$[**1**] in the solid state.

Complex	Absorption: λ / nm
$(\Delta_{LLL})_2$-K_3[**1**]	560, 434
$(\Lambda_{LLL})_2$-K_3[**1**]	550, 434
$(\Delta_{LLL})_2$-$[Co_3(aet)_6]$[**1**]	560, 437, 348
$(\Lambda_{LLL})_4$-$[Co_3(aet)_6]_2$[**2**]	580, 450, 360
$(\Lambda_{LLL})_4$-$[CoRh_2(aet)_6]$[**2**]	579, 539, 336
$(\Lambda_{LLL})_2$-$[Co(en)_3]$[**1**]	572, 436, 340

Complex	CD extrema: λ /10^3 nm
$(\Delta_{LLL})_2$-K_3[**1**]	509 (–), 447 (+), 404 (–), 376 (–)
$(\Lambda_{LLL})_2$-K_3[**1**]	522 (+), 449 (–),411 (+), 377 (–)
$(\Delta_{LLL})_2$-$[Co_3(aet)_6]$[**1**]	577 (–), 451 (+), 398 (–), 365 (–)
$(\Lambda_{LLL})_4$-$[Co_3(aet)_6]_2$[**2**]	560 (+), 460 (–), 395 (+), 355 (+)
$(\Lambda_{LLL})_4$-$[CoRh_2(aet)_6]$[**2**]	632 (–), 553 (+), 416 (+), 370 (+)
$(\Lambda_{LLL})_2$-$[Co(en)_3]$[**1**]	520 (+), 450 (–), 410 (+), 375 (+), 320 (+)

Chapter III. Chiral Recognition Behavior of $(\Delta_{LLL})_2$-$[M_3Co^{III}_2(L\text{-cys})_6]^{3-}$ toward $(\Delta)_2/(\Lambda)_2$-$[Co^{III}_3(aet)_6]^{3+}$ (M = Au^I, Ag^I)

III-1 Introduction

In Chapter II, the unique multiple inversions and structural conversion in the L-cysteinato Au^ICo^{III} system was demonstrated. The $Au^I_3Co^{III}_2$ pentanuclear complex-anion $(\Delta_{LLL})_2$-$[Au_3Co_2(L\text{-cys})_6]^{3-}$ ($(\Delta_{LLL})_2$-$[\mathbf{1}]^{3-}$) was inverted to the $(\Lambda_{LLL})_2$-$[Au_3Co_2(L\text{-cys})_6]^{3-}$ ($(\Lambda_{LLL})_2$-$[\mathbf{1}]^{3-}$) retaining the pentanuclear structure by controlling the solution pH, which were further converted to the $Au^I_6Co^{III}_4$ decanuclear complex-anion $(\Lambda_{LLL})_4$-$[Au_6Co_4(L\text{-cys})_{12}]^{6-}$ ($(\Lambda_{LLL})_2$-$[\mathbf{2}]^{6-}$) upon the crystallization with $[Co_3(aet)_6]^{3+}$. The detailed mechanism of the conversions was discussed based on the spectral measurements.

In this chapter, the chiralselective behavior of the cocrystallized compounds, $(\Delta_{LLL})_2$-$[Co_3(aet)_6][\mathbf{1}]$ and $(\Lambda_{LLL})_4$-$[Co_3(aet)_6]_2[\mathbf{2}]$, described in Chapter II is discussed in detail (Scheme 3-1). As mentioned in Chapter I, the optical resolution of the racemic compounds is one of the important subjects in the field of stereochemistry. The separation of one enantiomer using a diastereomeric nature is an effective method. The L-cysteinato multinuclear complexes are a good candidate for a resolving reagent toward racemic complex-cations during the cocrystallization process because of their structural features: (i) to have an anionic nature, (ii) to have multiple chiral centers on the metal centers (Δ/Λ), the bridging S atoms (*R*/*S*), and the C atom of L-cys (*R*), and (iii) to have free carboxylate groups available for the recognition site. Thus, the chirality of the complex-cation in $(\Delta_{LLL})_2$-$[Co_3(aet)_6][\mathbf{1}]$ and $(\Lambda_{LLL})_4$-$[Co_3(aet)_6]_2[\mathbf{2}]$ was checked by the separation of the complex-anion and complex-cation using column chromatography and the sequential absorption and CD spectral measurements.

For the comparison, the chiral behavior using $(\Delta_{LLL})_2$-$[Ag_3Co_2(L\text{-cys})_6]^{3-}$ ($(\Delta_{LLL})_2$-$[\mathbf{3}]^{3-}$),[1] which has a similar structure with $(\Delta_{LLL})_2$-$[\mathbf{1}]^{3-}$, having a $\{Ag^I_3\}$ moiety instead of the $\{Au^I_3\}$ moiety, was also investigated (Scheme 3-1). The introduction of the $\{Ag^I_3\}$ moiety may lead to the formation of intermolecular interactions using the Ag^I ion besides the amine and carboxylate groups. The structure of the obtained cocrystallized compound $(\Delta_{LLL})_2$-$[Co_3(aet)_6][\mathbf{3}]$ was determined by single-crystal X-ray analysis, and the chiralselectivity was investigated by the similar way as $(\Delta_{LLL})_2$-$[Co_3(aet)_6][\mathbf{1}]$ and $(\Lambda_{LLL})_4$-$[Co_3(aet)_6]_2[\mathbf{2}]$.

The structural differences in the three complex-anions, $(\Delta_{LLL})_2$-$[\mathbf{1}]^{3-}$, $(\Lambda_{LLL})_4$-$[\mathbf{2}]^{6-}$, and $(\Delta_{LLL})_2$-$[\mathbf{3}]^{3-}$, are the bridging metal ions (Au^I/Ag^I), the configuration around the terminal Co^{III} ions ($\Delta_{LLL}/\Lambda_{LLL}$), the orientation of the carboxylate groups

(equatorial/axial), and nuclearity (pentanuclear/decanuclear). The key factors that control the chiralselective behavior are discussed based on the X-ray crystal structures.

III-2 Experimental Section

III-2-1 Materials

All chemicals were of commercial grade and use without further purification. The starting materials, $(\Delta)_2/(\Lambda)_2$-$[Co_3(aet)_6](NO_3)$ and $(\Delta_{LLL})_2$-$K_3[Ag_3Co_2(L\text{-}cys)_6]$ were prepared by the method or modified method described in the literature.[1,2] The preparation of $(\Delta_{LLL})_2$-$[Co_3(aet)_6][Au_3Co_2(L\text{-}cys)_6]$ ($(\Delta_{LLL})_2$-$[Co_3(aet)_6]$[**1**]) and $(\Lambda_{LLL})_4$-$[Co_3(aet)_6]_2[Au_3Co_2(L\text{-}cys)_6]$ ($(\Lambda_{LLL})_4$-$[Co_3(aet)_6]_2$[**2**]) is described in Chapter II.

III-2-2 Preparation of $(\Delta_{LLL})_2$-$[Co^{III}_3(aet)_6][Ag^{I}_3Co^{III}_2(L\text{-}cys)_6]$ ($(\Delta_{LLL})_2$-$[Co^{III}_3(aet)_6]$[**3**])

To a solution containing 43 mg (0.051 mmol) of *rac*-$[Co_3(aet)_6](NO_3)_3\cdot H_2O$ in 10 mL of water was added a solution containing 50 mg (0.017 mmol) of $(\Delta_{LLL})_2$-$K_3[Ag_3Co_2(L\text{-}cys)_6]\cdot 10H_2O$ ($(\Delta_{LLL})_2$-K_3[**3**]$\cdot 10H_2O$) in 10 mL of water. The black solution was allowed to stand at room temperature for 2 weeks. The resulting black needle-like crystals of $(\Delta_{LLL})_2$-$[Co_3(aet)_6]$[**3**] were collected by filtration. Yield: 38 mg (53%). Calcd for $[Co_3(aet)_6][Ag_3Co_2(L\text{-}cys)_6]\cdot 8H_2O = C_{30}H_{82}N_{12}O_{20}S_{12}Co_5Ag_3$: C, 18.63; H, 4.27; N, 8.69%. Found: C, 18.53; H, 4.23; N, 8.69%. Electronic absorption spectrum in a $NaNO_3$ aqueous solution [λ / nm ($\log\varepsilon$ / mol^{-1} dm^3 cm^{-1})]: 558 (2.62), 439 (2.96), 346 (3.51), 279 (3.94), 253 (3.93). CD spectrum in a $NaNO_3$ aqueous solution [λ / nm ($\Delta\varepsilon$ / mol^{-1} dm^3 cm^{-1})]: 591 (–40.53), 537 (+33.27), 493 (–27.29), 346 (+55.11), 368 (–46.97), 326 (+56.71). One of the single crystals was used for X-ray measurement.

III-2-3 Physical Measurements

The electronic absorption spectra were recorded with a JASCO V-660 or a JASCO V-630 spectrophotometers using a 1 cm quartz cell at room temperature. The diffuse reflectance spectra were recorded on a JASCO V-570 spectrophotometer at room temperature by using $MgSO_4$. The CD spectra were recorded with a J-820 spectrometer at room temperature using a 1 cm quartz cell for the solution state and using KBr disks for the solid state. The IR spectra were recorded on a JASCO FT/IR-4100 infrared spectrometer using KBr disks at room temperature. The elemental analyses (C, H, N) were performed at Osaka University. X-ray fluorescence analyses were made on a HORIBA MESA-500 or SHIMADZU EDX-720 spectrometer. The ^{1}H NMR spectra were recorded with a JEOL ECA500 (500 MHz) spectrometer at room temperature in D_2O, using sodium 4,4’-dimethyl-4-silapentane-1-sulfonate (DSS) as the internal standard.

III-2-4 X-ray Structural Determination

The single-crystal X-ray diffraction measurements for $(\Delta_{LLL})_2$-$[Co_3(aet)_6]$[**3**] were performed on a Rigaku R-AXIS VII imaging plate area detector with a graphite monochromated MoKα radiation at –73℃. The intensity data were collected by the ω-scan technique and were empirically corrected for absorption. The structures were solved by direct methods using SHELXS-97.[3] The structure refinements were carried out using full-matrix least-squares (SHELXL-97).[3] All calculations were performed using the Yadokari-XG software package.[3] For $(\Delta_{LLL})_2$-$[Co_3(aet)_6]$[**3**], all non-hydrogen atoms except the water molecule were refined anisotropically, while the others are refined isotropically. Hydrogen atoms were included in calculated positions except those of water molecules.

III-3 Results and Discussion

III-3-1 Synthesis and Characterization

(a) $(\Delta_{LLL})_2$-[Co^{III}_3(aet)$_6$][$Au^{I}_3Co^{III}_2$(L-cys)$_6$] ($(\Delta_{LLL})_2$-[Co^{III}_3(aet)$_6$][**1**])

As mentioned in Chapter II, the reaction of $(\Delta_{LLL})_2$-K_3[**1**] and $(\Delta)_2/(\Lambda)_2$-$[Co_3(aet)_6](NO_3)_3$ in a 1:2 ratio in water gave black block crystals of $(\Delta_{LLL})_2$-$[Co_3(aet)_6][Au_3Co_2(L\text{-}cys)_6]$ ($(\Delta_{LLL})_2$-$[Co_3(aet)_6]$[**1**]). The IR, absorption, CD, and ^{1}H NMR spectra, elemental analysis, and X-ray analysis demonstrated that $(\Delta_{LLL})_2$-$[Co_3(aet)_6]$[**1**] consists of $(\Delta_{LLL})_2$-$[\mathbf{1}]^{3-}$ and $[Co_3(aet)_6]^{3+}$ in a 1:1 ratio, retaining the structure of both complex-anion and complex-cation. Focused on the chirality of the $[Co_3(aet)_6]^{3+}$ unit, both $(\Delta)_2$ and $(\Lambda)_2$ isomers of $[Co_3(aet)_6]^{3+}$ are contained in $(\Delta_{LLL})_2$-$[Co_3(aet)_6]$[**1**], and low chiralselectivity of $(\Delta_{LLL})_2$-$[\mathbf{1}]^{3-}$ toward $[Co_3(aet)_6]^{3+}$ is suggested. In this section, the chiral behavior of $(\Delta_{LLL})_2$-$[Co_3(aet)_6]$[**1**] is discussed in detail.

To investigate the chiral configuration of the incorporated complex-cation in the bulk sample of $(\Delta_{LLL})_2$-$[Co_3(aet)_6]$[**1**], the bulk sample was dissolved in water by adding a saturated $NaClO_4$ aqueous solution and chromatographed on a cation-exchange column (SP-Sephadex C-25). When the column was treated with water, a brown band containing $(\Delta_{LLL})_2$-$[\mathbf{1}]^{3-}$ was eluted, while a brownish green band containing $[Co_3(aet)_6]^{3+}$ was absorbed on the top of the column, which was eluted with a 0.3 M aqueous solution of $NaClO_4$. The absorption spectrum of the eluate containing the complex-anion shows an absorption band at 567 nm and a shoulder at 440 nm (Figure S1-1, see appendix). Its CD spectrum shows negative bands at 562 and 382 nm and a positive band at 435 nm. These spectral features are coincident with those of $(\Delta_{LLL})_2$-K_3[**1**], which indicates that the structure and chirality of the complex-anion are retained during the reaction. The absorption spectrum of the eluate containing the complex-cation shows an absorption shoulder at 590 nm and two sharp absorption bands at 440 and 345 nm (Figure S1-1, see appendix). Its CD spectrum shows quite weak negative bands at 610, 485, and 350 nm and positive bands at 540 and 435 nm (Figure S1-1, see appendix). This indicates that the $(\Delta)_2$ isomer of $[Co_3(aet)_6]^{3+}$ is predominantly incorporated in $(\Delta_{LLL})_2$-$[Co_3(aet)_6]$[**1**], but its chiralselectivity is low.

(b) $(\Lambda_{LLL})_4$-[Co^{III}_3(aet)$_6$]$_2$[$Au^{I}_6Co^{III}_4$(L-cys)$_{12}$] ($(\Lambda_{LLL})_4$-[Co^{III}_3(aet)$_6$]$_2$[**2**])

As mentioned in Chapter II, the reaction of $(\Delta_{LLL})_2$-K_3[**1**] and $(\Delta)_2/(\Lambda)_2$-$[Co_3(aet)_6](NO_3)_3$ in a 1:2 ratio in a basic aqueous solution, or the reaction of $(\Lambda_{LLL})_2$-K_3[**1**] and $(\Delta)_2/(\Lambda)_2$-$[Co_3(aet)_6](NO_3)_3$ in a 1:2 ratio in water, gave black block crystals of $(\Lambda_{LLL})_4$-$[Co_3(aet)_6]_2[Au_6Co_4(L\text{-}cys)_{12}]$ ($(\Lambda_{LLL})_4$-$[Co_3(aet)_6]_2$[**2**]). The

IR, absorption, CD, and ^{1}H NMR spectra, elemental analysis, and X-ray analysis demonstrated that $(\Lambda_{LLL})_4$-$[Co_3(aet)_6]_2$[**2**] consists of $(\Lambda_{LLL})_4$-[**2**]$^{6-}$ and $[Co_3(aet)_6]^{3+}$ in a 1:2 ratio, and it was found that the conversion from the $Au^{I}_3Co^{III}_2$ pentanulear structure to the $Au^{I}_6Co^{III}_4$ decanuclear structure for the complex-anion was observed with the retention of the structure of the complex-cation. Focused on the chirality of the $[Co_3(aet)_6]^{3+}$ cation, both $(\Delta)_2$ and $(\Lambda)_2$ isomers of $[Co_3(aet)_6]^{3+}$ are contained in $(\Lambda_{LLL})_4$-$[Co_3(aet)_6]_2$[**2**], and similarly, low chiralselectivity of $(\Lambda_{LLL})_4$-[**2**]$^{6-}$ toward $[Co_3(aet)_6]^{3+}$ is suggested. In this section, the chiral behavior of $(\Lambda_{LLL})_4$-$[Co_3(aet)_6]_2$[**2**] is discussed in detail.

To investigate the chiral configuration of the incorporated complex-cation in the bulk sample of $(\Lambda_{LLL})_4$-$[Co_3(aet)_6]_2$[**2**], the bulk sample was dissolved in water by adding a saturated $NaClO_4$ aqueous solution and chromatographed on a cation-exchange column (SP-Sephadex C-25). When the column was treated with water, a brown band containing $(\Lambda_{LLL})_4$-[**2**]$^{6-}$ was eluted, while a brownish green band containing $[Co_3(aet)_6]^{3+}$ was absorbed on the top of the column, which was eluted with a 0.3 M aqueous solution of $NaClO_4$. The absorption spectrum of the eluate containing the complex-anion shows an absorption shoulder at 565 nm and a sharp absorption band at 301 nm (Figure 3-1). Its CD spectrum shows positive bands at 575 and 390 nm and a negative band at 453 nm. These spectral features are coincident with those of $(\Lambda_{LLL})_2$-K_3[**1**], which indicates that the chirality of the complex-anion is retained but the $Au^{I}_6Co^{III}_4$ decanuclear structure was converted to the $Au^{I}_3Co^{III}_2$ pentanuclear structure during the column chromatography process. The absorption spectrum of the eluate containing the complex-cation shows three absorption bands at 590, 440, and 345 nm (Figure 3-1). Its CD spectrum shows negative bands at 610, 485, and 350 nm and positive bands at 540 and 435 nm (Figure 3-1). This CD spectral pattern is same as that of $(\Delta)_2$-$[Co_3(aet)_6]^{3+}$, but their intensity is weak. This indicates that the $(\Delta)_2$ isomer of $[Co_3(aet)_6]^{3+}$ is predominantly incorporated in $(\Lambda_{LLL})_4$-$[Co_3(aet)_6]_2$[**2**]. The calculation based on the absorption band at 440 nm and the CD band at 540 nm confirmed that the enantiomeric excess (*ee*) for the incorporated $(\Delta)_2$-$[Co_3(aet)_6]^{3+}$ in the bulk sample of $(\Lambda_{LLL})_4$-$[Co_3(aet)_6]_2$[**2**] is 22%.

(c) $(\Delta_{LLL})_2$-$[Co^{III}_3(aet)_6][Ag^{I}_3Co^{III}_2(L\text{-cys})_6]$ ($(\Delta_{LLL})_2$-$[Co^{III}_3(aet)_6]$[**3**])

Treatment of $(\Delta)_2/(\Lambda)_2$-$[Co_3(aet)_6](NO_3)_3$ with $(\Delta_{LLL})_2$-$K_3[Ag_3Co_2(L\text{-cys})_6]$ ($(\Delta_{LLL})_2$-K_3[**3**]) in a 2:1 ratio in water, followed by allowing to stand at room temperature, gave black needle-like crystals of $(\Delta_{LLL})_2$-$[Co_3(aet)_6][Ag_3Co_2(L\text{-cys})_6]$ ($(\Delta_{LLL})_2$-$[Co_3(aet)_6]$[**3**]). The IR spectrum of $(\Delta_{LLL})_2$-$[Co_3(aet)_6]$[**3**] shows a strong sharp C=O stretching band at 1605 cm^{-1}, suggestive of the presence of L-cys with the deprotonated carboxylate group (Figure 3-2). X-ray fluorescence spectroscopy

indicates that this product contains Au, Ag, and Co atoms. The elemental analytical data are in agreement with the formula for a 1:1 adduct of $[Co_3(aet)_6]^{3+}$ and $[\mathbf{3}]^{3-}$. The reflection and CD spectra in the solid state are shown in Figure 3-3. In the reflection spectrum, three bands at 582, 443, and 352 nm are observed, which is similar with those of $(\Delta_{LLL})_2$-K_3[**3**] and $(\Delta_{LLL})_2$-$[Co_3(aet)_6]$[**1**]. The CD spectrum shows a complicated pattern with negative bands at 618, 513, and 392 nm and positive bands at 555 and 459 nm, which is quite different from those of $(\Delta_{LLL})_2$-K_3[**3**] and $(\Delta_{LLL})_2$-$[Co_3(aet)_6]$[**1**]. The absorption and CD spectra of the crystals in a $NaNO_3$ aqueous solution are essentially the same as the reflection and CD spectra in the solid state. The absorption spectrum shows three absorption bands at 580, 440, and 340 nm, and the CD spectrum shows negative bands at 590, 490, and 370 nm and positive bands at 535 and 435 nm (Figure 3-4). The ^{1}H NMR spectrum in a $NaNO_3$ solution of D_2O shows one set of L-cys signals attributed to $(\Delta_{LLL})_2$-$[\mathbf{3}]^{3-}$ and one set of aet signals attributed to $[Co_3(aet)_6]^{3+}$, of which integration ratio indicates the presence of $(\Delta_{LLL})_2$-$[\mathbf{3}]^{3-}$ and $[Co_3(aet)_6]^{3+}$ in a 1:1 ratio (Figure 3-5). The structure of $(\Delta_{LLL})_2$-$[Co_3(aet)_6]$[**3**] was established by X-ray structural analysis, which shows the presence of a pentanuclear complex-anion and a trinuclear complex-cation in a 1:1 ratio, and only the $(\Delta_{LLL})_2$ and $(\Delta)_2$ isomers exist in crystal, respectively (*vide infra*).

To check the chirality of the complex-anion and the complex-cation in the bulk sample, the cationic and anionic parts are separated by column chromatography, and their absorption and CD spectra were measured. When the bulk sample of $(\Delta_{LLL})_2$-$[Co_3(aet)_6]$[**3**] was dissolved in a $NaClO_4$ aqueous solution and was chromatographed on a cation-exchange column (SP-Sephadex C-25), a purple band containing the complex-anion eluted with water, while a brownish green band containing the complex-cation was adsorbed on the top of the column. This cationic part was eluted with a 0.3 M aqueous solution of $NaClO_4$. The absorption spectrum of the purple band shows the bands at 570 and 440 nm, and its CD spectrum shows negative bands at 565 and 380 nm and a positive band at 440 nm (Figure 3-6). These spectral features are coincident with those of $(\Delta_{LLL})_2$-$[\mathbf{3}]^{3-}$, indicative of the retention of the Δ_{LLL} configurational $Ag^{I}{}_3Co^{III}{}_2$ pentanuclear structure during the reaction. For the cationic part, the absorption spectrum suggests the presence of $[Co_3(aet)_6]^{3+}$ based on the bands at 590 and 440 nm (Figure 3-6). In the CD spectrum, the spectral pattern and intensity are the same as those of $(\Delta)_2$-$[Co_3(aet)_6]^{3+}$ showing a negative band at 610 nm and a positive band at 540 nm (Figure 3-6), indicating that only the $(\Delta)_2$ isomer of $[Co_3(aet)_6]^{3+}$ is incorporated in $(\Delta_{LLL})_2$-$[Co_3(aet)_6]$[**3**]. This chiralselective uptake of $[Co_3(aet)_6]^{3+}$ is consistent with the X-ray structural analysis that showed the presence of only the $(\Delta)_2$ isomer of $[Co_3(aet)_6]^{3+}$ in crystal.

III-3-2 Crystal Structure of $(\Delta_{LLL})_2$-$[Co^{III}_3(aet)_6][Ag^{I}_3Co^{III}_2(L\text{-}cys)_6]$ ($(\Delta_{LLL})_2$-$[Co^{III}_3(aet)_6][\mathbf{3}]$)

X-ray crystallography demonstrated that $(\Delta_{LLL})_2$-$[Co_3(aet)_6][\mathbf{3}]$ consists of a trinuclear complex-cation ($[Co_3(aet)_6]^{3+}$) and a pentanuclear complex-anion ($(\Delta_{LLL})_2$-$[\mathbf{3}]^{3-}$) besides water molecules of crystallization in the asymmetric unit. The molecular and packing structures are shown in Figures 3-7, 3-8, 3-9, and 3-10. The crystallographic data are summarized in Table 3-1 and the selected bond distances and angles are listed in Table 3-2.

As shown in Figure 3-7, the complex-anion $(\Delta_{LLL})_2$-$[\mathbf{3}]^{3-}$ has an S-bridged $Ag^{I}_3Co^{III}_2$ pentanuclear structure, in which two $[Co(L\text{-}cys)_3]^{3-}$ units are bridged by three linear Ag^{I} atoms (av. Co–S = 2.242(86) Å, Co–N = 1.995(6) Å, Ag–S = 2.434(1) Å, S–Ag–S = 171.1°). As in $(\Delta_{LLL})_2$-$[\mathbf{1}]^{3-}$, the Co^{III} centers coordinated by three bidentate-N,S L-cys ligands take a Δ_{LLL} configuration, and the bridging S atoms adopt an *S* configuration to give only the $(\Delta_{LLL})_2(S)_6$ isomer. All six carboxylate groups in $(\Delta_{LLL})_2$-$[\mathbf{3}]^{3-}$ take an equatorial orientation, and the N,S-chelate rings adopt a thermodynamically stable *lel* (λ for Δ) conformation. Three S–Ag–S linkages are twisted in a left-handed manner such that three Ag^{I} atoms are close to each other (av. Ag···Ag = 3.053 Å). The complex-cation $[Co_3(aet)_6]^{3+}$ incorporated in $(\Delta_{LLL})_2$-$[Co_3(aet)_6][\mathbf{3}]$ exclusively adopts the $(\Delta)_2$ configuration, indicative of the chiralselective incorporation of the $(\Delta)_2$ isomer of $[Co_3(aet)_6]^{3+}$ in crystal.

Each $(\Delta_{LLL})_2$-$[\mathbf{3}]^{3-}$ anion is connected with four complex-anions; two of the four complex-anions are connected through Ag–OOC coordination bonds with a monodentate coordination mode (av. Ag–O = 2.619 Å), and the other two complex-anions are connected through hydrogen bonds between carboxylate and amine groups (av. NH···O = 3.063 Å), as shown in Figure 3-8. In addition, each $(\Delta_{LLL})_2$-$[\mathbf{3}]^{3-}$ anion is also connected with four complex-cations $[Co_3(aet)_6]^{3+}$; four carboxylate groups are hydrogen bonded with amine groups of the four complex-cations (av. NH···O = 2.895 Å), two of which coordinate to the Ag atoms of the neighboring complex-anions simultaneously (Figure 3-8). Thus, each $(\Delta_{LLL})_2$-$[\mathbf{3}]^{3-}$ anion is connected with four complex-anions and four complex-cations through the NH···O hydrogen bonds and Ag–O coordination bonds. On the other hand, each $(\Delta)_2$-$[Co_3(aet)_6]^{3+}$ cation is hydrogen-bonded with four adjacent complex-anions with the average NH···O distance of 3.048 Å (Figure 3-9). As a result, an anionic 2D sheet and a cationic 2D sheet are arranged alternately to form a hydrogen-bonding 3D network structure (Figure 3-10).

III-3-3 Chiralselectivity of $(\Delta_{LLL})_2$-$[M^I_3Co^{III}_2(L\text{-cys})_6]^{3-}$ (M^I = Au^I, Ag^I) and $(\Lambda_{LLL})_4$-$[Au^I_6Co^{III}_4(L\text{-cys})_{12}]^{6-}$ toward $(\Delta)_2/(\Lambda)_2$-$[Co^{III}_3(aet)_6]^{3+}$

As described above, the chiralselectivity of L-cysteinato Au^ICo^{III} or Ag^ICo^{III} complex-anions toward the racemic $[Co_3(aet)_6]^{3+}$ complex-cation was investigated. Treatment of $(\Delta_{LLL})_2$-$[Au_3Co_2(L\text{-cys})_6]^{3-}$ ($(\Delta_{LLL})_2$-[**1**]$^{3-}$) with $(\Delta)_2/(\Lambda)_2$-$[Co_3(aet)_6]^3$ gave the cocrystallized compound consisting of $(\Delta_{LLL})_2$-[**1**]$^{3-}$ and $[Co_3(aet)_6]^3$ in a 1:1 ratio. In this compound, the $(\Delta)_2$ isomer of $[Co_3(aet)_6]^3$ is preferentially selected, but its chiralselectivity is low. When $(\Lambda_{LLL})_2$-$[Au_3Co_2(L\text{-cys})_6]^{3-}$ ($(\Lambda_{LLL})_2$-[**1**]$^{3-}$) was treated with $[Co_3(aet)_6]^3$, the structural conversion of the complex-anion occurred to afford the cocrystallized compound $(\Lambda_{LLL})_4$-$[Co_3(aet)_6]_2$[**2**]. In $(\Lambda_{LLL})_4$-$[Co_3(aet)_6]_2$[**2**], the $(\Delta)_2$ isomer of $[Co_3(aet)_6]^3$ is also preferentially incorporated with an enantiomeric excess (*ee*) of 22%. On the other hand, the use of $(\Delta_{LLL})_2$-$[Ag_3Co_2(L\text{-cys})_6]^{3-}$ ($(\Delta_{LLL})_2$-[**3**]$^{3-}$) resulted in the selective uptake of $(\Delta)_2$-$[Co_3(aet)_6]^3$ exclusively upon the cocrystallization. From these results, it is speculated that the presence of Ag^I or Au^I centers in the complex-anions is the most important factor for the selective behavior toward racemic $[Co_3(aet)_6]^{3+}$, and the chirality of the Co^{III} centers as well as the nuclearity of the complex-anions also affect the chiralselectivity but as minor factors.

To elucidate the structural features that cause the different chiralselective behavior, the structures of the cocrystallized compounds are compared in detail, focused on the number of the intermolecular interactions between the complex-anion and the complex-caion. The carboxylate group of L-cys in the complex-anions can interact with the amine group of aet in the complex-cation. In $(\Delta_{LLL})_2$-$[Co_3(aet)_6]$[**1**], each $(\Delta_{LLL})_2$-[**1**]$^{3-}$ unit are connected to two complex-anions using two of the six free carboxylate groups, whereas other two carboxylate groups interact with the amine groups of the two complex-cations. Thus, each $(\Delta_{LLL})_2$-[**1**]$^{3-}$ unit is hydrogen-bonded with two complex-cations. In $(\Lambda_{LLL})_4$-$[Co_3(aet)_6]_2$[**2**], there exist twelve free carboxylate groups in the complex-anion unit. Four axially oriented carboxylate groups each forms an intramolecular hydrogen bond with the L-cys amine group, two of which also interact with the neighboring two complex-anions. Other two carboxylate groups are hydrogen bonded with the two complex-anions. Including the amine-donating hydrogen bonded two complex-anions, each complex-anion is connected with six complex-anions. Four carboxylate groups do not form a hydrogen bond, but make a pocket for the complex-cation. The remaining two carboxylate groups are hydrogen bonded with the amine groups of two complex-cations. Thus, only two intermolecular hydrogen bonding interactions between the complex-anion and complex-cation are formed in $(\Lambda_{LLL})_4$-$[Co_3(aet)_6]_2$[**2**]. On the other hand, in $(\Delta_{LLL})_2$-$[Co_3(aet)_6]$[**3**], intermolecular interactions not only through the hydrogen

bonds between the amine and carboxylate groups but also through the coordination bonds between the Ag^{I} ion and carboxylate group are formed. Thus, each complex-anion can be connected with many neighboring units. As a result, each complex-anion is connected with four complex-anions and four complex-cations.

In $(\Delta_{LLL})_2$-$[Co_3(aet)_6]$[**1**] that shows the low selectivity and $(\Lambda_{LLL})_4$-$[Co_3(aet)_6]_2$[**2**] that shows the better but still low selectivity, each complex-anion is connected with only two complex-cations, whereas four complex-cations are connected with each complex-anion in $(\Delta_{LLL})_2$-$[Co_3(aet)_6]$[**3**] that shows the excellent chiralselectivity. Thus, the number of the intermolecular interactions between the complex-anions and complex-cations in the crystal structure is considered to be essential for the chiralselective behavior upon the cocrystallization. Introduction of the Ag^{I} ion leads to the formation of the Ag–OOC coordination bonds besides hydrogen bonds, which resulted in the increase in the number of the intermolecular interactions, and thus, resulted in the excellent chiralselectivity in $(\Delta_{LLL})_2$-$[Co_3(aet)_6]$[**3**].

III-4 Summary

In this chapter, the chiralselectivity of three L-cysteinato complex-anions toward $(\Delta)_2/(\Lambda)_2$-$[Co_3(aet)_6]^{3+}$ was investigated. Treatment of $(\Delta_{LLL})_2$-$[Au_3Co_2(L\text{-}cys)_6]^{3-}$ ($(\Delta_{LLL})_2$-$[\mathbf{1}]^{3-}$) with $[Co_3(aet)_6]^{3}$ in water gave the cocrystallized compound of the starting materials, $(\Delta_{LLL})_2$-$[Co_3(aet)_6][\mathbf{1}]$. The separation of the complex-anion and complex-cation by column chromatography and the sequential absorption and CD spectral measurements showed that the $(\Delta)_2$ isomer of $[Co_3(aet)_6]^{3+}$ is preferentially incorporated in the bulk sample with low selectivity. In $(\Lambda_{LLL})_4$-$[Co_3(aet)_6]_2[\mathbf{2}]$, obtained by the treatment of $(\Lambda_{LLL})_2$-$[Au_3Co_2(L\text{-}cys)_6]^{3-}$ ($(\Lambda_{LLL})_2$-$[\mathbf{1}]^{3-}$) with $[Co_3(aet)_6]^{3+}$ in water, the $(\Delta)_2$ isomer of $[Co_3(aet)_6]^{3}$ is also preferentially selected in the bulk sample showing better chiralselectivity with the enantiomeric excess (*ee*) of 22%, which was confirmed by the column chromatography and the spectral measurements. The treatment of $(\Delta_{LLL})_2$-$[Ag_3Co_2(L\text{-}cys)_6]^{3-}$ ($(\Delta_{LLL})_2$-$[\mathbf{3}]^{3-}$) with $[Co_3(aet)_6]^{3}$ in water afforded the similar cocrystallized compound $(\Delta_{LLL})_2$-$[Co_3(aet)_6][\mathbf{3}]$. Remarkably, the $(\Delta)_2$ isomer of $[Co_3(aet)_6]^{3}$ was exclusively incorporated in the bulk sample of $(\Delta_{LLL})_2$-$[Co_3(aet)_6][\mathbf{3}]$. In $(\Delta_{LLL})_2$-$[Co_3(aet)_6][\mathbf{1}]$ and $(\Lambda_{LLL})_4$-$[Co_3(aet)_6]_2[\mathbf{2}]$, the low selective incorporation of $[Co_3(aet)_6]^{3}$ was observed, whereas $(\Delta_{LLL})_2$-$[Co_3(aet)_6][\mathbf{3}]$ showed the excellent selectivity. In the former two compounds, the complex-anions contain the Au^{I} linkers between the $[Co(L\text{-}cys)_3]^{3-}$ units, and the latter compound contains the Ag^{I} linkers in the complex-anion. Thus, it is speculated that the chirality of the Co^{III} centers in the complex-anions does not affect the chiralselectivity toward $[Co_3(aet)_6]^{3+}$, instead, the presence of the Ag^{I} centers in the complex-anions might lead to the excellent chiralselectivity. From the comparison of the packing structures of the three compounds, the number of the intermolecular interactions between the complex-anions and complex-cations is important for the chiralselective behavior. In the former two compounds containing the Au^{I} ions in the complex-anions, only two complex-cations are connected to each complex-anion through the hydrogen bonds. On the other hand, each complex-anion is surrounded by four complex-cations in $(\Delta_{LLL})_2$-$[Co_3(aet)_6][\mathbf{3}]$ containing the Ag^{I} ions in the complex-anion. The presence of the Ag^{I} ions instead of the Au^{I} ions leads to the formation of the Ag–OOC coordination bonds besides hydrogen bonds, which resulted in the increase in the number of the intermolecular interactions between the complex-anion and complex-cation, and thus resulted in the excellent chiralselectivity in $(\Delta_{LLL})_2$-$[Co_3(aet)_6][\mathbf{3}]$.

III-5 References

(1) T. Konno, K. Tokuda, T. Suzuki, K. Okamoto, *Bull*. *Chem*. *Soc*. *Jpn*. **1998**, *71*, 1049–1054.

(2) (a) G. R. Brubaker, B. E. Douglas, *Inorg*. *Chem*. **1967**, *6*, 1562–1566. (b) M. J. Heeg, E. L. Blinn, E. Deutsch, *Inorg*. *Chem*. **1985**, *24*, 1118–1120. (c) S. Miyanowaki, T. Konno, K. Okamoto, J. Hidaka, *Bull*. *Chem*. *Soc*. *Jpn*. **1988**, *61*, 2987–2989.

(3) (a) G. M. Sheldrick, *Acta Crystallogr*. **2008**, *A64*, 112–122. (b) C. Kabuto, S. Akine, E. Kwon, *J*. *Cryst*. *Soc*. *Jpn*. **2009**, *51*, 218–224.

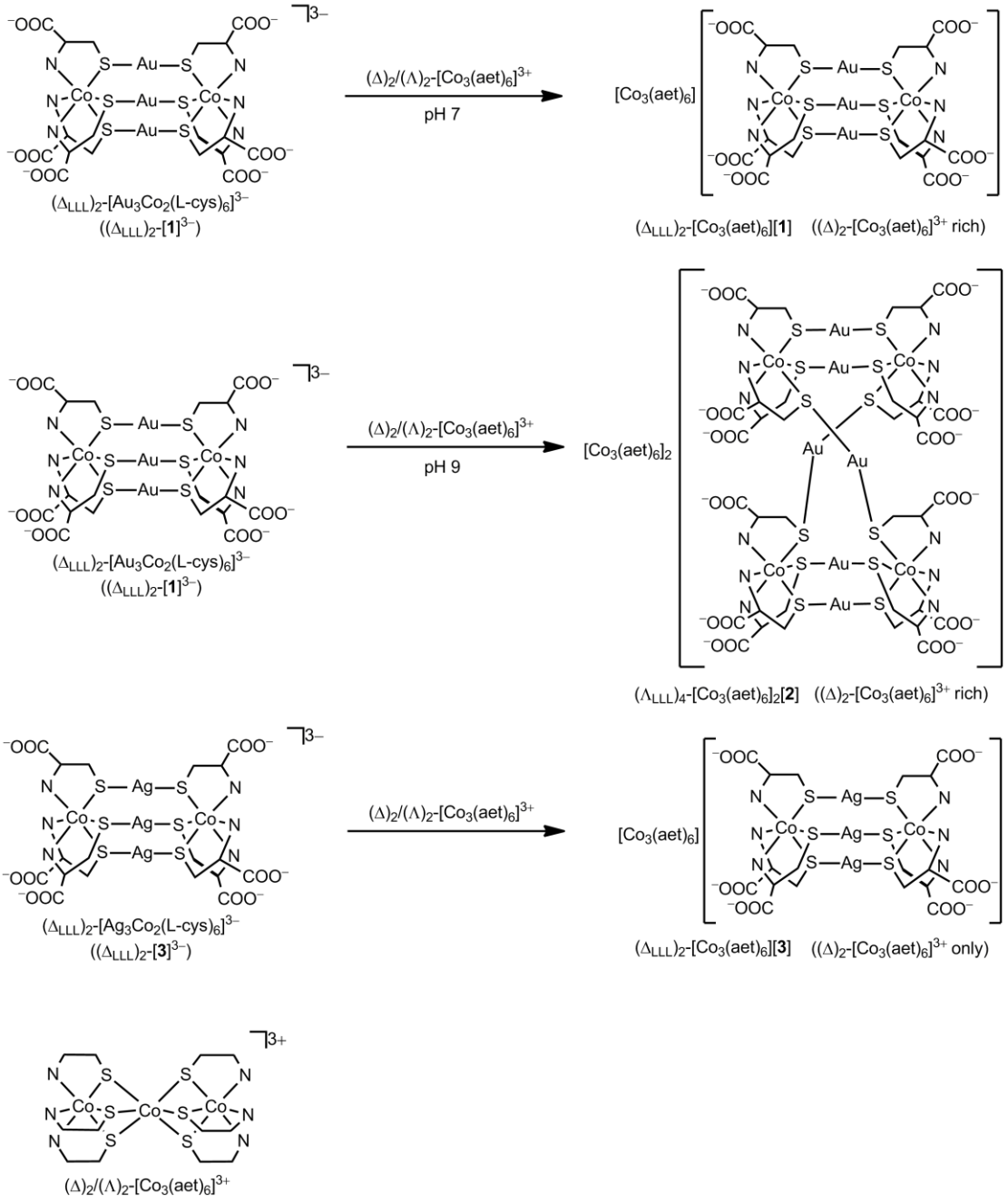

Scheme 3-1. Schematic representation of chiralselective crystallizations.

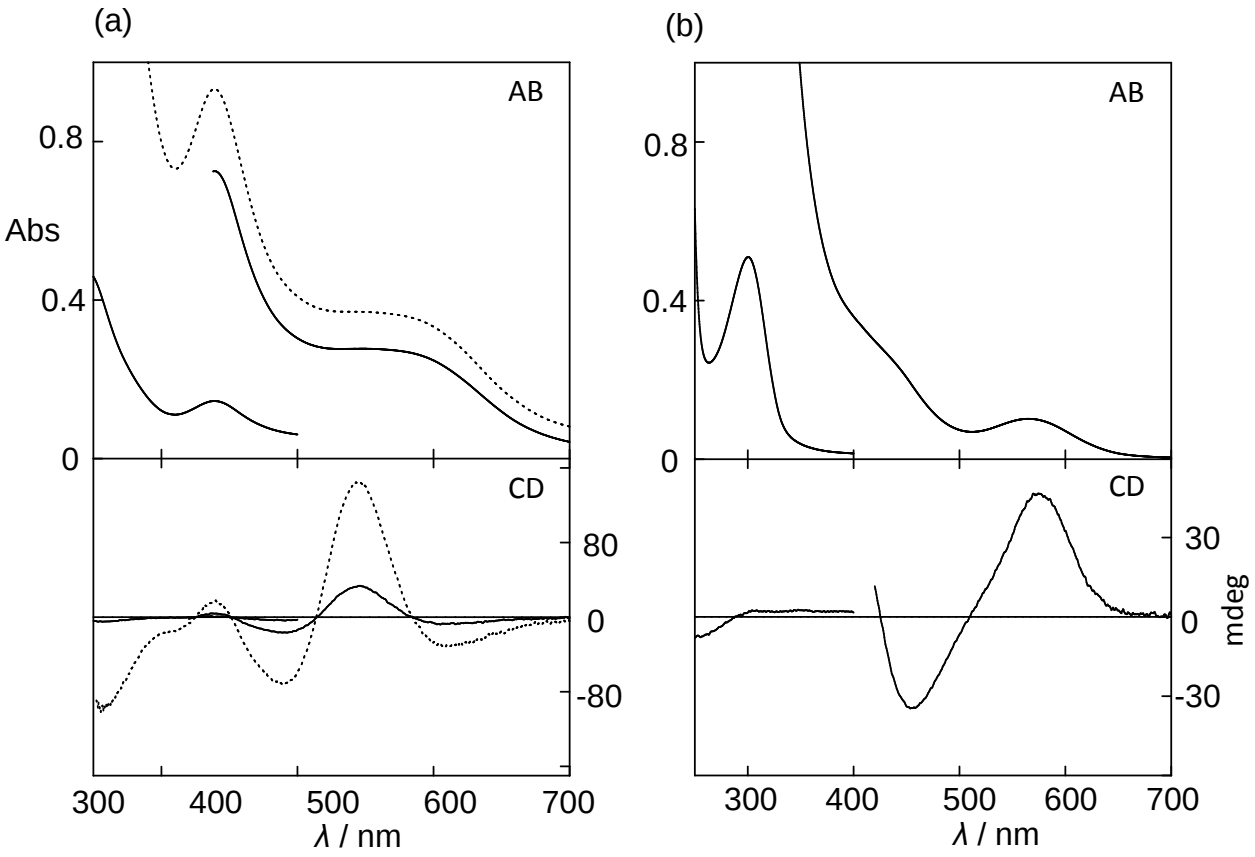

Figure 3-1. Absorption and CD spectra of (a) $[Co_3(aet)_6]^{3+}$ and (b) $(\Lambda_{LLL})_4$-[**2**]$^{6-}$ incorporated in $(\Lambda_{LLL})_4$-$[Co_3(aet)_6]_2$[**2**] in water (—), together with those of $(\Delta)_2$-$[Co_3(aet)_6]^{3+}$ (---).

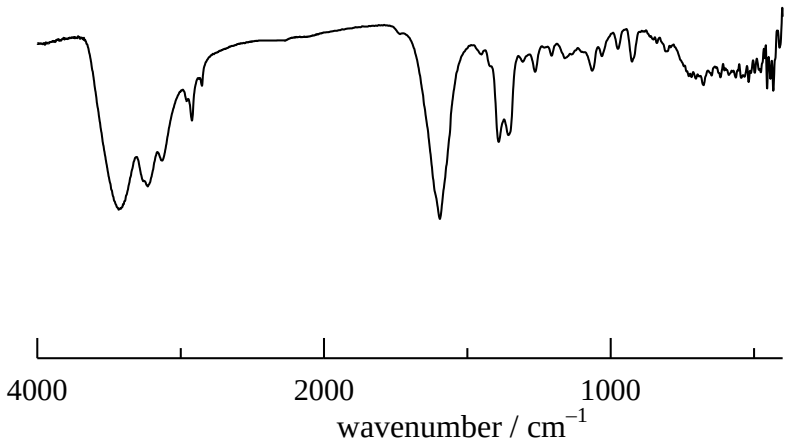

Figure 3-2. IR spectrum of $(\Delta_{LLL})_2$-$[Co_3(aet)_6]$[**3**] (KBr disk).

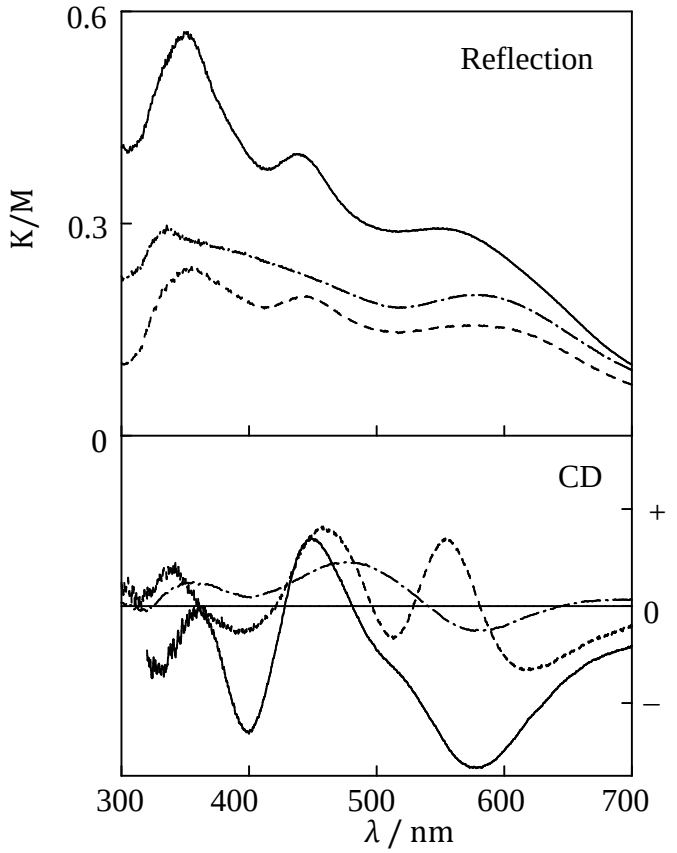

Figure 3-3. Reflection and CD spectra of $(\Delta_{LLL})_2$-$[Co_3(aet)_6]$[**1**] (—), $(\Delta_{LLL})_2$-$[Co_3(aet)_6]$[**3**] (---), and $(\Delta_{LLL})_2$-K_3[**3**] (-·-·-) in the solid state. For $(\Delta_{LLL})_2$-$[Co_3(aet)_6]$[**1**], reflection spectrum [λ / nm]: 560, 437, 352; CD spectrum [λ / nm]: 610 (–), 550 (+), 459 (+), 398 (–). For $(\Delta_{LLL})_2$-$[Co_3(aet)_6]$[**3**], reflection spectrum [λ / nm]: 557, 440, 350; CD spectrum [λ / nm]: 576 (–), 450 (+), 398 (–), 340 (+). For $(\Delta_{LLL})_2$-K_3[**3**], reflection spectrum [λ / nm]: 584, 355; CD spectrum [λ / nm]: 579 (–), 482 (+),400 (+), 352 (+).

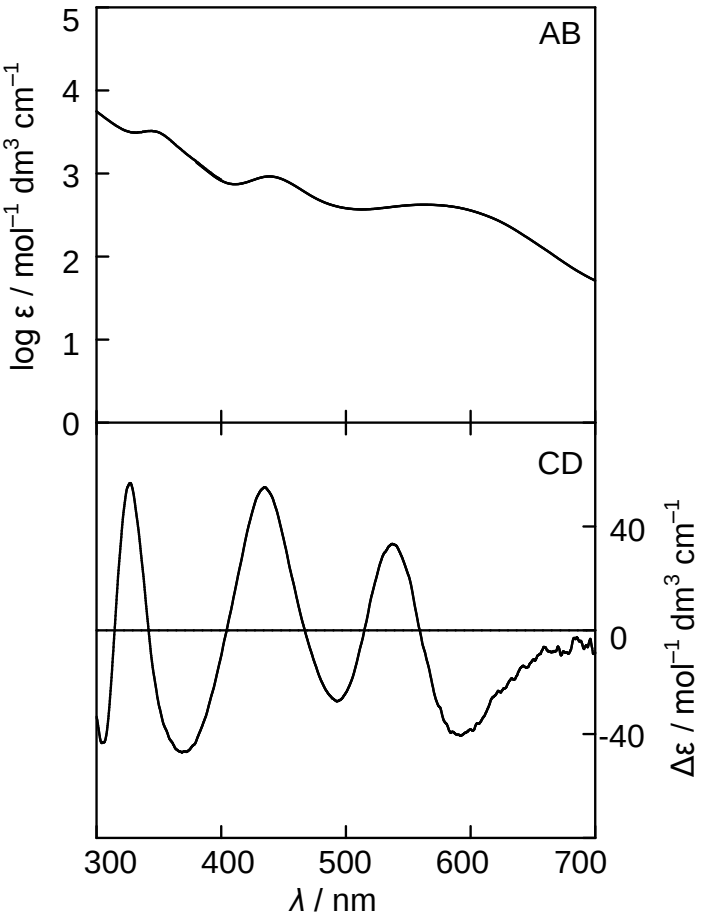

Figure 3-4. Absorption and CD spectra of $(\Delta_{LLL})_2$-$[Co_3(aet)_6]$[**3**] in a $NaNO_3$ aqueous solution.

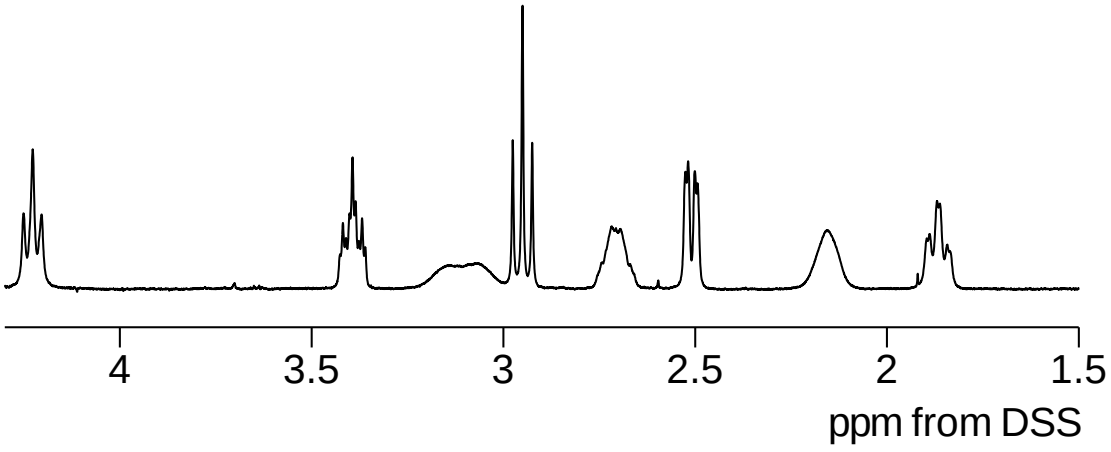

Figure 3-5. ^{1}H NMR spectrum of $(\Delta_{LLL})_2$-$[Co_3(aet)_6]$[**3**] in D_2O containing $NaNO_3$.

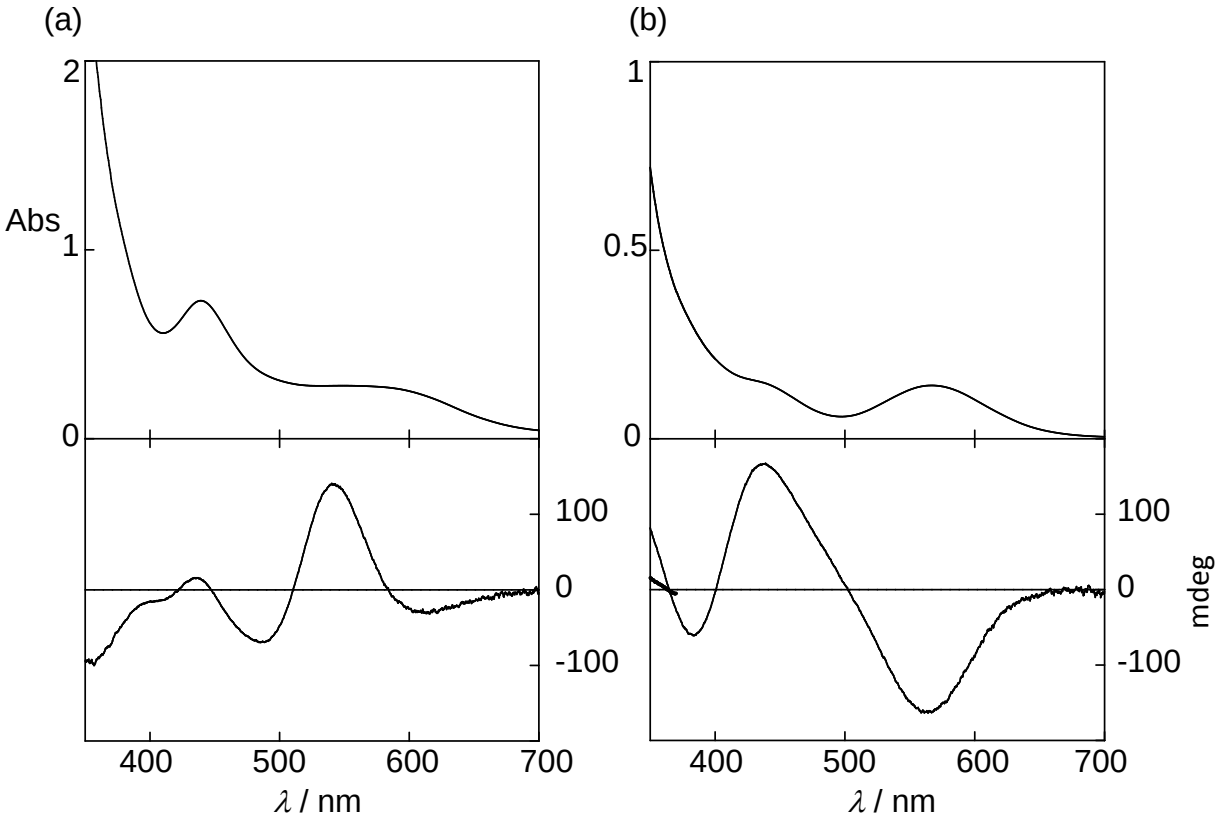

Figure 3-6. Absorption and CD spectra of (a) $[Co_3(aet)_6]^{3+}$ and (b) $[\mathbf{3}]^{3-}$ incorporated in $(\Delta_{LLL})_2$-$[Co_3(aet)_6][\mathbf{3}]$ in water.

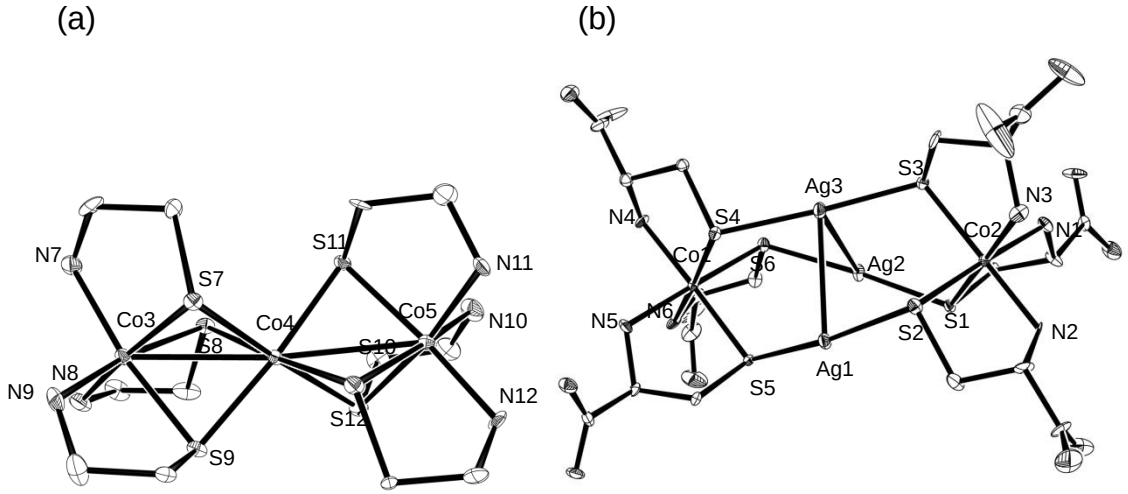

Figure 3-7. ORTEP drawings of (a) $[Co_3(aet)_6]^{3+}$ and (b) $(\Delta_{LLL})_2$-[**3**]$^{3-}$ in $(\Delta_{LLL})_2$-$[Co_3(aet)_6]$[**3**]. Hydrogen atoms are omitted for clarity.

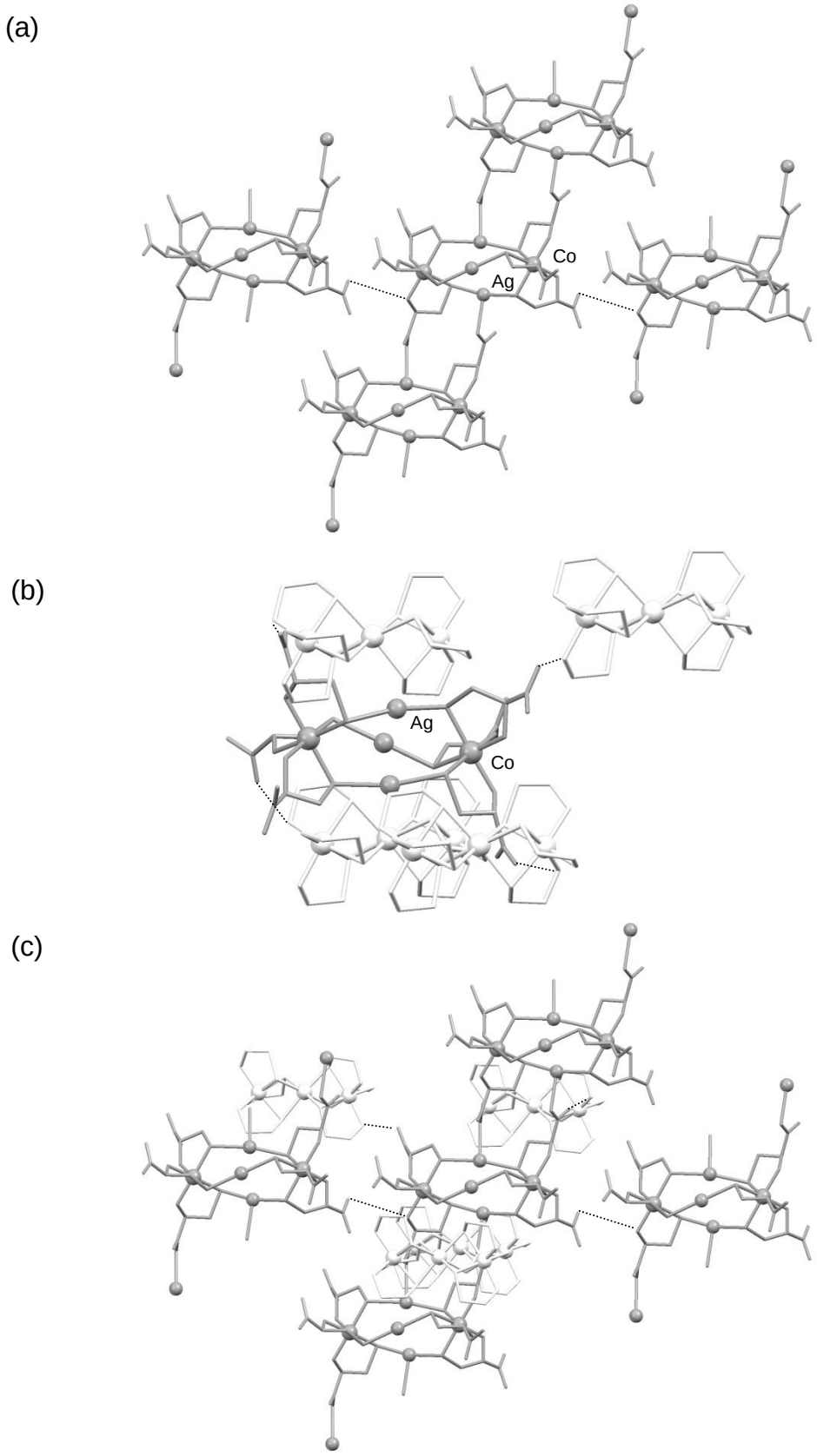

Figure 3-8. Perspective views of intermolecular interactions around each complex-anion in $(\Delta_{LLL})_2$-$[Co_3(aet)_6]$[**3**]. Interactions (a) with complex-anions, (b) with complex-cations, and (c) with both complex-anions and complex-cations.

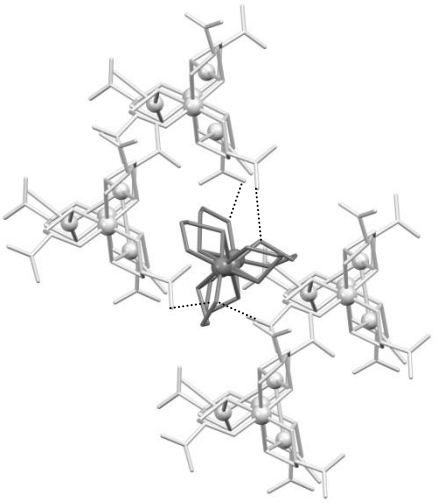

Figure 3-9. Perspective view of intermolecular interactions around each complex-cation in $(\Delta_{LLL})_2$-$[Co_3(aet)_6]$[**3**].

(a)

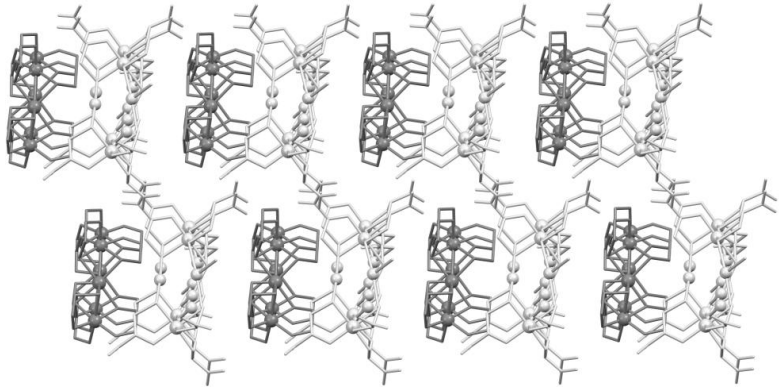

(b)

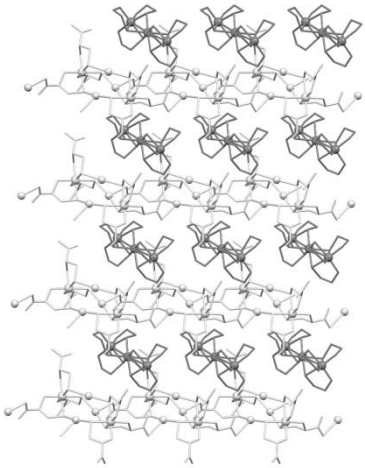

Figure 3-10. Packing structures of $(\Delta_{LLL})_2$-$[Co_3(aet)_6]$[**3**] viewing from (a) *a* axis and (b) *c* axis. Dark gray and light gray molecules represent complex-cation and complex-anion, respectively.

Table 3-1. Crystallographic data of $(\Delta_{LLL})_2$-$[Co_3(aet)_6][\mathbf{3}]$.

	$(\Delta_{LLL})_2$-$[Co_3(aet)_6][\mathbf{3}]\cdot 8H_2O$
Empirical formula	$C_{30}H_{66}Ag_3Co_5N_{12}O_{12}S_{12}$
Formula weight	1789.93
Crystal system	*P*1
Space group	triclinic
a / Å	10.02596(18)
b / Å	12.4445(2)
c / Å	14.3300(3)
α / °	70.511(5)
β / °	71.151(5)
γ / °	86.980(6)
V / Å ^{3}	1592.06(5)
Z	1
T / K	200(2)
R(int)	0.0211
ρ_{calcd} / g cm^{-3}	1.867
μ(Mo *K*α) / cm^{-1}	2.621
θ_{max}	54.98
total no. of data	12788
no. of unique data	11385
no. of parameters	297
*R*1, w*R*2 (I>2σ(I))[a,b]	0.0879, 0.2650
*R*1, w*R*2 (all data)[a,b]	0.0890, 0.2679

[a] $R1 = \Sigma(|(|F_o|-|F_c|)| / \Sigma(|F_o|)$, [b] $wR2 = [\Sigma w(F_o^2-F_c^2)^2 / \Sigma w(F_o^2)^2]^{1/2}$

Table 3-2. Selected bond distances and angles of $(\Delta_{LLL})_2$-$[Co_3(aet)_6]$[**3**].

Distances (Å)			
Ag(1)-S(2)	2.444(2)	O(1)-Ag(1)#2	2.501(8)
Ag(1)-S(5)	2.448(2)	Co(3)-N(7)	1.991(10)
Ag(1)-O(1)#1	2.501(8)	Co(3)-N(8)	2.020(10)
Ag(2)-S(1)	2.442(2)	Co(3)-N(9)	2.024(10)
Ag(2)-S(4)	2.447(3)	Co(3)-S(9)	2.220(3)
Ag(3)-S(3)	2.406(2)	Co(3)-S(7)	2.241(3)
Ag(3)-S(6)	2.416(2)	Co(3)-S(8)	2.257(3)
Co(1)-N(2)	1.983(8)	Co(4)-S(9)	2.235(2)
Co(1)-N(1)	1.983(9)	Co(4)-S(11)	2.237(3)
Co(1)-N(3)	1.989(9)	Co(4)-S(12)	2.246(3)
Co(1)-S(2)	2.225(3)	Co(4)-S(7)	2.253(3)
Co(1)-S(1)	2.248(2)	Co(4)-S(10)	2.270(3)
Co(1)-S(3)	2.256(3)	Co(4)-S(8)	2.300(3)
Co(2)-N(4)	1.987(8)	Co(5)-N(12)	1.977(10)
Co(2)-N(6)	1.996(8)	Co(5)-N(10)	2.005(10)
Co(2)-N(5)	1.998(9)	Co(5)-N(11)	2.013(10)
Co(2)-S(4)	2.227(3)	Co(5)-S(11)	2.224(3)
Co(2)-S(5)	2.245(3)	Co(5)-S(12)	2.235(3)
Co(2)-S(6)	2.252(2)	Co(5)-S(10)	2.241(3)

Angles (°)			
S(2)-Ag(1)-S(5)	167.61(9)	N(1)-Co(1)-S(3)	92.1(3)
S(1)-Ag(2)-S(4)	168.85(9)	N(3)-Co(1)-S(3)	86.6(3)
S(3)-Ag(3)-S(6)	176.82(9)	S(2)-Co(1)-S(3)	90.51(10)
N(2)-Co(1)-N(1)	90.7(4)	S(1)-Co(1)-S(3)	92.06(9)
N(2)-Co(1)-N(3)	90.2(4)	N(4)-Co(2)-N(6)	88.9(4)
N(1)-Co(1)-N(3)	89.7(4)	N(4)-Co(2)-N(5)	88.8(4)
N(2)-Co(1)-S(2)	86.7(3)	N(6)-Co(2)-N(5)	90.3(4)
N(1)-Co(1)-S(2)	177.2(3)	N(4)-Co(2)-S(4)	87.9(3)
N(3)-Co(1)-S(2)	91.5(3)	N(6)-Co(2)-S(4)	89.9(3)
N(2)-Co(1)-S(1)	91.3(3)	N(5)-Co(2)-S(4)	176.7(3)
N(1)-Co(1)-S(1)	88.3(2)	N(4)-Co(2)-S(5)	90.9(3)
N(3)-Co(1)-S(1)	177.5(3)	N(6)-Co(2)-S(5)	178.6(3)
S(2)-Co(1)-S(1)	90.55(9)	N(5)-Co(2)-S(5)	88.3(3)
N(2)-Co(1)-S(3)	175.7(3)	S(4)-Co(2)-S(5)	91.50(10)

Table 3-2. (continued).

N(4)-Co(2)-S(6)	175.5(3)	S(12)-Co(4)-S(7)	175.97(12)
N(6)-Co(2)-S(6)	87.1(3)	S(9)-Co(4)-S(10)	174.45(12)
N(5)-Co(2)-S(6)	93.3(3)	S(11)-Co(4)-S(10)	82.28(10)
S(4)-Co(2)-S(6)	90.02(10)	S(12)-Co(4)-S(10)	82.19(10)
S(5)-Co(2)-S(6)	93.12(10)	S(7)-Co(4)-S(10)	100.21(10)
N(7)-Co(3)-N(8)	98.4(5)	S(9)-Co(4)-S(8)	82.82(10)
N(7)-Co(3)-N(9)	91.2(4)	S(11)-Co(4)-S(8)	174.89(12)
N(8)-Co(3)-N(9)	93.1(4)	S(12)-Co(4)-S(8)	100.45(10)
N(7)-Co(3)-S(9)	171.4(3)	S(7)-Co(4)-S(8)	82.37(11)
N(8)-Co(3)-S(9)	90.2(4)	S(10)-Co(4)-S(8)	100.19(11)
N(9)-Co(3)-S(9)	88.1(3)	N(12)-Co(5)-N(10)	95.9(5)
N(7)-Co(3)-S(7)	86.1(3)	N(12)-Co(5)-N(11)	94.8(5)
N(8)-Co(3)-S(7)	171.4(4)	N(10)-Co(5)-N(11)	96.9(4)
N(9)-Co(3)-S(7)	94.1(3)	N(12)-Co(5)-S(11)	172.1(4)
S(9)-Co(3)-S(7)	85.42(10)	N(10)-Co(5)-S(11)	90.9(3)
N(7)-Co(3)-S(8)	96.2(3)	N(11)-Co(5)-S(11)	88.4(3)
N(8)-Co(3)-S(8)	88.6(3)	N(12)-Co(5)-S(12)	87.8(3)
N(9)-Co(3)-S(8)	172.0(3)	N(10)-Co(5)-S(12)	169.7(3)
S(9)-Co(3)-S(8)	84.13(10)	N(11)-Co(5)-S(12)	92.4(3)
S(7)-Co(3)-S(8)	83.60(10)	S(11)-Co(5)-S(12)	84.82(10)
S(9)-Co(4)-S(11)	95.09(10)	N(12)-Co(5)-S(10)	93.0(3)
S(9)-Co(4)-S(12)	92.71(10)	N(10)-Co(5)-S(10)	87.1(3)
S(11)-Co(4)-S(12)	84.28(10)	N(11)-Co(5)-S(10)	170.8(3)
S(9)-Co(4)-S(7)	84.77(10)	S(11)-Co(5)-S(10)	83.21(10)
S(11)-Co(4)-S(7)	92.81(11)	S(12)-Co(5)-S(10)	83.08(11)

Symmetry codes: (#1) x+1, y, z, (#2) x–1, y, z.

Table 3-3. Absorption and CD spectral data for $(\Delta_{LLL})_2$-$[Co_3(aet)_6]$[**3**] in a $NaNO_3$ aqueous solution.

Complex	Absorption maxima: λ / nm (log ε / mol^{-1} dm^3 cm^{-1})
$(\Delta_{LLL})_2$-$[Co_3(aet)_6]$[**3**]	558 (2.62), 439 (2.96), 346 (3.51), 279 (3.94), 253 (3.93)

Complex	CD extrema: λ / nm ($\Delta\varepsilon$ / mol^{-1} dm^3 cm^{-1})
$(\Delta_{LLL})_2$-$[Co_3(aet)_6]$[**3**]	591 (–40.53), 537 (+33.27), 493 (–27.29), 346 (+55.11), 368 (–46.97), 326 (+56.71)

Table 3-4. Reflection and CD spectral data for $(\Delta_{LLL})_2$-K_3[**3**] and $(\Delta_{LLL})_2$-$[Co_3(aet)_6]$[**3**] in the solid state.

Complex	Reflection maxima: λ / nm
$(\Delta_{LLL})_2$-K_3[**3**]	584, 335
$(\Delta_{LLL})_2$-$[Co_3(aet)_6]$[**3**]	582, 443, 352

Complex	CD extrema: λ / nm
$(\Delta_{LLL})_2$-K_3[**3**]	579 (–), 482 (+),400 (+), 352 (+)
$(\Delta_{LLL})_2$-$[Co_3(aet)_6]$[**3**]	618 (–), 555 (+), 513(–), 459 (+), 392 (–), 352 (–)

Chapter IV. Chiral Recognition Behavior of $(\Delta_{LLL})_2$-$[M_3Rh^{III}_2(L\text{-cys})_6]^{3-}$ (M = Au^I, Ag^I) toward $(\Delta)_2/(\Lambda)_2$-$[Co^{III}_3(aet)_6]^{3+}$

IV-1 Introduction

In the previous study and this study described in Chapter III, it was shown that L-cysteinato multinuclear complex-anions act as a resolving reagent toward racemic complex-cations through the cocrystallization. When $(\Delta_{LLL})_2$- and $(\Lambda_{LLL})_2$-$[Co_3(L\text{-cys})_6]^{3-}$ were treated with $(\Delta)_2/(\Lambda)_2$-$[Co_3(aet)_6]^{3+}$ and $(\Delta)_2/(\Lambda)_2$-$[Ag_3Co_2(aet)_6]^{3+}$, $(\Lambda_{LLL})_2$-$[Co_3(L\text{-cys})_6]^{3-}$ selected the $(\Delta)_2$-$[Co_3(aet)_6]^{3+}$ and $(\Lambda)_2$-$[Ag_3Co_2(aet)_6]^{3+}$ with an excellent enantiomeric excess (*ee*) of ~100%, whereas $(\Delta_{LLL})_2$-$[Co_3(L\text{-cys})_6]^{3-}$ showed only low chiralselectivity.[1] From the X-ray structural analysis, the orientation of the carboxylate groups in the complex-anions is essential for the chiralselective behavior. That is, in $(\Delta_{LLL})_2$-$[Co_3(L\text{-cys})_6]^{3-}$ having the equatorially oriented carboxylate groups, the efficient hydrogen bonding interactions between the complex-anions are formed, which leads to the less number of the intermolecular interactions between the complex-anions and complex-cations. On the other hand, in $(\Lambda_{LLL})_2$-$[Co_3(L\text{-cys})_6]^{3-}$ having the axially oriented carboxylate groups, there exist much number of intermolecular interactions between the complex-anions and the complex-cations, which resulted in the excellent chiralselectivity. In addition, further structural inspection showed that the presence of the Ag^I ion also contributes to the good chiralselectivity, because the Ag^I ion can form an additional interaction with the carboxylate group. In fact, the use of $(\Delta_{LLL})_2$-$[Ag_3Co_2(L\text{-cys})_6]^{3-}$ ($(\Delta_{LLL})_2$-$[\mathbf{3}]^{3-}$) also led to the excellent chiralselectivity toward $(\Delta)_2/(\Lambda)_2$-$[Co_3(aet)_6]^{3+}$, as shown in Chapter III. On the other hand, the complex-anion $(\Delta_{LLL})_2$-$[Au_3Co_2(L\text{-cys})_6]^{3-}$ ($(\Delta_{LLL})_2$-$[\mathbf{1}]^{3-}$) only showed the low chiralselectivity in spite of the similar structure, because the Au^I ions cannot form a coordination bond.

In this chapter, the chiral behavior of two complex-anions, $(\Delta_{LLL})_2$-$[Au_3Rh_2(L\text{-cys})_6]^{3-}$ ($(\Delta_{LLL})_2$-$[\mathbf{4}]^{3-}$) and $(\Delta_{LLL})_2$-$[Ag_3Rh_2(L\text{-cys})_6]^{3-}$ ($(\Delta_{LLL})_2$-$[\mathbf{5}]^{3-}$), is investigated. Both complex-anions were crystallized with $[Co_3(aet)_6]^{3+}$ to form cocrystallized compounds, $(\Delta_{LLL})_2$-$[Co_3(aet)_6][\mathbf{4}]$ and $(\Delta_{LLL})_2$-$[Co_3(aet)_6][\mathbf{5}]$ (Scheme 4-1). The chirality of the complex-cation $[Co_3(aet)_6]^{3+}$ was checked by the similar method described in Chapter III. In addition, the possibility of the chiral and structural conversions observed in the L-cysteinato Au^ICo^{III} system shown in Chapter II was also studied. The influence of the inert Rh^{III} centers to the chiral behavior such as chiral inversions and chiralselectivity is discussed. And also, the important structural features for the excellent chiralselectivity toward $[Co_3(aet)_6]^{3+}$ are proposed, by comparing the structures and chiralselectivity of

the seven cocrystallized compounds, $(\Delta_{LLL})_2$-$[Co_3(aet)_6]$[**1**], $(\Lambda_{LLL})_4$-$[Co_3(aet)_6]_2$[**2**], $(\Delta_{LLL})_2$-$[Co_3(aet)_6]$[**3**], $(\Delta_{LLL})_2$-$[Co_3(aet)_6]$[**4**], $(\Delta_{LLL})_2$-$[Co_3(aet)_6]$[**5**], $(\Delta_{LLL})_2$-$[Co_3(aet)_6][Co_3(\text{L-cys})_6]$, and $(\Lambda_{LLL})_2$-$[Co_3(aet)_6][Co_3(\text{L-cys})_6]$, including two reported compounds.

IV-2 Experimental Section

IV-2-1 Materials

All chemicals were of commercial grade and use without further purification. The starting material $(\Delta)_2/(\Lambda)_2$-$[Co_3(aet)_6](NO_3)_3 \cdot H_2O$ was prepared by the method described in the literature.[2]

IV-2-2 Preparation of $M_3Rh_2^{III}$ ($M = Au^I, Ag^I$) Complexes

(a) $(\Delta_{LLL})_2$-$K_3[Au^I_3Rh^{III}_2(L\text{-cys})_6]$ ($(\Delta_{LLL})_2$-K$_3$[4])

To a suspension of (Δ_{LLL})-$H_3[Rh(L\text{-cys-}N,S)_3]$ (0.30 g, 0.65 mmol) in 15 mL of water was added an aqueous solution of KOH (0.5 M) until the suspension became a clear solution. To the yellow solution was added a solution containing $HAuCl_4$ (0.40 g, 0.96 mmol) and 2,2'-thiodiethanol (0.1 mL) in 15 mL of water. The yellow solution was stirred at room temperature for 2 h, and the resulting yellow powder was collected by filtration. The yellow powder was dissolved in water by adding KOH aqueous solution (0.5 M), to which was added a large amount of EtOH. The precipitated yellow powder of $(\Delta_{LLL})_2$-K_3[**4**]$\cdot 11H_2O$ were collected by filtration. Yield: 0.48 g (81%). Anal. Calcd for $K_3[Au_3Rh_2(L\text{-cys})_6] \cdot 11H_2O$ = $C_{18}H_{52}Au_3Rh_2S_6N_6O_{23}K_3$: C, 11.83; H, 2.87; N, 4.60%. Found: C, 11.79; H, 2.76; N, 4.56%. IR (KBr, cm^{-1}): 1608 (ν_{COO}-). Absorption spectrum in H_2O [λ / nm ($\log\varepsilon$ / mol^{-1} dm^3 cm^{-1})]: 365 (3.37), 302 (3.87)^{sh}, 250 (4.65)^{sh}, 214 (4.84). CD spectrum in H_2O [λ / nm ($\Delta\varepsilon$ / mol^{-1} dm^3 cm^{-1})]: 380 (–28.27), 343 (+10.68), 266 (–187.27), 226 (+221.81).

(b) $(\Delta_{LLL})_2$-$H_4[Ag^I_3Rh^{III}_2(L\text{-cys})_6](NO_3)$ ($(\Delta_{LLL})_2$-H_4[5](NO_3))

To a yellow suspension of (Δ_{LLL})-$H_3[Rh(L\text{-cys-}N,S)_3]$ (0.10 g, 0.22 mmol) in 5 mL of water was added an aqueous solution of KOH (0.5 M) until the suspension became a clear solution. To the yellow solution was added a solution of $AgNO_3$ (0.056 g, 0.33 mmol) in 5 mL of water. The mixture was stirred at room temperature for 1 h. After filtration, a HNO_3 aqueous solution (1 M, 0.5 mL) was added to the yellow filtrate. The precipitated yellow powder $(\Delta_{LLL})_2$-H_4[**5**]NO_3 was collected by filtration. Yield: 105 mg (62%). Anal. Calcd for $H_4[Ag_3Rh_2(L\text{-cys})_6](NO_3) \cdot 11H_2O$ = $C_{18}H_{56}Ag_3Rh_2S_6N_7O_{26}$: C, 14.35%; H, 3.75%; N, 6.51%. Found: C, 14.08%; H, 3.55%; N, 6.57%. IR (KBr, cm^{-1}): 1717 (ν_{COOH}), 1605 (ν_{COO}-), 1383 (ν_{NO3}-). Absorption spectrum in H_2O [λ / nm ($\log\varepsilon$ / mol^{-1} dm^3 cm^{-1})]: 374 (3.21), 316 (3.6)^{sh}, 275 (4.3)^{sh}, 228 (4.80). CD spectrum in H_2O [λ / nm ($\Delta\varepsilon$ / mol^{-1} dm^3 cm^{-1})]: 380 (–20.01), 338 (+11.33), 239 (–86.53), 219 (+155.1).

IV-2-3 Preparation of Cocrystallized Compounds

(a) $(\Delta_{LLL})_2$-$[Co^{III}_3(aet)_6][Au^{I}_3Rh^{III}_2(L\text{-}cys)_6]$ ($(\Delta_{LLL})_2$-$[Co^{III}_3(aet)_6][4]$)

To a solution containing 50 mg (0.027 mmol) of $(\Delta_{LLL})_2$-K_3[**4**]·$11H_2O$ in 5 mL of water was added a solution containing 46 mg (0.055 mmol) of $(\Delta)_2/(\Lambda)_2$-$[Co_3(aet)_6](NO_3)_3$·H_2O in 5 mL of water. The black solution was allowed to stand at room temperature for 1 week. The resulting black crystals of $(\Delta_{LLL})_2$-$[Co_3(aet)_6]$[**4**] were collected by filtration. Yield: 44 mg (65%). Calcd for $[Co_3(aet)_6][Au_3Rh_2(L\text{-}cys)_6]$·$17H_2O$ = $C_{30}H_{100}N_{12}O_{29}S_{12}Co_3Rh_2Au_3$: C, 14.69; H, 4.11; N, 6.85%. Found: C, 14.73; H, 4.14; N, 6.83%. IR (KBr, cm^{-1}): 1603 (ν_{COO}-). Absorption spectrum in a $NaNO_3$ aqueous solution [λ / nm (logε / mol^{-1} dm^3 cm^{-1})]: 575 (3.27), 432 (3.79), 345 (4.30), 289 (4.52). CD spectrum in a $NaNO_3$ aqueous solution [λ / nm ($\Delta\varepsilon$ / mol^{-1} dm^3 cm^{-1})]: 610 (–0.28), 545 (+1.67), 484 (–0.68), 379 (–30.48), 341 (+9.46), 265 (–185.40). One of the single crystals was used for X-ray measurement.

(b) $(\Delta_{LLL})_2$-$[Co^{III}_3(aet)_6][Ag^{I}_3Rh^{III}_2(L\text{-}cys)_6]$ ($(\Delta_{LLL})_2$-$[Co^{III}_3(aet)_6][5]$)

To a yellow suspension containing 50 mg (0.033 mmol) of $(\Delta_{LLL})_2$-H_4[**5**](NO_3)·$11H_2O$ in 5 mL of water was added an aqueous solution of KOH (0.1 M, 6.5 mL) until the suspension became a clear solution. To the yellow solution was added a solution containing 46 mg (0.055 mmol) of $(\Delta)_2/(\Lambda)_2$-$[Co_3(aet)_6](NO_3)_3$·H_2O in 10 mL of water. The mixture was allowed to stand at room temperature for 2 weeks. The resulting black crystals of $(\Delta_{LLL})_2$-$[Co_3(aet)_6]$[**5**] were collected by filtration. Yield: 40 mg (60%). Calcd for $[Co_3(aet)_6][Ag_3Rh_2(L\text{-}cys)_6]$·$9H_2O$ = $C_{30}H_{84}N_{12}O_{21}S_{12}Co_3Rh_2Ag_3$: C, 17.68; H, 4.12; N, 8.25%. Found: C, 17.69; H, 4.12; N, 8.20%. IR (KBr, cm^{-1}): 1596 (ν_{COO}-). Absorption spectrum in a saturated $NaNO_3$ aqueous solution [λ / nm (logε / mol^{-1} dm^3 cm^{-1})]: 585 (3.36), 439 (3.70), 346 (4.31), 276 (4.65). CD spectrum in a $NaNO_3$ aqueous solution [λ / nm ($\Delta\varepsilon$ / mol^{-1} dm^3 cm^{-1})]: 606 (–3.69), 543 (+16.63), 487 (–8.47), 439 (+1.12), 376 (–19.69), 330 (+11.26), 304 (–9.28), 283 (+14.75), 241 (–56.74). One of single crystals was used for X-ray measurement.

IV-2-4 Physical Measurements

The electronic absorption spectra were recorded with a JASCO V-660 or a JASCO V-630 spectrophotometers using a 1 cm quartz cell at room temperature. The diffuse reflectance spectra were recorded on a JASCO V-570 spectrophotometer at room temperature by using $MgSO_4$. The CD spectra were recorded with a J-820 spectrometer at room temperature using a 1 cm quartz cell for the solution state and using KBr disks for the solid state. The IR spectra were recorded on a JASCO

FT/IR-4100 infrared spectrometer using KBr disks at room temperature. The elemental analyses (C, H, N) were performed at Osaka University. X-ray fluorescence analyses were made on a HORIBA MESA-500 or SHIMADZU EDX-720 spectrometer. The ^{1}H NMR spectra were recorded with a JEOL ECA500 (500 MHz) spectrometer at room temperature in D_2O, using sodium 4,4'-dimethyl-4-silapentane-1-sulfonate (DSS) as the internal standard.

IV-2-5 X-ray Structural Determination

Single-crystal X-ray diffraction measurements for $(\Delta_{LLL})_2$-H_4[**5**]$(NO_3)\cdot 9H_2O$, $(\Delta_{LLL})_2$-$[Co_3(aet)_6]$[**4**]$\cdot 16H_2O$, and $(\Delta_{LLL})_2$-$[Co_3(aet)_6]$[**5**]$\cdot 6H_2O$ were performed on a Rigaku R-AXIS VII imaging plate area detector with a graphite monochromated Mo Kα radiation at –73^{o}C. The intensity data were collected by the ω-scan technique and were empirically corrected for absorption. The structures were solved by direct methods using SHELXS-97.[3] The structure refinements were carried out using full-matrix least-squares (SHELXL-97).[3] All calculations were performed using the Yadokari-XG software package.[3] For $(\Delta_{LLL})_2$-H_4[**5**]$(NO_3)\cdot 9H_2O$, non-hydrogen atoms except the disordered atoms were refined anisotropically, while the others are refined isotropically. Hydrogen atoms were included in calculated positions except those of water molecules. A quarter of NO_3^- was not refined because of the severe disorder. For $(\Delta_{LLL})_2$-$[Co_3(aet)_6]$[**4**], all non-hydrogen atoms except the C, O, and disordered N atoms were refined anisotropically, while the others are refined isotropically. Hydrogen atoms were included in calculated positions except those of aet ligands and water molecules. For $(\Delta_{LLL})_2$-$[Co_3(aet)_6]$[**5**], all non-hydrogen atoms except the water molecule were refined anisotropically, while the others are refined isotropically. Hydrogen atoms were included in calculated positions except those of water molecules.

IV-3 Results and Discussion

IV-3-1 Synthesis and Characterization

(a) (Δ_{LLL})$_2$-K$_3$[Au$^{I}_3$Rh$^{III}_2$(L-cys)$_6$] ((Δ_{LLL})$_2$-K$_3$[4])

Treatment of Δ_{LLL}-H$_3$[Rh(L-cys)$_3$] with Au^{I} in a 2:3 ratio in water in the presence of KOH gave a yellow powder. This yellow crude product was dissolved in water by adding a KOH aqueous solution, and then a large amount of EtOH was added to it to give a yellow powder of (Δ_{LLL})$_2$-K$_3$[**4**].

As shown in Figure 4-1, the IR spectrum of (Δ_{LLL})$_2$-K$_3$[**4**] shows the band at 1608 cm^{-1} assigned to COO^{-}, suggestive of the presence of L-cys. The X-ray fluorescence spectroscopy implies that (Δ_{LLL})$_2$-K$_3$[**4**] contains Au and Rh atoms, and elemental analytical data are agreement with the formula for K$_3$[Au$_3$Rh$_2$(L-cys)$_6$]·11H$_2$O. The ^{1}H NMR spectrum in D$_2$O shows two methylene signals (δ 3.17 and 3.29 ppm) and one methine signal (δ 3.00 ppm) attributed to the L-cys ligand (Figure 4-2). The presence of single set of signals suggests that (Δ_{LLL})$_2$-K$_3$[**4**] has a symmetrical structure with all L-cys ligands being equivalent. The absorption spectrum of (Δ_{LLL})$_2$-K$_3$[**4**] in water shows absorption bands at 365, 302, 250, and 214 nm (Figure 4-3, Table 4-5). The CD spectrum shows negative bands at 380 and 266 nm and positive bands at 343 and 226 nm (Figure 4-3, Table 4-5). The absorption and CD spectral features are similar to those of (Δ_{LLL})$_2$-H$_4$[**5**](NO$_3$) (*vide infra*), suggesting that (Δ_{LLL})$_2$-[**4**]$^{3-}$ has a similar S-bridged Au$^{I}_3$Rh$^{III}_2$ pentanuclear structure with that of (Δ_{LLL})$_2$-[**5**]$^{3-}$ having a {Au$^{I}_3$} moiety instead of the {Ag$^{I}_3$} moiety in (Δ_{LLL})$_2$-[**5**]$^{3-}$, in which two Δ_{LLL} configurational [Rh(L-cys)$_3$]$^{3-}$ units are triply bridged by three linear Au^{I} ions. Unfortunately, many attempts to obtain single crystals suitable for X-ray analysis were unsuccessful.

(b) (Δ_{LLL})$_2$-H$_4$[Ag$^{I}_3$Rh$^{III}_2$(L-cys)$_6$](NO$_3$) ((Δ_{LLL})$_2$-H$_4$[5](NO$_3$))

Reaction of Δ_{LLL}-H$_3$[Rh(L-cys)$_3$] with Ag^{I} in a 2:3 ratio in water in the presence of KOH gave a yellow solution. When a HNO$_3$ aqueous solution was added to it, a yellow powder appeared immediately. The yellow product of (Δ_{LLL})$_2$-H$_4$[**5**](NO$_3$) was collected by filtration.

The IR spectrum of (Δ_{LLL})$_2$-H$_4$[**5**](NO$_3$) shows the presence of L-cys and NO$_3^-$ based on the band at 1717 cm^{-1} assigned to COOH and the band at 1605 cm^{-1} assigned to COO$^-$ for L-cys, and the band at 1383 cm^{-1} for NO$_3^-$, respectively (Figure 4-1). This indicates the presence of cationic species by the protonation on some of the carboxylate groups. The X-ray fluorescence spectroscopy implies that (Δ_{LLL})$_2$-H$_4$[**5**](NO$_3$) contains Ag and Rh atoms, and elemental analytical data are agreement with the formula for H$_4$[Au$_3$Co$_2$(L-cys)$_6$](NO$_3$)·9H$_2$O. The ^{1}H NMR

spectrum in D_2O in the presence of base shows a single set of L-cys signals with two methylene signals (δ 2.78 and 3.32 ppm) and one methine signal (δ 2.86 ppm) (Figure 4-2). Single crystals of $(\Delta_{LLL})_2$-H_4[**5**](NO_3) suitable for X-ray analysis were obtained by the reaction of $(\Delta_{LLL})_4$-$K_6[Rh_4Zn_4O(L\text{-cys})_{12}]$ with $AgNO_3$ in water in an acidic condition. The X-ray analysis demonstrated that $(\Delta_{LLL})_2$-H_4[**5**](NO_3) has an S-bridged $Ag^{I}_3Rh^{III}_2$ pentanuclear structure in $H_4[Ag_3Rh_2(L\text{-cys})_6](NO_3)$, in which two Δ_{LLL}-$[\mathbf{5}]^{3-}$ moieties are bridged by three linear Ag^{I} atoms (*vide infra*). The absorption spectrum of $(\Delta_{LLL})_2$-H_4[**5**](NO_3) in water in the presence of base shows absorption bands at 374, 316, 275, and 228 nm (Figure 4-3, Table 4-5). The CD spectrum shows negative bands at 380 and 239 nm and positive bonds at 338 and 219 nm (Figure 4-3, Table 4-5).

(c) $(\Delta_{LLL})_2$-$[Co^{III}_3(aet)_6][Au^{I}_3Rh^{III}_2(L\text{-cys})_6]$ ($(\Delta_{LLL})_2$-$[Co^{III}_3(aet)_6][4]$)

Treatment of $(\Delta_{LLL})_2$-$K_3[Au_3Rh_2(L\text{-cys})_6]$ ($(\Delta_{LLL})_2$-K_3[**4**]) with $(\Delta)_2/(\Lambda)_2$-$[Co_3(aet)_6](NO_3)_3$ in a 1:2 ratio in water, followed by allowing to stand at room temperature for 1 week, gave black block crystals of $(\Delta_{LLL})_2$-$[Co_3(aet)_6]$[**4**]. The similar reaction in a basic aqueous solution also gave the same compound $(\Delta_{LLL})_2$-$[Co_3(aet)_6]$[**4**], which is different from the reaction using $(\Delta_{LLL})_2$-$[\mathbf{1}]^{3-}$ that showed the chiral and structural conversions, as described in Chapter II.

The IR spectrum shows a strong sharp C=O stretching band at 1604 cm^{-1} assigned to COO^-, suggestive of the presence of L-cys (Figure 4-4). X-ray fluorescence spectroscopy indicates that this compound contains Au, Rh, and Co atoms, and the elemental analytical data are in agreement with the formula for a 1:1 adduct of $[Co_3(aet)_6]^{3+}$ and $[\mathbf{4}]^{3-}$. The ^1H NMR spectrum of $(\Delta_{LLL})_2$-$[Co_3(aet)_6]$[**4**] in a $NaNO_3$ solution of D_2O shows the presence of $(\Delta_{LLL})_2$-$[\mathbf{4}]^{3-}$ and $[Co_3(aet)_6]^{3+}$ in a 1:1 ratio (Figure 4-5). The reflection and CD spectra of the crystals in the solid state are shown in Figure 4-6. The reflection spectrum shows three bands at 607, 446, and 356 nm, and the CD spectrum shows negative bands at 500, 356, 327, and 302 nm and positive bands at 560 and 420 nm. The absorption spectrum of the crystals in a $NaNO_3$ aqueous solution is similar to those of $[Co_3(aet)_6]^{3+}$, showing four absorption bands at 575, 432, 345, and 289 nm (Figure 4-7). The CD spectrum in the range of 700 to 400 nm is reminiscent of that of $(\Delta)_2$-$[Co_3(aet)_6]^{3+}$, showing negative bands at 610 and 484 nm and a positive band at 545 nm, but the intensity is weak (Figure 4-7). On the other hand, in the short wavelength region, the spectral pattern is similar to that of $(\Delta_{LLL})_2$-$[\mathbf{4}]^{3-}$, showing negative bands at 379 and 265 nm and a positive band at 341 nm with a reasonable intensity. These absorption and CD spectra indicate the presence of $(\Delta_{LLL})_2$-$[\mathbf{4}]^{3-}$ and $[Co_3(aet)_6]^{3+}$, and the $(\Delta)_2$ isomer of the complex-cation is incorporated preferentially. Single-crystal X-ray analysis demonstrated that

$(\Delta_{LLL})_2$-$[Co_3(aet)_6]$[**4**] is composed of $(\Delta_{LLL})_2$-$[\mathbf{4}]^{3-}$ and $[Co_3(aet)_6]^{3+}$ in a 1:1 ratio (*vide infra*), and the chiral preference of the $[Co_3(aet)_6]^{3+}$ unit was not determined due to the severe disorder of the $(\Delta)_2$ and $(\Lambda)_2$ isomers of $[Co_3(aet)_6]^{3+}$.

To investigate the chiralselective incorporation of the complex-cation in $(\Delta_{LLL})_2$-$[Co_3(aet)_6]$[**4**], the bulk sample was dissolved in water by adding a saturated $NaClO_4$ aqueous solution and chromatographed on a cation-exchange column (SP-Sephadex C-25). When the column was treated with water, a yellow band containing $(\Delta_{LLL})_2$-$[\mathbf{4}]^{3-}$ was eluted, while a brownish green band containing $[Co_3(aet)_6]^{3+}$ was adsorbed on the top of the column. This adsorbed band was eluted with a 0.3 M aqueous solution of $NaClO_4$. The absorption spectrum of the eluate containing the complex-anion shows a sharp absorption band at 363 nm (Figure S1-2, see appendix). Its CD spectrum shows a negative band at 378 nm and a positive band at 342 nm. These spectral features are coincident with those of $(\Delta_{LLL})_2$-$[\mathbf{4}]^{3-}$, which indicates that the structure and chirality of the complex-anion are retained during the reaction. The absorption spectrum of the eluate containing the complex-cation shows an absorption shoulder at 590 nm and two sharp absorption bands at 440 and 350 nm, and the CD spectrum shows a negative band at 610 nm and positive bands at 540, 490, 435, and 350 nm (Figure S1-2, see appendix). This CD spectral pattern is same as that of $(\Delta)_2$-$[Co_3(aet)_6]^{3+}$, but the intensity is quite weak. This indicates that the $(\Delta)_2$ isomer of $[Co_3(aet)_6]^{3+}$ is predominantly incorporated in $(\Delta_{LLL})_2$-$[Co_3(aet)_6]$[**4**], but its chiralselectivity is low.

(d) $(\Delta_{LLL})_2$-$[Co^{III}_3(aet)_6][Ag^{I}_3Rh^{III}_2(L\text{-cys})_6]$ ($(\Delta_{LLL})_2$-$[Co^{III}_3(aet)_6]$[5])

Treatment of the racemic $(\Delta)_2/(\Lambda)_2$-$[Co_3(aet)_6](NO_3)_3$ with $(\Delta_{LLL})_2$-$H_4[Ag_3Rh_2(L\text{-cys})_6](NO_3)$ ($(\Delta_{LLL})_2$-H_4[**5**](NO_3)) in a 2:1 ratio in water, followed by allowing to stand at room temperature, gave black needle-like crystals of $(\Delta_{LLL})_2$-$[Co_3(aet)_6][Ag_3Rh_2(L\text{-cys})_6]$ ($(\Delta_{LLL})_2$-$[Co_3(aet)_6]$[**5**]).

The IR spectrum of $(\Delta_{LLL})_2$-$[Co_3(aet)_6]$[**5**] shows a strong sharp C=O stretching band at 1597 cm^{-1}, suggestive of the presence of L-cys with the deprotonated carboxylate group (Figure 4-4). X-ray fluorescence spectroscopy indicates that this product contains Ag, Rh, and Co atoms. The elemental analytical data are in agreement with the formula for a 1:1 adduct of $[Co_3(aet)_6]^{3+}$ and $[\mathbf{5}]^{3-}$. The ^1H NMR spectrum in a $NaNO_3$ solution of D_2O shows one set of L-cys signals attributed to $(\Delta_{LLL})_2$-$[\mathbf{5}]^{3-}$ and one set of aet signals attributed to $[Co_3(aet)_6]^{3+}$, of which integration ratio indicates the presence of $(\Delta_{LLL})_2$-$[\mathbf{5}]^{3-}$ and $[Co_3(aet)_6]^{3+}$ in a 1:1 ratio (Figure 4-5). The reflection and CD spectra in the solid state are shown in Figure 4-6. In the reflection spectrum, three bands at 600, 443, and 357 nm were observed, of which pattern is similar to that of $[Co_3(aet)_6]^{3+}$. The CD spectrum shows a negative band at

398 nm and positive bands at 560, 452, 340, and 285 nm. The CD pattern in the long wavelength region is similar to that of $(\Delta)_2$-$[Co_3(aet)_6]^{3+}$, whereas the pattern in the short wavelength region is similar to that of $(\Delta_{LLL})_2$-$[\mathbf{5}]^{3-}$. The absorption and CD spectra of the crystals in a $NaNO_3$ aqueous solution are essentially the same as the reflection and CD spectra in the solid state. The absorption spectrum shows four absorption bands at 580, 439, 346, and 276 nm, of which spectral pattern is similar to that of $[Co_3(aet)_6]^{3+}$. The CD spectrum shows negative bands at 606, 487, 376, 304, and 241 nm and positive bands at 543, 439, 330, and 283 nm (Figure 4-7). The CD spectral pattern in the long wavelength region also resembles that of $(\Delta)_2$-$[Co_3(aet)_6]^{3+}$, indicating that $(\Delta_{LLL})_2$-$[Co_3(aet)_6][\mathbf{5}]$ contains the $(\Delta)_2$ isomer of $[Co_3(aet)_6]^{3+}$ preferentially. X-ray structural analysis of $(\Delta_{LLL})_2$-$[Co_3(aet)_6][\mathbf{5}]$ shows the presence of $(\Delta_{LLL})_2$-$[\mathbf{5}]^{3-}$ and $[Co_3(aet)_6]^{3+}$ in a 1:1 ratio, and only the $(\Delta_{LLL})_2$ and $(\Delta)_2$ isomers exist in crystal (*vide infra*).

To check the chirality of the complex-anion and the complex-cation in the bulk sample, the cationic and anionic parts are separated by column chromatography, and their absorption and CD spectra were measured. When the bulk sample of $(\Delta_{LLL})_2$-$[Co_3(aet)_6][\mathbf{5}]$ was dissolved in a $NaClO_4$ aqueous solution and was chromatographed on a cation-exchange column (SP-Sephadex C-25), a yellow band containing the complex-anion eluted with water, and a brownish green band containing the complex-cation was eluted with a 0.3 M aqueous solution of $NaClO_4$. The absorption spectrum of the yellow band shows a band at 375 nm, and its CD spectrum shows a negative band at 379 nm and a positive band at 337 nm (Figure 4-8). These spectral features are coincident with those of $(\Delta_{LLL})_2$-$[\mathbf{5}]^{3-}$, indicative of the retention of the Δ_{LLL} configurational $Ag^{I}_3Rh^{III}_2$ pentanuclear structure during the reaction. For the cationic part, the absorption spectrum suggests the presence of $[Co_3(aet)_6]^{3+}$ based on the bands at 590 and 440 nm (Figure 4-8). In the CD spectrum, the spectral pattern and intensity are same as those of $(\Delta)_2$-$[Co_3(aet)_6]^{3+}$ showing the bands at 610 and 540 nm (Figure 4-8), indicating that only the $(\Delta)_2$ isomer of $[Co_3(aet)_6]^{3+}$ is incorporated in $(\Delta_{LLL})_2$-$[Co_3(aet)_6][\mathbf{5}]$. This excellent chiralselectivity toward $[Co_3(aet)_6]^{3+}$ is consistent with the X-ray structural analysis that showed the presence of only the $(\Delta)_2$ isomer of $[Co_3(aet)_6]^{3+}$ in crystal.

IV-3-3 Crystal Structures of Complexes

(a) $(\Delta_{LLL})_2$-$H_4[Ag^{I}_3Rh^{III}_2(L\text{-}cys)_6](NO_3)$ ($(\Delta_{LLL})_2$-$H_4[\mathbf{5}](NO_3)$)

The crystal structure of $(\Delta_{LLL})_2$-$H_4[\mathbf{5}](NO_3)\cdot 9H_2O$ was established by single-crystal X-ray crystallography. The asymmetric unit contains a half of $(\Delta_{LLL})_2$-$H_4[\mathbf{5}]^{+}$, a quarter of nitrate anion, and water molecules. Another quarter nitrate anion was not refined due to the severe disorder. The molecular and packing structures are shown in

Figures 4-9, 4-10, and 4-11. The crystallographic data are summarized in Table 4-1, and the selected bond distances and angles are listed in Table 4-2.

As shown in Figure 4-9, $(\Delta_{LLL})_2$-H_4[**5**]$^+$ has an S-bridged $Ag^I_3Rh^{III}_2$ pentanuclear structure. Each Rh^{III} atom has an octahedral geometry coordinated by three bidentate L-cys-*N*,*S* ligands in a facial fashion (av. Rh–S = 3.146 Å, Rh–N = 2.097 Å), and adopts a Δ configuration. In this mononuclear unit, two of the three L-cys ligands have protonated carboxy groups and the other has a deprotonated carboxylate group. Two Δ_{LLL}-H_2[Rh(L-cys)$_3$]$^-$ units are linked by three linear Au^I atoms through S atoms (av. Ag–S = 2.41 Å, S–Ag–S = 172°). All six S atoms adopt an *S* configuration, and only the $(\Delta_{LLL})_2(S)_6$ isomer exists in crystal. The L-cys N,S-chelate rings in the Δ configurational [Rh(L-cys)$_3$]$^{3-}$ units adopt a *lel* (λ for Δ) conformation with free COO^- groups pointing to an equatorial orientation. Three Ag^I atoms are arranged in a triangle form with the averaged Ag···Ag distance of 3.03 Å, indicative of the presence of an argyrophilic interaction,[4] These three S–Ag–S linkages are twisted to form a triple-stranded helical structure with a left handedness. The $(\Delta_{LLL})_2$-H_4[**5**]$^+$ units are connected to each other through intermolecular Ag···Ag interactions (av. Ag···Ag = 2.935 Å) to form a dimeric structure (Figure 4-10). In addition, two carboxylate groups in each $(\Delta_{LLL})_2$-H_4[**5**]$^+$ unit bind to two Ag^I atoms from two different adjacent units (av. Ag–O = 2.65 Å), which completes a 1D chain made up of the dimers (Figure 4-10). The 1D chains are further connected to each other through intermolecular COOH···OOC hydrogen bonds (av. O···O = 2.49 Å) to construct a columnar structure with large cavities that accommodate water molecules (Figure 4-11).

(b) $(\Delta_{LLL})_2$-[Co^{III}_3(aet)$_6$][$Au^I_3Rh^{III}_2$(L-cys)$_6$] ($(\Delta_{LLL})_2$-[Co^{III}_3(aet)$_6$][4])

The crystal structure of $(\Delta_{LLL})_2$-[Co_3(aet)$_6$][**4**] is isomorphous with $(\Delta_{LLL})_2$-[Co_3(aet)$_6$][**1**], consisting of a complex-cation [Co_3(aet)$_6$]$^{3+}$ and a complex-anion $(\Delta_{LLL})_2$-[**4**]$^{3-}$ besides water molecules of crystallization. The molecular and packing structures are shown in Figures 4-12, 4-13, 4-14, and 4-15. The crystallographic data are summarized in Table 4-1 and the selected bond distances and angles are listed in Table 4-3.

The complex-anion of $(\Delta_{LLL})_2$-[**4**]$^{3-}$ in $(\Delta_{LLL})_2$-[Co_3(aet)$_6$][**4**] has an S-bridged $Au^I_3Rh^{III}_2$ pentanuclear structure (Figure 4-12). Each Rh^{III} center is in an N_3S_3 octahedral environment coordinated by three bidentate-*N*,*S* L-cys ligands (av. Rh–S = 2.335(8) Å, Rh–N = 2.126(3) Å). Two [Rh(L-cys)$_3$]$^{3-}$ units are linked by three Au^I ions, and each Au^I center is in an S_2 linear coordination environment (av. Au–S = 2.305(6) Å, S–Au–S = 173.4°). Two Rh^{III} centers take a Δ_{LLL} configuration, and all six S atoms adopt an *S* configuration to give only the $(\Delta_{LLL})_2(S)_6$ isomer. The L-cys

N,S-chelate rings in the Δ_{LLL} configurational $[Co(L\text{-}cys)_3]^{3-}$ units adopt a *lel* (λ for Δ) conformation with free COO^- groups pointing to an equatorial orientation. There exist intramolecular aurophilic interactions between the triangular Au^I ions (av. Au···Au = 3.034(6) Å), and three S–Au–S linkages have a left-handed helical arrangement. For the cationic part, the S-bridged Co^{III}_3 trinuclear structure is retained, and it was found that the $(\Delta)_2$ and $(\Lambda)_2$ isomers are disordered in a ca. 3:2 ratio. In the packing structure, $(\Delta_{LLL})_2$-[**4**]$^{3-}$ units are connected to each other through hydrogen bonds between the amine and carboxylate groups (av. NH···O = 2.86 Å) to form a hydrogen-bonded 1D chain structure (Figure 4-13). The 1D chains are arranged in a parallel manner, and the disordered $[Co_3(aet)_6]^{3+}$ units are incorporated between the chains through hydrogen bonds (av. NH···O = 2.31 Å), such that each complex-cation is surrounded by two complex-anions (Figure 4-14). Each complex-anion is surrounded by two complex-anions and two complex-cations (Figure 4-14), and as a result, complex-anions and complex-cations are alternately arranged to construct a 3D hydrogen-bonding network structure (Figure 4-15).

(c) $(\Delta_{LLL})_2$-$[Co^{III}_3(aet)_6][Ag^I_3Rh^{III}_2(L\text{-}cys)_6]$ ($(\Delta_{LLL})_2$-$[Co^{III}_3(aet)_6]$[5])

X-ray crystallography demonstrated that $(\Delta_{LLL})_2$-$[Co_3(aet)_6]$[**5**] consists of a complex-cation $[Co_3(aet)_6]^{3+}$ and a complex-anion $(\Delta_{LLL})_2$-[**5**]$^{3-}$ besides water molecules of crystallization in the asymmetric unit. The molecular and packing structures are shown in Figures 4-16, 4-17, 4-18 and 4-19. The crystallographic data are summarized in Table 4-1, and the selected bond distances and angles are listed in Table 4-4.

As shown in Figure 4-16, the complex-anion $(\Delta_{LLL})_2$-[**5**]$^{3-}$ has an S-bridged $Ag^I_3Rh^{III}_2$ pentanuclear structure, in which two $[Rh(L\text{-}cys)_3]^{3-}$ units are bridged by three linear Ag^I atoms (av. Rh–S = 2.316 Å, Rh–N = 2.114 Å, Ag–S = 2.421 Å, S–Ag–S = 171.54°). As in $(\Delta_{LLL})_2$-[**4**]$^{3-}$, the Rh^{III} centers coordinated by three bidentate-*N*,*S* L-cys ligands adopt a Δ_{LLL} configuration, and the bridging S atoms adopt an *S* configuration to give only the $(\Delta_{LLL})_2(S)_6$ isomer. All six carboxylate groups in $(\Delta_{LLL})_2$-[**5**]$^{3-}$ take an equatorial orientation, and the N,S-chelate rings adopt a thermodynamically stable *lel* (λ for Δ) conformation. Three S–Ag–S linkages are twisted in a left-handed manner such that three Ag^I atoms are close to each other (av. Ag···Ag = 3.106 Å). The complex-cation $[Co_3(aet)_6]^{3+}$ incorporated in $(\Delta_{LLL})_2$-$[Co_3(aet)_6]$[**5**] exclusively adopts the $(\Delta)_2$ configurations, indicative of the chiralselective uptake of the $(\Delta)_2$ isomer of $[Co_3(aet)_6]^{3+}$ in crystal.

Each complex-anion $(\Delta_{LLL})_2$-[**5**]$^{3-}$ is connected with six complex-anions; two of the six complex-anions are connected through Ag···OOC interaction bonds with a monodentate coordination mode (av. Ag···OOC = 2.729 Å), and the other four

complex-anions are connected through hydrogen bonds between carboxylate and amine groups (av. NH···O = 3.007 Å), as shown in Figure 4-17. In addition, each complex-anion $(\Delta_{LLL})_2$-[**5**]$^{3-}$ is also connected with four complex-cations $[Co_3(aet)_6]^{3+}$ through the hydrogen bonds between the carboxylate groups of $(\Delta_{LLL})_2$-[**5**]$^{3-}$ and the amine groups of complex-cations (av. NH···O = 2.97 Å) (Figure 4-17). Thus, each $(\Delta_{LLL})_2$-[**5**]$^{3-}$ anion is connected with six complex-anions and four complex-cations through the NH···O hydrogen bonds and Ag···O coordination bonds. Each $(\Delta)_2$-$[Co_3(aet)_6]^{3+}$ cation is hydrogen-bonded with four adjacent complex-anions with the average NH···O distance of 3.060(5) Å (Figure 4-18). As a result, anionic and cationic part alternately arranged to construct a 3D network structure (Figure 4-19).

IV-3-4 Chiralselectivity of $(\Delta_{LLL})_2$-$[M^{I}_3Rh^{III}_2(L\text{-cys})_6]^{3-}$ (M^{I} = Au^{I}, Ag^{I}) toward $(\Delta)_2/(\Lambda)_2$-$[Co^{III}_3(aet)_6]^{3+}$

The chiralselective behavior of two complex-anions, $(\Delta_{LLL})_2$-[**4**]$^{3-}$ and $(\Delta_{LLL})_2$-[**5**]$^{3-}$, toward $(\Delta)_2/(\Lambda)_2$-$[Co_3(aet)_6]^{3+}$ was investigated. It was found that these two complex-anions containing the $[Rh(L\text{-cys})_3]^{3-}$ units showed the similar chiralselective ability with those containing the $[Co(L\text{-cys})_3]^{3-}$ units. When $(\Delta_{LLL})_2$-[**4**]$^{3-}$ was reacted with $(\Delta)_2/(\Lambda)_2$-$[Co_3(aet)_6]^{3+}$, the cocrystallized compound $(\Delta_{LLL})_2$-$[Co_3(aet)_6]$[**4**] was obtained. In this compound, the $(\Delta)_2$ isomer of $[Co_3(aet)_6]^{3+}$ was preferentially incorporated, but its selectivity is low. The similar reaction using $(\Delta_{LLL})_2$-[**5**]$^{3-}$ instead of $(\Delta_{LLL})_2$-[**4**]$^{3-}$ also gave the cocrystallized compound $(\Delta_{LLL})_2$-$[Co_3(aet)_6]$[**5**], but the chiralselective behavior is quite different. In $(\Delta_{LLL})_2$-$[Co_3(aet)_6]$[**5**], the $(\Delta)_2$ isomer of $[Co_3(aet)_6]^{3+}$ was exclusively incorporated.

This difference can be also discussed by comparing the packing structures. In $(\Delta_{LLL})_2$-$[Co_3(aet)_6]$[**4**], each complex-anion is surrounded by two complex-anions and two complex-cations through the hydrogen bonds between the amine and carboxylate groups. Each complex-cation is surrounded by two complex-anions through hydrogen bonds. On the other hand, in $(\Delta_{LLL})_2$-$[Co_3(aet)_6]$[**5**], each complex-anion is connected with six complex-anions and four complex-cations through the NH···O hydrogen bonds and Ag–OOC coordination bonds, while each complex-cation is hydrogen-bonded with four adjacent complex-anions. From the comparison of these two packing structures, it was found that the number of the intermolecular interactions is different to each other. In $(\Delta_{LLL})_2$-$[Co_3(aet)_6]$[**5**] containing the Ag^{I} ion in the complex-anion, the coordination bonds between the Ag^{I} ion and carboxylate groups were formed in addition to the hydrogen bonding interactions. Thus, the ten complexes are connected to each complex-anion, and concomitantly, the four complexes are connected to each complex-cation. As a result, the tight packing structure was formed in $(\Delta_{LLL})_2$-$[Co_3(aet)_6]$[**5**], which leads to the excellent

chiralselectivity. Namely, the effective chiral recognition toward $(\Delta)_2$-$[Co_3(aet)_6]^{3+}$ was achieved by means of increasing the intermolecular interactions through the introduction of the Ag^I ions. On the other hand, in $(\Delta_{LLL})_2$-$[Co_3(aet)_6]$[**4**] containing the Au^I ion in the complex-anion, no significant intermolecular interaction using the Au^I ion was observed, and thus, the less number of the intermolecular interactions were formed. As a result, the looser packing structure was formed in $(\Delta_{LLL})_2$-$[Co_3(aet)_6]$[**4**], which leads to the less chiralselective ability of $(\Delta_{LLL})_2$-$[\mathbf{4}]^{3-}$ toward $[Co_3(aet)_6]^{3+}$.

IV-3-5 Chiralselectivity of Complex-anions Containing L-Cysteinate toward $(\Delta)_2/(\Lambda)_2$-$[Co^{III}_3(aet)_6]^{3+}$

Commonly, the L-cysteinato multinuclear complexes have (i) multiple chiral centers on the metal centers (Δ/Λ), the bridging S atoms (*R*/*S*), and the C atom of L-cys (*R*), (ii) an anionic nature, and (iii) several carboxylate groups available for the chiral recognition sites. Thus, these complexes can act as a resolving reagent toward racemic complex-cations. The chiralselective behavior of the seven L-cysteinato multinuclear complex-anions, $(\Delta_{LLL})_2$-$[Co_3(L\text{-}cys)_6]^{3-}$, $(\Lambda_{LLL})_2$-$[Co_3(L\text{-}cys)_6]^{3-}$, $(\Delta_{LLL})_2$-$[Au_3Co_2(L\text{-}cys)_6]^{3-}$ ($(\Delta_{LLL})_2$-$[\mathbf{1}]^{3-}$), $(\Lambda_{LLL})_4$-$[Au_6Co_4(L\text{-}cys)_{12}]^{6-}$ ($(\Lambda_{LLL})_4$-$[\mathbf{2}]^{6-}$), $(\Delta_{LLL})_2$-$[Ag_3Co_2(L\text{-}cys)_6]^{3-}$ ($(\Delta_{LLL})_2$-$[\mathbf{3}]^{3-}$), $(\Delta_{LLL})_2$-$[Au_3Rh_2(L\text{-}cys)_6]^{3-}$ ($(\Delta_{LLL})_2$-$[\mathbf{4}]^{3-}$), and $(\Delta_{LLL})_2$-$[Ag_3Rh_2(L\text{-}cys)_6]^{3-}$ ($(\Delta_{LLL})_2$-$[\mathbf{5}]^{3-}$), toward the complex-cation, $(\Delta)_2/(\Lambda)_2$-$[Co_3(aet)_6]^{3+}$, was investigated up to now, including the literature.

Comparing the chiralselectivity of $(\Delta_{LLL})_2$-$[Co_3(L\text{-}cys)_6]^{3-}$ and $(\Lambda_{LLL})_2$-$[Co_3(L\text{-}cys)_6]^{3-}$, $(\Lambda_{LLL})_2$-$[Co_3(L\text{-}cys)_6]^{3-}$ selects the $(\Delta)_2$ isomer of $[Co_3(aet)_6]^{3+}$ exclusively (*ee* ~100%), whereas $(\Delta_{LLL})_2$-$[Co_3(L\text{-}cys)_6]^{3-}$ preferentially selects the $(\Lambda)_2$ isomer of $[Co_3(aet)_6]^{3+}$ (*ee* ~20%). The factor that controls the excellent/poor selectivity was considered as the different orientation of the free carboxylate groups. The $(\Delta_{LLL})_2$-$[Co_3(L\text{-}cys)_6]^{3-}$ complex-anion has equatorially oriented carboxylate groups, which leads to the formation of the efficient double hydrogen bonding interactions between the complex-anions, and the further interaction with the complex-cation is difficult to be formed. On the other hand, the $(\Lambda_{LLL})_2$-$[Co_3(L\text{-}cys)_6]^{3-}$ complex-anion has axially oriented carboxylate groups, and thus, the hydrogen bonds between the complex-anions and between the complex-anion and the complex-cation can be equally formed. As a result, each complex-anion is surrounded by two complex-anions and three complex-cations. Thus, the complex-anion having the Λ_{LLL} configurational mononuclear units with axially oriented carboxylate groups is a good candidate for a resolving agent compared with that having the Δ_{LLL} configurational mononuclear units with equatorially oriented carboxylate groups.

The complex-anions, $(\Delta_{LLL})_2$-[**1**]$^{3-}$ and $(\Delta_{LLL})_2$-[**4**]$^{3-}$, containing a $\{Au^{I}_3\}$ unit instead of the central Co^{III} ion in $(\Delta_{LLL})_2$-$[Co_3(L\text{-cys})_6]^{3-}$ were found to show the poor selectivity toward $(\Delta)_2/(\Lambda)_2$-$[Co_3(aet)_6]^{3+}$. In both cases, the $(\Delta)_2$ isomer of $[Co_3(aet)_6]^{3+}$ were partially selected. This low selectivity is explained by the same reason as $(\Delta_{LLL})_2$-$[Co_3(L\text{-cys})_6]^{3-}$. In both cocrystallized compounds, the complex-anions have the equatorially oriented carboxylate groups, and the efficient double hydrogen bonding interactions are formed between the complex-anions, which leads to the less number of the intermolecular interactions between the complex-anion and the complex-cation, and the poor selectivity toward the complex-cation.

Considering the speculation that the Λ_{LLL} configurational multinuclear complex-anions act as an efficient resolving reagent than the Δ_{LLL} configurational complex-anions, the complex-anions $(\Lambda_{LLL})_2$-[**1**]$^{3-}$ and $(\Lambda_{LLL})_2$-[**4**]$^{3-}$ should show the good chiralselectivity. Unfortunately, the preparation of $(\Lambda_{LLL})_2$-[**4**]$^{3-}$ was failed by the similar reaction with that of $(\Lambda_{LLL})_2$-[**1**]$^{3-}$, because of the inertness of the Rh^{III} centers and the thermodynamical stability of both the *lel* conformation of the chelate ring and the equatorial orientation of the carboxylate groups. As described in Chapter II, $(\Lambda_{LLL})_2$-[**1**]$^{3-}$ was successfully prepared, but was structurally converted to $(\Lambda_{LLL})_4$-[**2**]$^{6-}$ upon the crystallization with $[Co_3(aet)_6]^{3+}$. Thus, the chiralselective behavior between $(\Delta_{LLL})_2$-[**1**]$^{3-}$ and $(\Lambda_{LLL})_2$-[**1**]$^{3-}$ could not be compared, but the investigation of the chiralselectivity of $(\Lambda_{LLL})_4$-[**2**]$^{6-}$ was performed. As a result, it was found that $(\Lambda_{LLL})_4$-[**2**]$^{6-}$ selects the $(\Delta)_2$ isomer of $[Co_3(aet)_6]^{3+}$ partially (*ee* 22%). This chiralselectivity is lower than expected, although the slight increase in the chiralselectivity of $(\Lambda_{LLL})_4$-[**2**]$^{6-}$ compared with $(\Delta_{LLL})_2$-[**1**]$^{3-}$ was observed. This can be explained by the orientation of the carboxylate groups. In $(\Lambda_{LLL})_4$-[**2**]$^{6-}$, only four of the twelve carboxylate groups orient an axial direction due to the steric hindrance, and the remaining eight carboxlate groups orient an equatorial direction, which might promote the formation of the intermolecular interactions between the complex-anions. Thus, only two complex-cations connected to each complex-anion, and the chiral recognition ability is not so good.

Finally, the influence of the introduction of the Ag^{I} ions is discussed. Both complex-anions $(\Delta_{LLL})_2$-[**3**]$^{3-}$ and $(\Delta_{LLL})_2$-[**5**]$^{3-}$ containing a $\{Ag^{I}_3\}$ unit between the terminal $(\Delta_{LLL})_2$-$[M(L\text{-cys})_6]^{3-}$ (M = Co^{III}, Rh^{III}) units showed the excellent chiralselectivity toward $(\Delta)_2/(\Lambda)_2$-$[Co_3(aet)_6]^{3+}$ in spite of the Δ_{LLL} configuration of the terminal $(\Delta_{LLL})_2$-$[M(L\text{-cys})_6]^{3-}$ units. The coordination geometry of the central Co^{III} center in $(\Delta_{LLL})_2$-$[Co_3(L\text{-cys})_6]^{3-}$ is satisfied by the six S atoms from two $(\Delta_{LLL})_2$-$[M(L\text{-cys})_6]^{3-}$ units, and the Au^{I} ions in $(\Delta_{LLL})_2$-[**1**]$^{3-}$ is in a rigid linear coordination geometry. Therefore, it is difficult to form another coordination bond to the central Co^{III} and Au^{I} ions. On the other hand, the Ag^{I} ions can take various

coordination number and geometry like two-coordination, three-coordination, and four-coordination, and thus, the the two-coordinated Ag^{I} ions in $(\Delta_{LLL})_2$-[**3**]$^{3-}$ and $(\Delta_{LLL})_2$-[**5**]$^{3-}$ are easily coordinated by additional ligands. As a result, in both $(\Delta_{LLL})_2$-[Co_3(aet)$_6$][**3**] and $(\Delta_{LLL})_2$-[Co_3(aet)$_6$][**5**], the Ag^{I} ion is coordinated by the carboxylate group in the neighboring complex-anion, and the hydrogen bonds between the complex-anion and the complex-cation are easy to be formed considering the Coulomb repulsion. In fact, each complex-anions are connected to four complex-cations in both cocrystallized compounds.

From the above discussion, it was speculated that the following structural features of the complex-anions with L-cysteinate are important for the excellent chiralselectivity: (i) to have additional interaction sites, such as two-coordinated Ag^{I} centers, besides the amine and carboxylate groups and (ii) to have axially oriented carboxylate groups.

IV-4 Summary

In this chapter, the chiralselective behavior of $(\Delta_{LLL})_2$-$[Au_3Rh_2(L\text{-cys})_6]^{3-}$ ($(\Delta_{LLL})_2$-$[\mathbf{4}]^{3-}$) and $(\Delta_{LLL})_2$-$[Ag_3Rh_2(L\text{-cys})_6]^{3-}$ ($(\Delta_{LLL})_2$-$[\mathbf{5}]^{3-}$) toward $(\Delta)_2/(\Lambda)_2$-$[Co_3(aet)_6]^{3+}$ was investigated. The reaction of $(\Delta_{LLL})_2$-$[\mathbf{4}]^{3-}$ with $(\Delta)_2/(\Lambda)_2$-$[Co_3(aet)_6]^{3+}$ in water gave the cocrystallized compound $(\Delta_{LLL})_2$-$[Co_3(aet)_6][\mathbf{4}]$, and the similar reaction of $(\Delta_{LLL})_2$-$[\mathbf{5}]^{3-}$ with $(\Delta)_2/(\Lambda)_2$-$[Co_3(aet)_6]^{3+}$ in water also gave the cocrystallized compound $(\Delta_{LLL})_2$-$[Co_3(aet)_6][\mathbf{5}]$. These compounds consist of the complex-anion and complex-cation in a 1:1 ratio, and it was found that the structures of both complex-anion and complex-cation were retained during the reaction. The separation of the complex-anion and complex-cation by column chromatography and the sequential absorption and CD spectral measurements showed that the $(\Delta)_2$ isomer of $[Co_3(aet)_6]^{3+}$ was preferencially incorporated in $(\Delta_{LLL})_2$-$[Co_3(aet)_6][\mathbf{4}]$ with a low chiralselectivity, whereas only the $(\Delta)_2$ isomer of $[Co_3(aet)_6]^{3+}$ was incorporated in $(\Delta_{LLL})_2$-$[Co_3(aet)_6][\mathbf{5}]$ (*ee* ~100%). This difference is caused by the different intermolecular interactions between the complex-anion and the complex-cation. In $(\Delta_{LLL})_2$-$[Co_3(aet)_6][\mathbf{4}]$, each complex-anion is surrounded by two complex-anions and two complex-cations, whereas in $(\Delta_{LLL})_2$-$[Co_3(aet)_6][\mathbf{5}]$, each complex-anion is surrounded by six complex-anions and four complex-cations. In $(\Delta_{LLL})_2$-$[Co_3(aet)_6][\mathbf{4}]$, only the hydrogen bonds between the carboxylate and amine groups are formed, and the central $\{Au^{I}_3\}$ moiety does not contribute to the formation of the intermolecular interactions. On the other hand, in $(\Delta_{LLL})_2$-$[Co_3(aet)_6][\mathbf{5}]$, the central $\{Ag^{I}_3\}$ moiety is coordinated by the carboxylate group of the neighboring complex-anion, and the intermolecular interactions were formed through coordination bonds as well as hydrogen bonds. Thus, the different number of the intermolecular interactions between $(\Delta_{LLL})_2$-$[Co_3(aet)_6][\mathbf{4}]$ and $(\Delta_{LLL})_2$-$[Co_3(aet)_6][\mathbf{5}]$ was observed, which leads to the different chiralselective ability of $(\Delta_{LLL})_2$-$[\mathbf{4}]^{3-}$ and $(\Delta_{LLL})_2$-$[\mathbf{5}]^{3-}$ toward $(\Delta)_2/(\Lambda)_2$-$[Co_3(aet)_6]^{3+}$.

By comparing the chiralselective behavior of the L-cysteinato multinuclear complex-anions, it was speculated that the factor that controls the selectivity is the number of the intermolecular interactions between the complex-anion and the complex-cation. The chiralselectivity becomes better as increasing the number of the interactions. In order to increase the cation-anion interactions, the following structural features of the complex-anions might be important: (i) to have additional interaction sites, such as two-coordinated Ag^{I} centers, besides the amine and carboxylate groups and (ii) to have axially oriented carboxylate groups.

IV-5 References

(1) (a) H. Q. Yuan, A. Igashira-Kamiyama, K. Tsuge, T. Konno, *Chem*. *Lett*. **2009**, *38*, 704–705. (b) H. Q. Yuan, A. Igashira-Kamiyama, T. Konno, *Chem*. *Lett*. **2011**, *40*, 285–287.

(2) (a) M. J. Heeg, E. L. Blinn, E. Deutsch, *Inorg*. *Chem*. **1985**, *24*, 1118–1120. (b) S. Miyanowaki, T. Konno, K. Okamoto, J. Hidaka, *Bull*. *Chem*. *Soc*. *Jpn*. **1988**, *61*, 2987–2989.

(3) (a) G. M. Sheldrick, *Acta Crystallogr*. **2008**, *A64*, 112–122. (b) C. Kabuto, S. Akine, E. Kwon, *J*. *Cryst*. *Soc*. *Jpn*. **2009**, *51*, 218–224.

(4) (a) A. N. Khlobystov, A. J. Blake, N. R. Champness, D. A. Lemenovskii, A. G. Majouga, N. V. Zyk, M. Schröder, *Coord*. *Chem*. *Rev*. **2001**, *222*, 155–192. (b) M. J. Katz, K. Sakai, D. B. Leznoff, *Chem*. *Soc*. *Rev*. **2008**, *37*, 1884–1895.

(a)

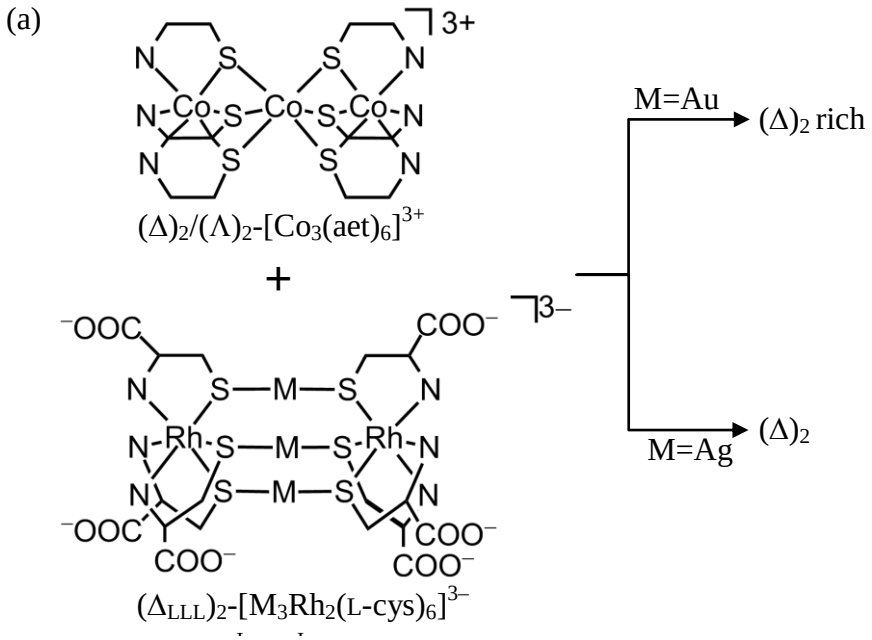

(b)

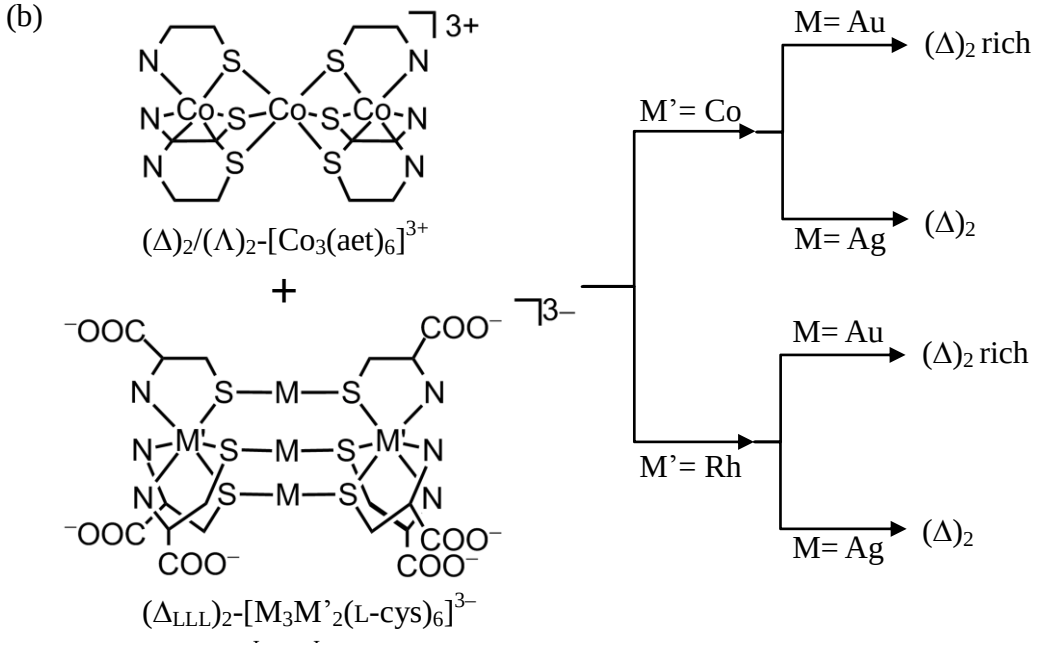

Scheme 4-1. Schemeatic representation of chiralselective crystallizations.

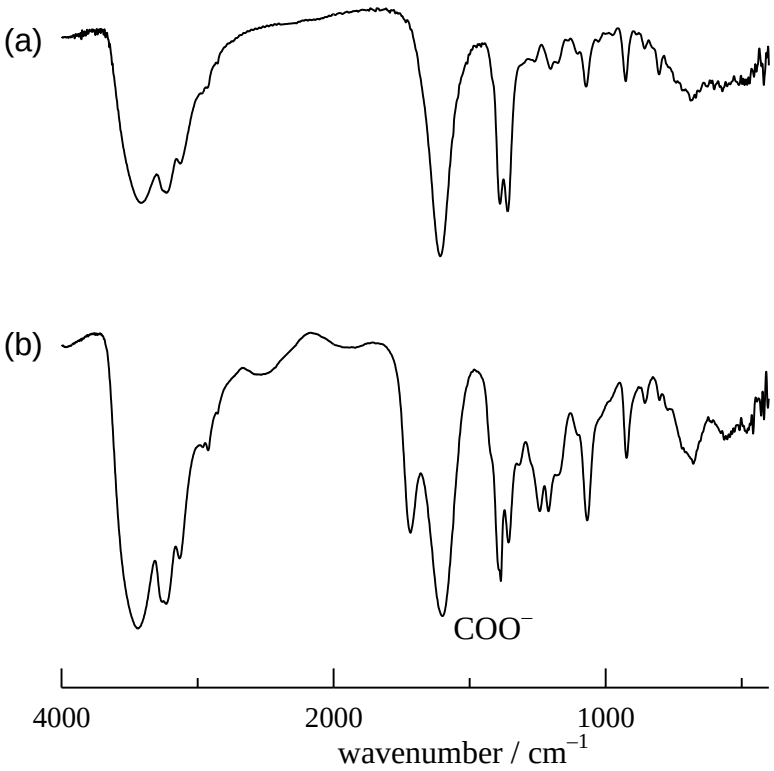

Figure 4-1. IR spectra of (a) $(\Delta_{LLL})_2$-K_3[**4**] and (b) $(\Delta_{LLL})_2$-H_4[**5**](NO_3) (KBr disk).

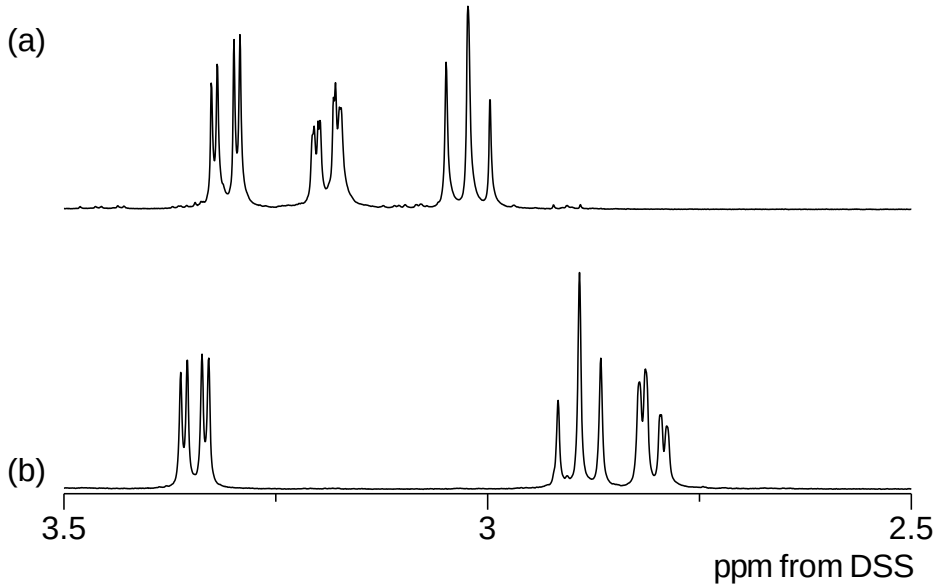

Figure 4-2. ^{1}H NMR spectra of (a) $(\Delta_{LLL})_2$-K_3[**4**] in D_2O and (b) $(\Delta_{LLL})_2$-H_4[**5**](NO_3) in D_2O in the presence of base.

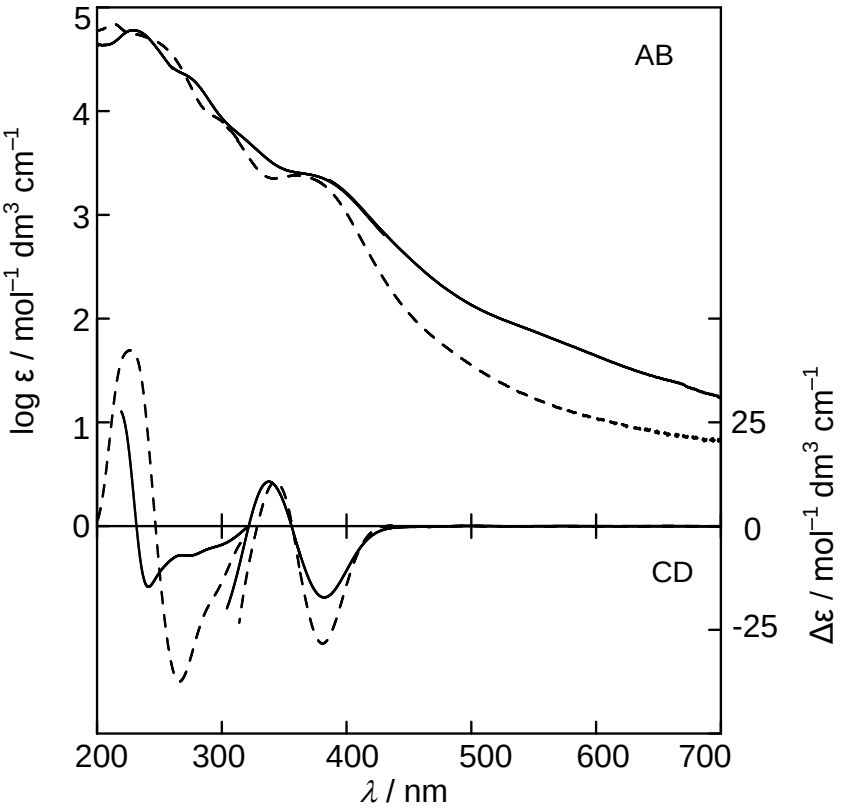

Figure 4-3. Absorption and CD spectra of $(\Delta_{LLL})_2$-K_3[**4**] in water (---) and $(\Delta_{LLL})_2$-H_4[**5**](NO_3) in water in the presence of base (—).

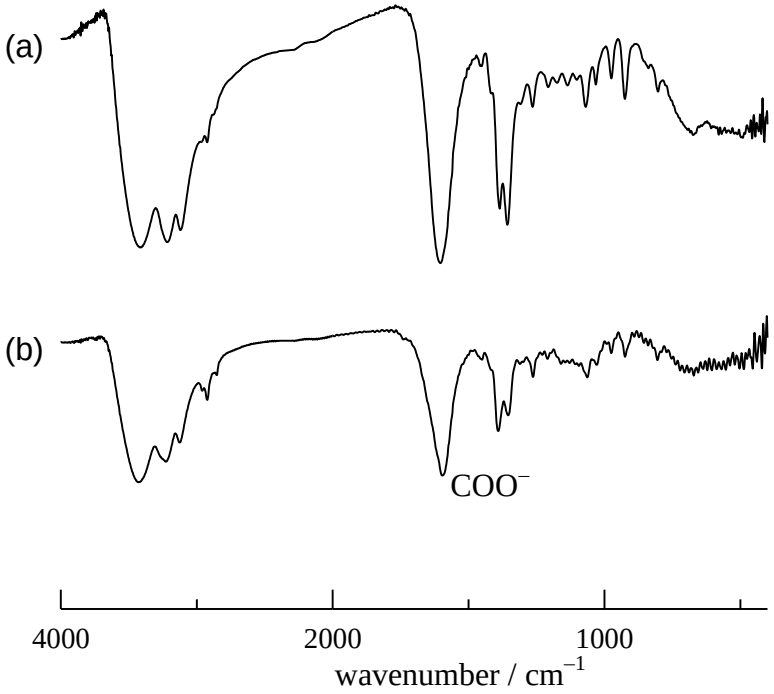

Figure 4-4. IR spectra of complex salts (a) $(\Delta_{LLL})_2$-$[Co_3(aet)_6]$[**4**] and (b) $(\Delta_{LLL})_2$-$[Co_3(aet)_6]$[**5**] (KBr disk).

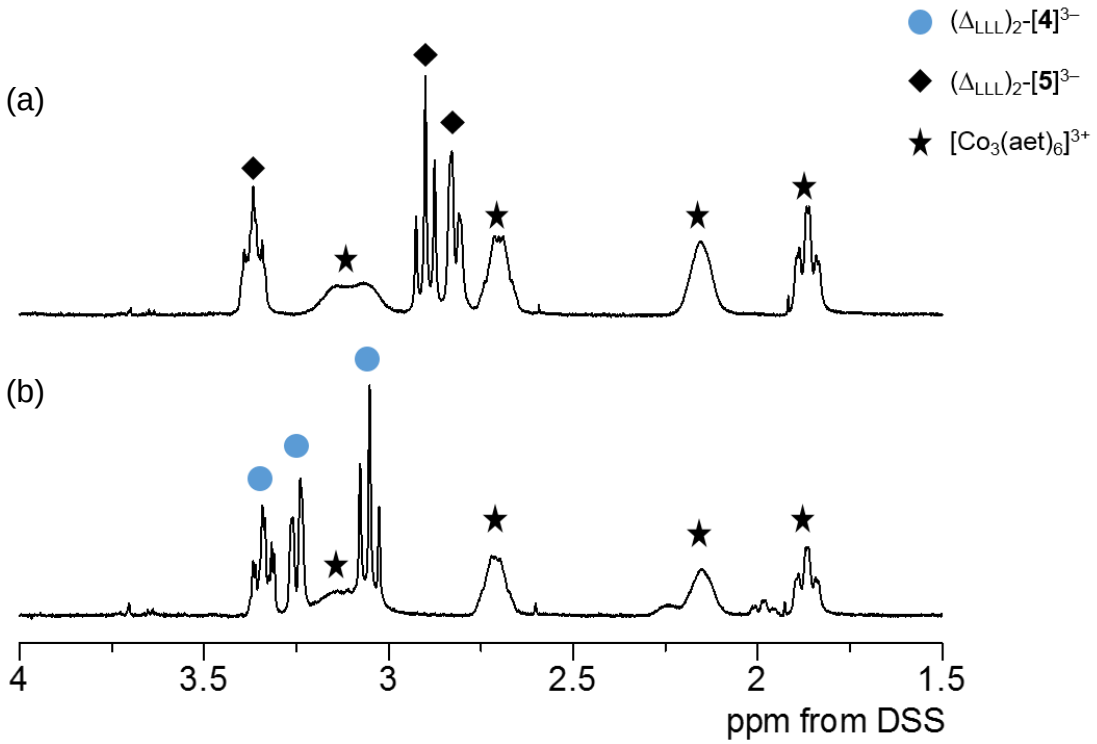

Figure 4-5. The ^{1}H NMR spectra of crystals of (a) $(\Delta_{LLL})_2$-[Co_3(aet)$_6$][**4**] and (b) $(\Delta_{LLL})_2$-[Co_3(aet)$_6$][**5**] in a $NaNO_3$ solution of D_2O.

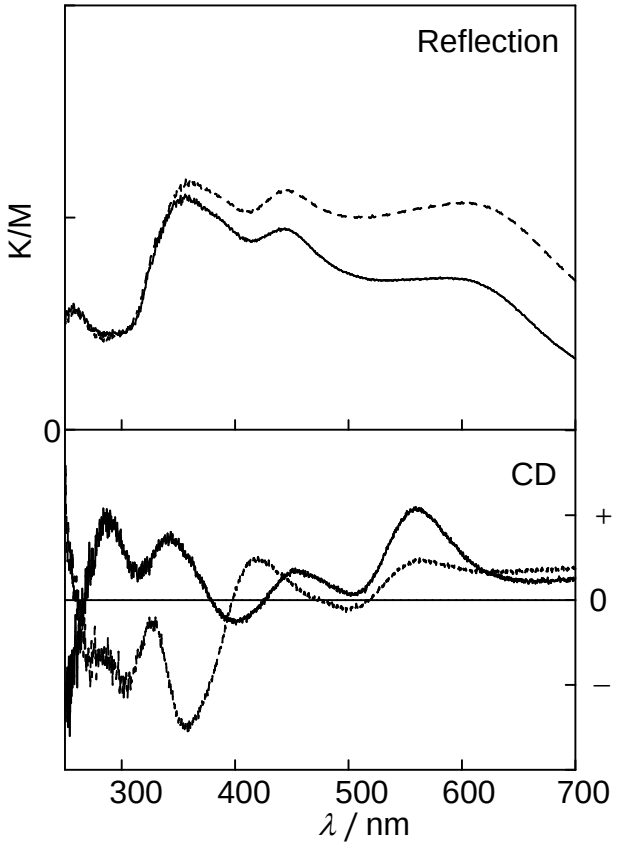

Figure 4-6. Reflection and CD spectra of $(\Delta_{LLL})_2$-$[Co_3(aet)_6]$[**4**] (---) and $(\Delta_{LLL})_2$-$[Co_3(aet)_6]$[**5**] (—) in the solid state. For $(\Delta_{LLL})_2$-$[Co_3(aet)_6]$[**4**], reflection spectrum [λ / nm]: 607, 446, 356; CD spectrum [λ / nm]: 560 (+), 500 (–), 420 (+), 356 (–), 327 (–), 302 (–). For $(\Delta_{LLL})_2$-$[Co_3(aet)_6]$[**5**], reflection spectrum [λ / nm]: 600, 443, 357; CD spectrum [λ / nm]: 560 (+), 505 (+), 452 (+), 398 (–), 340 (+), 315 (+), 285 (+).

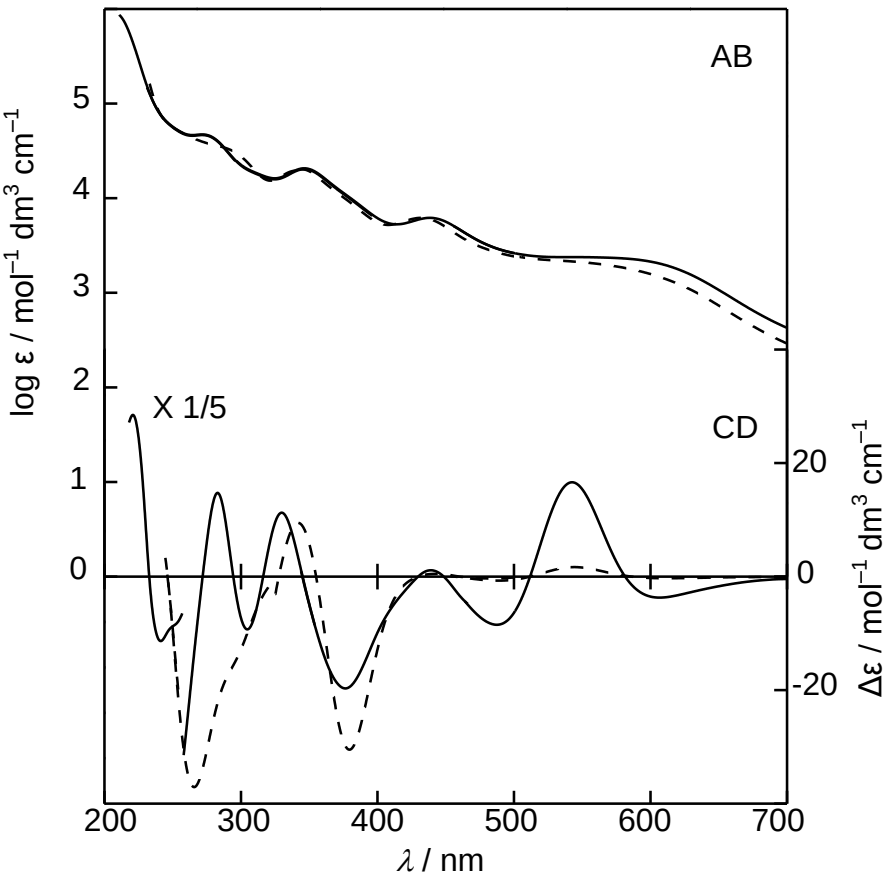

Figure 4-7. Absorption and CD spectra of $(\Delta_{LLL})_2$-$[Co_3(aet)_6]$[**4**] (---) and $(\Delta_{LLL})_2$-$[Co_3(aet)_6]$[**5**] (—) in a $NaNO_3$ aqueous solution. For $(\Delta_{LLL})_2$-$[Co_3(aet)_6]$[**4**], absorption spectrum [λ / nm (logε / mol^{-1} dm^3 cm^{-1})]: 575 (3.27), 432 (3.79), 345 (4.30), 289 (4.52); CD spectrum [λ / nm ($\Delta\varepsilon$ / mol^{-1} dm^3 cm^{-1})]: 610 (–0.28), 545 (+1.67), 484 (–0.68), 379 (–30.48), 341 (+9.46), 265 (–185.40). For $(\Delta_{LLL})_2$-$[Co_3(aet)_6]$[**5**], absorption spectrum [λ / nm (logε / mol^{-1} dm^3 cm^{-1})]: 585 (3.36), 439 (3.70), 346 (4.31), 276 (4.65); CD spectrum [λ / nm ($\Delta\varepsilon$ / mol^{-1} dm^3 cm^{-1})]: 606 (–3.69), 543 (+16.63), 487 (–8.47), 439 (+1.12), 376 (–19.69), 330 (+11.26), 304 (–9.28), 283 (+14.75), 241(–56.74).

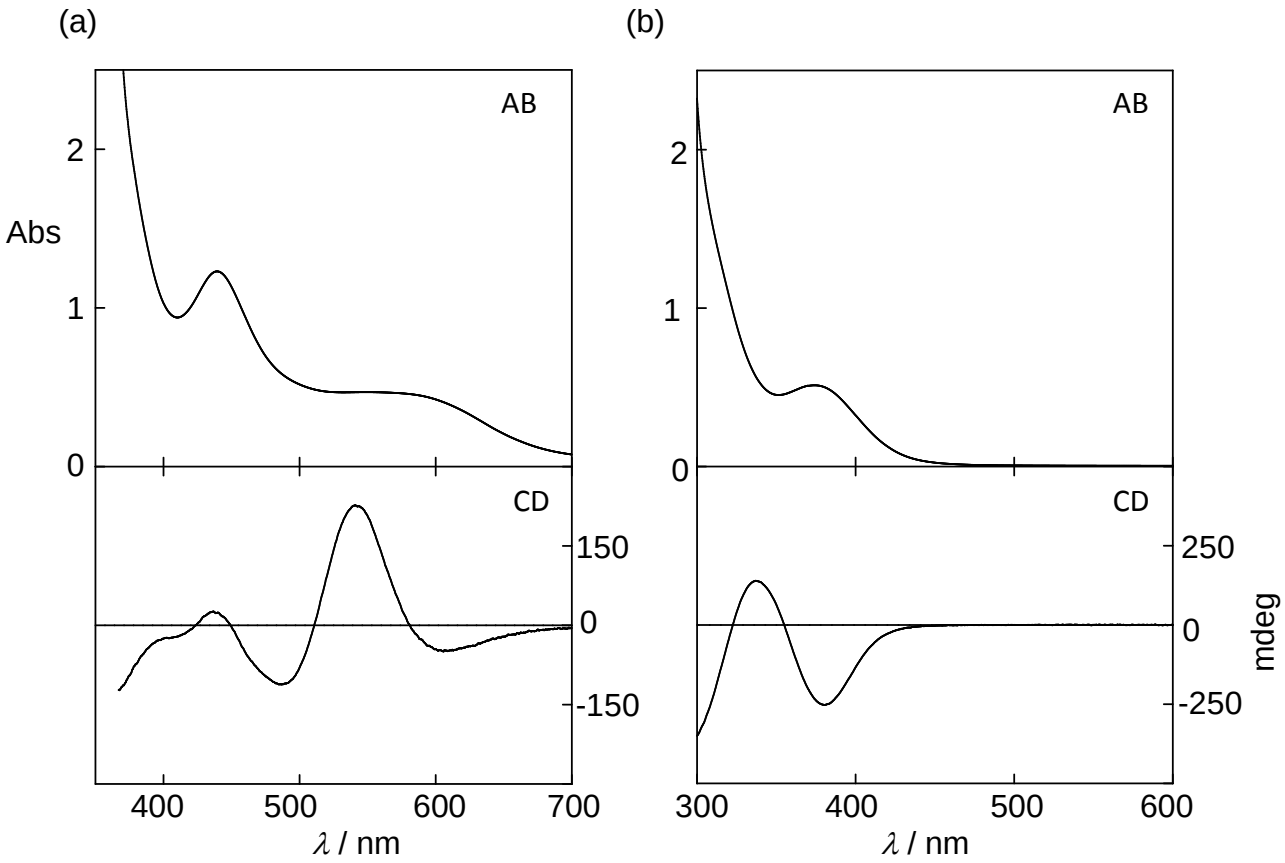

Figure 4-8. Absorption and CD spectra of (a) $[Co_3(aet)_6]^3$ and (b) $[\mathbf{5}]^{3-}$ incorporated in $(\Delta_{LLL})_2$-$[Co_3(aet)_6][\mathbf{5}]$ in water.

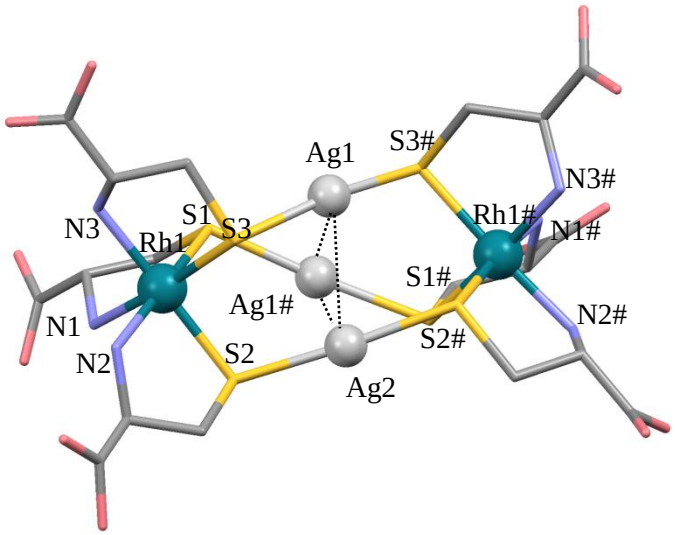

Figure 4-9. A perspective view of $(\Delta_{LLL})_2$-[**5**]$^{3-}$ in $(\Delta_{LLL})_2$-H_4[**5**](NO_3) with the atomic labeling scheme. Symmetry code: (#) –x+1, y, –z.

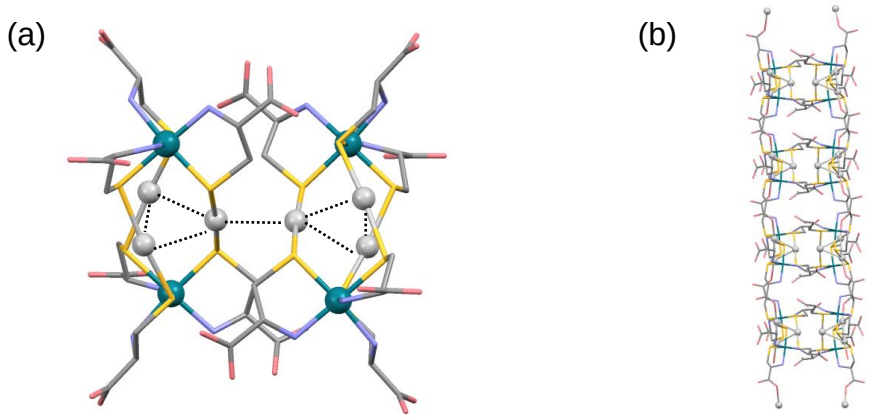

Figure 4-10. (a) A dimer structure formed by an Ag···Ag contact and (b) a 1D chain structure formed by Ag–OOC bonds.

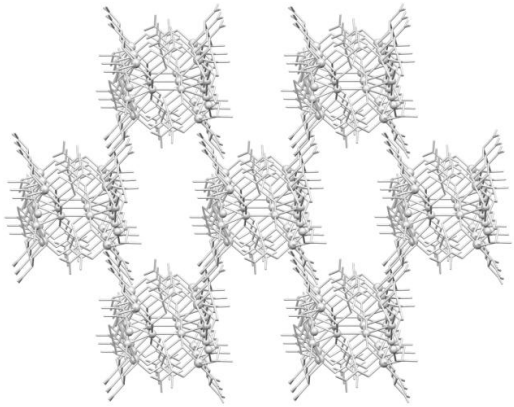

Figure 4-11. A 3D structure formed by COOH···OOC hydrogen bonds in $(\Delta_{LLL})_2$-H_4[**5**](NO_3).

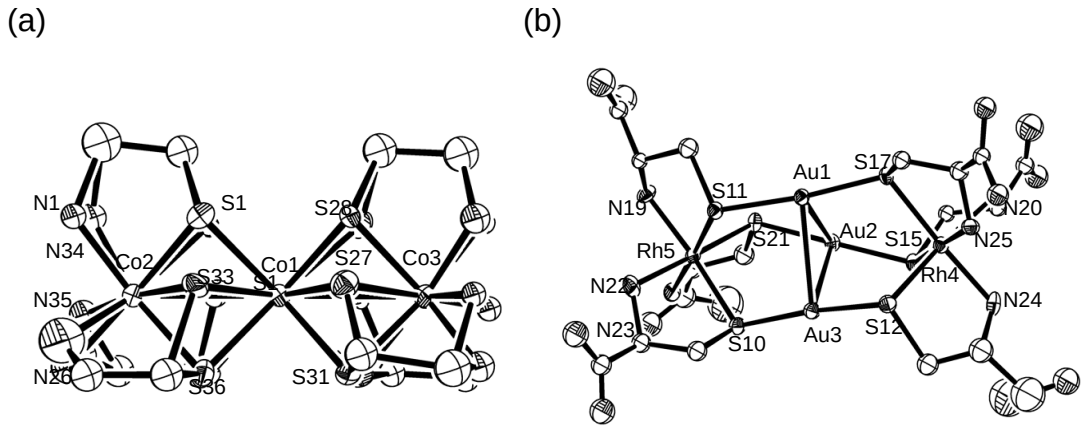

Figure 4-12. ORTEP drawings of (a) $[Co_3(aet)_6]^{3+}$ and (b) $(\Delta_{LLL})_2$-[**4**]$^{3-}$ in $(\Delta_{LLL})_2$-$[Co_3(aet)_6]$[**4**]. Hydrogen atoms are omitted for clarity.

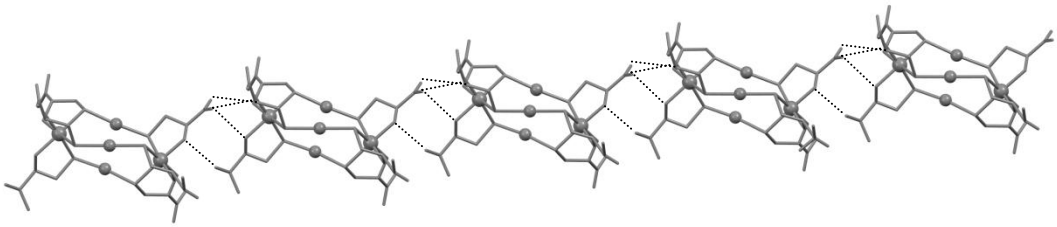

Figure 4-13. Perspective view of 1D chain structure of the complex-anion in $(\Delta_{LLL})_2$-$[Co_3(aet)_6]$[**4**]. Dashed lines represent hydrogen bonds.

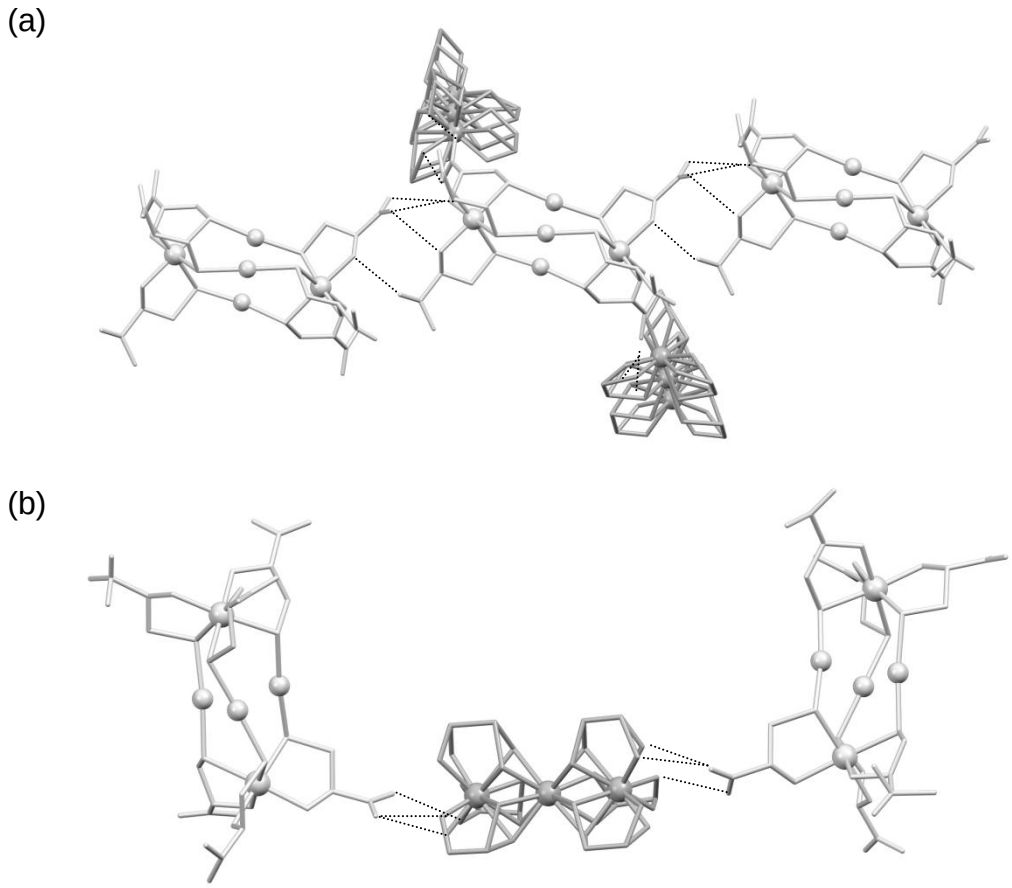

Figure 4-14. Intermolecular interactions (a) around each complex-anion and (b) around each complex-cation in $(\Delta_{LLL})_2$-$[Co_3(aet)_6]$[**4**].

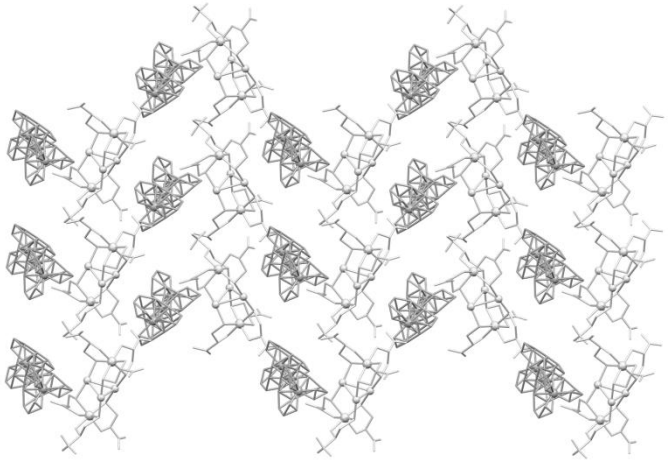

Figure 4-15. Packing structure of $(\Delta_{LLL})_2$-$[Co_3(aet)_6]$[**4**] viewing from *a* axis. Dark gray and light gray molecules represent complex-cation and complex-anion, respectively.

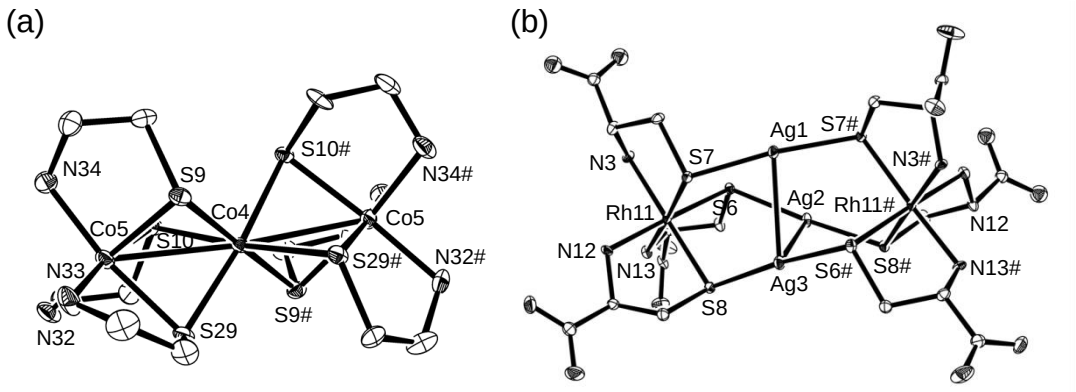

Figure 4-16. ORTEP drawings of (a) $[Co_3(aet)_6]^{3+}$ and (b) $(\Delta_{LLL})_2$-[**5**]$^{3-}$ in $(\Delta_{LLL})_2$-$[Co_3(aet)_6]$[**5**]. Hydrogen atoms are omitted for clarity.

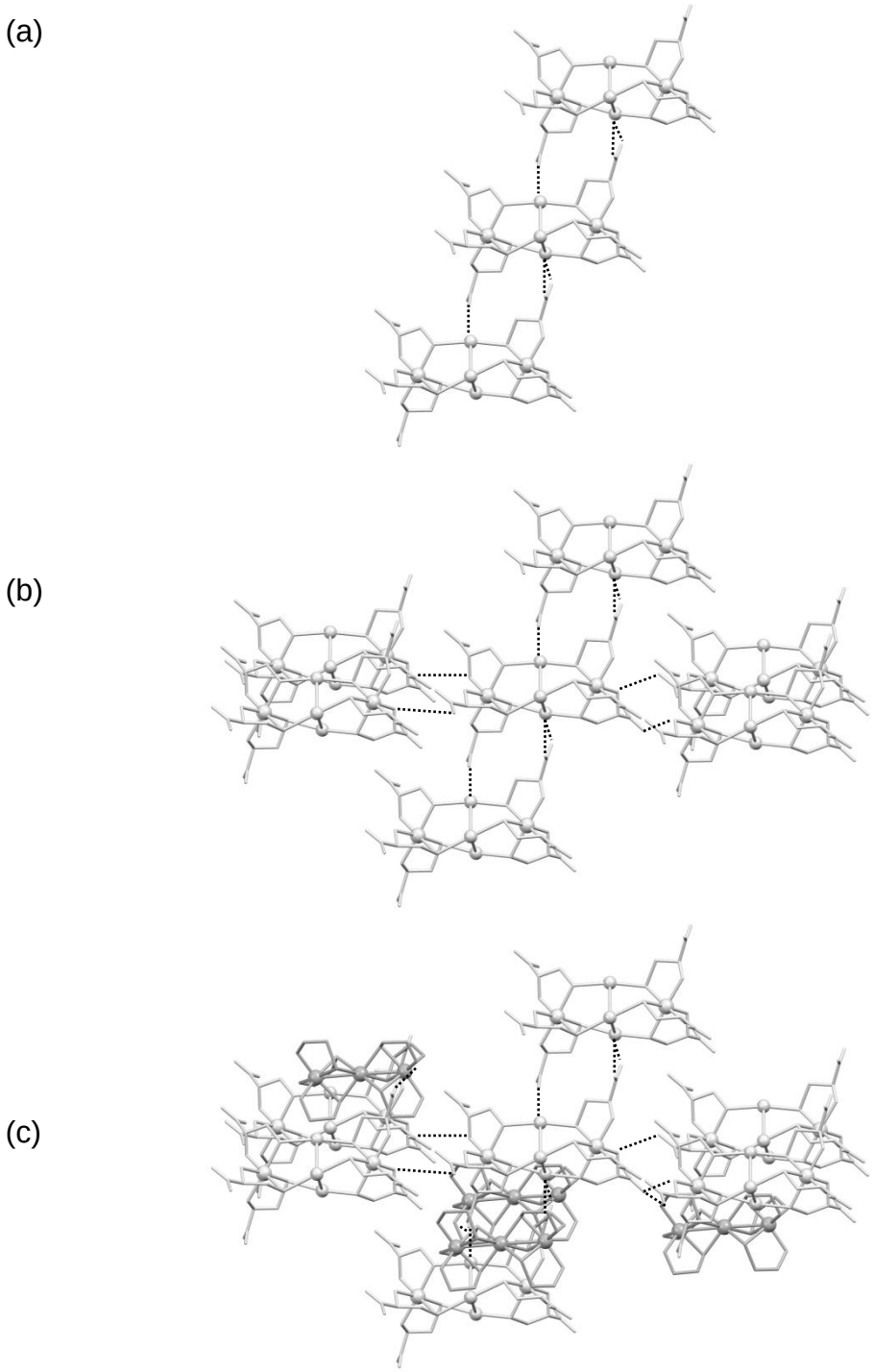

Figure 4-17. Perspective views of intermolecular interactions around each complex-anion in $(\Delta_{LLL})_2$-$[Co_3(aet)_6]$[**5**]. (a) Anion-anion interactions through the Ag–OOC coordination bonds, (b) all anion-anion interactions through the Ag–OOC coordination bonds and NH···O hydrogen bonds, and (c) all anion-anion and anion-cation intermolecular interactions.

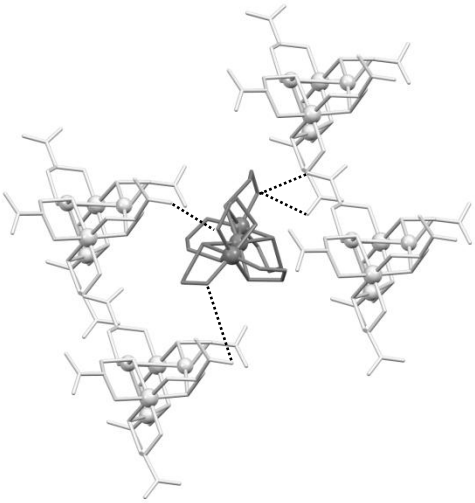

Figure 4-18. Perspective view of intermolecular interactions around each complex-cation in $(\Delta_{LLL})_2$-$[Co_3(aet)_6]$[**5**].

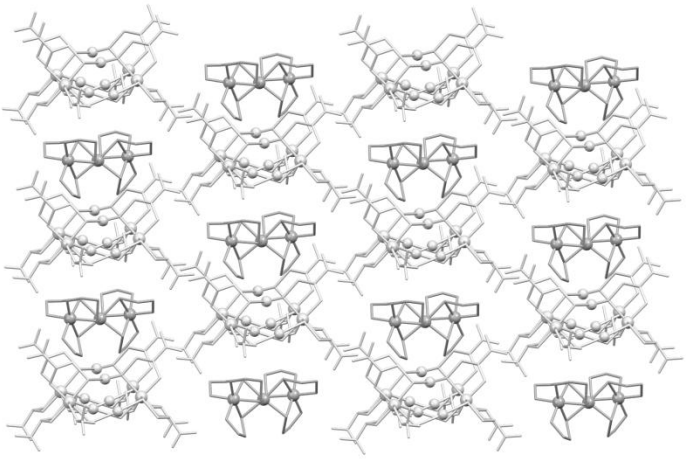

Figure 4-19. Packing structure of $(\Delta_{LLL})_2$-$[Co_3(aet)_6]$[**5**]. Dark gray and light gray molecules represent complex-cation and complex-anion, respectively.

Table 4-1. Crystallographic data of complexes.

	$(\Delta_{LLL})_2$-H_4[**5**]$(NO_3)\cdot 9H_2O$	$(\Delta_{LLL})_2$-[Co_3(aet)$_6$][**4**]$\cdot 17H_2O$	$(\Delta_{LLL})_2$-[Co_3(aet)$_6$][**5**]$\cdot 9H_2O$
Empirical formula	$C_{18}H_{52}Ag_3N_7O_{24}Rh_2S_6$	$C_{30}H_{104}Au_3Co_3N_{12}O_{31}Rh_2S_{12}$	$C_{30}H_{30}Ag_3Co_3N_{12}O_{20}Rh_2S_{12}$
Formula weight	2449.18	2449.18	1969.60
Crystal system	Orthorhombic	Monoclinic	Monoclinic
Space group	*I*222	$P2_1$	*C*2
a / Å	10.024(2)	12.902(9)	26.5781(5)
b / Å	18.725(5)	26.58(2)	12.5092(3)
c / Å	24.813(7)	13.130(10)	10.2204(2)
β / °		115.54(3)	109.336(8)
V / Å ^{3}	4657(2)	4062(5)	3206.31(12)
Z	4	2	4
T / K	200(2)	200(2)	200(2)
R(int)	0.0337	0.0588	0.0183
ρ_{calcd} / g cm^{-3}	2.100	2.002	1.813
μ(Mo Kα) / cm^{-1}	2.285	6.771	2.615
θ_{Max}	54.96	54.96	54.96
total no. of data	5350	31698	12890
no. of unique data	5270	18194	6988
no. of parameters	249	590	359
*R*1, w*R*2 (*I*>2σ(*I*))[a,b]	0.0337, 0.0344	0.0657, 0.1662	0.0284, 0.0617
*R*1, w*R*2 (all data)[a,b]	0.0982, 0.0977	0.0824, 0.1738	0.0312, 0.0622

[a] $R1 = (\Sigma|(|F_o| - |F_c|)|)/(\Sigma|F_o|)$, [b] $wR2 = [\{\Sigma w(F_o^2 - F_c^2)^2\}/(\Sigma w|F_o^2|^2)]^{1/2}$

Table 4-2. Selected bond distances and angles of $(\Delta_{LLL})_2$-H_4[**5**](NO_3).

		Distances (Å)	
Rh1-S1	2.3161(14)	Rh1-N1	2.101(4)
Rh1-S2	2.3222(12)	Rh1-N2	2.097(5)
Rh1-S3	2.3062(13)	Rh1-N3	2.093(4)
Ag1-S1	2.4184(15)	Ag1-Ag2	2.9889(8)
Ag2-S2	2.3865(12)	Ag2-Ag2#2	2.9354(13)
Ag1-S3#1	2.4198(14)	Ag1-Ag1#1	3.1095(10)
		Angles (º)	
N3-Rh1-N2	90.02(18)	N3-Rh1-S3	85.22(13)
N3-Rh1-N1	91.06(18)	N2-Rh1-S3	92.27(17)
N2-Rh1-N1	90.2(2)	N3-Rh1-S1	91.49(14)
S3-Rh1-S2	92.16(5)	N1-Rh1-S1	85.39(13)
S1-Rh1-S2	93.55(5)	N2-Rh1-S2	85.20(13)
S3-Rh1-S1	92.25(5)	N1-Rh1-S2	92.48(13)
N1-Rh1-S3	175.55(13)	Ag1#1-Ag2-Ag1	62.69(3)
N2-Rh1-S1	175.34(17)	Ag2-Ag1-Ag1#1	58.656(12)
N3-Rh1-S2	174.06(13)	Ag2#2-Ag2-Ag1	148.657(13)

Symmetry codes: (#1) –x+1, y, –z, (#2) –x+1, –y, z.

Table 4-3. Selected bond distances and angles of $(\Delta_{LLL})_2$-$[Co_3(aet)_6]_2$[**4**].

Distances (Å)			
Au(1)-S(5)	2.298(4)	Co(1)-S(9A)	2.233(8)
Au(1)-S(2)	2.303(4)	Co(1)-S(7B)	2.289(11)
Au(2)-S(1)	2.306(4)	Co(1)-S(8A)	2.317(8)
Au(2)-S(4)	2.323(4)	Co(2)-S(10B)	2.246(11)
Au(3)-S(3)	2.299(4)	Co(2)-S(7A)	2.253(8)
Au(3)-S(6)	2.302(4)	Co(2)-S(11A)	2.259(9)
Rh(1)-N(1)	2.085(13)	Co(2)-S(11B)	2.260(11)
Rh(1)-N(3)	2.116(15)	Co(2)-S(9A)	2.262(8)
Rh(1)-N(2)	2.155(14)	Co(2)-S(9B)	2.275(10)
Rh(1)-S(3)	2.322(4)	Co(2)-S(8A)	2.279(8)
Rh(1)-S(2)	2.344(4)	Co(2)-S(12B)	2.282(10)
Rh(1)-S(1)	2.345(4)	Co(2)-S(10A)	2.291(9)
Rh(2)-N(6)	2.099(15)	Co(2)-S(12A)	2.301(8)
Rh(2)-N(5)	2.114(13)	Co(2)-S(8B)	2.302(10)
Rh(2)-N(4)	2.168(13)	Co(2)-S(7B)	2.328(11)
Rh(2)-S(6)	2.326(4)	Co(3)-N(12B)	1.75(4)
Rh(2)-S(5)	2.334(4)	Co(3)-N(10B)	1.86(4)
Rh(2)-S(4)	2.340(4)	Co(3)-N(12A)	1.97(3)
Co(1)-N(8A)	1.92(3)	Co(3)-N(10A)	2.01(3)
Co(1)-N(7A)	1.93(3)	Co(3)-N(11B)	2.06(6)
Co(1)-N(9B)	1.93(4)	Co(3)-N(11A)	2.13(4)
Co(1)-N(8B)	1.96(3)	Co(3)-S(12A)	2.215(8)
Co(1)-N(9A)	2.02(2)	Co(3)-S(10A)	2.240(8)
Co(1)-N(7B)	2.12(4)	Co(3)-S(11A)	2.257(11)
Co(1)-S(8B)	2.175(10)	Co(3)-S(10B)	2.267(11)
Co(1)-S(9B)	2.183(10)	Co(3)-S(11B)	2.271(10)
Co(1)-S(7A)	2.232(8)	Co(3)-S(12B)	2.293(12)

Angles (º)			
S(5)-Au(1)-S(2)	172.19(14)	N(1)-Rh(1)-S(3)	87.6(4)
S(1)-Au(2)-S(4)	174.47(14)	N(3)-Rh(1)-S(3)	85.8(5)
S(3)-Au(3)-S(6)	173.69(14)	N(2)-Rh(1)-S(3)	174.8(4)
N(1)-Rh(1)-N(3)	89.6(6)	N(1)-Rh(1)-S(2)	177.3(4)
N(1)-Rh(1)-N(2)	92.8(5)	N(3)-Rh(1)-S(2)	89.0(5)
N(3)-Rh(1)-N(2)	89.0(6)	N(2)-Rh(1)-S(2)	85.0(4)
S(3)-Rh(1)-S(2)	94.55(16)	N(1)-Rh(1)-S(1)	85.7(4)

Table 4-3. (continued)

N(3)-Rh(1)-S(1)	175.3(5)	N(8B)-Co(1)-S(8B)	93.1(9)
N(2)-Rh(1)-S(1)	90.8(4)	N(9A)-Co(1)-S(8B)	138.9(8)
S(3)-Rh(1)-S(1)	94.37(15)	N(7B)-Co(1)-S(8B)	92.5(11)
S(2)-Rh(1)-S(1)	95.71(15)	N(8A)-Co(1)-S(9B)	123.1(9)
N(6)-Rh(2)-N(5)	90.2(6)	N(7A)-Co(1)-S(9B)	133.1(9)
N(6)-Rh(2)-N(4)	89.1(6)	N(9B)-Co(1)-S(9B)	88.8(12)
N(5)-Rh(2)-N(4)	91.5(5)	N(8B)-Co(1)-S(9B)	95.6(10)
N(6)-Rh(2)-S(6)	86.1(4)	N(9A)-Co(1)-S(9B)	72.8(8)
N(5)-Rh(2)-S(6)	89.3(4)	N(7B)-Co(1)-S(9B)	170.9(11)
N(4)-Rh(2)-S(6)	175.1(4)	S(8B)-Co(1)-S(9B)	88.1(4)
N(6)-Rh(2)-S(5)	175.3(4)	N(8A)-Co(1)-S(7A)	93.7(9)
N(5)-Rh(2)-S(5)	85.4(4)	N(7A)-Co(1)-S(7A)	91.3(8)
N(4)-Rh(2)-S(5)	89.3(4)	N(9B)-Co(1)-S(7A)	134.7(12)
S(6)-Rh(2)-S(5)	95.57(16)	N(8B)-Co(1)-S(7A)	126.6(9)
N(6)-Rh(2)-S(4)	90.1(4)	N(9A)-Co(1)-S(7A)	174.6(8)
N(5)-Rh(2)-S(4)	177.6(4)	N(7B)-Co(1)-S(7A)	73.5(11)
N(4)-Rh(2)-S(4)	86.2(4)	S(8B)-Co(1)-S(7A)	38.6(4)
S(6)-Rh(2)-S(4)	93.02(16)	S(9B)-Co(1)-S(7A)	101.8(3)
S(5)-Rh(2)-S(4)	94.18(16)	N(8A)-Co(1)-S(9A)	169.4(8)
N(8A)-Co(1)-N(7A)	100.3(11)	N(7A)-Co(1)-S(9A)	90.3(8)
N(8A)-Co(1)-N(9B)	117.1(15)	N(9B)-Co(1)-S(9A)	69.4(12)
N(7A)-Co(1)-N(9B)	53.1(14)	N(8B)-Co(1)-S(9A)	137.6(10)
N(8A)-Co(1)-N(8B)	37.1(12)	N(9A)-Co(1)-S(9A)	90.5(8)
N(7A)-Co(1)-N(8B)	112.2(12)	N(7B)-Co(1)-S(9A)	124.3(11)
N(9B)-Co(1)-N(8B)	95.3(15)	S(8B)-Co(1)-S(9A)	102.8(3)
N(8A)-Co(1)-N(9A)	88.9(11)	S(9B)-Co(1)-S(9A)	47.0(3)
N(7A)-Co(1)-N(9A)	92.9(11)	S(7A)-Co(1)-S(9A)	86.1(3)
N(9B)-Co(1)-N(9A)	47.0(14)	N(8A)-Co(1)-S(7B)	142.2(9)
N(8B)-Co(1)-N(9A)	54.5(11)	N(7A)-Co(1)-S(7B)	69.0(8)
N(8A)-Co(1)-N(7B)	65.5(13)	N(9B)-Co(1)-S(7B)	86.2(12)
N(7A)-Co(1)-N(7B)	40.9(13)	N(8B)-Co(1)-S(7B)	178.5(10)
N(9B)-Co(1)-N(7B)	89.3(16)	N(9A)-Co(1)-S(7B)	126.6(8)
N(8B)-Co(1)-N(7B)	93.4(14)	N(7B)-Co(1)-S(7B)	86.9(11)
N(9A)-Co(1)-N(7B)	111.9(13)	S(8B)-Co(1)-S(7B)	85.5(4)
N(8A)-Co(1)-S(8B)	71.2(9)	S(9B)-Co(1)-S(7B)	84.1(4)
N(7A)-Co(1)-S(8B)	125.2(8)	S(7A)-Co(1)-S(7B)	52.2(4)
N(9B)-Co(1)-S(8B)	171.4(12)	S(9A)-Co(1)-S(7B)	42.7(3)

Table 4-3. (continued)

N(8A)-Co(1)-S(8A)	86.1(8)	S(9B)-Co(2)-S(12B)	99.6(4)
N(7A)-Co(1)-S(8A)	171.8(8)	S(8A)-Co(2)-S(12B)	135.3(3)
N(9B)-Co(1)-S(8A)	128.3(12)	S(10B)-Co(2)-S(10A)	50.4(4)
N(8B)-Co(1)-S(8A)	76.0(9)	S(7A)-Co(2)-S(10A)	93.3(3)
N(9A)-Co(1)-S(8A)	92.3(8)	S(11A)-Co(2)-S(10A)	83.7(3)
N(7B)-Co(1)-S(8A)	141.2(11)	S(11B)-Co(2)-S(10A)	41.0(4)
S(8B)-Co(1)-S(8A)	51.9(3)	S(9A)-Co(2)-S(10A)	176.9(3)
S(9B)-Co(1)-S(8A)	43.3(3)	S(9B)-Co(2)-S(10A)	137.3(4)
S(7A)-Co(1)-S(8A)	83.1(3)	S(8A)-Co(2)-S(10A)	98.8(3)
S(9A)-Co(1)-S(8A)	83.3(3)	S(12B)-Co(2)-S(10A)	101.1(3)
S(7B)-Co(1)-S(8A)	102.8(3)	S(10B)-Co(2)-S(12A)	39.1(4)
S(10B)-Co(2)-S(7A)	135.1(4)	S(7A)-Co(2)-S(12A)	174.3(3)
S(10B)-Co(2)-S(11A)	101.0(4)	S(11A)-Co(2)-S(12A)	83.3(3)
S(7A)-Co(2)-S(11A)	99.3(3)	S(11B)-Co(2)-S(12A)	99.8(3)
S(10B)-Co(2)-S(11B)	84.9(4)	S(9A)-Co(2)-S(12A)	100.1(3)
S(7A)-Co(2)-S(11B)	78.2(3)	S(9B)-Co(2)-S(12A)	83.3(3)
S(11A)-Co(2)-S(11B)	50.2(4)	S(8A)-Co(2)-S(12A)	94.1(3)
S(10B)-Co(2)-S(9A)	132.5(4)	S(12B)-Co(2)-S(12A)	50.3(4)
S(7A)-Co(2)-S(9A)	84.9(3)	S(10A)-Co(2)-S(12A)	81.9(3)
S(11A)-Co(2)-S(9A)	94.1(3)	S(10B)-Co(2)-S(8B)	103.7(4)
S(11B)-Co(2)-S(9A)	136.0(4)	S(7A)-Co(2)-S(8B)	37.3(3)
S(10B)-Co(2)-S(9B)	95.7(4)	S(11A)-Co(2)-S(8B)	132.6(4)
S(7A)-Co(2)-S(9B)	98.3(3)	S(11B)-Co(2)-S(8B)	92.6(4)
S(11A)-Co(2)-S(9B)	133.7(4)	S(9A)-Co(2)-S(8B)	97.9(3)
S(11B)-Co(2)-S(9B)	175.5(4)	S(9B)-Co(2)-S(8B)	82.9(4)
S(9A)-Co(2)-S(9B)	45.6(3)	S(8A)-Co(2)-S(8B)	51.0(3)
S(10B)-Co(2)-S(8A)	78.5(3)	S(12B)-Co(2)-S(8B)	171.6(4)
S(7A)-Co(2)-S(8A)	83.5(3)	S(10A)-Co(2)-S(8B)	82.0(3)
S(11A)-Co(2)-S(8A)	176.2(3)	S(12A)-Co(2)-S(8B)	138.2(4)
S(11B)-Co(2)-S(8A)	133.3(3)	S(10B)-Co(2)-S(7B)	173.4(4)
S(9A)-Co(2)-S(8A)	83.5(3)	S(7A)-Co(2)-S(7B)	51.4(4)
S(9B)-Co(2)-S(8A)	42.9(3)	S(11A)-Co(2)-S(7B)	77.3(4)
S(10B)-Co(2)-S(12B)	84.1(4)	S(11B)-Co(2)-S(7B)	98.6(4)
S(7A)-Co(2)-S(12B)	134.3(4)	S(9A)-Co(2)-S(7B)	42.0(3)
S(11A)-Co(2)-S(12B)	41.0(3)	S(9B)-Co(2)-S(7B)	81.2(4)
S(11B)-Co(2)-S(12B)	84.8(4)	S(8A)-Co(2)-S(7B)	102.7(3)
S(9A)-Co(2)-S(12B)	78.6(3)	S(12B)-Co(2)-S(7B)	90.6(4)

Table 4-3. (continued)

S(10A)-Co(2)-S(7B)	135.1(4)	N(11B)-Co(3)-S(11A)	72.7(13)
S(12A)-Co(2)-S(7B)	134.3(4)	N(11A)-Co(3)-S(11A)	86.0(11)
S(8B)-Co(2)-S(7B)	81.8(4)	S(12A)-Co(3)-S(11A)	85.3(3)
N(12B)-Co(3)-N(10B)	97.7(19)	S(10A)-Co(3)-S(11A)	84.9(3)
N(12B)-Co(3)-N(12A)	36.4(15)	N(12B)-Co(3)-S(10B)	93.5(14)
N(10B)-Co(3)-N(12A)	112.1(15)	N(10B)-Co(3)-S(10B)	88.0(13)
N(12B)-Co(3)-N(10A)	70.5(16)	N(12A)-Co(3)-S(10B)	125.7(8)
N(10B)-Co(3)-N(10A)	30.8(14)	N(10A)-Co(3)-S(10B)	76.1(9)
N(12A)-Co(3)-N(10A)	95.9(11)	N(11B)-Co(3)-S(10B)	169.8(9)
N(12B)-Co(3)-N(11B)	96.4(18)	N(11A)-Co(3)-S(10B)	141.0(12)
N(10B)-Co(3)-N(11B)	93(2)	S(12A)-Co(3)-S(10B)	39.7(4)
N(12A)-Co(3)-N(11B)	63.0(16)	S(10A)-Co(3)-S(10B)	50.8(4)
N(10A)-Co(3)-N(11B)	109.7(16)	S(11A)-Co(3)-S(10B)	100.5(3)
N(12B)-Co(3)-N(11A)	118.1(18)	N(12B)-Co(3)-S(11B)	165.3(14)
N(10B)-Co(3)-N(11A)	66.8(16)	N(10B)-Co(3)-S(11B)	96.7(14)
N(12A)-Co(3)-N(11A)	92.2(13)	N(12A)-Co(3)-S(11B)	137.5(8)
N(10A)-Co(3)-N(11A)	92.6(13)	N(10A)-Co(3)-S(11B)	122.6(9)
N(11B)-Co(3)-N(11A)	33.1(19)	N(11B)-Co(3)-S(11B)	85.6(9)
N(12B)-Co(3)-S(12A)	68.0(14)	N(11A)-Co(3)-S(11B)	70.6(11)
N(10B)-Co(3)-S(12A)	120.3(13)	S(12A)-Co(3)-S(11B)	102.1(3)
N(12A)-Co(3)-S(12A)	90.0(8)	S(10A)-Co(3)-S(11B)	41.3(4)
N(10A)-Co(3)-S(12A)	95.8(9)	S(11A)-Co(3)-S(11B)	50.1(4)
N(11B)-Co(3)-S(12A)	143.9(19)	S(10B)-Co(3)-S(11B)	84.2(4)
N(11A)-Co(3)-S(12A)	171.0(11)	N(12B)-Co(3)-S(12B)	81.0(14)
N(12B)-Co(3)-S(10A)	142.5(14)	N(10B)-Co(3)-S(12B)	171.2(13)
N(10B)-Co(3)-S(10A)	73.3(13)	N(12A)-Co(3)-S(12B)	72.0(8)
N(12A)-Co(3)-S(10A)	174.1(8)	N(10A)-Co(3)-S(12B)	143.4(9)
N(10A)-Co(3)-S(10A)	87.8(9)	N(11B)-Co(3)-S(12B)	95.6(19)
N(11B)-Co(3)-S(10A)	120.0(13)	N(11A)-Co(3)-S(12B)	121.5(11)
N(11A)-Co(3)-S(10A)	92.3(11)	S(12A)-Co(3)-S(12B)	51.1(4)
S(12A)-Co(3)-S(10A)	85.0(3)	S(10A)-Co(3)-S(12B)	102.3(3)
N(12B)-Co(3)-S(11A)	116.6(14)	S(11A)-Co(3)-S(12B)	40.9(3)
N(10B)-Co(3)-S(11A)	143.7(14)	S(10B)-Co(3)-S(12B)	83.4(4)
N(12A)-Co(3)-S(11A)	91.5(8)	S(11B)-Co(3)-S(12B)	84.3(4)
N(10A)-Co(3)-S(11A)	172.5(9)		

Table 4-4. Selected bond distances and angles of $(\Delta_{LLL})_2$-$[Co_3(aet)_6]_2$[**5**].

Distances (Å)			
Ag(1)-S(7)#1	2.4192(12)	Co(4)-S(29)#2	2.2723(15)
Ag(1)-S(7)	2.4192(12)	Co(4)-Co(5)	2.8582(8)
Ag(1)-Ag(2)	2.9782(6)	Co(4)-Co(5)#2	2.8583(8)
Ag(1)-Ag(2)#1	2.9783(6)	Co(5)-N(33)	1.992(5)
Ag(2)-S(8)#1	2.4200(13)	Co(5)-N(32)	1.993(6)
Ag(2)-S(6)	2.4222(12)	Co(5)-N(34)	2.012(5)
Ag(2)-Ag(2)#1	3.3678(7)	Co(5)-S(9)#2	2.2139(16)
Rh(11)-N(3)	2.104(4)	Co(5)-S(10)#2	2.2341(15)
Rh(11)-N(13)	2.115(3)	Co(5)-S(29)	2.2423(17)
Rh(11)-N(12)	2.121(4)	S(6)-C(18)	1.836(5)
Rh(11)-S(6)	2.3047(10)	S(7)-C(15)	1.838(5)
Rh(11)-S(8)	2.3239(12)	S(8)-C(16)	1.840(5)
Rh(11)-S(7)	2.3319(13)	S(8)-Ag(2)#1	2.4200(13)
Co(4)-S(9)#2	2.2338(15)	S(9)-C(35)#2	1.826(6)
Co(4)-S(9)	2.2339(15)	S(9)-Co(5)#2	2.2140(16)
Co(4)-S(10)	2.2629(14)	S(10)-C(36)#2	1.851(6)
Co(4)-S(10)#2	2.2629(14)	S(10)-Co(5)#2	2.2341(15)
Co(4)-S(29)	2.2723(15)		

Angles (º)			
S(7)#1-Ag(1)-S(7)	173.21(7)	N(13)-Rh(11)-S(6)	176.84(12)
S(7)#1-Ag(1)-Ag(2)	80.82(3)	N(12)-Rh(11)-S(6)	85.76(12)
S(7)-Ag(1)-Ag(2)	104.90(3)	N(3)-Rh(11)-S(8)	175.58(11)
S(7)#1-Ag(1)-Ag(2)#1	104.90(3)	N(13)-Rh(11)-S(8)	86.08(11)
S(7)-Ag(1)-Ag(2)#1	80.82(3)	N(12)-Rh(11)-S(8)	87.65(12)
Ag(2)-Ag(1)-Ag(2)#1	68.860(19)	S(6)-Rh(11)-S(8)	94.32(4)
S(8)#1-Ag(2)-S(6)	170.72(4)	N(3)-Rh(11)-S(7)	86.06(12)
S(8)#1-Ag(2)-Ag(1)	97.17(3)	N(13)-Rh(11)-S(7)	91.50(12)
S(6)-Ag(2)-Ag(1)	76.93(3)	N(12)-Rh(11)-S(7)	177.14(12)
S(8)#1-Ag(2)-Ag(2)#1	75.12(3)	S(6)-Rh(11)-S(7)	91.61(4)
S(6)-Ag(2)-Ag(2)#1	95.60(3)	S(8)-Rh(11)-S(7)	93.68(4)
Ag(1)-Ag(2)-Ag(2)#1	55.570(9)	S(9)#2-Co(4)-S(9)	90.14(8)
N(3)-Rh(11)-N(13)	89.52(16)	S(9)#2-Co(4)-S(10)	95.98(5)
N(3)-Rh(11)-N(12)	92.80(15)	S(9)-Co(4)-S(10)	83.51(5)
N(13)-Rh(11)-N(12)	91.12(16)	S(9)#2-Co(4)-S(10)#2	83.51(5)
N(3)-Rh(11)-S(6)	90.09(11)	S(9)-Co(4)-S(10)#2	95.98(5)

Table 4-4. (continued)

S(10)-Co(4)-S(10)#2	179.27(9)	N(33)-Co(5)-S(9)#2	87.74(17)
S(9)#2-Co(4)-S(29)	83.72(5)	N(32)-Co(5)-S(9)#2	171.5(2)
S(9)-Co(4)-S(29)	173.75(6)	N(34)-Co(5)-S(9)#2	91.04(16)
S(10)-Co(4)-S(29)	98.27(6)	N(33)-Co(5)-S(10)#2	171.97(18)
S(10)#2-Co(4)-S(29)	82.19(5)	N(32)-Co(5)-S(10)#2	94.80(19)
S(9)#2-Co(4)-S(29)#2	173.74(6)	N(34)-Co(5)-S(10)#2	88.38(15)
S(9)-Co(4)-S(29)#2	83.72(5)	S(9)#2-Co(5)-S(10)#2	84.63(6)
S(10)-Co(4)-S(29)#2	82.19(5)	N(33)-Co(5)-S(29)	93.33(17)
S(10)#2-Co(4)-S(29)#2	98.27(6)	N(32)-Co(5)-S(29)	86.6(2)
S(29)-Co(4)-S(29)#2	102.45(8)	N(34)-Co(5)-S(29)	171.22(15)
N(33)-Co(5)-N(32)	92.4(2)	S(9)#2-Co(5)-S(29)	84.88(6)
N(33)-Co(5)-N(34)	94.3(2)	S(10)#2-Co(5)-S(29)	83.51(6)
N(32)-Co(5)-N(34)	97.4(2)		

Symmetry codes: (#1) –x,y,–z, (#2) –x+1,y,–z+1.

Table 4-5. Absorption and CD spectral data for $(\Delta_{LLL})_2$-K_3[**4**] in water and $(\Delta_{LLL})_2$-H_4[**5**](NO_3) in water in the presence of base.

Complex	Absorption maxima: λ / nm (log ε / mol^{-1} dm^3 cm^{-1})
$(\Delta_{LLL})_2$-K_3[**4**]	365 (3.37), 302 (3.87), 250 (4.65), 214 (4.84)
$(\Delta_{LLL})_2$-H_4[**5**](NO_3)	374 (3.21), 316 (3.6), 275 (4.3), 228 (4.80).

Complex	CD extrema: λ / nm ($\Delta\varepsilon$ / mol^{-1} dm^3 cm^{-1})
$(\Delta_{LLL})_2$-K_3[**4**]	380 (–28.27), 343 (+10.68), 266 (–187.27), 226 (+221.81)
$(\Delta_{LLL})_2$-H_4[**5**](NO_3)	380 (–20.01), 338 (+11.33), 239 (–86.53), 219 (+155.1)

Table 4-6. Absorption and CD spectral data for $(\Delta_{LLL})_2$-[Co_3(aet)$_6$][**4**] and $(\Delta_{LLL})_2$-[Co_3(aet)$_6$][**5**] in a $NaNO_3$ aqueous solution.

Complex	Absorption maxima: λ / nm (log ε / mol^{-1} dm^3 cm^{-1})
$(\Delta_{LLL})_2$-[Co_3(aet)$_6$][**4**]	575 (3.27), 432 (3.79), 345 (4.30), 289 (4.52)
$(\Delta_{LLL})_2$-[Co_3(aet)$_6$][**5**]	585 (3.36), 439 (3.70), 346 (4.31), 276 (4.65).

Complex	CD extrema: λ / nm ($\Delta\varepsilon$ / mol^{-1} dm^3 cm^{-1})
$(\Delta_{LLL})_2$-[Co_3(aet)$_6$][**4**]	610 (–0.28), 545 (+1.67), 484 (–0.68), 379 (–30.48), 341 (+9.46), 265 (–185.40)
$(\Delta_{LLL})_2$-[Co_3(aet)$_6$][**5**]	606 (–3.69), 543 (+16.63), 487 (–8.47), 439 (+1.12), 376 (–19.69), 330 (+11.26), 304 (–9.28), 283 (+14.75), 241 (–56.74)

Table 4-7. Reflection and CD spectral data for $(\Delta_{LLL})_2$-[Co_3(aet)$_6$][**4**] and $(\Delta_{LLL})_2$-[Co_3(aet)$_6$][**5**] in the solid state.

Complex	Reflection maxima: λ / nm
$(\Delta_{LLL})_2$-[Co_3(aet)$_6$][**4**]	607, 446, 356
$(\Delta_{LLL})_2$-[Co_3(aet)$_6$][**5**]	600, 443, 357

Complex	CD extrema: λ / nm
$(\Delta_{LLL})_2$-[Co_3(aet)$_6$][**4**]	560 (+), 500 (–), 420 (+), 356 (–), 327 (–), 302 (–)
$(\Delta_{LLL})_2$-[Co_3(aet)$_6$][**5**]	560 (+), 505 (+), 452 (+), 398 (–), 340 (+), 315 (+), 285 (+)

Chapter V. Conclusion

In this study, the chiral behavior of the L-cysteinato pentanuclear complex-anions, $(\Delta_{LLL})_2$-$[Au_3Co_2(L\text{-cys})_6]^{3-}$ ($(\Delta_{LLL})_2$-[**1**]$^{3-}$), $(\Delta_{LLL})_2$-$[Ag_3Co_2(L\text{-cys})_6]^{3-}$ ($(\Delta_{LLL})_2$-[**3**]$^{3-}$), $(\Delta_{LLL})_2$-$[Au_3Rh_2(L\text{-cys})_6]^{3-}$ ($(\Delta_{LLL})_2$-[**4**]$^{3-}$), and $(\Delta_{LLL})_2$-$[Ag_3Rh_2(L\text{-cys})_6]^{3-}$ ($(\Delta_{LLL})_2$-[**5**]$^{3-}$), was investigated. Since these complex-anions have multiple chiral centers and free carboxylate groups available for metal-coordination donor or hydrogen-bond acceptor, these complex-anions can act as a resolving reagent toward cationic racemic metal complexes during the cocrystallization process. In this thesis, the chiralselective behavior of the complex-anions toward $(\Delta)_2/(\Lambda)_2$-$[Co_3(aet)_6]^{3+}$, together with the unique chiral and structural conversion of $(\Delta_{LLL})_2$-[**1**]$^{3-}$, was reported.

In Chapter II, it was demonstrated that the S-bridged $Au^{I}_3Co^{III}_2$ complex-anion, $(\Delta_{LLL})_2$-[**1**]$^{3-}$, was converted to the S-bridged $Au^{I}_6Co^{III}_4$ complex-anion, $(\Lambda_{LLL})_4$-$[Au_6Co_4(L\text{-cys})_{12}]^{6-}$ ($(\Lambda_{LLL})_4$-[**2**]$^{6-}$), by the reaction with $(\Delta)_2/(\Lambda)_2$-$[Co_3(aet)_6]^{3+}$ in a basic aqueous solution. The reaction of $(\Delta_{LLL})_2$-[**1**]$^{3-}$ and $[Co_3(aet)_6]^{3+}$ in a neutral aqueous solution gave black crystals of $(\Delta_{LLL})_2$-$[Co_3(aet)_6]$[**1**] with retention of both the cationic and anionic structures, whereas a similar reaction in a basic solution gave the cocrystallized compound $(\Lambda_{LLL})_4$-$[Co_3(aet)_6]_2$[**2**]. From the spectral measurements, it was found that $(\Delta_{LLL})_2$-[**1**]$^{3-}$ is subject to the multiple chiral inversion on the Co^{III} centers and bridging S atoms to give $(\Lambda_{LLL})_2$-[**1**]$^{3-}$, which is induced by the pH control. Subsequently, the structural conversion to $(\Lambda_{LLL})_4$-[**2**]$^{6-}$ occurred upon the crystallization with $[Co_3(aet)_6]^{3+}$, which might be promoted by the stabilization through the formation of many intramolecular aurophilic interactions. The good shape matching of the complex-cation and the complex-anion also contributes to the conversion. The creation of such a unique coordination compound that has relatively inert metal centers and shows a multiple chiral inversion and a structural conversion is unprecedented. Furthermore, $(\Lambda_{LLL})_4$-[**2**]$^{6-}$ was converted back to $(\Lambda_{LLL})_2$-[**1**]$^{3-}$ by dissolution.

In Chapter III, the chiralselective behavior of the $Au^{I}Co^{III}$ and $Ag^{I}Co^{III}$ multinuclear complex-anions toward $(\Delta)_2/(\Lambda)_2$-$[Co_3(aet)_6]^{3+}$ was reported. The chirality of the complex-cation $[Co_3(aet)_6]^{3+}$ in the cocrystallized compound, $(\Delta_{LLL})_2$-$[Co_3(aet)_6]$[**1**], was checked by column chromatography and the subsequent absorption and CD spectral measurements. As a result, the $(\Delta)_2$ isomer of $[Co_3(aet)_6]^{3}$ is preferentially incorporated with a low chiralselectivity. The chiralselectivity of the cocrystallized compound, $(\Lambda_{LLL})_4$-$[Co_3(aet)_6]_2$[**2**], was also checked by a similar way, and it was found that the $(\Delta)_2$ isomer of $[Co_3(aet)_6]^{3}$ is preferentially incorporated with an enantiomeric excess (*ee*) of 22%. The chiralselectivity of $(\Lambda_{LLL})_4$-[**2**]$^{6-}$ is better, but is still not so good. The chiralselectivity of $(\Delta_{LLL})_2$-$[Ag_3Co_2(L\text{-cys})_6]^{3-}$ ($(\Delta_{LLL})_2$-[**3**]$^{3-}$) was also investigated for the comparison. Remarkably, the $(\Delta)_2$ isomer of $[Co_3(aet)_6]^{3}$ was

exclusively incorporated in the cocrystallized compound $(\Delta_{LLL})_2$-$[Co_3(aet)_6]$[**3**]. From the comparison of the structures of three compounds, it is speculated that the chirality of the Co^{III} centers in the complex-anions does not affect the chiralselectivity toward $[Co_3(aet)_6]^{3+}$, and the bridging metal ions (Au^I/Ag^I) might lead to the different chiralselectivity. The number of the intermolecular interactions between the complex-anion and the complex-cation may be important for the chiralselective behavior. In the two Au^ICo^{III} compounds showing the low selectivity, only two complex-cations are connected to each complex-anion through hydrogen bonds. On the other hand, each complex-anion is surrounded by four complex-cations in the Ag^ICo^{III} compound showing the excellent selectivity. The presence of the Ag^I ions instead of Au^I leads to the formation of intermolecular Ag–OOC coordination bonds, besides hydrogen bonds. This resulted in the increase in the number of intermolecular interactions, and thus, resulted in the excellent chiralselectivity in $(\Delta_{LLL})_2$-$[Co_3(aet)_6]$[**3**].

In Chapter IV, $(\Delta_{LLL})_2$-[**4**]$^{3-}$ and $(\Delta_{LLL})_2$-[**5**]$^{3-}$ were newly synthesized by the reaction of $(\Delta_{LLL})_2$-$[Rh(L\text{-}cys)_3]^{3-}$ with Au^I and Ag^I, respectively, and their chiral behavior such as the chiral inversion and the chiralselectivity toward $(\Delta)_2$/$(\Lambda)_2$-$[Co_3(aet)_6]^{3+}$ was investigated. Treatment of $(\Delta_{LLL})_2$-[**4**]$^{3-}$ with base did not lead to the chiral inversion, which is due to the inertness of Rh^{III} centers. For the chiralselectivity, both complex-anions were cocrystallized with $[Co_3(aet)_6]^{3+}$ to give $(\Delta_{LLL})_2$-$[Co_3(aet)_6]$[**4**] and $(\Delta_{LLL})_2$-$[Co_3(aet)_6]$[**5**]. In $(\Delta_{LLL})_2$-$[Co_3(aet)_6]$[**4**], the $(\Delta)_2$ isomer of $[Co_3(aet)_6]^{3+}$ was preferencially incorporated, whereas only the $(\Delta)_2$ isomer of $[Co_3(aet)_6]^{3+}$ was incorporated in $(\Delta_{LLL})_2$-$[Co_3(aet)_6]$[**5**] (*ee* ~100%). This difference might be also caused by the different intermolecular interactions between the complex-anion and the complex-cation. In $(\Delta_{LLL})_2$-$[Co_3(aet)_6]$[**4**], each complex-anion is hydrogen-bonded with two complex-cations in addition to two complex-anions, whereas in $(\Delta_{LLL})_2$-$[Co_3(aet)_6]$[**5**], each complex-anion is surrounded by six complex-anions and four complex-cations through hydrogen bonds and Ag–O coordination bonds.

By comparing the chiralselective behavior of the seven L-cysteinato multinuclear complex-anions including the previously reported complex-anions, $(\Delta_{LLL})_2$-$[Co_3(L\text{-}cys)_6]^{3-}$ and $(\Lambda_{LLL})_2$-$[Co_3(L\text{-}cys)_6]^{3-}$, it was assumed that the increase in the number of the intermolecular interactions between complex-anions and complex-cations is important for controlling the chiralselectivity. The chiralselectivity becomes better as the increase in the intermolecular interactions. In order to increase the cation-anion interactions, the following structural features of the complex-anions might be important: (i) to have additional interaction sites, such as coordinated Ag^I centers, besides the amine and carboxylate groups and (ii) to have axially oriented carboxylate groups.

In summary, this study demonstrated the fascinating chiral behavior in the L-cysteinato multinuclear complex-anions. As shown in Chapter II, $(\Delta_{LLL})_2$-[**1**]$^{3-}$ was converted to $(\Lambda_{LLL})_2$-[**1**]$^{3-}$ by treatment with base, and then was converted to $(\Lambda_{LLL})_4$-[**2**]$^{6-}$ upon the crystallization with $[Co_3(aet)_6]^{3+}$. It should be noted that the cooperative multiple chiral inversion occurred from $(\Delta_{LLL})_2(S)_6$ to $(\Lambda_{LLL})_2(R)_6$ retaining the $Au^{I}_3Co^{III}_2$ pentanuclear structure in the chiral inversion process. Thus, this system belongs to "strongly correlated chiral system" that shows cooperative multiple chiral inversion. In addition, the conversion from $(\Lambda_{LLL})_2$-[**1**]$^{3-}$ to $(\Lambda_{LLL})_4$-[**2**]$^{6-}$ can be considered as the aggregation of the chiral centers in one molecule. Thus, the construction of the $Au^{I}Co^{III}$ coordination system that shows the multiple chiral inversion and enhancement was achieved. This system contains relatively inert metal centers (Au^{I} and Co^{III} centers) that lead to the formation of relatively stable structures needed for the devices for use. Thus, this study provides not only the fundamental understanding for the chiral behavior in coordination chemistry, but also the further development of chiral switching systems in material science. Furthermore, the investigation of the chiralselectivity of the multinuclear complex-anions toward the multinuclear complex-cation showed that the increase in the intermolecular interaction sites between complex-anions and complex-cations leads to the excellent chiralselectivity. To achieve this, the introduction of several non-covalent bonding sites into complexes should be required.